POSITRON IMPACT IONISATION PHENOMENA

A thesis submitted to the University of London
for the degree of Doctor of Philosophy

J.Moxom
Department of Physics and Astronomy
University College London

October 1993

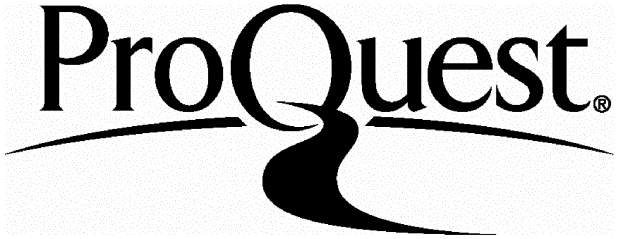

Abstract

A magnetically guided beam of nearly-monoenergetic slow positrons has been used to study positron impact ionisation phenomena in gases. A novel hemispherical scattering cell incorporating an efficient ion extraction and detection system has been developed and has been utilised throughout this work.

The energy spectra for the electrons ejected around 0° relative to the incident beam, following positron impact ionisation of Ar, have been measured by a time-of-flight method and a retarding electric field analyzer. The angular acceptance of the electron detection system has been estimated and used to compare the measured spectra with the double differential cross-sections calculated by Mandal *et al* (1986), Sil *et al* (1991) and Schultz and Reinhold (1990). The importance of the electron-capture-to-the-continuum process is discussed in this context and found to be minor at small forward angles, in contrast to the case of heavy positively charged projectiles.

The apparatus was modified to produce a pulsed beam of slow positrons and utilised to measure in detail the total ionisation cross-section (Q_t^+) for a variety of atomic and molecular targets. For Ar, He and H_2, Q_t^+ which includes contributions from Ps formation, has been subtracted from corresponding total cross-sections, in order to deduce the behaviour of the elastic scattering cross-section (Q_{el}) in the vicinity of the Ps formation threshold (E_{Ps}). Here a small change in the gradient of Q_{el} has been found.

The energy dependencies of the Q_t^+ for He, Ne and Ar, close to E_{Ps} have been interpreted in terms of threshold theory. In the case of Ar the outgoing Ps appears to be predominantly s-wave in character. For He and Ne the analysis suggests that the Ps contains significant contributions from a number of partial waves.

In the case of O_2, structure in Q_t^+ has been found, which

is attributed to coupling between two inelastic channels, namely Ps formation and excitation to the Schuman-Runge continuum.

Contents

Chapter 3. Ejected Electron Energy Spectra in Low Energy Positron-Atom Collisions

Chapter 4. Total Ionisation Cross-Sections in Positron-Gas Collisions

Figure Captions

Table Captions

Acknowledgements

Acknowledgements are due to:

G. Laricchia for supervision and encouragement;

M. Charlton, W. E. Meyerhof and members of the experimental positron group at UCL for useful discussion and practical help;

E. J. C. Oldfield and I. E. Rangue for technical advice.

CHAPTER 1

INTRODUCTION

1.1 Historical Background

The existence of anti-matter was first predicted by Dirac (1930a), following his formulation of the relativistically invariant Schrodinger equation for free electrons in an electromagnetic field. Solutions were obtained which corresponded to states of the particles with negative energies. These arise as a direct consequence of Einstein's equation for the total energy (E) of a particle of rest mass (m_0) and momentum (p)

$$E^2=m_0^2c^4+p^2c^2 \qquad (1.1)$$

where c is the speed of light, in vacuum.

Dirac proposed that the vacuum should be considered to consist of an infinite and uniform sea of electrons occupying all the negative energy states below $-m_0c^2$, the Pauli exclusion principle forbidding the transition of free electrons from positive energy states to the occupied negative states. An electron may, however, be excited from a negative to a positive energy level, leaving behind a "hole". This hole, in an otherwise filled sea of electrons, would appear to possess the properties of a particle with positive mass and charge.

At the time of Dirac's work, the only known positively charged elementary particle was the proton. Dirac proposed that the holes in the negative energy states were protons and that the differences between the masses of the proton and electron were due to interactions between the electrons. However, Weyl (1931) showed that the hole had to correspond

to a new particle with the same mass as an electron and this particle (or anti-electron) was named the positron.

Positrons were first observed by Anderson (1932) in a cloud chamber study of cosmic rays. The tracks produced by these particles were initially attributed to protons. However, Blackett and Occhialini (1933), using a similar experimental technique, showed that the observed particles had the same mass as an electron. The existence of the positron was thus confirmed.

It was suggested by Mohorovicic (1934) that a quasi-stable hydrogenic bound state of a positron and electron may exist. This bound state was named positronium (Ps) by Ruark (1945) and soon received considerable theoretical attention (e.g. Wheeler 1946 and Fulton and Martin 1954). Its existence was experimentally verified by Deutch (1951) whilst measuring positron lifetimes in gases.

The positron is intrinsically of great interest as a readily available example of anti-matter. Positrons can be obtained from the decay of certain radionuclides and have become powerful probes of a wide range of physical phenomena. The possibility of annihilation of a positron with its anti-particle, the electron, has made possible the investigation of such phenomena by a number of experimental techniques which rely on the detection of the annihilation photons. These are discussed in § 1.3.

Positrons may be formed into nearly mono-energetic beams and these have been used, among other things, to study the interaction of positrons with single atoms(molecules) at well defined energies. This has provided unique information of a complementary nature to that available from electron scattering. The complementarity arises because, as a projectile the positron has the same mass but opposite charge sign to an electron. Thus, a comparison of collision cross-sections for positron and electron projectiles may highlight the effects of the projectile charge sign, correlation and exchange on collision processes. A channel unique to positron scattering is Ps formation. This and other aspects of

positron-atom(molecule) collisions, resulting in target ionisation have been investigated during the course of the work presented in this thesis.

In this chapter a discussion of the physical properties of positrons and Ps is followed by a brief review of some of the experimental techniques used in positron physics. This is followed by a summary of some of the available data for positron collision cross-sections, with emphasis on those which are particularly relevant to the present work.

1.2 Basic Properties of Positrons and Ps

The annihilation of a low energy positron with an electron will almost always result in the emission of a number of γ-ray photons. If the two particles annihilate from rest, the total energy of the photons will be equal to the sum of the rest mass energies of the annihilating pair, $2m_oc^2$. This is approximately 1.022MeV. The number of photons emitted is dictated by the conservation of charge parity (P_c). A single photon has $P_c = -1$, so for a system of n photons

$$P_c = (-1)^n \qquad (1.2)$$

Yang (1950) showed that the selection rule for positron annihilation into n photons is

$$(-1)^n = (-1)^{L+S} \qquad (1.3)$$

where L and S are the total angular momentum and spin of the positron-electron system.

Figure 1.1 shows the Feynman diagrams for positron annihilation into up to four photons. The probability of annihilation by each of these processes is approximately proportional to α^m, where m is the number of vertices representing a photon interaction on the Feynman diagram and α is the fine structure constant ($\approx 1/137$). The most probable annihilation mode is that resulting in the emission of two

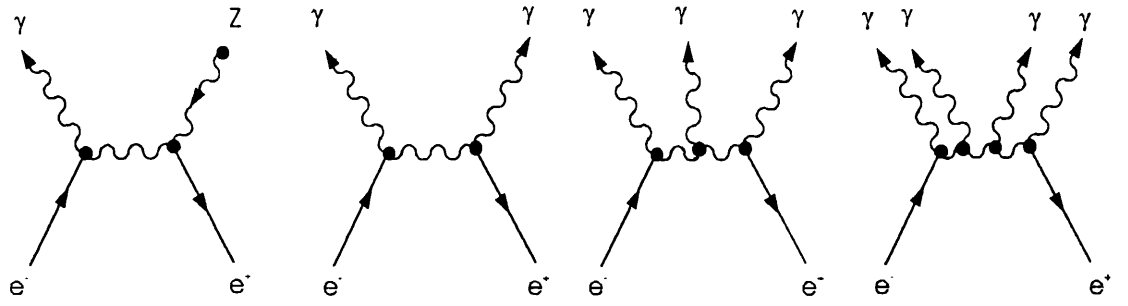

Figure 1.1. Feynman diagrams for positron annihilation into 1-4 photons.

photons. One and three photon emission both have m = 3, however single photon annihilation is less likely by a factor of around α^3, since it requires the presence of a third body to conserve momentum. Annihilation into four photons is the least probable annihilation mode shown, but has recently been observed by Adachi *et al* (1990) who measured the branching ratio for 4γ to 2γ decay as $(1.30\pm0.31)\times10^{-6}$ in accord with theory (e.g. McCoyd 1965,Billoire *et al* 1978). Radiationless annihilation is also possible and is an Auger-like process, in which a positron annihilates with a bound electron, the excess energy causing an inner-shell electron to be ejected from the atom. This process was first predicted by Brunings (1934). Its branching ratio was calculated by Massey and Burhop (1938) and more recently by Mikhailov and Porsev (1992), who estimated a cross-section for this process of the order of $10^{-28}cm^2$.

Ps can be formed in two different ground states, depending on the relative spin orientation of its constituents. If the particles have anti-parallel spins then para-positronium (p-Ps) is formed; if the spin orientations are parallel, ortho-positronium (o-Ps) results. The total angular momentum (J = L + S) of ground state o-Ps is 1, giving rise to three sub-states with magnetic quantum numbers m = -1, 0, 1, whereas for p-Ps, the total angular momentum is

zero and hence m = 0. The ratio of the cross sections for o-Ps to p-Ps formation therefore are 3:1. According to the above arguments and equation 1.3, o-Ps will decay predominantly into three photons and p-Ps into two. In the latter case, the two photons, as viewed from the centre of mass (c.m.) frame, are emitted at 180° to each other and have equal energies (≈511keV). Measurements of the photon energy and deviation from co-linearity in the lab-frame, may be used to obtain information about the momentum of the annihilating pair, as discussed in section 1.3. The three photons from the decay of o-Ps are emitted co-planarly with an energy distribution which was calculated by Ore and Powell (1949) and has been measured by Chang Tian-Bao *et al* (1985). Both sets of results are shown in figure 1.2.

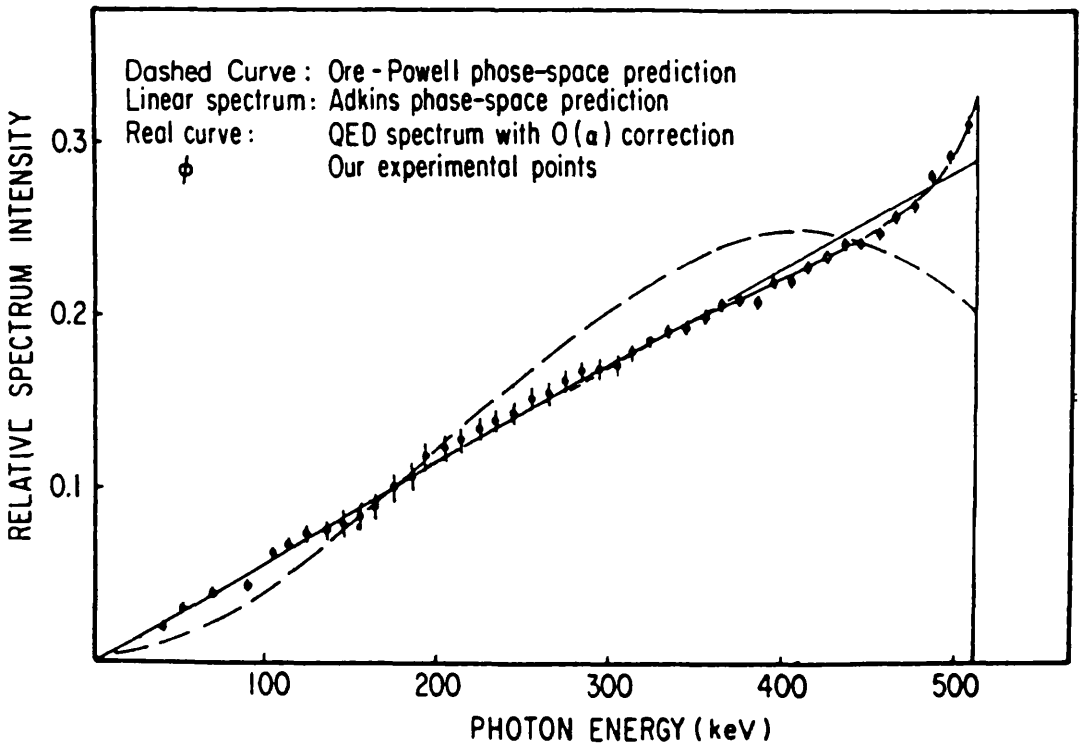

Figure 1.2. The 3-γ energy distribution from the decay of o-Ps measured by Chang Tian-Bao *et al* (1985) compared with theory (see text).

Dirac (1930b) calculated the cross section for two photon annihilation ($\sigma_{2\gamma}$) of a non-relativistic, free electron-positron pair as

$$\sigma_{2\gamma}(e^-) = \frac{\pi r_0^2 c}{v} \qquad (1.4)$$

where v is the relative velocity of the positron and electron and $r_o=e^2/(4\pi\epsilon_o m_o c^2)$ is the classical electron radius.

For positrons in a gas this equation has been modified (e.g. Heyland *et al* 1982) to

$$\sigma_{2\gamma}(A) = \frac{\pi r_0^2 c Z_{eff}(v)}{v} \qquad (1.5)$$

where $Z_{eff}(v)$ is an empirical quantity representing the effective number of electrons per atom seen by a positron with velocity v. It may be significantly greater than the atomic number due to long range interactions. At the collision velocities typically encountered in positron beam experiments, $\sigma_{2\gamma}(A)$ is of the order of $10^{-26}m^2$ for $Z_{eff} = 1$. Since the 3-γ decay mode is around 376 times less likely (from the spin averaged decay rate ratio), direct annihilation has a negligible cross-section in comparison with most other atomic collision processes, at these energies.

Ps is purely leptonic, making it an ideal system with which to study the bound state aspects of quantum electrodynamics. Structurally, Ps is similar to a hydrogen atom, with approximately half its reduced mass, twice its Bohr radius (1.05Å) and a binding energy, in a state of principal quantum number n, given by $(6.8/n^2)$eV. Figure 1.3 shows a comparison of the n = 1 and n = 2 energy levels of H and Ps. The magnetic moment of a positron is around 667 times that of the proton, making the spin-orbit and spin-spin interactions comparable in magnitude, thus removing the distinction between fine and hyperfine structure evident in

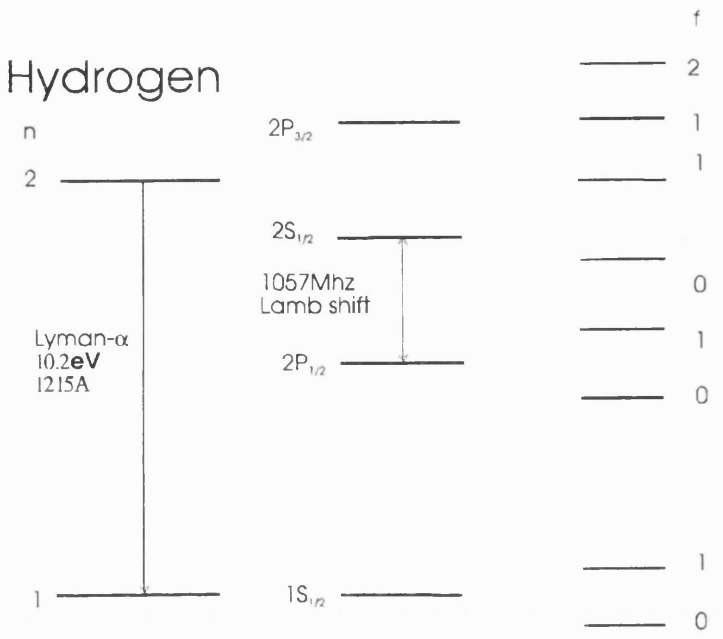

Positronium

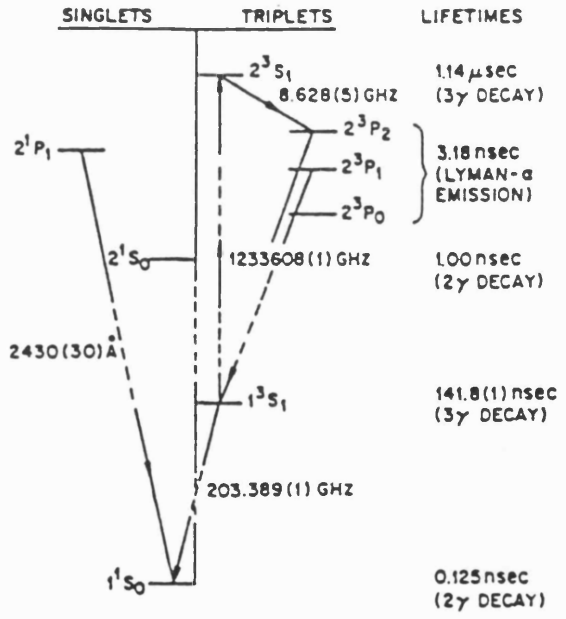

Figure 1.3. A schematic diagram of the n = 1 and n = 2 states of H and Ps.

H.

The vacuum annihilation rate of p-Ps (λ_p) has been calculated to be $7.9852 ns^{-1}$ by Harris and Brown (1957) and the most recently calculated value of the decay rate for o-Ps (λ_o) is $(7.03830 \pm 0.00007) \mu s^{-1}$ (Adkins 1983). λ_p has been measured by Gidley *et al* (1982) who employed a magnetic field to mix p-Ps with the m = 0 sub-state of o-Ps. A value for λ_p of $(7.994 \pm 0.011) ns^{-1}$ was obtained, in agreement with theory.

However, discrepancies exist between theory and experiment in the case of λ_o. Here, the most recent measurement is $(7.0482 \pm 0.0016) ns^{-1}$ (Nico *et al* 1991) and is around 6.2 of its standard deviations above the theoretical value. Nico and co-workers have considered carefully the possibility that this discrepancy might be due to systematic effects, but having attempted to eliminate possible sources of error, have suggested that higher order terms are necessary in the calculation.

1.3 Experimental Techniques

Positrons with a broad distribution of velocities may be obtained from the β^+ decay of radionuclides. Two commonly used sources are ^{22}Na and ^{58}Co, the decay schemes and branching ratios of which are shown in figure 2.1. In the early swarm-type experiments, these positrons were injected directly into the sample under investigation and information about their interactions with the medium was obtained by observation of the annihilation γ-rays. Over the years, much useful information has been gained from these types of experiments and among their major achievements are the observation of Ps and the measurement of its lifetimes.

Additionally, the positron has proved to be a sensitive probe with which to study defects in crystal structures. A missing ion core may create a potential well in the periodic lattice potential. Such a defect may extend over a region sufficiently large in comparison with the de Broglie

wavelength of a thermalised positron and result in the localisation of the positron wave-function at the defect site. When a positron becomes trapped at a vacancy defect, the overlap of its wave-function with that of the more energetic core electrons decreases, relative to the less tightly bound conduction electrons. For reasons explained below, this may lead to an observable reduction in the deviation from co-linearity and Doppler-shift of the annihilation γ-rays. There is also a reduction in the electron density at a vacancy site resulting in an increase in the mean positron lifetime. These effects may be used to estimate the defect concentration in the sample as well as the type of defects present. The ability of thermally activated vacancies to trap positrons in this way was first demonstrated by MacKenzie *et al* (1967) and has subsequently been extensively studied (e.g. see review by Schultz and Lynn 1988).

1.3.1 Two-Photon Angular Correlation Measurements

The technique involving the measurement of the angular correlation of annihilation radiation (ACAR) has been widely used to study the annihilation of positrons in solids, liquids and gases. If a positron annihilates via the two photon decay mode then, in the c.m. frame, the two photons will be emitted co-linearly, as already mentioned. In the lab-frame a deviation of the photons from co-linearity (θ) may be used to deduce the c.m. momentum of the positron-electron pair at the moment of annihilation. In ACAR experiments it is this angular deviation that is measured.

When a thermalised positron annihilates in a solid it contributes very little to the c.m. momentum of the annihilating pair, since, on average, there is only one positron in the sample at any time. It can therefore continue to loose energy until it occupies a level near the bottom of its own band. The electron however, is likely to posses

significantly higher energy because of the effect that the Pauli exclusion principle has on the sea of electrons in the sample. The range of values of θ is therefore almost entirely due to the momentum distribution of the electrons. Figure 1.4 shows a schematic diagram of a typical ACAR apparatus. A positron source (e.g ^{22}Na) is placed directly adjacent, or immersed in, the sample so as to maximise the fraction of implanted β^+ particles. In most solids the positrons achieve near thermal equilibrium in a few ps and eventually annihilate with an electron with lifetimes typically of the order of 10^{-10}s. In ACAR experiments the annihilation radiation is monitored by two detectors placed a few metres away. One of the detectors is rotated about the sample, in order to measure the coincidence rate between the two detectors as a function of θ. In this way an ACAR spectrum is acquired. The angular resolution of such an apparatus is mainly determined by geometric factors such as the angular acceptance of the detectors and the dimensions of the source and sample. Figure 1.5a) shows the two dimensional (2D) ACAR spectra for p-Ps annihilating in quartz. The very low momentum of the annihilating pair is reflected in the sharp peak, unlike the 2D-ACAR distribution for single crystal Cu shown in figure 1.5b). Here the distribution is much broader, due to the fact that the positrons annihilate with more energetic electrons.

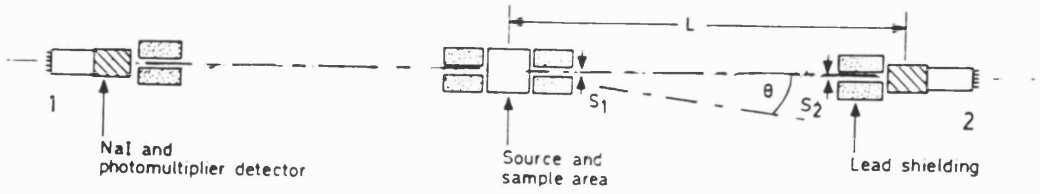

Figure 1.4. A schematic diagram of a typical ACAR apparatus.

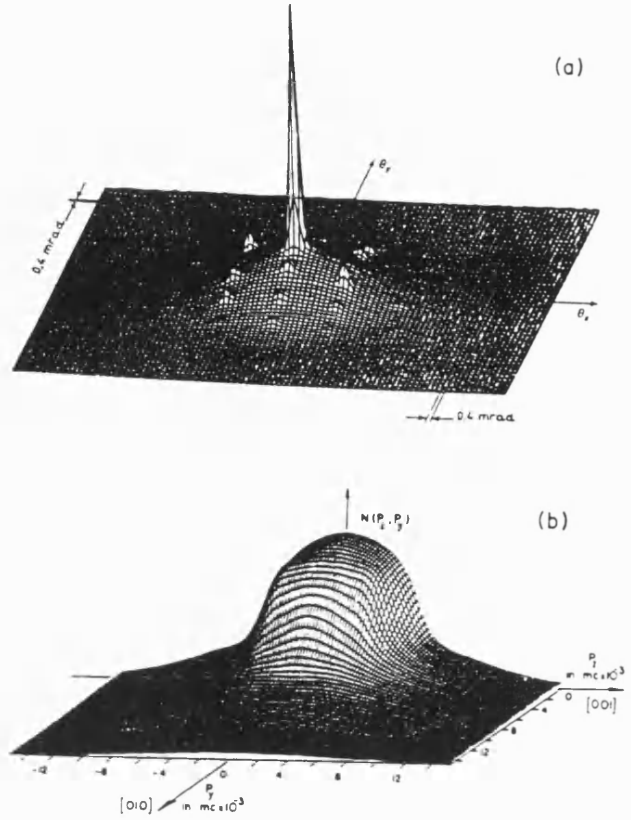

Figure 1.5. 2-D ACAR spectra of positrons annihilating in a) single crystal quartz (Manuel 1981) and b) Cu (Haghgooie *et al* 1978).

1.3.2 The Doppler Broadening Technique

The Doppler broadening technique may also yield information about the momentum distribution of electrons in a solid. It relies on the measurement of the Doppler shift of the energy of the annihilation photons, caused by the motion of the annihilating pair. The c.m. kinetic energy of the annihilating pair ($E_{c.m.}$) in the lab frame is related to the shift $h\Delta\nu$ by

$$E_{c.m.} = \frac{(h\Delta\nu)^2}{m_o c^2} \qquad (1.6)$$

The Doppler shift of the two-γ annihilation radiation may cause the corresponding photo-peak in the energy spectrum to become broadened. The degree of broadening may then be related to the momentum distribution of the electrons.

The energy of the annihilation radiation is usually monitored using high resolution detectors [e.g. Ge(Li)] with a set-up of the type shown in figure 1.6.

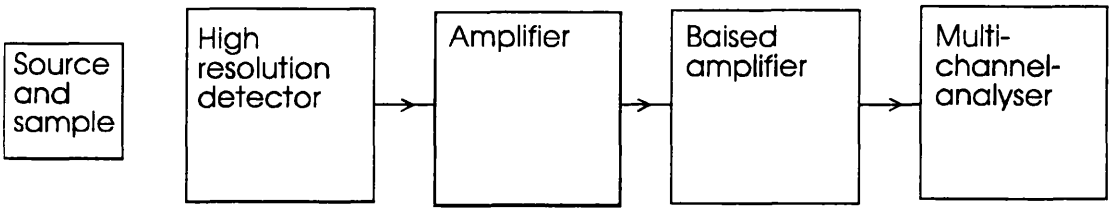

Figure 1.6. A typical arrangement for measuring Doppler broadening spectra.

As well as studying the annihilation of positrons in solids, the technique has been used to monitor the in flight annihilation of p-Ps and to observe the formation of Ps^-, (Mills 1981) the bound state of a positron and two electrons, the existence of which was predicted by Wheeler (1946). The technique has also been used to monitor the formation of approximately mono-energetic Ps in charge exchange reactions of positrons with He (Brown 1986).

1.3.3 The Lifetime Technique

The positron lifetime technique was pioneered by Shearer and Deutch (1949) who obtained lifetime spectra of positrons annihilating in various gases. Lifetime experiments have

since been applied to study interactions of positrons with liquids and solids. Although the associated instrumentation has improved, the basic principle of lifetime measurements has remained the same. A typical apparatus used to measure positron lifetimes in gases is that of Coleman *et al* (1975), shown in figure 1.70a). A 1.28MeV γ-ray follows the emission of a positron from the ^{22}Na source within around 10^{-12}s and is detected by a fast plastic scintillator, optically coupled to a photo-multiplier tube. This is used to generate a start pulse for the timing system. A second detector is used to generate stop pulses from the annihilation γ-rays of positrons diffusing through the gas. A lifetime spectrum is built up from a large number of such events. A lifetime spectrum obtained in this way by Coleman *et al* (1975) for Ar gas at 297K and a gas pressure of 6.3 amagats is shown in figure 1.7b).

After background subtraction the spectrum can be divided into three regions. The prompt peak at the left hand side of the spectrum is caused by the decay of p-Ps and annihilation of positrons in the source and chamber walls. This is followed by a shoulder region which is due to the annihilation of free positrons before thermalisation. The remainder of the spectrum is the sum of two exponential decay curves, corresponding to the annihilation of thermalised positrons and o-Ps. The two components are separated by fitting an exponential to the slower o-Ps component and subtracting this from the spectrum to obtain the free positron component. This spectrum is typical of those obtained for most gases although, in general, molecular gases have no resolvable shoulder region. This is due to the rapid thermalisation of the free positrons caused by the existence of vibrational and excitational energy levels extending down to thermal energies. This type of analysis has resulted in the extraction of information about the slowing down of positrons, their lifetimes in the media, the formation probability of Ps and its lifetime in the media.

In solids, the lifetime technique has yielded

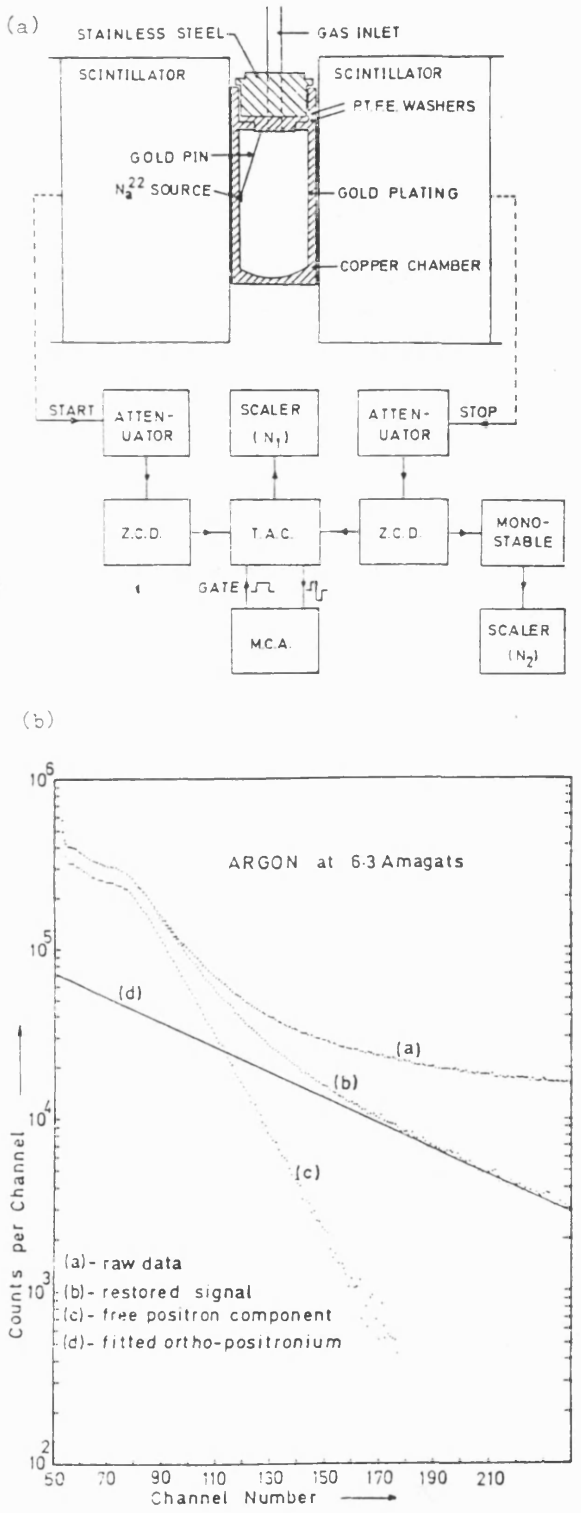

Figure 1.7. a) The apparatus used by Coleman *et al* (1975) to measure positron lifetimes in gases and b) a lifetime spectrum for positrons annihilating in Ar (Coleman *et al* 1975).

information complementary to that obtained using ACAR and Doppler-broadening techniques.

1.4 The Development of Slow Positron Beams

The techniques mentioned above are constrained by the broad energy and angular distribution of the incident positrons. A significant advance in the field of experimental positron physics came with the development of tunable, nearly mono-energetic beams of low energy positrons. Such beams are produced by slowing down β^+ particles, from a radioactive source or pair production by bremsstrahlung radiation, to near thermal energies using a solid state moderator. Figure 1.8 shows the differential yield of re-emitted positrons from W(110) in comparison with the normalised β^+ spectrum from ^{58}Co (from Schultz and Lynn 1988). This demonstrates that at low energies, moderation is several orders of magnitude more efficient than energy selection as a method for obtaining slow positrons.

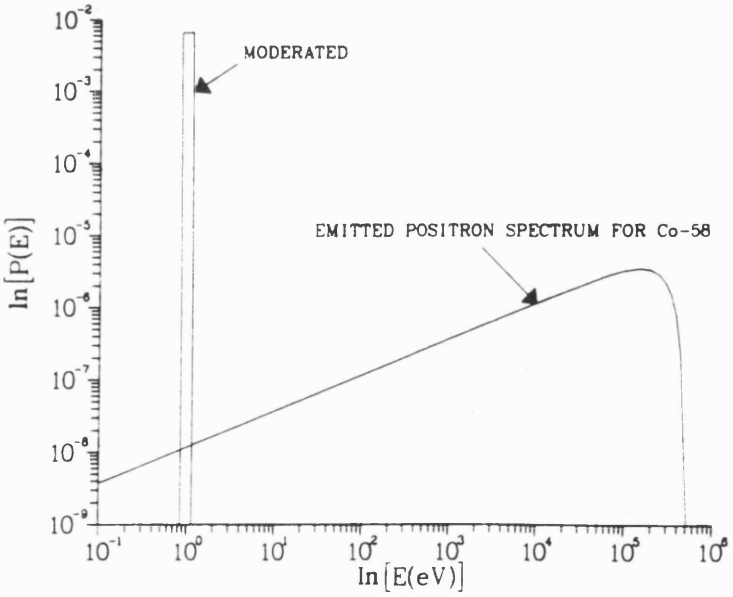

Figure 1.8. Comparison of the slow positron yield from a W(100) moderator with the β^+ spectrum from a ^{58}Co source.

The possibility that positrons with near thermal energies could be obtained by implanting β^+ particles from a radioactive source into a solid was first suggested by Madansky and Rasetti (1950). They estimated that the efficiency of such a moderator would be determined by the ratio between the positron diffusion length and the mean implantation depth of the incident β^+ particles. This they calculated to be of the order of 10^{-3} for the samples used in their experiment. Here, a ^{64}Cu positron source with an activity of (10-30)mCi was used to irradiate various samples including Pt, glass and mica. The slow positrons were to be confined by a magnetic field and detected by observing γ-rays from their annihilation on an Al foil, around 80cm from the sample. Unfortunately, Madansky and Rasetti (1950) were unable to detect any low energy positrons, probably due to the low sensitivity of their apparatus and defective samples. They did however, attribute the zero yield to positron trapping in the samples and Ps formation; two processes that have subsequently been shown to be of great importance.

The first observation of slow positron emission from a metal surface was made by Cherry (1958). Positrons were found to be emitted with energies of less than 10eV from Cr plated mica when irradiated with β^+ particles from a ^{22}Na source. The ratio between the number of slow positrons to fast β^+ particles was found to be around 10^{-8}.

The importance of this result was largely unappreciated until 1969, when Madey (1969) performed a similar experiment with polyethylene and Groce *et al* (1969) reported that a slow positron flux with energies of a few eV had been obtained from Au. Here an Au surface was bombarded with fast positrons obtained from pair production in a Ta converter by the bremsstrahlung radiation produced by a 55MeV beam of electrons from a linear accelerator. This work was extended by Costello *et al* (1972) who measured the energy distributions of slow positrons emitted from an approximately 200Å thick layer of Au, deposited on mica, CsBr and Al substrates. The energy distributions were measured using a

time of flight technique and were found to peak between 0.75 and 2.90eV. It was proposed for the first time that this energy was due to a negative positron work function of the surface. Costello *et al* (1972a) went on to use this flux of slow positrons to make the first positron-atom total scattering cross section measurements. This work is discussed in § 1.5.

A positron work function (ϕ_+) may be defined, in an analogous way to the electron work function (ϕ_-) as the minimum energy required to move a positron from a point well inside the surface to a point well outside. If ϕ_+ is negative, positrons are ejected from the surface with kinetic energies approximately equal to ϕ_+.

Lang and Kohn (1971) defined ϕ_- as

$$\phi_- = \Delta\varphi - \mu_- \qquad (1.7)$$

where μ_- is the bulk chemical potential of the electrons, relative to the mean electrostatic potential in the metal interior and $\Delta\varphi$ is the rise in mean electrostatic potential across the surface. The surface dipole, $\Delta\varphi$, is caused by the electron gas from the metal interior, spilling out beyond the last atomic layer and into the vacuum. This is shown in figure 1.9. Here the ion-core potential is represented by a uniform background, equal to the average interstitial potential, according to the jellium model. The combined effect of this and the electron gas, which as already mentioned, spills out of the surface, creates a dipole moment across the surface and tends to bind electrons to the solid.

Tong (1972) proposed that the surface dipole contribution to ϕ_+ should have an equal magnitude but opposite sign to $\Delta\varphi$ and hence

$$\phi_+ = -\Delta\varphi - \mu_+ \qquad (1.8)$$

where μ_+ is the bulk chemical potential of a positron, relative to the mean electrostatic potential in the metal interior. Since the surface dipole has the opposite sign for a positron, this will tend to make positrons escape from the

surface. It is the cancellation between μ_+ and $\Delta\varphi$ that causes ϕ_+ to be close to zero, or negative in many cases. The potentials a positron or electron sees close to a metal surface are represented in figure 1.9. This shows that for a positron there is an attractive potential well just outside the surface. This is due to the image potential seen by the positron at large distances and the correlation with the electron gas spilling out of the metal surface at small distances.

Tong (1972) predicted negative values of ϕ_+ of a few electron-Volts for Al, Mg, Cu and Au. The work function of Au has since been experimentally measured to be positive (Nieminen and Hodges 1976, Lynn 1980 [unpublished]). The

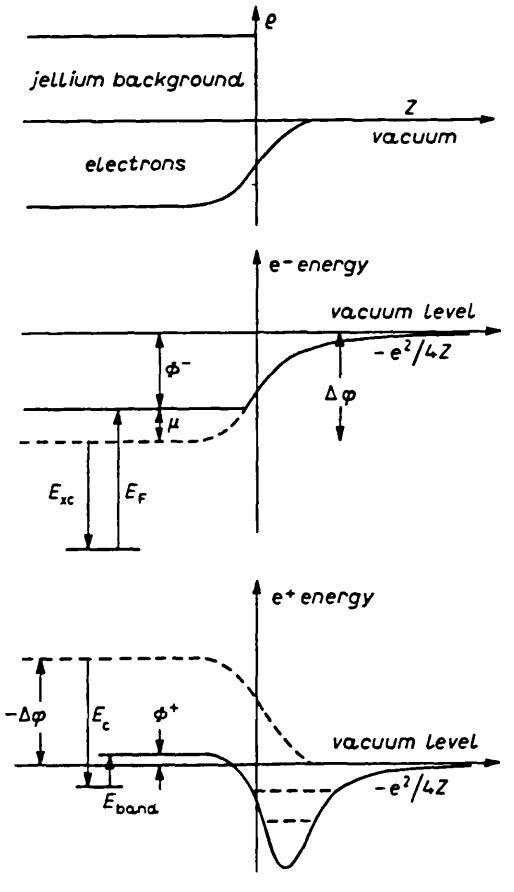

Figure 1.9. The potentials seen by a positron and an electron near the surface of a metal.

results of Costello *et al* (1972) may therefore be ascribed to epithermal positron emission or sample impurities causing ϕ_+ to become negative.

A 300-fold improvement in moderation efficiency was achieved by Canter *et al* (1972) from an Au moderator consisting of vanes arranged in the form of a venetian blind coated with MgO. This was bombarded with fast positrons from ^{22}Na to obtain a flux of slow positrons. The energy spread of the slow positrons was around 3eV and the moderation efficiency was approximately $3x10^{-5}$. This was used to measure the total cross-section of He as discussed in § 1.5.

An alternative method of slow positron beam production was developed by Stein *et al* (1974). A B target was bombarded with 4.75MeV protons from a Van de Graff generator to produce positrons from the decay of ^{11}C, produced by the reaction $^{11}B(p,n)^{11}C$. The B target also acted as the moderator and positrons emitted from the surface were extracted electrostatically, with an energy spread of around 0.1eV. The efficiency of this type of moderator was estimated to be around 10^{-7}. These slow positrons were used to make the first observation of a Ramsauer-Townsend minimum in positron elastic scattering cross-sections, as discussed in § 1.5.

Further study of the moderation properties of various poly-crystalline moderators was carried out by Pendyala *et al* (1976). An increase in slow positron yields after heat treatment was reported, with the highest yield obtained from Cu after baking at 450K for several hours.

Until the work of Mills *et al* (1978), all investigations had been performed with samples of unknown structure and purity. This had hindered progress in the understanding of the moderation process. Mills *et al* (1978) investigated positron emission from clean single crystal surfaces of Al, Cr and Si, with known crystal orientations, bombarded with positrons of known energies. A ^{58}Co source and Pt moderator was used to produce a flux of slow positrons of variable mean energy, which were used to bombard targets with energies from (0.1-3.0)keV. The annihilation of positrons at the target was

measured by detection of the annihilation γ-rays and the energy spectrum of the slow positrons was determined by recording the annihilation rate as a function of a negative potential applied to the target. The energy distributions were measured for different target temperatures up to 500°C. Mills *et al* (1978) proposed the following mechanism for the thermalisation, diffusion and emission of positrons from metals.

After implantation in a moderator material, β^+ particles with energies less than a few MeV may initially lose kinetic energy to electrons in the bulk of the solid by inelastic processes such as core excitation, plasmon emission and electron-hole pair creation. Nieminen and Oliva (1980) estimated that such positrons would have reached energies of a few eV after around 10^{-13}s. After this, near-thermal equilibrium with the lattice is achieved, predominantly by phonon scattering in around 10^{-12}s (Perkins and Carbotte 1970). A typical non-thermal positron will diffuse about 30Å in this time. Therefore, positrons impacting the surface with energies in the keV range, will thermalise before reaching the surface, since the mean implantation depth will be of the order of 100Å (Mills *et al* 1978). At the surface the surviving positrons may form Ps, become trapped in a surface state, be reflected or, if the surface has a negative ϕ_+, be ejected into the vacuum.

Murray and Mills (1980) measured the moderation efficiency of Cu and Al as a function of ϕ_+ by varying the crystal orientation and the amount of S on the surface. The result for Cu is shown in figure 1.10, showing an increase in efficiency as ϕ_+ is made more negative.

Dale *et al* (1980) then measured the slow positron yield from a variety of samples with different structural characteristics. The highest moderation efficiency was around $7\text{x}10^{-4}$ from poly-crystalline W vanes that had been chemically etched and heated to 2200°C. Dale *et al* (1980) showed that the heat treatment was a more important factor than surface cleanliness in determining moderator efficiency, since

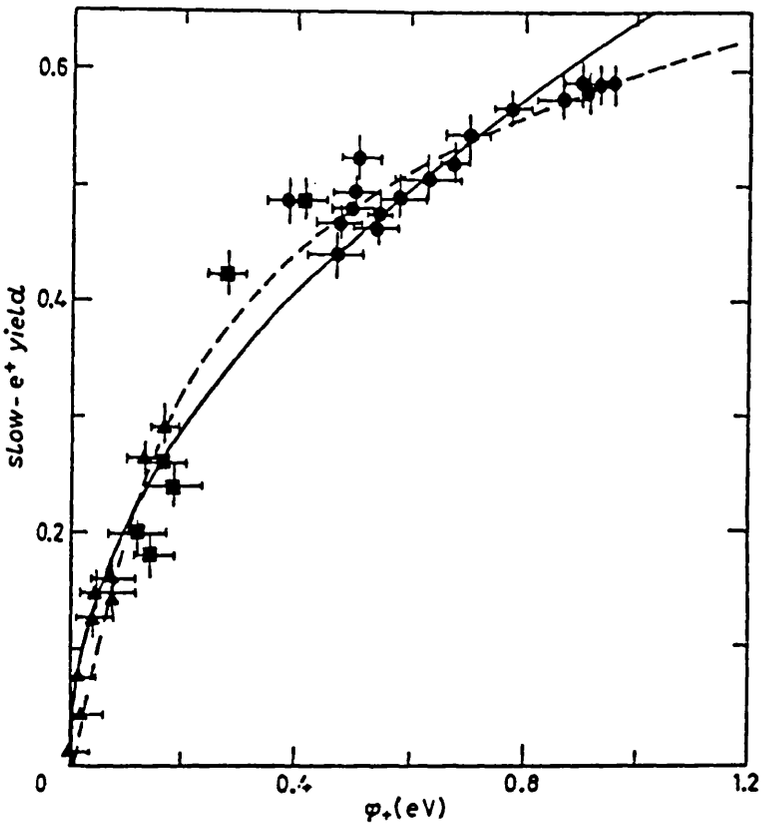

Figure 1.10. The slow positron yield from a Cu surface as a function of ϕ_+ (Murray and Mills 1980).

annealing increases the degree of atomic order in the moderator. This causes there to be fewer defects which may act as positron traps (as mentioned in § 1.3).

Using a clean, single crystal W sample, Vehanen *et al* (1983) obtained a moderation efficiency of around 3×10^{-3}, which is around 75% the maximum possible efficiency, as calculated by Vehanen and Makinen (1985).

Some of the different source-moderator geometries that have been employed are shown in figure 1.11. Figure 1.11a) shows the back-scattering configuration in which β^+ particles are implanted onto a flat, usually single crystal, material and slow positrons are extracted from the same surface. If this is clean, positrons are emitted almost normally with

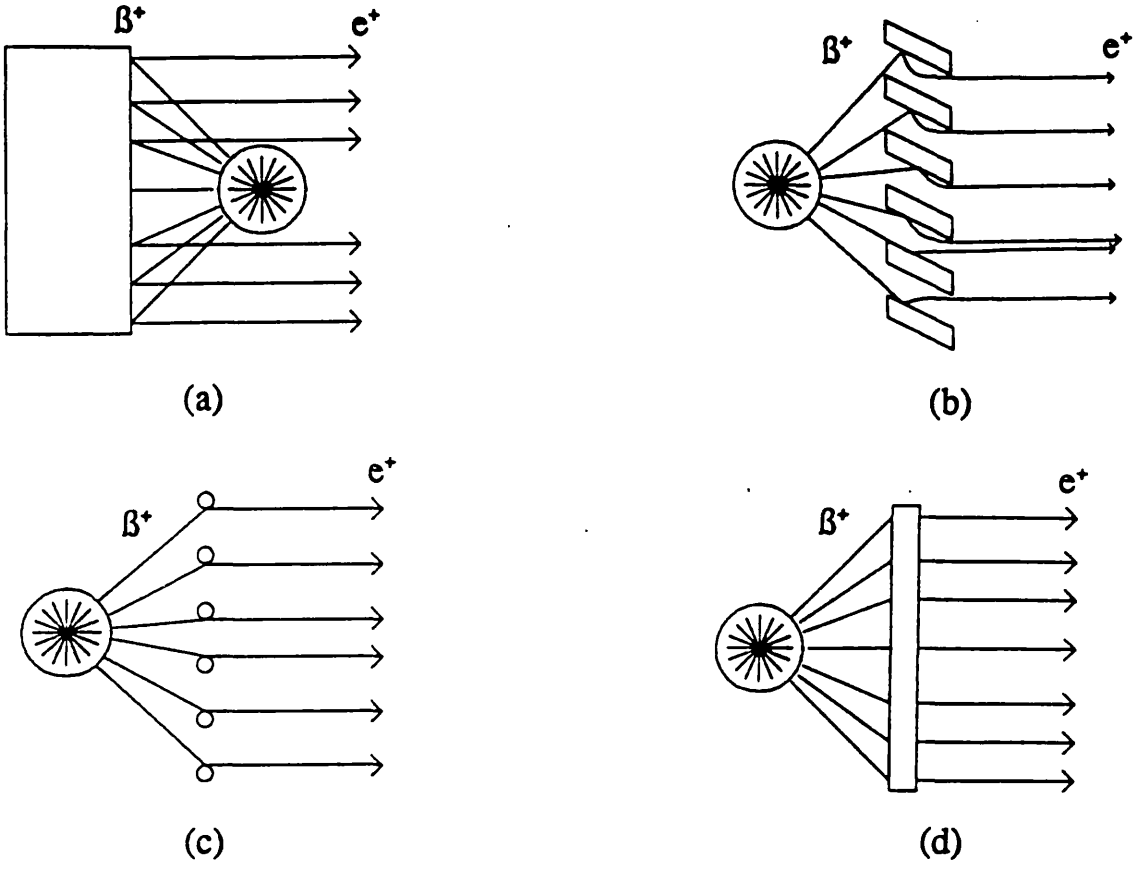

Figure 1.11. Typical source/moderator arrangements showing a) backscattering b) vane c) grid and d) transmission configurations.

only a small transverse component due to thermal energies. A disadvantage of this arrangement is that the source obscures part of the moderator and so this geometry is only suitable for small sources with high specific activities e.g. ^{58}Co deposited on a needle or ribbon. Figures 1.11b) and c) show vane and grid arrangements. Here the positrons emerge from the same surface as that entered by the β^+ particles but are extracted from the side opposite the source. With this geometry the size of the source holder is unimportant and commercially obtained ^{22}Na sources may be employed. The vane arrangement may be arranged to intercept the majority of the incident flux emitted in its direction, however the grid system has the advantage of ease of fabrication, although the partial transparency may result in the transmission of some

of the β^+ flux. Figure 1.11d) shows the transmission mode geometry in which positrons diffuse through moderators of thickness of a few thousand Å. This configuration results in narrow energy and angular distributions and simplifies electron optics since the input and output may be electrically screened.

All the moderation techniques described above use negative work function materials. However, new high efficiency moderators have been developed based on materials possessing positive values of ϕ_+, these are the solid rare gas (RGS) and field assisted (FA) RGS moderators.

Mills and Gullikson (1986) condensed Ne, Ar, Kr and Xe onto a cup type moderator and measured the yield of slow positrons. Ne was found to be the most efficient moderator at around $7x10^{-3}$. In this case, the energy distribution of the re-emitted positrons was around 0.58eV FWHM. The high efficiency is attributed to the wide band gap, in terms of the "hot positron" model. Here an implanted positron may lose kinetic energy by inelastic processes, until reaching the band gap. Then the only means of energy loss is via phonon excitation. Since the maximum energy for phonon excitation is small (e.g. $83x10^{-2}$eV for Ar, Schwentner *et al* 1975) the diffusion length before thermalisation is increased. Hence, a significant number may reach the surface with energies in excess of ϕ_+ and be re-emitted into the vacuum.

Merrison *et al* (1992) increased the efficiency of solid Ar and Kr moderators by a factor of around 3, by covering the RGS with a thin layer of O_2 and charging the surface by low energy electron bombardment. The enhanced yield was ascribed to the effect of the electric field on bulk diffusion and surface properties.

Extraction and transport of slow positrons from the moderator is usually achieved by a system of electric and magnetic fields. Under the influence of conservative forces, Liouville's theorem states that the volume of an ensemble of particles in phase space is constant. This can be expressed as

$$B(E) = \frac{I}{d^2 E \sin^2\theta} = constant \qquad (1.9)$$

where B(E) is the brightness per unit energy and E, I, d and θ are the energy, intensity, diameter and angular divergence of the beam respectively. Hence, for a constant beam energy and intensity, d may only be reduced by increasing θ and vice-versa. Mills (1980) pointed out that the constraints of equation 1.9 do not apply to the moderation process since it is non-conservative and that by focusing a beam onto smaller areas in successive stages of re-moderation, B(E) may be increased several orders of magnitude, with relatively small loss in intensity.

The first brightness enhanced beam was constructed by Frieze *et al* (1985) who succeeded in increasing the brightness of a positron beam by around 30 times, with a loss in intensity of around 80%. A more recent apparatus implemented by Brandes *et al* (1988) has increased B(E) by a factor of 500 and was used to produce a scanning positron micro-beam. This beam was focused to dimensions of around (10 x 50)μm and was scanned across a test grid while monitoring the intensity of annihilation radiation. This intensity, measured as a function of beam position, was used to generate a 1-D image of the grid.

1.5 Positron-Atom(Molecule) Cross-Sections

With the advent of tunable beams of low energy positrons it soon became possible to investigate positron-atom(molecule) interactions under single collision regimes and at specified energies. Today these studies include partial cross-sections for a number of scattering channels, some differential investigations of elastic scattering and ionisation processes.

1.5.1 Total Cross-Sections

The first positron-atom(molecule) cross-sections to be measured were total cross-sections (Q_t). Experiments to measure Q_t usually involve measuring the attenuation of a beam of particles of well defined energies, passing through a region containing the target gas. Under ideal conditions, Q_t can be obtained from the Beer-Lambert expression

$$Q_t = \frac{1}{nl} \ln \frac{I_0}{I} \qquad (1.10)$$

where I and I_0 are the transmitted (unscattered) and incident beam fluxes respectively and n is the number density of the gas along an interaction region of length l.

The most significant systematic errors are usually those involved in determining n, l and I, since n depends on the target gas temperature and pressure and may vary along the interaction region, l may be difficult to determine due to spiralling and end effects and I may be difficult to determine because of positrons elastically scattered through small angles. In most Q_t measurements with positrons, the attenuation (I/I_0) is either measured directly or inferred from time of flight (TOF) measurements.

The first positron Q_t measurement was made for He by Costello *et al* (1972a) using a TOF technique. With improved beam fluxes, values of Q_t have now been measured with higher precision, for a wide range of atomic and molecular gases. The first to be studied were the noble gases, since these exist in atomic form at room temperature. These targets have been extensively studied over a wide range of impact energies and the level of agreement between the various experiments is in general, reasonably good.

Figure 1.12 shows most of the experimental values of Q_t for positron-He scattering in the range (0-30)eV along with a selection of theoretical data. In the experiment of Stein *et al* (1978) the attenuations were obtained by measuring beam currents, whilst in those of Mizogawa *et al* (1985), Coleman

et al (1979), Canter *et al* (1972) and Wilson (1978) (corrected by Sinapius *et al* 1980), attenuations were derived from TOF spectra. An important feature of this cross-section is the Ramsauer-Townsend minimum around 2eV, first observed in positron scattering by Stein *et al* (1978). A similar effect has been observed in Q_t for Ne (e.g. Stein *et al* 1978) and, to a lesser extent, in Ar (e.g. Kauppila *et al* 1976). The importance of Ps formation can also be seen, with its threshold (E_{Ps}) at 17.78eV, around which energy the cross-section is seen to rise abruptly. This rise in Q_t is typical of all the inert and many molecular gases.

The Ramsauer-Townsend minimum was first observed in Q_t for electron scattering (Ramsauer 1921,1923, Townsend and Bailey 1922 and Ramsauer and Kollath 1929). It is a quantum

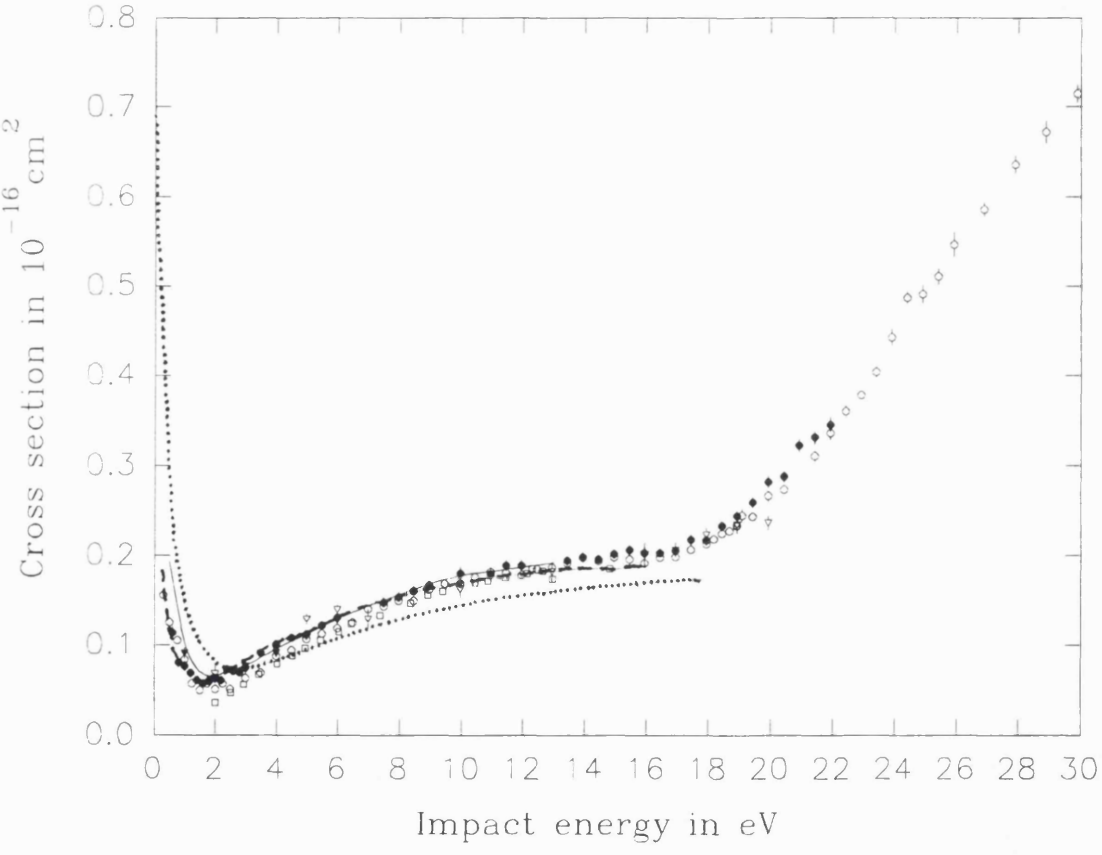

Figure 1.12. Q_t for positron-He scattering: Stein *et al* (1978), ○; Mizogawa *et al* (1985), •; Canter *et al* (1972), ▽; Sinapius *et al* (1980), ▼; Coleman *et al* (1979), □; Amusia *et al* (1976), dashed line; Wadhera *et al* (1981), solid line; McEachran *et al* (1978) dotted line.

mechanical effect and occurs when the s-wave phase shift becomes approximately equal to an integral multiple of π, causing the cross-section to become small. For positron scattering the effect arises in a slightly different way. Here, the cancellation between the static and polarisation interactions may become almost complete at certain energies, causing the phase shift to become close to zero. This then causes a minimum in the cross-section.

The Ramsauer-Townsend minimum is also evident in all of the theoretical results shown in figure 1.12, although there are small discrepancies as to its magnitude and position. Values of Q_t were derived by Wadhera *et al* (1981) by summing contribution from s-, p-, and d-wave phase shifts calculated by Humberston (1979), Humberston and Campeanu (1980) and Drachman (1966) respectively. Higher order partial wave contributions obtained by O'Malley *et al* (1961) in a Born approximation calculation were also included. These results agree well with experiment above the minima, but are slightly greater at lower energies. Also shown are the results of the polarised-orbital calculation by McEachran *et al* (1978) and the random-phase approximation calculation of Amusia *et al* (1976). The results of McEachran *et al* (1978) are significantly in excess of the experimental values at low energies, but fall below the measured values at higher energies, by around 11% at E_{Ps}. The results of Amusia *et al* (1976) agree well with the experimental values at all energies studied. This may however be fortuitous since the variational calculations of Humberston (1979) and Humberston and Campeanu (1980) are believed to be more accurate.

At low energies the values of Q_t for electron scattering from the inert gases greatly exceeds that for positron scattering, in the case of He, by up to two orders of magnitude around the Ramsauer-Townsend minimum at 2eV. This is illustrated in figure 1.13, which shows the smoothed values of Q_t for positron scattering (Stein *et al* 1978, Kauppila *et al* 1981) and electron scattering (Kauppila *et al* 1981). The positron and electron cross-sections are found to

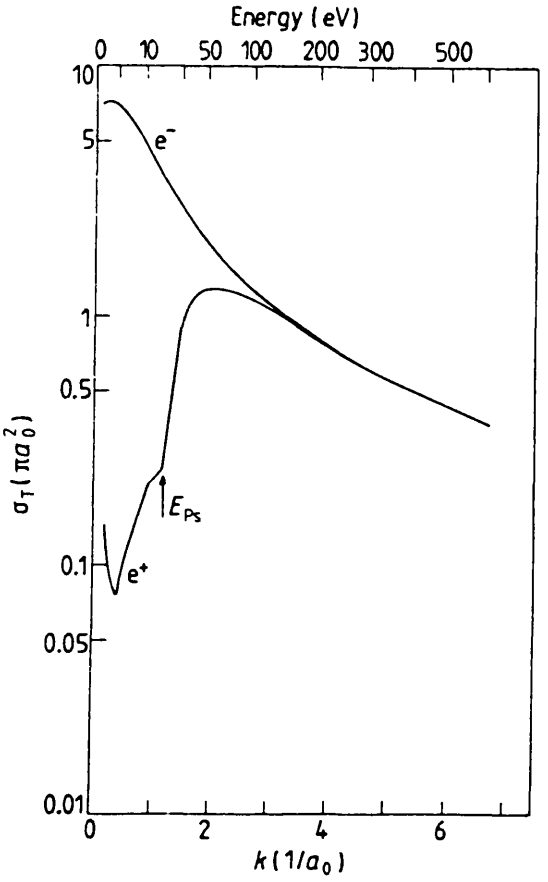

Figure 1.13. Q_t in He for positrons (Stein *et al* 1978, Kauppila *et al* 1981) and electrons (Kauppila *et al* 1981).

merge, at around 200eV, an energy considerably lower than expected from theory (e.g. Dewangan and Walters 1977, who predict the cross-sections will merge at around 2keV). The merging of the cross-sections may be qualitatively understood as follows.

The static interaction between the projectile and the Coulomb field of the target is attractive for the electron and repulsive for the positron. However, the polarisation interaction, caused by the distortion of the charge distribution of the target by the projectile, is always attractive. Thus, at low energies, there is an addition of the two interactions in the case of electron scattering, and a cancellation for positron scattering, resulting in larger values of Q_t for electrons scattering. As the energy of the projectile is increased, the target polarisation interaction

diminishes, and eventually becomes negligible in comparison with the static interaction, which has the same magnitude for both projectiles. This causes the two cross-sections to merge at high energies.

Recently the investigation of Q_t has been extended to unstable targets, namely the alkali atoms and atomic H. Stein *et al* (1985) reported the first measurements of Q_t for positron scattering from K over the energy range from 5eV to 49eV. This experiment was performed by measuring the attenuation of a projectile beam, passing through an oven containing the target gas. Both the electron and positron cross-sections were found to be similar, to within around 25%, over the entire energy range, unlike all the room temperature gases previously studied. It was suggested by Stein *et al* (1985) that the similarity was due to the high polarizability of K causing the polarisation interaction to overwhelmingly dominate the static interaction, thus causing the strength of the interactions to be approximately equal for the two projectiles. This work was extended to K and Na over a wider range of energies (3-102)eV by Kwan *et al* (1991). The similarity between the electron and positron results was also noted for Na and the cross-sections for the two projectiles were found to merge at the unusually low energy of around 40eV, below which the electron cross-section was smaller than the corresponding positron cross-section, in qualitative agreement with theory (Ward *et al* 1989, Walters 1976, Phelps and Lin 1981).

Following a closer examination of the low energy part of the cross-sections, Parikh *et al* (1993) have found evidence of unexpected behaviour in Q_t for K and Rb. For both targets, Q_t for positron scattering, was found to contain broad maxima around 6eV. Below this energy Q_t was found to decrease, with decreasing impact energy down to 1eV the lowest energy studied. This contrasted with the results of 5-state close-coupling calculations by Ward *et al* (1989) and McEachran *et al* (1991), which continue to rise at low energies. Parikh *et al* (1993) point out that this structure may be artificial and

due to incomplete discrimination against forward scattering, but showed that these effects could not fully account for the discrepancy between theory and experiment.

Zhou *et al* (1993) have recently reported preliminary measurements of Q_t for electron and positron scattering from H. This experiment was performed by measuring the attenuation of a projectile beam passing through a chamber filled with a mixture of H and H_2 obtained from an r.f. discharge tube. Absolute values of Q_t were obtained by normalising the electron results to the results of de Heer *et al* (1977) and applying the same normalisation constant to the positron data. They obtained reasonable agreement with the calculations of Winick and Reinhardt (1978) and Walters (1988). As a consistency check, Stein *et al* (1993) estimated Q_t by summing the elastic (Walters 1988), Ps formation (Sperber *et al* 1992) and single ionisation (Spicher *et al* 1990) cross-sections. The result of the summation is significantly in excess of the values of Q_t, measured by Zhou *et al* (1993), implying some inconsistencies between the values for the various cross-sections.

1.5.2 Excitation Cross-Sections

The first inelastic positron scattering cross-section to be investigated experimentally was that of excitation (Q_{ex}). Coleman and Hutton (1980) and Coleman *et al* (1982) first measured Q_{ex} for He for energies up to 10eV above threshold using a TOF method. Positrons were guided by a uniform magnetic field and timed over a flight path which included a short scattering cell. The TOF spectra for impact energies up to 10eV above the first excitation threshold (E_{ex}) at 20.6eV contained a peak corresponding to positron scattering at small angles with an energy loss of 20.6eV, attributed to the 1^1S-2^1S transition. From this the values for Q_{ex} for the 1^1S-2^1S transition shown in figure 1.14 were obtained.

Sueoka (1982,1989) used a similar technique, with an

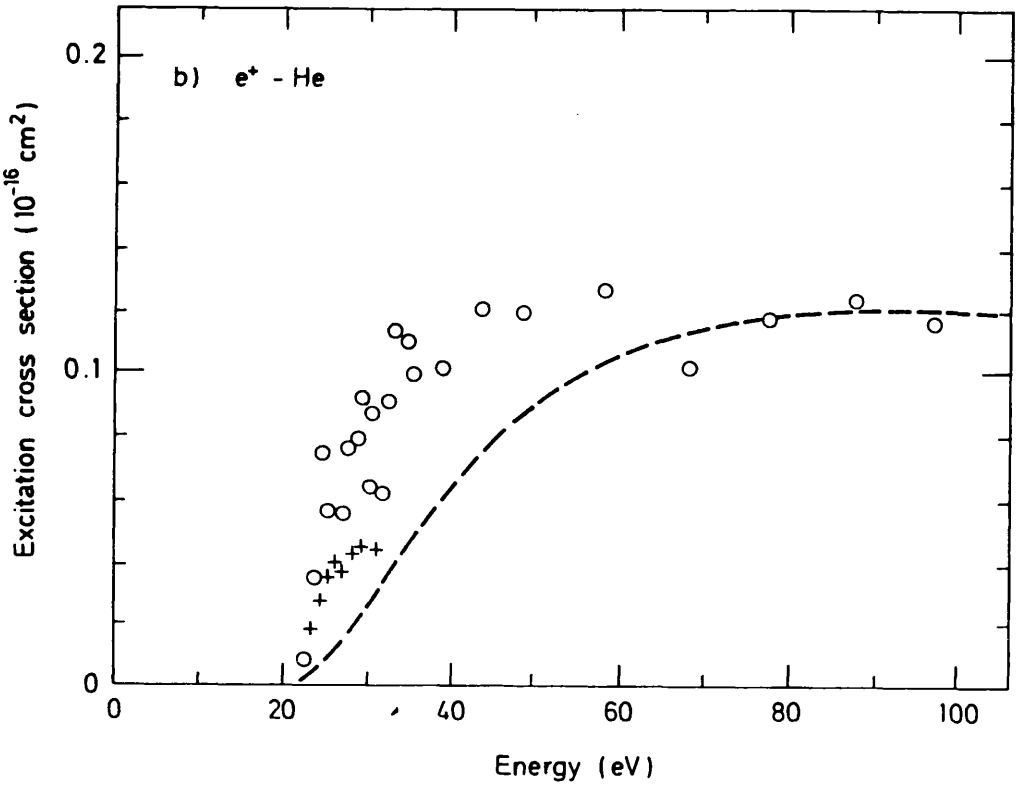

Figure 1.14. Q_{ex} for positron-He scattering: Sueoka (1989), o; Coleman *et al* (1982), +; Parcell *et al* (1983,1987) (1S-2S and 1S-2P), dashed line.

additional retarding element to discriminate against ionisation events and obtained values for Q_{ex} in He, up to 120eV. These measurements which are thought to comprise the 1^1S-1^2S and 1^1S-2^1P transitions, are shown along with those of Coleman *et al* (1982) in figure 1.14. Comparison with the results of a distorted-wave approximation calculation by Parcell *et al* (1983,1987) shows the experimental results being higher at low energies although the data of Sueoka *et al* (1989) are in good agreement with theory above 60eV. Values of Q_{ex} been calculated more recently by Hewitt *et al* (1992) and Ficocelli-Varracchio and Parcell (1992). These are compared with experiment and discussed in the context of the present work in § 5.2.

1.5.3 Elastic Scattering Cross-Sections.

Below the Ps formation threshold, the angle integrated elastic scattering cross-section (Q_{el}) is equal to Q_t. However, interest has recently turned to the behaviour of Q_{el} at energies just above E_{Ps}. This has followed from the suggestion that there may be threshold effects in the form of Wigner-like cusps around E_{Ps} by Campeanu *et al* (1987) and Fromme *et al* (1988). More recently however, the experimental data of Coleman *et al* (1992) and Moxom *et al* (1993) indicate that the magnitude of the effect may be very much smaller than expected. This work is discussed fully in chapter 5.

The first attempt to obtain angular information about positron-atom scattering was made by Jaduszliwer and Paul (1973,1974). Here the number of scattered positrons reaching a detector was measured as the strength of an axial magnetic field was varied. From this, values of the differential elastic scattering cross-sections ($d\sigma_{el}/d\Omega$) for He, Ne and Ar were derived. However, these early measurements have subsequently been superseded.

A TOF technique was employed by Coleman and McNutt (1979) to obtain $d\sigma_{el}/d\Omega$. They studied Ar at impact energies up to 8.7eV and obtained values for $d\sigma_{el}/d\Omega$ at angles between 20° and 60°. Positrons were passed through a 10mm long scattering cell, guided by a strong (140G) magnetic field and timed over a flight path of around 25cm. The forward scattered positrons arrived at the detector with delayed flight times, due to the increased distances travelled and the angular distribution was derived from these flight times. There is good accord between these and the normalised results of a polarised-orbital calculation by McEachran *et al* (1979) and a semi-empirical polarisation potential calculation by Schrader (1979), as shown in figure 1.15.

A crossed beam technique, similar to that commonly used in electron scattering experiments, was employed by Hyder *et al* (1986) to measure $d\sigma_{el}/d\Omega$ for electron and positron scattering in Ar, in the range 30°-135° and for impact

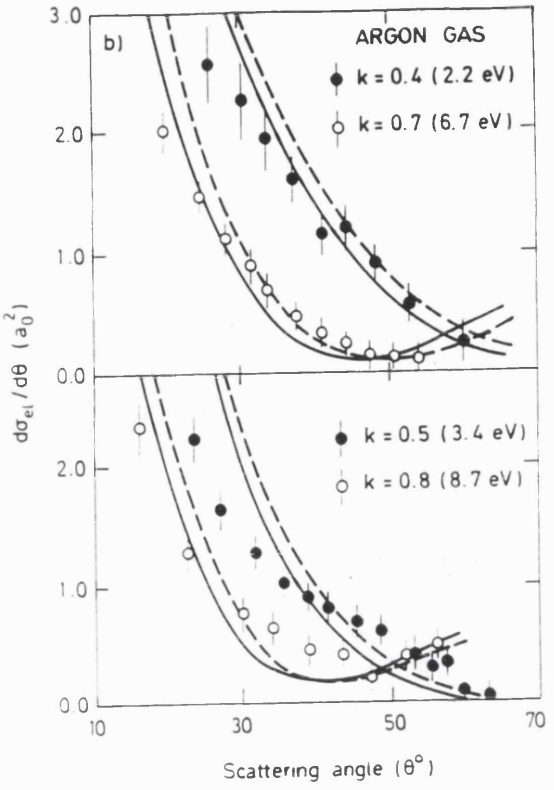

Figure 1.15. $d\sigma_{el}/d\Omega$ for positron-Ar scattering. Experiment: Coleman and McNutt (1979), •○. Theory: Schrader (1979), solid line; McEachran et al (1979), dashed line (see text).

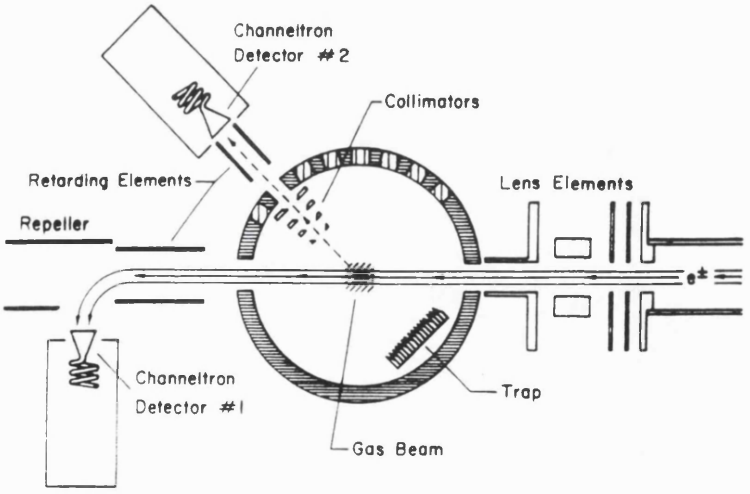

Figure 1.16. A schematic diagram of the apparatus used by Hyder *et al* (1986) to measure $d\sigma_{el}/d\Omega$.

energies from 100eV to 300eV. This apparatus is shown in figure 1.16. The primary beam was monitored using channeltron 1 whilst elastically scattered particles could be detected by channeltron 2. This detector had an angular acceptance of around ±8° and a retarding element was used to discriminate against inelastically scattered projectiles. Some of the results for positron and electron scattering at 100eV and 200eV are shown in figure 1.17. All the data were normalised at 90°. The positron results were normalised to the theoretical values of $d\sigma_{el}/d\Omega$ calculated by McEachran and Stauffer (1986) and Nahar and Wadhera (1987), which are almost identical at angles above 30° and the electron results

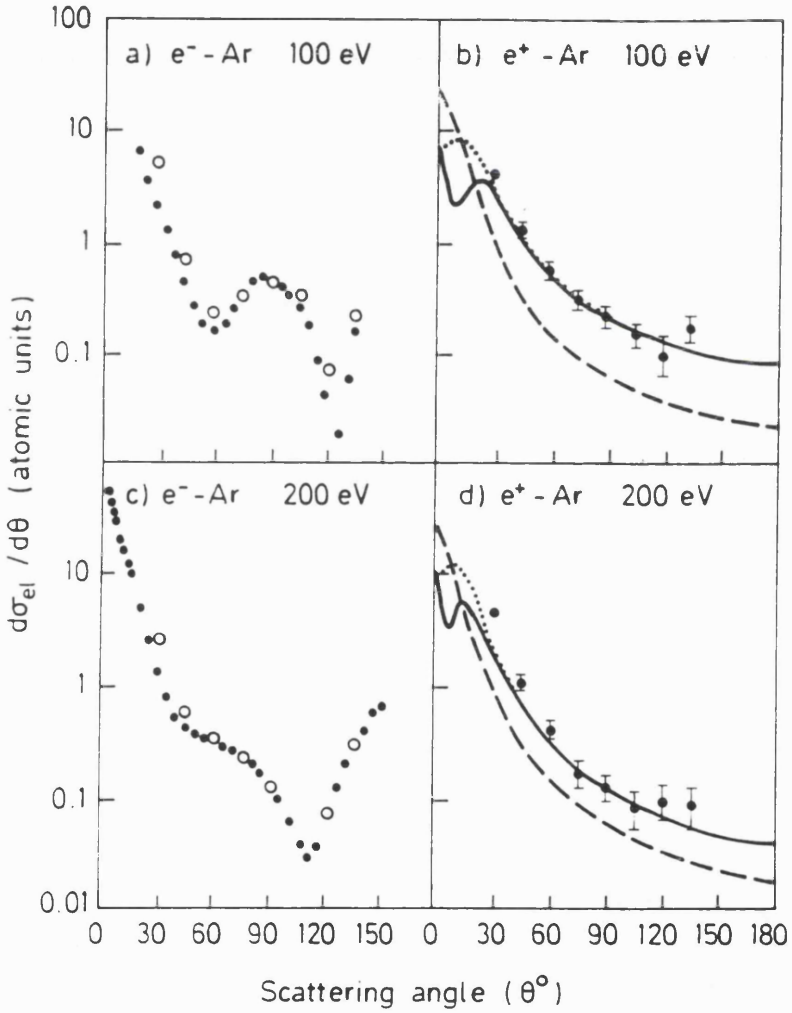

Figure 1.17. $d\sigma_{el}/d\Omega$ for positron/electron-Ar scattering: Hyder *et al* (1986), ● o; Srivastava *et al* (1981), •; McEachran and Stauffer (1986), solid line; Joachain and Potvliege (1987), dashed line; Nahar and Wadhera (1987), dotted line.

were normalised to existing experimental data (Srivastava *et al* 1981 and Dubois and Rudd 1975). Data for both projectiles were found to be in good accord with that used for normalisation, at all but the lowest energies. This discrepancy is attributed to geometric factors by Hyder *et al* (1986). Also shown in figure 1.17 are the results of Joachain and Potvliege (1987) which are significantly lower than those of McEachran and Stauffer (1986) and Nahar and Wadhera (1987) above 30°. If the experimental data were normalised to these results at 90°, they would still lie slightly above theory at small angles.

Smith *et al* (1989) extended the work of Hyder *et al* (1986) to lower energies as shown in figure 1.18. This figure

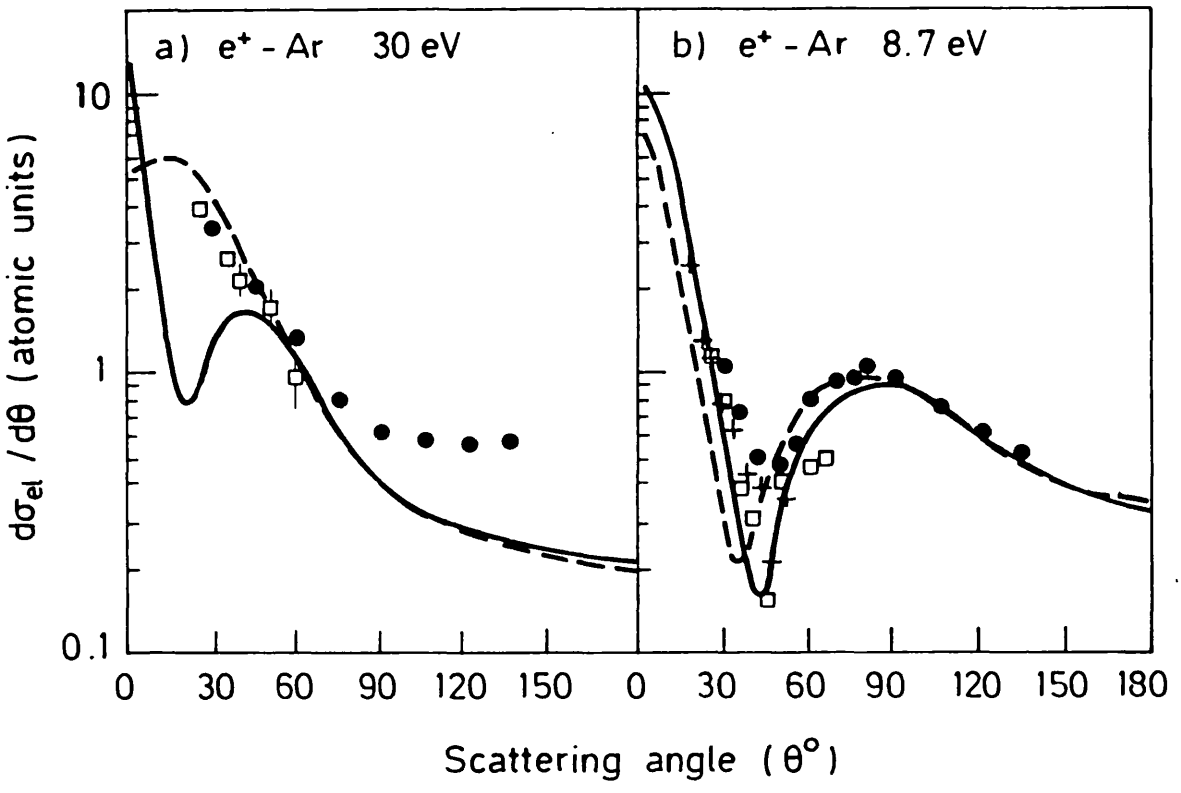

Figure 1.18. $d\sigma_{el}/d\Omega$ for positron-Ar scattering. a) 30eV. Experiment: Floeder *et al* (1988),□; Smith *et al* (1989),●. Theory: Bartschat *et al* (1988), dashed line; McEachran and Stauffer (1986), solid line. b) 8.7eV. Experiment: Floeder *et al* (1988),□; Smith *et al* (1989),●; Coleman and McNutt (1979),+. Theory: McEachran and Stauffer (1986), solid line; Montgomery and LaBahn (1970), dashed line.

also shows the results of a similar crossed beam experiment, performed by Floeder *et al* (1988), for positron scattering off Ar, in the angular range 26°-65° and at energies of 8.5eV and 30eV. At 30eV, the theoretical results of McEachran and Stauffer (1986) contain a minimum around 20°. There is no evidence of this in the experimental data of Floeder *et al* (1988), or Smith *et al* (1989) and in addition, the data of Smith *et al* (1989) display a significantly different shape at larger angles. The minimum at 20° is not present in the optical-potential calculation of Bartschat *et al* (1988), which is in good accord with experiment below 60°. At 8.7eV (figure 1.18b) the experimental results of Floeder *et al* (1988) and Coleman and McNutt (1979) exhibit a deep minimum at around 40°, in good agreement with McEachran and Stauffer (1986). The results of Smith *et al* (1989) are in qualitative agreement, however the minimum is significantly shallower.

Dou *et al* (1992) measured $d\sigma_{el}/d\Omega$ as a function of impact energy at a fixed angle. This was accomplished using the technique and apparatus of Hyder *et al* (1986). Shown in figure 1.19 are their results for positron scattering in Ar at 90° for energies in the range (12-300)eV. The structure

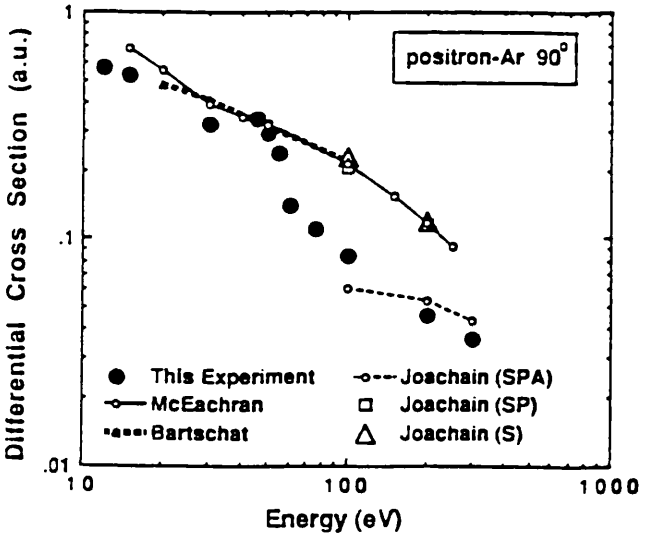

Figure 1.19. $d\sigma_{el}/d\Omega$ for Ar at 90°, plotted as a function of impact energy (Dou *et al* 1992).

takes the form of a drop in $d\sigma_{ei}/d\Omega$ of around a factor of 2 between 55eV and 60eV. Other measurements taken at 60° and 120° show similar structure at around the same energy. Its origin is not yet fully understood, but it was suggested by Dou (1991) that it may be related to the coupled-channel shape-resonance found by Higgins and Burke (1991) in the Ps formation cross-section in positron-H collisions. These structures appear around energies where the ionisation cross-section reaches its maximum value and may be caused by complex channel coupling effects.

1.5.4 Ionisation

The processes of single ionisation and Ps formation have been the subject of extensive investigation and are reviewed in the context of the present work in chapter 4. Charlton *et al* (1988,1989) have studied the phenomenon of double ionisation and defined the quantity $R^{(2)}$ as the ratio of the double to single ionisation cross-sections. This was measured in He, Ne and Ar up to 5keV using the apparatus of Knudsen *et al* (1990), shown in figure 4.6. Values of $R^{(2)}$ for positron impact on He are shown in figure 1.20, where they are compared with $R^{(2)}$ for electrons, protons and anti-protons (Charlton *et al* 1988,1989, Andersen *et al* 1987). The positron curve merges with that for protons at energies in excess of 2MeV/amu, where both are significantly smaller than those for the negatively charged projectiles. This is predominantly due to differences in Q_i^{2+}, since at these velocities the single ionisation cross-sections merge, in accord with the first Born approximation. This shows that the effect is due to Q_i^{2+} being smaller for the positively charged particles and that the differences in Q_i^{2+} at high energies are caused by the projectile charge and not its mass. Charlton *et al* (1988,1989) ascribe the difference between the positron and proton results at lower energies, to the lower kinetic energies of the lighter particles.

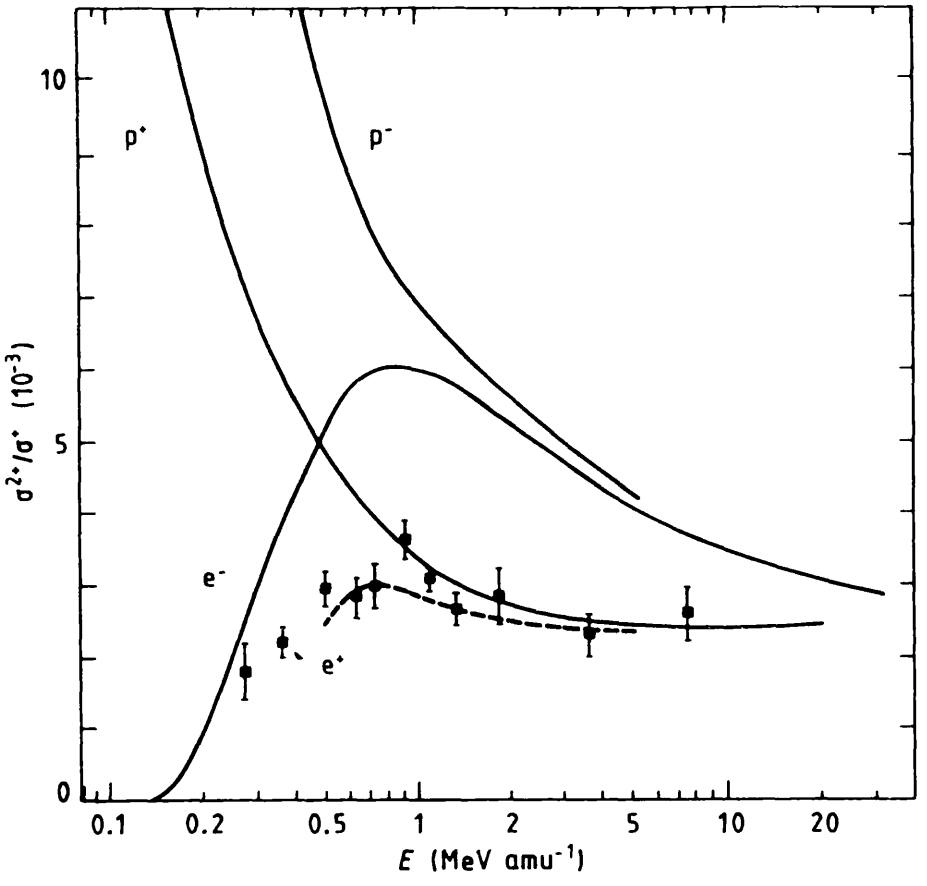

Figure 1.20. $R^{(2)}$ for positrons, electrons, protons and anti-protons. (Charlton *et al* 1988, 1989, Andersen *et al* 1987).

1.6 The Aims and Motivation for the Present Work

The motivation of the present work has been to further the study of positron interactions with gases. In particular, those processes which result in ionisation namely, Ps formation, direct ionisation and a special case of ionisation known as electron capture to the continuum (ECC).

It has been suggested that positron impact ionisation of gases may lead to structures at characteristic energies in the doubly and triple differential cross-sections, caused by ECC. This process is due to correlation between scattered positively charged projectiles and ejected electrons and is well known from collisions involving protons and heavy

positively charged ions (e.g. Crooks and Rudd 1970, Rodbro and Andersen 1979, Knudsen *et al* 1986). It has been proposed that this effect may also be manifest in the energy spectra of electrons ejected following positron impact ionisation. However discrepancies exist among the available theoretical results. Brauner and Briggs (1986), Mandal *et al* (1986) and Sil *et al* (1991) predict a pronounced cusp in such spectra, while Schultz and Reinhold (1990) expect a small ridge. The aim of the work described in chapter 3 has been to asses the significance of this process in positron-Ar collisions and to provide guidance for theory.

Another important positron impact ionisation processes is Ps formation. In the work described in chapter 4, the combined cross-section for this and direct ionisation (i.e. the total ionisation cross-section, Q_t^+) has been measured, in detail for a number of gases. This work was performed in order to study the energy dependence of Q_t^+, which is entirely due to Ps formation close to its threshold (E_{Ps}), and to derive new values for Q_{el} in the vicinity of E_{Ps} since here, as already mentioned, Wigner cusps may exist in Q_{el} (e.g. Campeanu *et al* 1987, Fromme *et al* 1988).

The aim of this work is therefore to add to the body of knowledge concerning the interactions of charged particles with atoms and molecules, thereby aiding the understanding of some of the most fundamental aspects of atomic physics.

CHAPTER 2

THE EXPERIMENTAL APPARATUS

2.1 The General Layout of the Apparatus

The positron beam used throughout this work was obtained by the moderation of β^+ particles emitted from commercially obtained radioisotopes. These fast positrons were moderated in energy using annealed W meshes and were formed into a beam using simple electrostatic optics. The positron beam was guided along an evacuated beam-line by a longitudinal magnetic field and traversed an interaction region consisting of a differentially pumped gas scattering cell, incorporating a novel ion extraction system. The beam-line was terminated by a charged particle detector.

For the measurement of ejected electron energy spectra described in chapter 3, a device (tagger) was used, which enabled positrons to be timed as they traversed the interaction region. The beam tagger and its principles of operation are described in § 3.3. For the measurement of total ionisation cross-sections, a Wien filter was placed between the source and interaction region to reduce the background contributions from fast particles in the beam. This, and other modifications that were carried out to improve the beam characteristics, are discussed in chapter 4.

The parts of the apparatus that were common to both types of experiment are discussed in this chapter and include the source and moderator assembly, the beam transport and vacuum systems, and the scattering cell and ion extractor.

2.2 The β^+ Source and Moderator

The radio-isotopes that were used as positron sources in this work were ^{22}Na and ^{58}Co. The decay schemes and branching ratios for β^+ and electron capture (E.C.) for these isotopes are shown in figure 2.1.

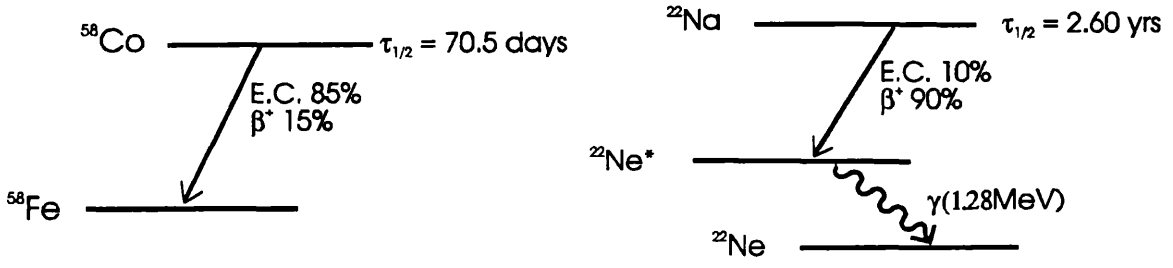

Figure 2.1. The decay schemes and branching ratios of ^{22}Na and ^{58}Co.

The two ^{22}Na sources were supplied by Amersham International and came in the form of a 4mm spot deposited on a 4mm thick Pt disc with a diameter of 18mm. The sources were sealed with a 10μm Ti window. This was estimated to allow around 41% of the β^+ particles emitted by the source to escape in the forward direction (Massoumi *et al* 1988). ^{22}Na has a half life of approximately 2.6 years and the activities of these sources were around 4mCi and 70mCi at the time of the experiments described below. The ^{58}Co source was electroplated onto a small area in the centre of a copper foil and was supplied in this form by Dupont Ltd. The half life of ^{58}Co is around 71 days and

the activity of this source was around 10mCi at the time of use.

The vacuum chamber housing the source and moderator assembly is shown in figure 2.2. This chamber consisted of two concentric stainless steel cylinders, with axis perpendicular to that of the beam-line. The source and moderator were located in the centre of these cylinders. The source was mounted on the end of a retractable manipulator shaft, which enabled the source to be withdrawn from the moderator and the central cylinder to be rotated, to allow the safe removal of the central lead plug, on which the moderator was mounted. The high level of radiation in the source region was shielded by partially filling the central cylinder with lead and surrounding the outer cylinder with lead bricks. The ^{22}Na sources were attached to the source holder, as shown in figure 2.3a). The ^{58}Co source was retained underneath a brass cap, with a 6mm hole in its centre, as shown in figure 2.3b). In both cases the source holder was attached to the end of the manipulator shaft by an M8 thread.

The moderator, shown in figure 2.3a), typically consisted of four or five superimposed, 90% transmission annealed W meshes, with an diameter of around 14mm. The annealing process, described in detail by Zafar *et al* (1988,1989), was carried out in a W oven formed by two strips of W foil, between which the moderator meshes were placed. The oven was heated by passing a current through the foils. The annealing cycle consisted of repeatedly raising the moderator temperature to around 2000°C for a few seconds, in a pressure of less than 10^{-1} torr. The heating process was initially accompanied by an increase in the pressure in the vacuum chamber, caused by emission of surface contaminants from the moderator and oven. The annealing cycle was repeated for up to several hours, and was continued until the oven could be raised to this temperature without causing the pressure in the vacuum chamber to rise appreciably.

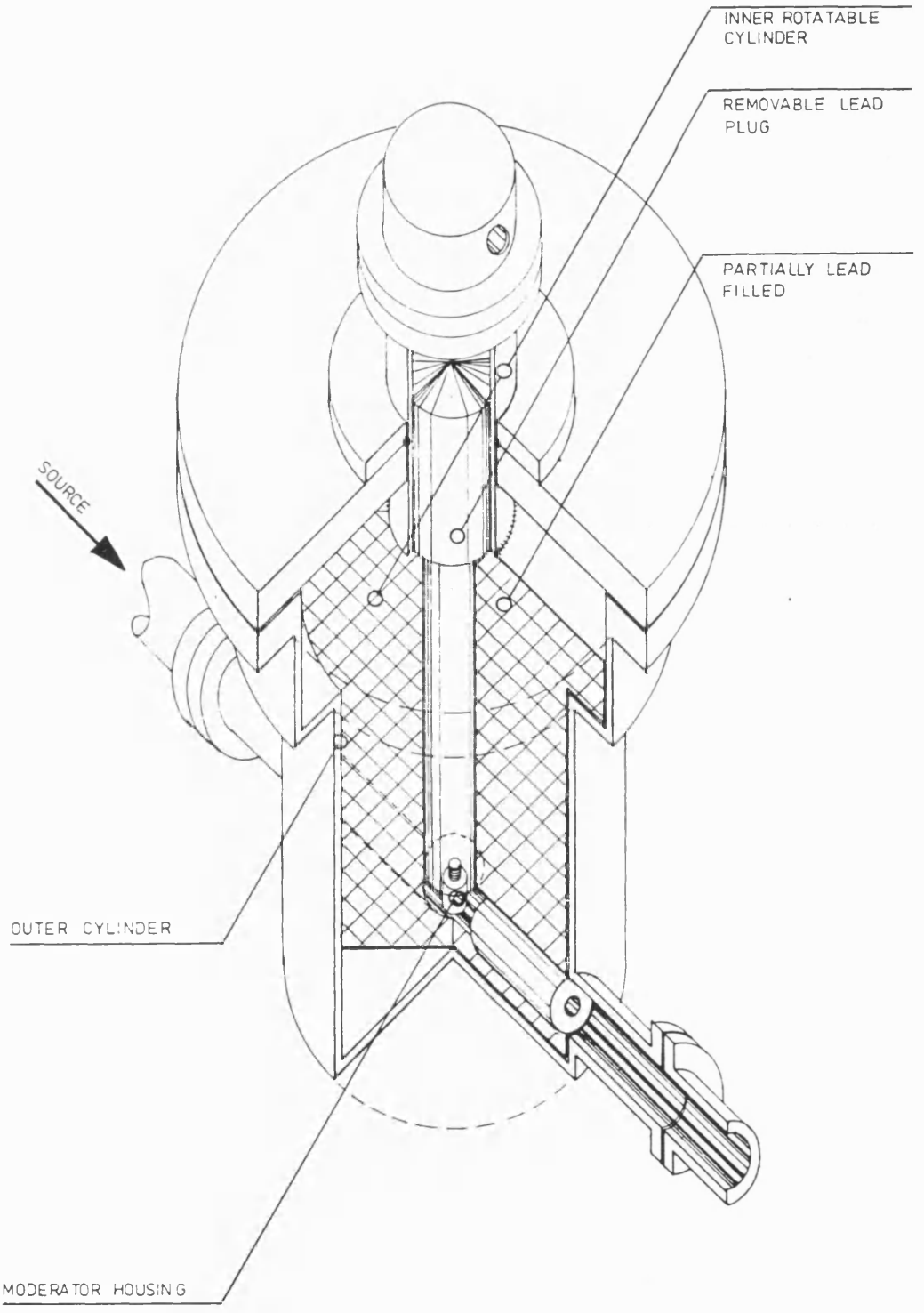

Figure 2.2. A cutaway diagram of the chamber housing the source and moderator assembly.

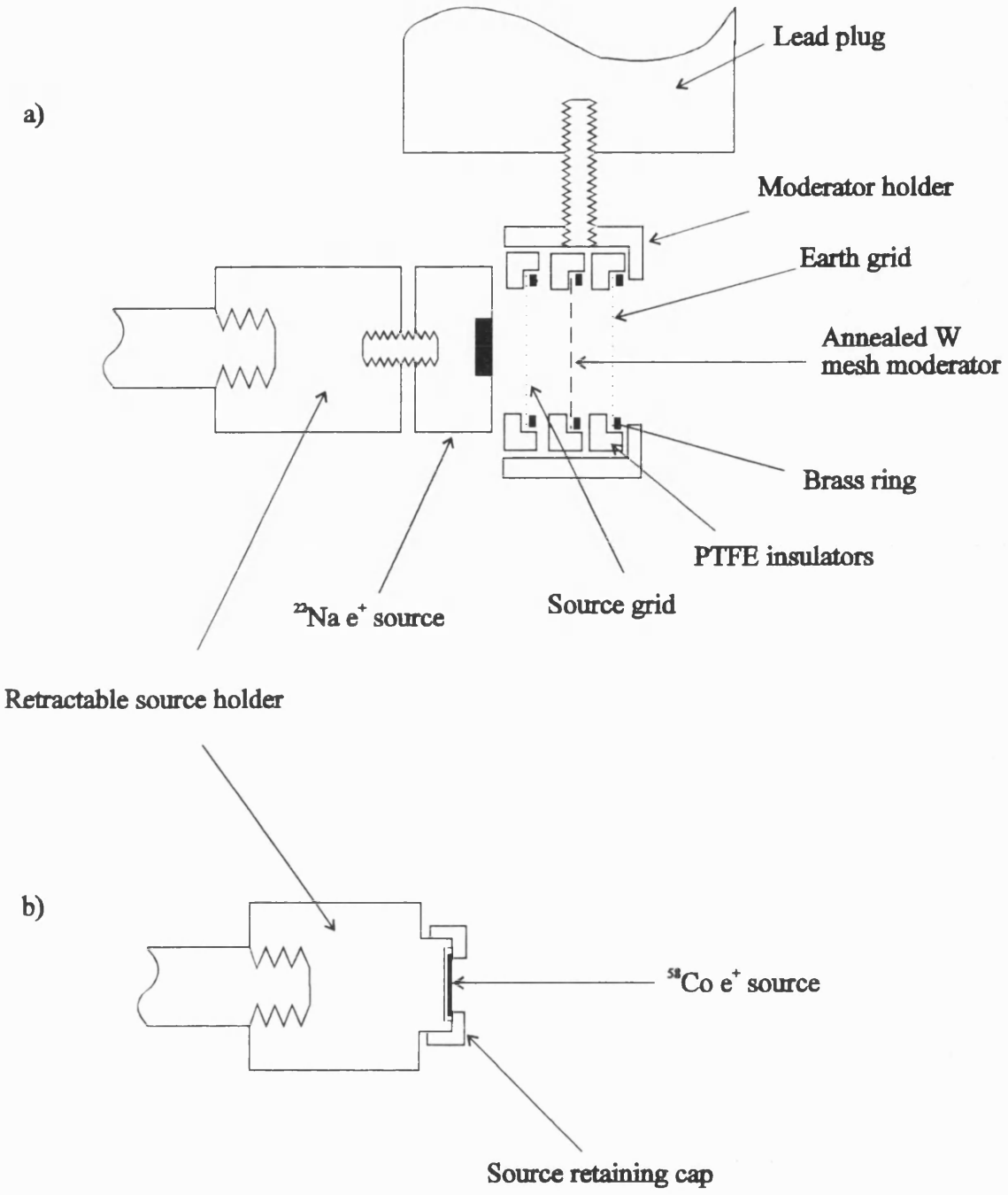

Figure 2.3. A schematic diagram of the source and moderator holder showing a) the ^{22}Na source and b) the ^{58}Co source (not drawn to scale).

The moderator meshes and grids were held in the grid holder shown in figure 2.3a). The grid holder consisted of a 9mm long brass sleeve with an internal diameter of 17mm, into which were inserted the annular PTFE insulators used to support the grids. The grids and moderator were held in position by brass rings, press fitted into the recesses of the PTFE insulators. Electrical connections were made to the grids via the brass rings. An unannealed 90% transmission W grid, placed around 2mm in front of the moderator, was grounded. By applying a positive potential (V_m) to the moderator, positrons which were re-emitted from its surface were accelerated in the forward direction. These slow positrons had kinetic energies (E) given by

$$E=eV_m+\Delta E \qquad (2.1)$$

where ΔE is the kinetic energy with which a positron left the moderator. As mentioned in chapter 1, most of these positrons will thermalise before being re-emitted, and since a positron may scatter from contaminants on the moderator surface, ΔE can have any value up to around $|\phi_+|$, where ϕ_+ is the negative positron work function of the moderator surface. The value of ϕ_+ therefore determines the maximum intrinsic energy spread of the positron beam. This was measured for the W mesh moderators used in this work, in the manner described in § 4.3, to be around (2.8±0.25)eV, in agreement with the value of ϕ_+ for clean W surfaces, annealed in-situ under UHV conditions (Jacobsen *et al* 1990).

A second 90% transmission W grid placed immediately behind the moderator was held at a slightly more positive potential, sufficient to cause positrons emitted from the rear of the moderator to be reflected back towards the meshes. Some of these positrons passed through the moderator, resulting in an approximate two-fold increase in the beam intensity.

2.3 The Beam Transport and Vacuum System

The beam transport and vacuum system are shown schematically in figure 2.4. A vacuum of the order of 10^{-6} torr was maintained in all parts of the apparatus, except the scattering cell, by four oil vapour diffusion pumps, backed by three mechanical rotary pumps. The source and moderator chamber was evacuated by an Edwards E02 diffusion pump backed by an Edwards ED50 rotary pump. The regions either side of the scattering cell, and the chamber housing the ion detector, were evacuated by two Edwards E04 diffusion pumps. The diffusion pump prior to the scattering cell was backed by an Edwards ED250 rotary pump. The diffusion pumps for the ion detector chamber and the region after the scattering cell were backed by a single Edwards two stage rotary pump.

The beam was guided through the apparatus by a longitudinal magnetic field of up to around 100G. From the tagging chamber to the end of the beam-line, this was produced by a series of current carrying coils with internal diameters of around 20cm, distributed along the beam-line as shown. Two coils of around 30cm in diameter were placed around the source and moderator chamber, and the beam was guided from here to the tagging chamber by a magnetic field set up inside a 1m long solenoid with a 15° bend. The bend in the solenoid reduced the number of fast particles, such as energetic electrons and positrons, in the beam and prevented a line-of-sight path from the source to the interaction region. Additional shielding from γ-rays emitted by the source was achieved by a lead collimator at the source end of the solenoid, and lead bricks placed around the bend. An additional coil was placed around each end of the solenoid to reduce end effects. By varying the magnetic field strength in various parts of the apparatus, the beam transport characteristics could be optimised, for example, to maximise the incident beam intensity or the

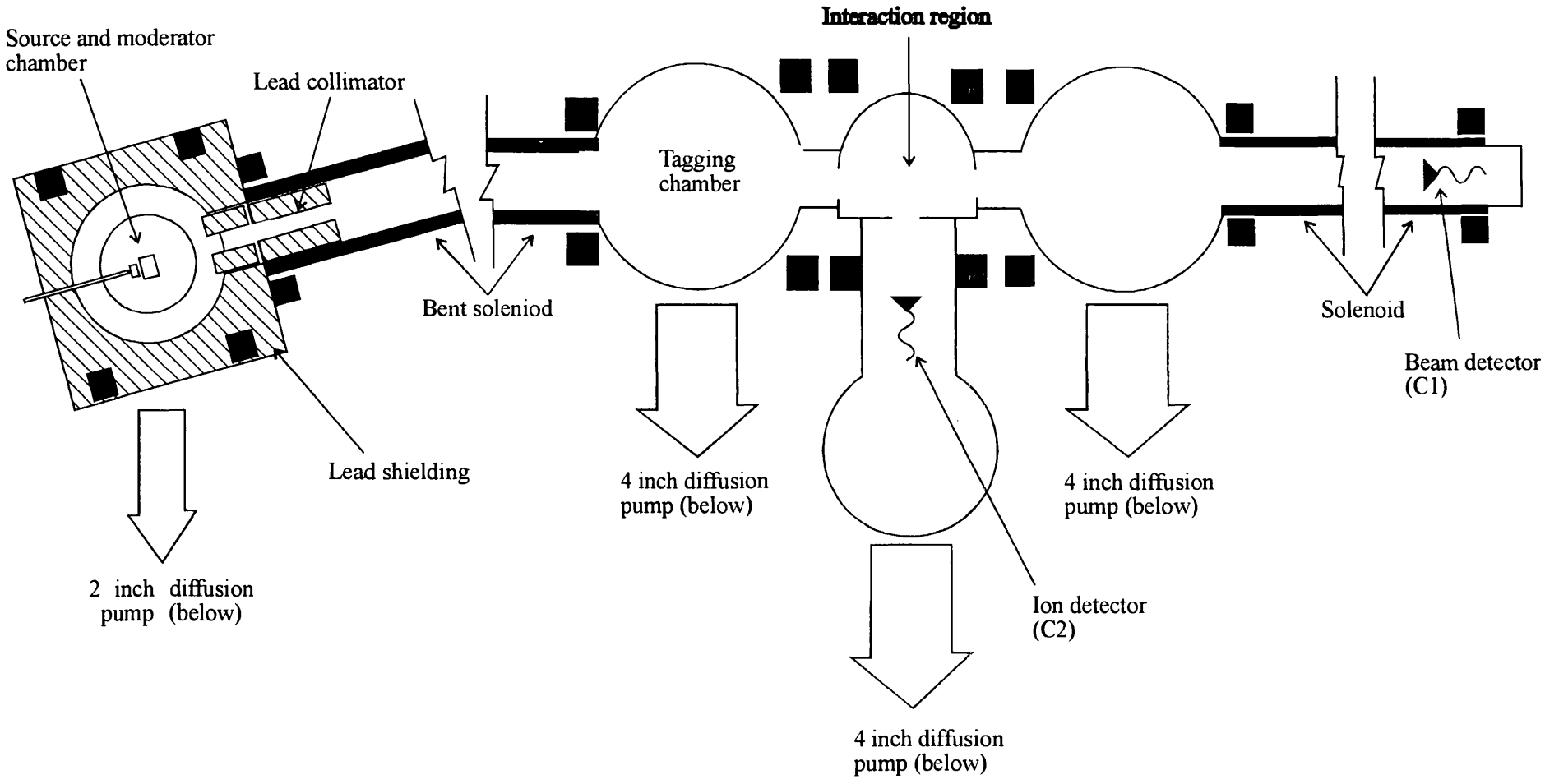

Figure 2.4 A schematic diagram of the positron beam transport and vacuum system (not drawn to scale). The solid black areas represent coil windings.

confinement of scattered particles, or to parallelise the beam.

If a charged particle passes from one region in which the magnitude of the guiding magnetic field is B_1, to another region in which the magnetic field strength is B_2, then provided that the magnetic field strength varies slowly, the pitch angles of the particle, relative to the magnetic field, in the two regions will be related by

$$\frac{B_1}{B_2} = \frac{\sin^2\alpha_1}{\sin^2\alpha_2} \qquad (2.2)$$

where α_1 and α_2 are the pitch angles in the regions where the magnetic field strengths are B_1 and B_2 respectively. Thus if $B_1 > B_2$ it follows that $\alpha_1 > \alpha_2$. Hence, if a positron beam passes to a region of reduced magnetic field strength, its distribution of pitch angles may be reduced. This technique may be used to "parallelise" a positron beam as it traverses the interaction region, if the magnetic field strength at the interaction region is lower than that at the moderator. However, the divergence of the magnetic field caused by the field strength gradient and the increased Larmor radii, may cause the beam diameter to increase. The low magnetic field strength in the interaction region may also fail to confine scattered particles. The magnetic field configurations were chosen with these criteria in mind. In the experiment described in chapter 3, the magnetic field strength around the scattering cell was around 10G. This low magnetic field strength was chosen in order to limit the confinement of scattered particles to those with small pitch angles. The angular acceptance of the beam transport in this case is discussed in § 3.2.1. In the work described in chapter 4 the magnetic field strength in the interaction region was increased to around 50G, in order to transport the beam through the scattering cell without colliding with the apertures.

2.4 The Scattering Cell and Ion Extractor

The differentially pumped scattering cell and the ion extractor are depicted in figure 2.5a). Ions were extracted from the interaction region by a radial electric field. This enabled ions to be extracted from anywhere within the scattering cell and transported to an ion detector in a separate vacuum chamber.

The scattering cell was hemispherical, with a diameter of around 90mm. The hemispherical wall of the cell was machined from a block of aluminium and was coated with graphite to prevent surface oxidation from becoming electrically charged. The graphite coating also reduced the secondary electron emission coefficient of the cell surface from 2-9 for AlO_2, to around 1. This helped to reduce the probability of secondary electrons being ejected into the interaction region by stray charged particles. 8mm diameter entrance and exit apertures in the sides of the cell allowed the beam to pass through the scattering cell parallel to the base of the hemisphere, such that the distance between the beam axis and the planar surface of the scattering cell was 19.5mm. The base of the cell comprised six concentric circular electrodes etched onto a printed circuit board (PCB). By applying suitable potentials to these electrodes a radial electric field was set up inside the scattering cell. These potentials were derived from the resistor chain shown in figure 2.5b). Capacitors were incorporated into the circuit to neutralise the effects of stray capacitance between the electrodes, allowing the ion extractor to be pulsed on and off without the pulses suffering distortion. The radial electric field caused ions to be focused onto the centre of the electrode array where a 4mm diameter hole enabled extraction. After passing through the hole ions were focused onto the cone of a Ceratron detector (C2). This device is a single-channel continuous-dynode, ceramic electron

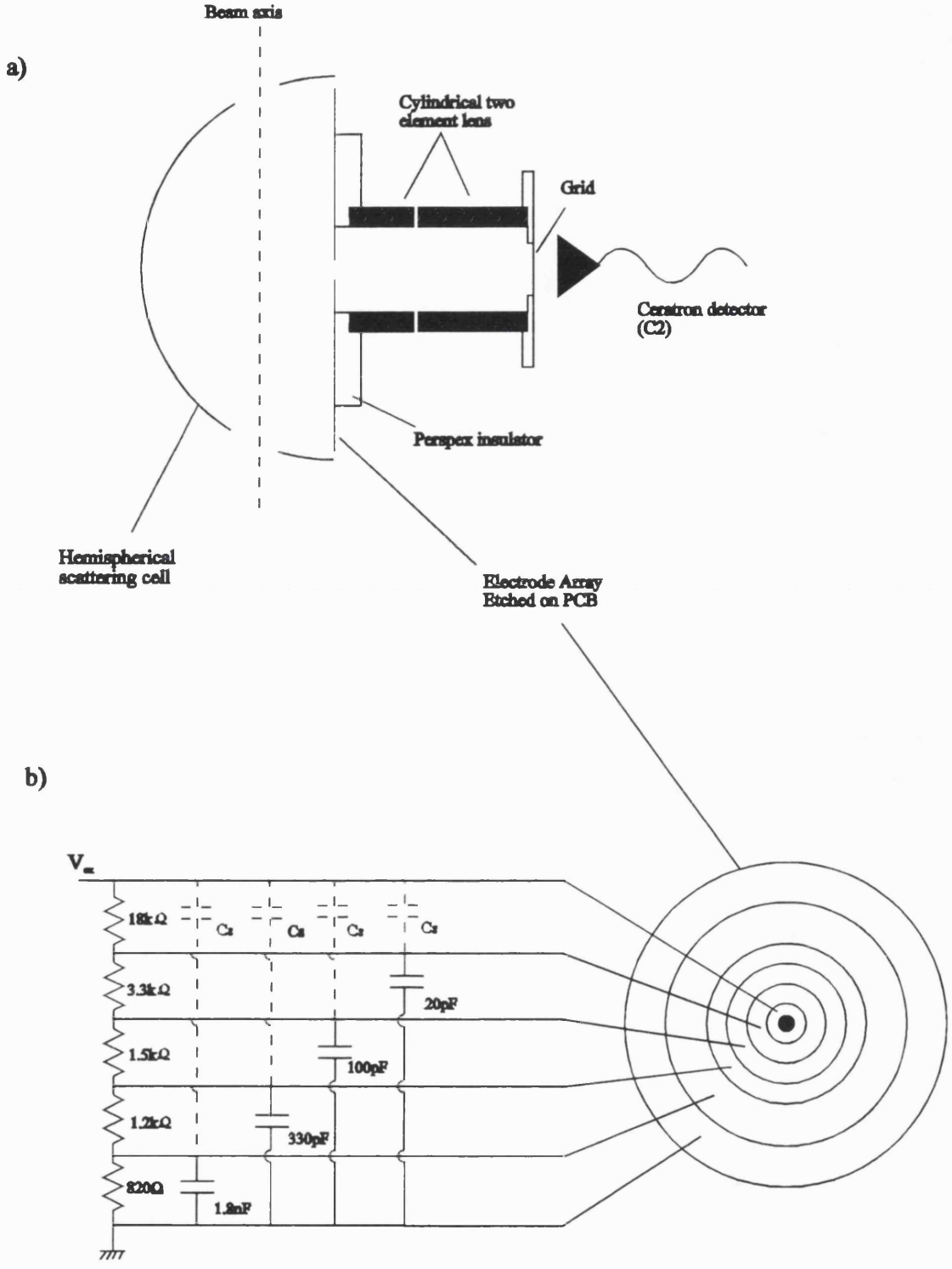

Figure 2.5. A schematic diagram showing a) the ion extractor and scattering cell and b) the network used to derive suitable potentials for the ion extractor electrodes.

multiplier (type EMW-6081 supplied by Murata Ltd) and was housed in a separate vacuum chamber under the low vacuum conditions ($<10^{-5}$ torr) necessary for its efficient operation. The ion focusing was achieved using a two element electrostatic lens. The first element was electrically connected to the central electrode of the ion extractor, while the second element was held at -3.1kV. The action of this lens caused ions emerging from the extraction hole with widely divergent trajectories to be focused onto the active area of C2.

The front cone of C2 was held at -3kV causing ions to strike its cone with sufficient kinetic energies to be efficiently detected. For a similar type of detector, manufactured by Phillips, the detection efficiency specified by the manufacturers is around 50% for "protons or positive ions" at this impact energy. No detection efficiency data is available from Murata, however, it is expected to be similar. The back of C2 was grounded and the collector was held at 200V. The potential for the collector was supplied via a 10MΩ series resistor and signal pulses were extracted by means of a 1nF decoupling capacitor. A 95% transmission Cu grid, in front of C2, was held at -3.1kV. This grid caused secondary electrons to be reflected back towards the cone of C2, thereby increasing its detection efficiency.

The sample gases were leaked into the middle of the scattering cell through an Edwards LV5 needle valve and the pressure was measured, in the middle of the cell, using an MKS 220-1 Baratron capacitance manometer, with an accuracy of ±5%, as quoted by the manufacturers.

2.5 The Performance of the Ion Extractor

The performance of the ion-extractor was simulated using the software package SIMION 4.0. This allowed the trajectories and

flight times of ions passing through the ion extractor to be predicted. The ion flight times and the ion extraction and detection efficiencies, were measured and compared with the results of the simulation, in order to verify that the device was operating as expected. The ion lifetimes in the scattering cell were also measured. Knowledge of these characteristics allowed the operating parameters of the apparatus to be optimised and background contributions to be estimated, as discussed in chapters 3 and 4.

2.5.1 A Computer Simulation of the Ion Trajectories

The result of a computer simulation of trajectories of ions through the ion-extractor is shown in figure 2.6. This shows the trajectories of singly ionised Ar atoms (Ar^+), the heaviest ions to be encountered in this work. The ions begin their trajectories with no kinetic energy and from starting points spaced 5mm apart inside the scattering cell, along the central axis of the beam-line. The simulation predicted that ions originating from anywhere along this line could be extracted from the interaction region and transported to C2. Trajectories were also simulated for the same ions originating along lines corresponding to the edges of the beam. The simulation predicted that all such ions would be successfully transported to C2 and indicated that ions would reach C2 from anywhere within the overlap of the beam and the target gas, inside the scattering cell. The focusing properties of the ion-extractor were simulated in the same way for H_2 ions (H_2^+), the lightest ions to be encountered. The ion trajectories were similar to those of Ar^+.

The magnetic field used to transport the beam, when incorporated in the simulation, had no significant effect on the ion trajectories. It did however have the beneficial effect

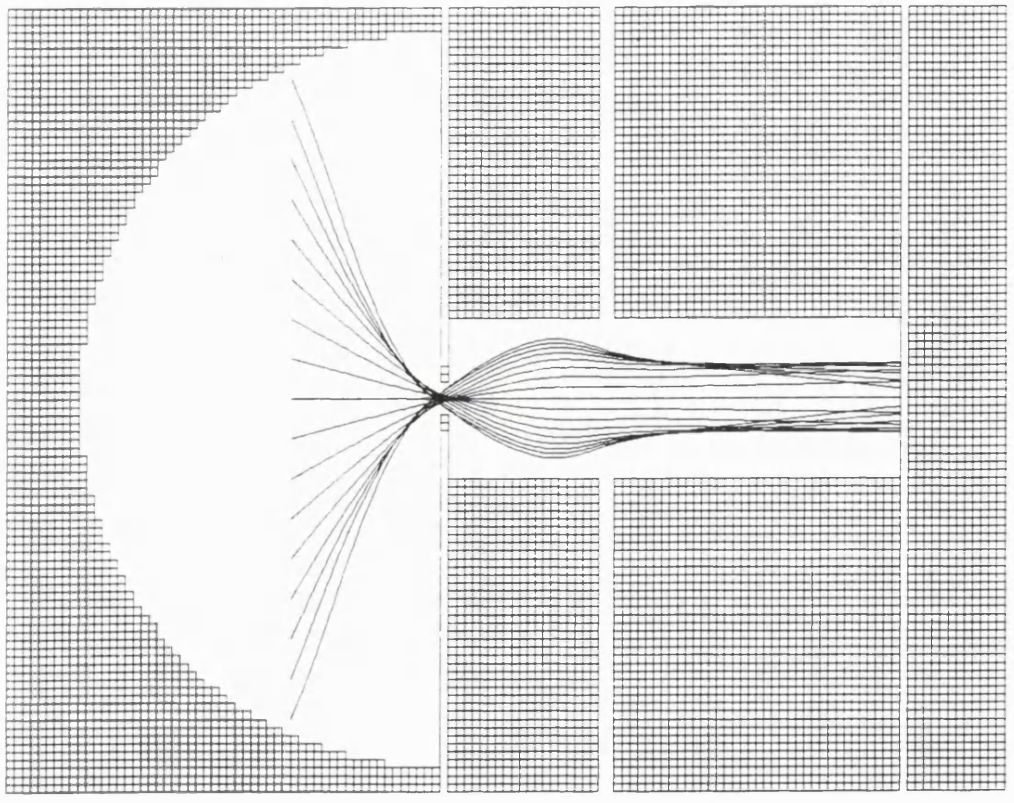

Figure 2.6. A computer simulation of ion trajectories through the ion extractor.

of preventing secondary electrons ejected from the grid and lens elements in front of C2 from passing back through the extraction hole and into the interaction region.

In order to asses the effect of the random thermal motion of the ions on their extraction efficiency, trajectories were simulated for Ar^+ and H_2^+ with kinetic energies of 35meV, the approximate mean thermal energy at room temperature. The trajectories were started from various points in the interaction region, with initial velocity vectors incremented over 4π. No significant de-focusing was noted and it was concluded that the thermal motion of the ions would not cause the extraction efficiency to be reduced.

2.5.2 The Ion Extraction Efficiency

The ion extraction efficiency (ϵ_i) is defined as the ratio between the ion production rate in the scattering cell and the ion count rate at C2. ϵ_i was estimated by passing a beam of positrons of a known intensity, through the scattering cell, whilst measuring the count rate at C2. The cell was filled with a target gas to a known pressure and the ion production rate was estimated from a knowledge of its ionisation cross-section. The mean energy of the beam was chosen such that contributions from Ps formation would be negligible. The ion count rate was also measured at different gas pressures to investigate the effect of pressure on the extraction efficiency.

Pulses from C2 were used to trigger a constant fraction discriminator and counted on a timed scaler. A positron beam with a mean kinetic energy of around 620eV was passed through the scattering cell, which was filled with Ar gas to pressures of up to 4.4μmHg, as measured on the Baratron. The beam intensity was measured using the Ceratron detector (C1) at the end of the beam-line. This was also a Murata EMW 6081 device. The potential on the cone of C1 was around 500V, resulting in an impact energy of around 1.1keV. At this energy the positron detection efficiency is around 80% (Sueoka 1982a). The count rate at C2 was found to saturate at approximately $350s^{-1}$ when the potential applied to the central electrode of the ion-extractor (V_{ex}) reached around -5V. These measurements were made with a d.c. extraction field, and not the pulsed field described below, in order to measure the intrinsic extraction efficiency of the radial electric field. ϵ_i was measured with a gas pressure of approximately 1μmHg and V_{ex} = -5V. At this pressure, around 8% of the beam was expected to be scattered (Kauppila *et al* 1981) and multiple scattering effects were therefore expected to be negligible. The electric field in the scattering cell due to V_{ex} was not expected to significantly perturb the

beam, since V_{ex} was small in comparison with the beam energy.

At this energy the contribution to the ion-yield from Ps formation was expected to be negligible in comparison with the single ionisation cross-section (Q_i^+). This may be inferred by extrapolation of the Ps formation cross-section (Q_{Ps}) measured by Fornari *et al* (1983) to higher impact energies. The value of Q_i^+ of Ar, measured by Knudsen *et al* (1990) was then used to estimate the ion production rate. The contribution, albeit small, from double ionisation of around 3.5% (Charlton *et al* 1989) was also included. The measured value of ϵ_i was (82±11)%. The uncertainty is that associated with the value of Q_i^+ from Knudsen *et al* (1990) and does not include systematic effects such as the uncertainty in the areal gas density or the detection efficiency of C2.

The ion count rate is plotted as a function of gas pressure in figure 2.7. The ion count rate rises almost

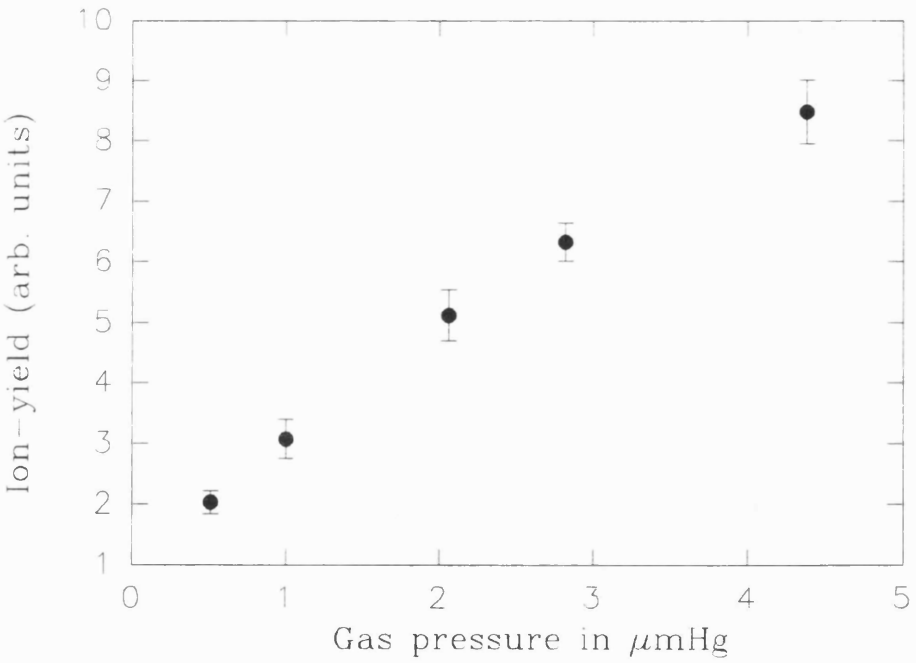

Figure 2.7. The variation of the ion-yield with gas pressure in the scattering cell.

linearly, up to around 4.4μmHg, the highest pressure investigated. This shows that the ion extraction efficiency is not greatly affected by the target gas pressure over this range, indicating that the effects of ion scattering on their journey to the detector are small.

2.5.3 The Ion Flight Times and their Lifetimes in the Scattering Cell

An ion lifetime is the time elapsed between its formation in the scattering cell and its recombination (probably by a collision with the cell wall) in the absence of an electric field in this region. This may occur due to thermal motion of the ions in the scattering cell. The effect is therefore expected to be dependent on the mass of the ions.

An ion flight time is the time taken for an ion to be transported from its formation point in the interaction region to C2 by the ion-extractor. This depends upon the ion charge-to-mass ratio and the magnitude of the potential applied to the ion-extractor.

These measurements were made using a beam of electrons with an arbitrarily chosen mean energy of around 50eV and an intensity of around $2000s^{-1}$. The scattering cell was filled with the target gas to a pressure of around 1μmHg. Signals from C1 and C2 were converted into fast negative going logic pulses by two constant fraction discriminators, CFD1 and CFD2, as shown in figure 2.8. Following the detection of an electron by C1 a pulse of -180V, with a duration of around 15μs, was applied to the ion-extractor, causing any ions present in the scattering cell to begin their journey to C2. Ion flight times were measured with the delay unit shown in figure 2.8 removed from the circuit. The high voltage pulses for the ion extractor were obtained from a MOSFET pulse amplifier. This unit was triggered

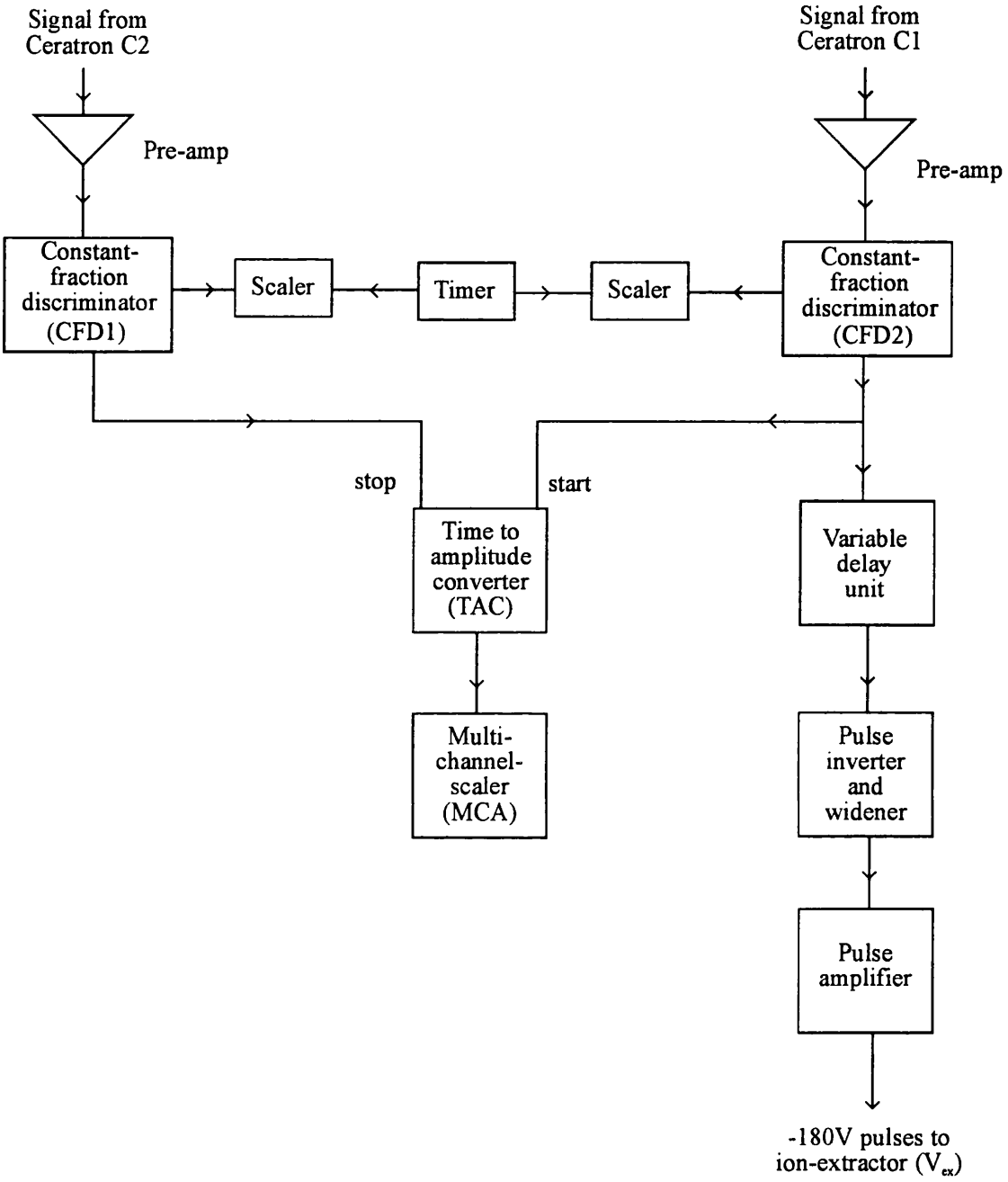

Figure 2.8. A schematic diagram of the circuit used to measure ion lifetimes in the scattering cell and flight times to the detector.

by signals from CFD1, which were inverted and widened to 15μs. The timing pulses from CFD1 and CFD2 were used as the start and stop signals respectively, for a time to amplitude converter (TAC). Output pulses from the TAC were processed and stored on a multi-channel-analyzer (MCA), thus generating an ion-flight-time spectrum.

Ion TOF spectra were measured for Ar and H_2, the heaviest and lightest of the targets used in this work. These spectra are shown in figure 2.9. In the case of Ar the distribution has its onset at around 3.8μs after the extraction field was pulsed on. The intensity rises to a broad maximum between around 5μs and 7μs and then gradually falls to zero by around 13μs. For H_2^+ the distribution has its onset around 0.8μs, reaches its maximum value around 1.4μs and falls to close to zero by around 2.4μs. The computer simulation predicted that flight times for ions would range between 4.0μs and 13.0μs, for Ar^+ and between 0.9μs and 2.7μs for H_2^+, in good agreement with the measured values.

Ion lifetimes were determined by delaying the onset of the extraction pulses relative to the signals from C1, using a variable delay unit. The ion-yield was measured as a function of this delay and used to obtain ion lifetime distributions. The intrinsic propagation delay of the electronics of 220ns and the times taken for the scattered electrons to reach C1 were estimated to be negligible in comparison to the ion lifetimes and flight times. Positive going pulses from the discriminators were counted on two scalers, enabled by a digital electronic timer, thus allowing the ion count rate (N_I) and the beam intensity (N_e) to be determined. The TAC and MCA played no part in the measurement of ion lifetimes.

The ion-yields (N_I/N_e) fell from a maximum value with no added delay, to a minimum value, caused by random extraction, as the delay was increased. The ion yields were differentiated with respect to the delay, to obtain the ion lifetime

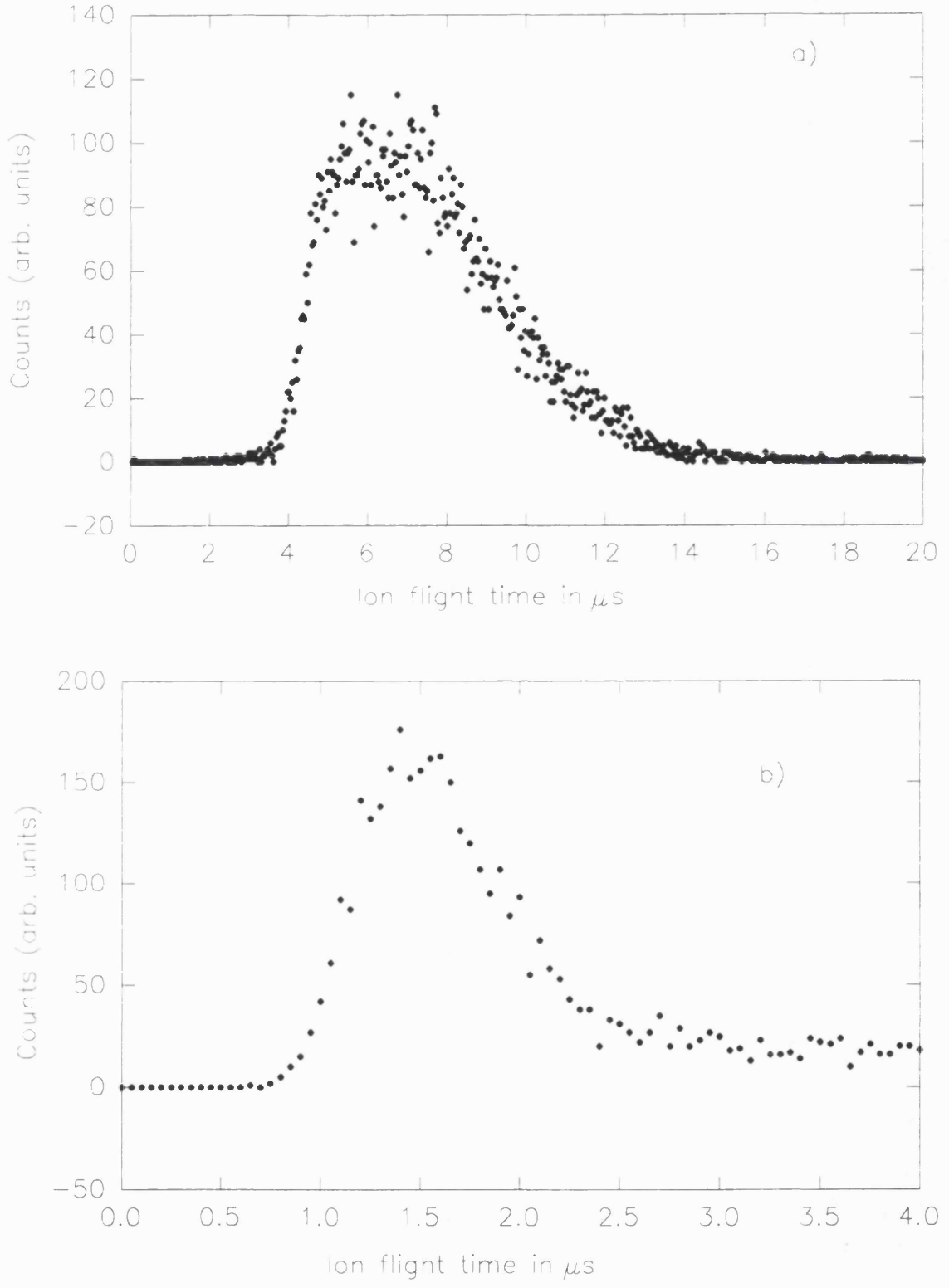

Figure 2.9. Distribution of ion-flight-times for a) Ar and b) H_2.

distributions shown in figure 2.10 for He, Ar and H_2. The vertical axes of three distributions have been arbitrarily normalised to each other for comparison. In each case the intensity rapidly rises to a maximum, before gradually decreasing to around zero. The maximum ion lifetimes were around 150μs, 70μs and 40μs for Ar, He and H_2 respectively, in broad agreement with the expected $m^{1/2}$ dependence, where m is the ion mass.

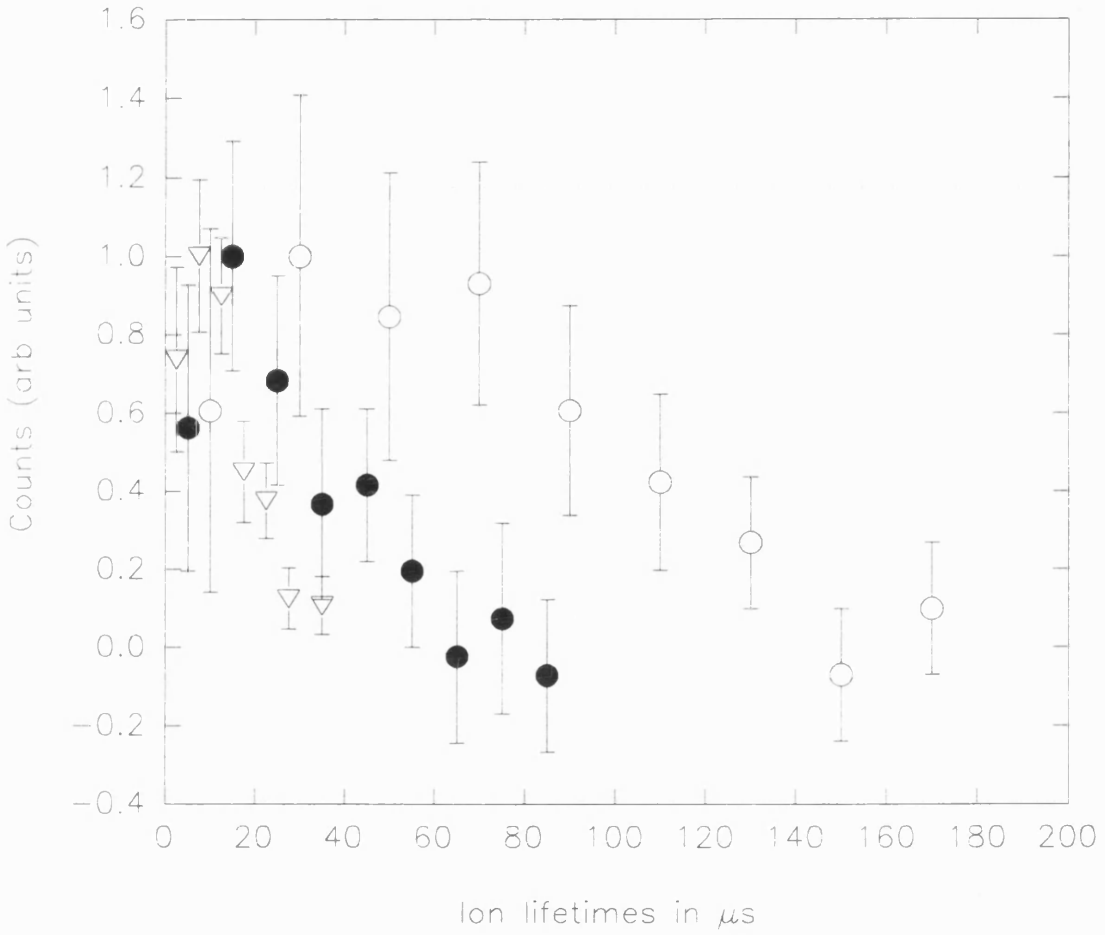

Figure 2.10. Distributions of ion lifetimes in the scattering cell for Ar o, He ● and H_2 ∇.

2.6 Summary

The main components of the apparatus used in this work have been described, with particular attention to the features which allow the system to be used to study ionisation phenomena. A novel scattering cell, incorporating an efficient ion extraction system, has been described along with the electronic circuit employed to characterise its performance.

CHAPTER 3

EJECTED ELECTRON ENERGY SPECTRA IN LOW ENERGY POSITRON-ATOM COLLISIONS

3.1 Introduction

Impact ionisation of an atomic target by a positively charged projectile may take place by a number of different processes. If an ejected electron is captured by the scattered projectile, then charge transfer will have taken place. If an electron leaves the target as a free particle, then direct ionisation will have occurred. In this case the energy and angular distributions of the ejected electrons may be strongly influenced by post-collision interactions. In particular, the Coulomb interaction between a scattered projectile and an ejected electron may cause the two particles to emerge from a collision with a high degree of correlation. If the relative velocity of the outgoing particles is close to zero, the ejected electron may be considered to have been transferred to a continuum state of the projectile. This process has been called electron capture to the continuum (ECC) and may give rise to a cusp-like peak in the ejected electron energy spectrum, having a maximum when the velocities of the scattered projectiles ($\underline{v}_p$) and ejected electrons ($\underline{v}_e$) are equal. The ECC peak is a well known feature of the electronic energy spectra arising from the ionisation by the impact of protons and positive ions of gaseous targets (e.g. Crooks and Rudd 1970, Rodbro and Andersen 1979, Knudsen *et al* 1986) and from thin foils (Harrison and Lucas 1970). ECC is most likely to occur when $\underline{v}_p$ is comparable to that of the target electron involved (Rodbro and Andersen 1979). At such velocities, these projectiles are unlikely to be significantly deflected by an

ionising collision, due to their relatively large mass. Hence, the ECC electrons usually have a narrow angular distribution around the direction of the incident beam.

It has recently been proposed that ECC may also result in structures in the ejected electron energy spectra arising from positron impact ionisation. (Brauner and Briggs 1986, Mandal *et al* 1986, Sil *et al* 1991, Schultz and Reinhold 1990). Since a positron has the same mass as an electron, ECC would result in all the available kinetic energy being shared approximately equally between the two particles and the process would be characterised by the emission of electrons with a distribution of kinetic energies peaked at E_{ECC} where

$$E_{ECC}=\frac{E_{+}-E_{I}}{2} \qquad (3.1)$$

Here E_I is the ionisation potential of the target and E_+ is the mean kinetic energy of the incident positrons. However, the ECC electrons may not necessarily be forwardly peaked, since a positron may well be deflected to wide angles by such a collision (e.g. Schultz and Olson 1988, Sil *et al* 1991).

3.1.1 ECC in Ionisation by Protons and Positive Ions

The first evidence of ECC was obtained by Rudd *et al* (1966), while studying proton impact ionisation of He and H_2. They measured the doubly differential ionisation cross-sections ($d^2\sigma/dEd\Omega$), differential in electron energy (E) and emission angle, over a range of impact energies from 100keV to 300keV. For electron emission at small angles, significant discrepancies were found with the first order Born approximation calculation of Oldham (1965). This calculation did not account for correlation in the final state and predicted that the electron energy distribution would fall almost monotonically with energy as shown in figure 3.1. For both targets Rudd *et al* (1966) found that $d^2\sigma/dEd\Omega$ at 10°, the smallest angle investigated, was found to contain ridges or

humps when plotted against E. The humps occurred around energies for which $\underline{v}_e = \underline{v}_p$. Following a suggestion by Oldham (1967), it was proposed that this was due to electrons being carried along in a continuum state of the protons.

Salin (1969) used the more elaborate distorted-wave Born-approximation to calculate $d^2\sigma/dEd\Omega$ for 300keV proton impact on H. Here correlation was accounted for by a Coulomb distortion of the final state wave function. The forward enhancement in $d^2\sigma/dEd\Omega$ observed by Rudd *et al* (1966) for $\underline{v}_e \approx \underline{v}_p$, was successfully reproduced, however a quantitative comparison with the experimental results was not possible due to the different targets employed by the two groups.

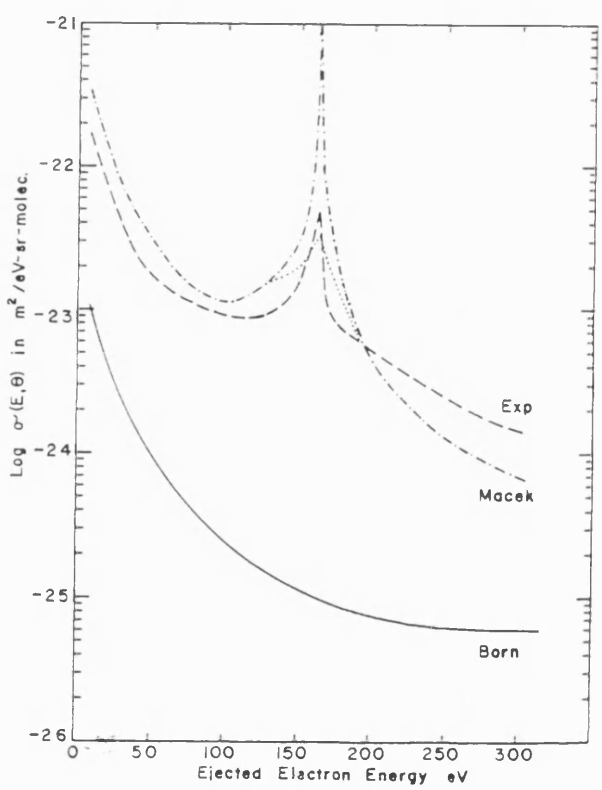

Figure 3.1. Cross-section for electrons ejected from He at 0° by 300keV protons (Macek 1970), dash-dot line; 1.4° Macek (1970), dotted line; 0° (Crooks and Rudd 1970), dashed line.

Macek (1970) calculated $d^2\sigma/dEd\Omega$ for He and H_2 bombarded by 300keV protons, using Fadeev's three body scattering formalism. The structures in $d^2\sigma/dEd\Omega$, noted by Rudd *et al* (1966) for emission at 10° were accurately reproduced and the results for both targets were found to be in reasonable agreement with the experimental values. In addition, a pronounced cusp in the ejected electron energy distribution was predicted for electrons emitted at 0°, when $\underline{v}_e = \underline{v}_p$.

This was experimentally verified by Crooks and Rudd (1970), who measured $d^2\sigma/dEd\Omega$, for electron emission around 0° for He bombarded by 100-300keV protons. The results for 300keV impact are shown in figure 3.1. Also shown are those of Macek (1970) for electron emission at 0° and 1.4°. Both the experimental and theoretical results contain a similar cusp-like peak at around 163eV, the ejection energy corresponding to $\underline{v}_e = \underline{v}_p$. The magnitude of the experimental peak lies between the theoretical curves for 0° and 1.4°. This is attributed to the ±1.4° angular resolution of the apparatus.

Harrison and Lucas (1970) observed similar structures in the energy spectra of secondary electrons ejected in the forward direction, by proton and H_2 ions transmitted through thin C and Au foils. The ejected electron energy distributions were found to contain ECC peaks, over a range of incident energies from 110keV to 320keV.

Experimental studies of this process have now been extended to other targets (e.g. Ne and Ar, Rodbro and Andersen 1979) and multiply charged projectiles (Knudsen *et al* 1986). Rodbro and Andersen (1979) measured $d^2\sigma/dEd\Omega$ for proton impact at energies in the range (15-1500)keV and found the yield of ECC electrons to reach a maximum when $\underline{v}_p \approx 1.4\underline{v}_i$, where $\underline{v}_i$ is the orbital velocity of the target electron involved. For increasing impact energies the ECC yield was found to fall off in a similar way to that for capture to bound states.

3.1.2 ECC in Ionisation by Positrons

Some recent calculations (Brauner and Briggs 1986, Mandal *et al* 1986, Sil *et al* 1991) predict that ECC may also result in the presence of cusp-like structures in the ejected electron energy spectra arising from positron impact ionisation. On the other hand, a classical calculation by Schultz and Reinhold (1990) indicates that ECC may only result in a slight enhancement of the electron energy distribution, in the form of a ridge around E_{ECC}. Schultz and Reinhold (1990) point out that the wide angular distribution of the scattered positrons may cause the ECC electrons to be distributed over a wide range of angles, diminishing the magnitude of any structures in $d^2\sigma/dEd\Omega$. The results of Schultz and Reinhold (1990), Mandal *et al* (1986) and Sil *et al* (1991) are shown in figures 3.2 and those of Brauner and Briggs (1986) in figure 3.3.

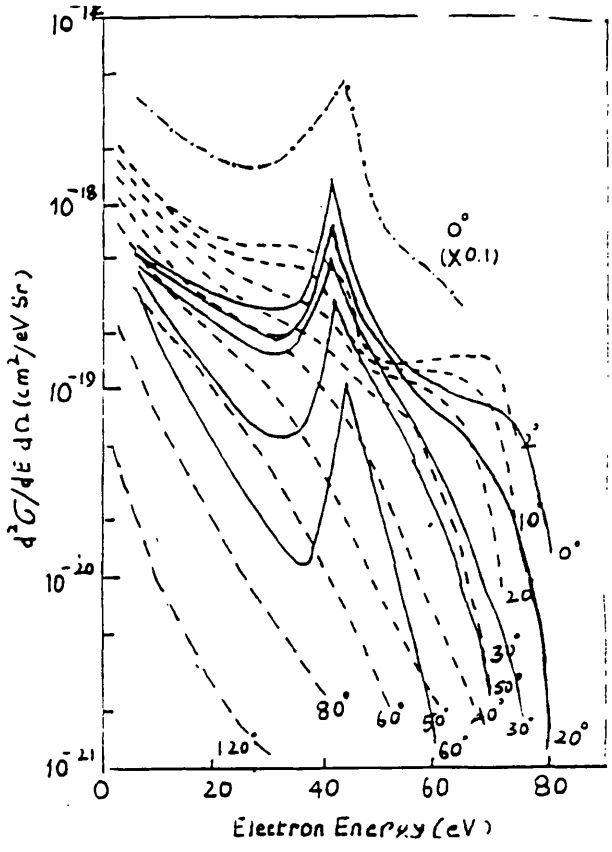

Figure 3.2. $d^2\sigma/dEd\Omega$ for electron emission from H by 100eV positrons. Solid line, Sil *et al* (1991); dashed line, Schultz and Reinhold (1990); dash-dot line, Mandal *et al* (1986) x0.1.

Mandal *et al* (1986) used the three body Fadeev formalism to calculate $d^2\sigma/dEd\Omega$ for 100eV positron impact ionisation of H. The result of their calculation, which was for electron emission at 0° relative to the incident beam, is shown in figure 3.2. The electron energy distribution was found to contain a pronounced cusp, peaked at E_{ECC} as given by equation 3.1.

By employing the same final state wave functions as Brauner and Briggs (1986) (see below), Sil *et al* (1991) calculated $d^2\sigma/dEd\Omega$ for 100eV positron impact on H. This calculation was performed for a range of emission angles from (0-60)° and predicted that there should be ECC cusps in $d^2\sigma/dEd\Omega$, for all emission angles investigated. These results are also shown in figure 3.2.

In a classical trajectory Monte-Carlo calculation, Schultz and Reinhold (1990) obtained a different result for the same system. The resulting variation of $d^2\sigma/dEd\Omega$ with electron energy is shown in figure 3.2, for a range of emission angles from 2° to 120°. Also shown are the scaled results of Mandal *et al* (1986) for comparison. In contrast

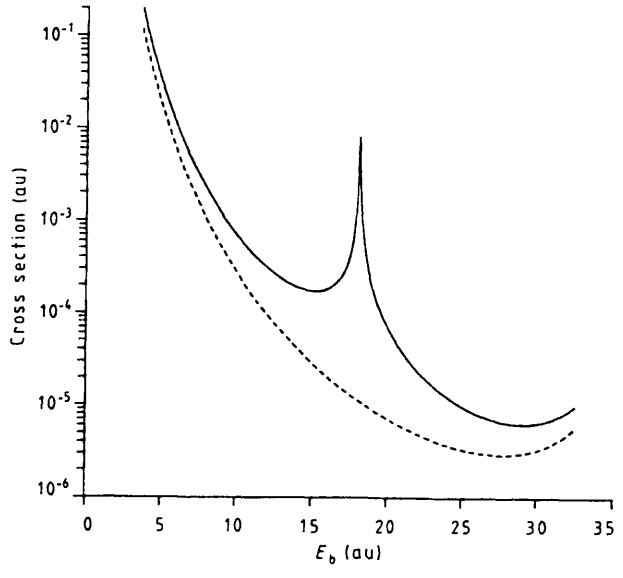

Figure 3.3. Triple differential cross-section for electron emission from H, at 0°, by 1keV positrons (Brauner and Briggs 1986).

with the findings of Mandal *et al* (1986) and Sil *et al* (1991), the results of Schultz and Reinhold (1990) do not contain the pronounced cusps, due to ECC. Instead, small ridges are present around E_{ECC}, for ejection angles up to 30°. Schultz and Reinhold (1990) attribute the near absence of a cusp in their results to the scattering of positrons to wide angles. Therefore, although ECC may occur, such electrons may be distributed over a wide range of angles and the magnitude of the peak in $d^2\sigma/dEd\Omega$ may be significantly reduced.

Brauner and Briggs (1986) calculated the triple differential cross-section at 0°, as a function of the electron emission energy. They used a first order Born-approximation with an electron-positron Coulomb wave in the final state. For collisions of 1keV positrons with H, a cusp was predicted around E_{ECC}, as shown in figure 3.3. These authors also predicted the existence of a dip or anti-cusp in the cross-section when the projectile is an electron.

Experimental evidence for the existence of this anti-cusp was recently obtained by Guang-yan *et al* (1992) who measured the triple differential cross-sections for electron scattering from He and Ar over a range of incident energies from 600eV to 1000eV. This complemented the work of Yamazaki *et al* (1990) who measured the electron energy spectra, in the forward direction, for electrons emitted from carbon foils by anti-proton impact. These authors also found evidence of an anti-cusp. However, the interpretation of their results is complicated by effects of target thickness and a high background of energetic secondary electrons.

3.1.3 Experimental Evidence of ECC in Positron-Atom Collisions and the Present Work

In an experiment to measure the ionisation cross-section of He, Coleman (1986) also measured retarding field spectra of the ejected electrons. This was done by applying a variable potential to a grid in front of the electron detector,

causing only those electrons with kinetic energies greater than a certain value to be detected. The results for 200eV impact are shown in figure 3.4. This indicates that the vast majority of electrons are ejected at velocities much smaller than the scattered projectile.

The first evidence that electrons may be emitted with energies close to E_{ECC} was obtained in a similar way by Charlton *et al* (1987). Results are shown in figure 3.5 for 200eV positron impact on Ne, plotted as a function of a reduced retarding voltage to facilitate comparison with the theoretical results of Brauner and Briggs (1986) which are shown integrated and normalised for comparison. When plotted in this way, E_{ECC} corresponds to around 0.5V/eV. The electron count rate appears to fall to a plateau, with values just above zero, before falling to around zero by 0.5V/eV, indicating that there is some electron emission around E_{ECC}. However, the large statistical uncertainties of these results inhibit a firm conclusion.

In order to determine the significance of ECC in positron-atom collisions, and to provide some guidance for theory, the present work has been carried out. The kinetic energies of electrons, ejected in the forward direction from an Ar target by positron impact have been measured and compared with theoretical expectations. Ar was chosen as a target because of its comparatively high ionisation cross-section (Knudsen *et al* 1990). Two different approaches were employed to measure the electron energies: a time-of-flight (TOF) technique and a retarding electric field method. In both cases the remnant ion was detected and used to gate the data acquisition system, so that data was only recorded from events associated with ionisation of the target. In this way it was possible to discriminate between electrons ejected from the target atoms and the large background of secondary electrons ejected from other parts of the apparatus, such as grids and apertures, by stray positrons and electrons.

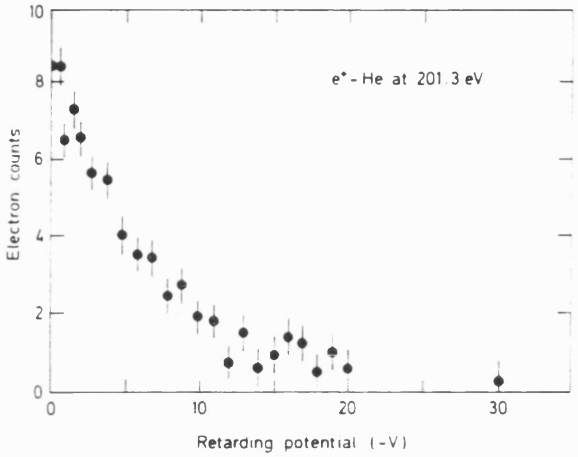

Figure 3.4. Electron count rate versus retarding potential (Coleman 1986).

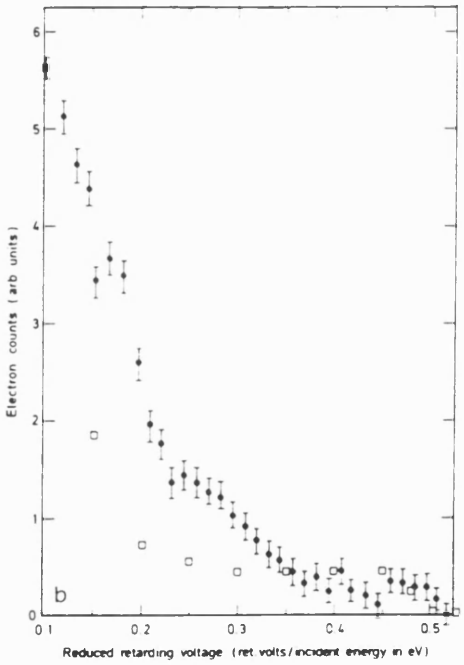

Figure 3.5. Results of Brauner and Briggs (1986) integrated and normalised, □; Results of Charlton *et al* (1987) for 200eV positron impact on Ne, •.

3.2 Experimental Details

The apparatus is shown schematically in figure 3.6, in the configuration used to make TOF measurements. Its main features are described in detail in chapter 2. In order to measure electron flight-times, a beam tagger prior to the scattering cell was employed and a flight tube and repeller grid were incorporated after the scattering cell. The retarding field profiles were measured, with the tagger removed from the beam-line, using an analyzer grid in front of the electron detector (C1).

A primary positron beam was obtained by the moderation of β^+ particles emitted by radioactive positron sources, using W meshes. The TOF measurements were made with a 4mCi ^{22}Na source resulting in a primary beam with an intensity of around $4x10^3 s^{-1}$. The beam was accelerated to a mean energy of around 350eV before being guided to a second moderator (M2), incorporated in the beam tagger. The operation of this device is described in section 3.3. The retarding field measurements were made with a beam with an intensity of around $3x10^4 s^{-1}$, derived from a 70mCi ^{22}Na source. The beam was in this case transported to the interaction region with the tagger retracted from the beam-line.

The interaction region comprised the gas scattering cell and ion extractor described in section 2.4. Following positron impact ionisation of gas atoms, electrons ejected in the forward direction were transported along a flight-tube of around 1m in length by a uniform magnetic field set up inside a solenoid. The electrons were detected at the end of the beam-line using C1, as shown in figure 3.6.

A repeller grid, between two earth grids approximately 9mm apart, was placed just after the exit aperture of the scattering cell. A potential of around 500V was applied to this grid in order to prevent positrons from travelling further along the beam-line and liberating secondary electrons from grids near the electron detector, C1, resulting in a distortion of the measured electron energy

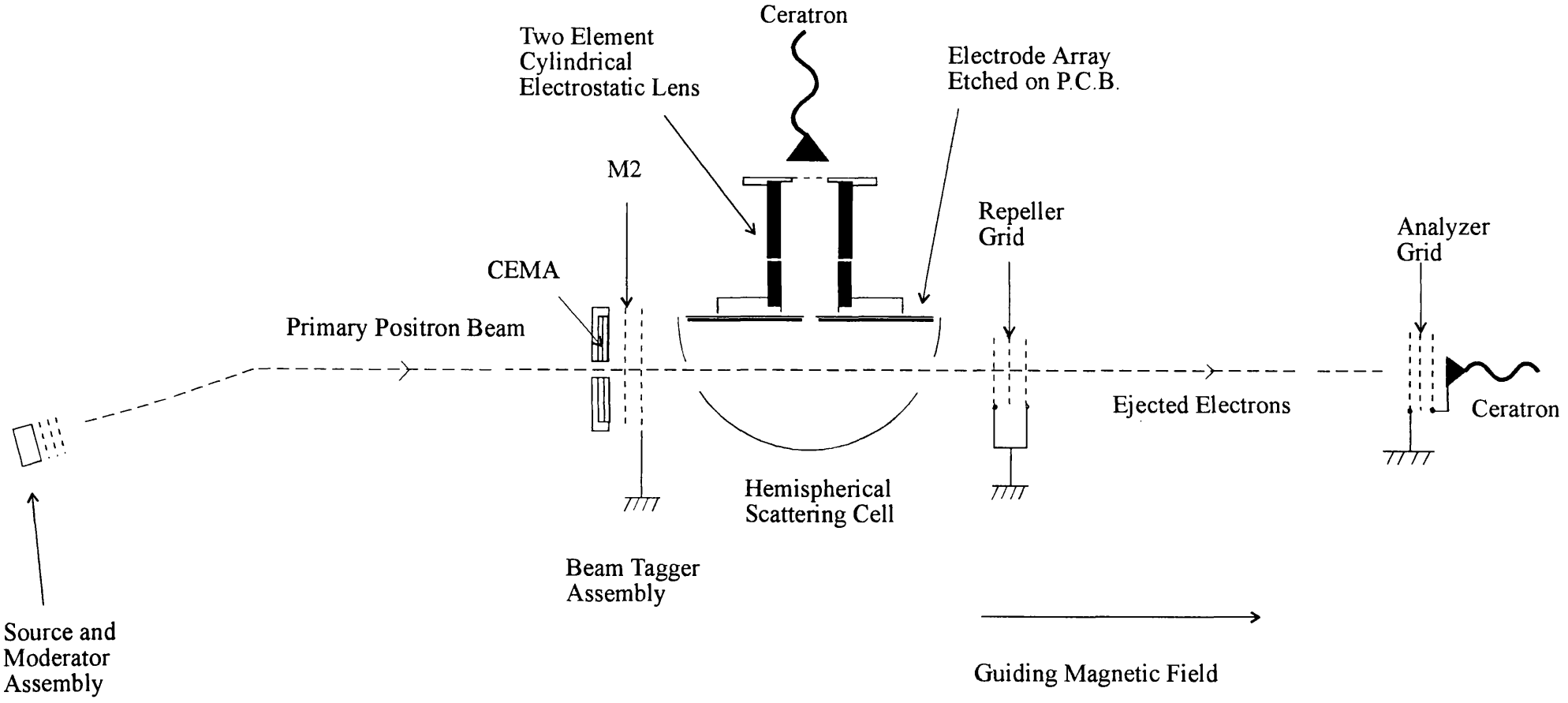

Figure 3.6 A schematic diagram of the apparatus used to measure ejected electron energy spectra (not drawn to scale).

spectra. The use of this grid did however cause positrons to be reflected back through the interaction region. The effects of multiple traversals are discussed below.

The magnetic field strength from the scattering cell onwards was reduced to around 10G, in order to reduce the pitch angles of the incident positrons and to limit the angular acceptance of the electron detection system, so that only those electrons ejected at small angles, relative to the beam axis, would be confined by the magnetic field to reach C1. By limiting the detection system to accept only those electrons with small transverse components of kinetic energy, the measured longitudinal component was approximately equal to the total kinetic energy. Additionally, according to certain theories, the ECC electrons were expected to be ejected at small angles in the forward direction.

3.2.1 The Transmission Probability Function

In order to estimate the angular acceptance of the electron detection system, the transmission probability function, $T(E,\theta)$, of the apparatus was estimated. $T(E,\theta)$ is defined as the probability of an ejected electron passing through the exit aperture of the scattering cell and reaching the active area of the detector, as a function of emission energy (E) and angle (θ), relative to the incident beam. $T(E,\theta)$ was estimated by solving the equations of motion for electrons with a given E and θ but with a large number of different starting co-ordinates, equally spaced over the entire range of possible starting points within the interaction region. The ratio between the total number of trajectories and the number of trajectories passing through the exit aperture of the scattering cell and reaching the detector was then used as an estimate of the transmission probability.

Throughout this derivation, the magnetic field strength is assumed to be uniform and not time varying. In vector notation, the equation of motion of a charged particle with

velocity $\underline{v}$, in a magnetic field $\underline{B}$ may be written

$$\frac{d\underline{v}}{dt} = \frac{q}{m}(\underline{v} \times \underline{B}) \qquad (3.2)$$

where q and m are the charge and mass of the particle respectively. If a cartesian co-ordinate system is chosen so that the z-axis is parallel to $\underline{B}$, equation (3.2) may be re-written

$$\frac{d\underline{v}}{dt} = \omega_c (v_y \hat{x} - v_x \hat{y}) \qquad (3.3)$$

where

$$\omega_c = \frac{qB}{m} \qquad (3.4)$$

and v_x and v_y are the components of velocity in the directions of the x and y axes. Solving equation (3.3), to find the particles position (x,y,z) as a function of time, it can easily be shown that

$$x(t) = -\frac{V_\perp}{\omega_c}\cos(\omega_c t + \eta) + x_0 + \frac{V_\perp}{\omega_c}\cos\eta \qquad (3.5.a)$$

$$y(t) = \frac{V_\perp}{\omega_c}\sin(\omega_c t + \eta) + y_0 - \frac{V_\perp}{\omega_c}\sin\eta \qquad (3.5.b)$$

$$z(t) = v_\parallel t + z_0 \qquad (3.5.c)$$

where (x_0, y_0, z_0) are the starting co-ordinates of the particle, η is the initial angle of its trajectory, relative to the y axis and $v_\perp$ and $v_\parallel$ are the components of velocity parallel and perpendicular to $\underline{B}$ when t = 0.

Using equations (3.5.a) to (3.5.c) the radial distance of an ejected electron from the beam axis may be calculated as a function of its distance along that axis. Thus, for a given starting point and initial velocity, it is possible to

calculate whether a trajectory will pass through the exit aperture of the scattering cell and reach the active area of the detector, since the position and radius of both are known.

A computer code was written to perform this task for around 32×10^3 trajectories for each different value of E and θ. The starting points of the trajectories were equally spaced over the region of overlap between the beam and target gas, inside the scattering cell, and were incremented in steps of 5mm along the z-axis and 1mm along the x and y-axes whilst η was varied over 360° in steps of 10°. The number of trajectories that passed through the exit aperture of the scattering cell and reached the detector were counted and the ratio between this number and the total number of trajectories was taken to be the transmission probability for

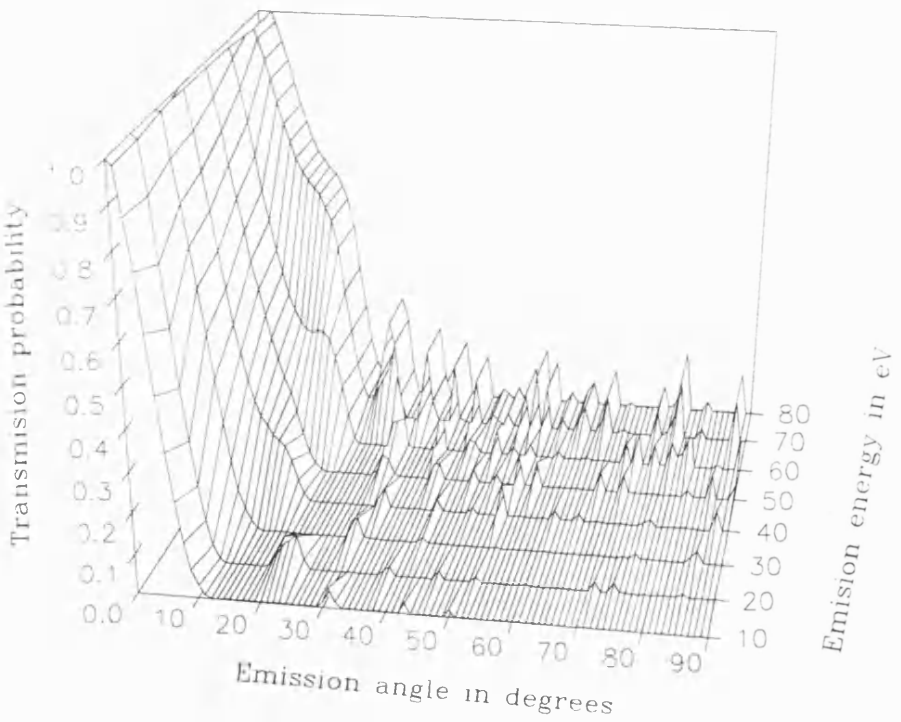

Figure 3.7. The estimated transmission probability function, T(E,θ), of the apparatus.

that value of E and θ. This was repeated for different values of E and θ to obtain the transmission probability function illustrated in figure 3.7.

$T(E,\theta)$ is strongly forward peaked around 0°, as required, and falls to around zero between 10° and 20° for E between 10eV and 80eV. For a given E, as θ is increased from zero, the Larmor radius of the particle will increase until it is large in comparison with the radius of the exit aperture, reducing its probability of passing through, thus causing $T(E,\theta)$ to be forwardly peaked. At larger emission angles however, $T(E,\theta)$ appears to contain a number of minor peaks. If both the distance from the starting point of a trajectory to the exit aperture of the cell and the distance from this point to C1 are both integer multiples of the particles pitch distance, then, even if the Larmor radius is far greater than the radius of the aperture, the particle may still pass through the aperture and reach C1. This is the reason for the secondary peaks in $T(E,\theta)$. However, this method of estimating $T(E,\theta)$ is rather crude and its results are not expected to be exact. The calculation was performed under the assumptions of a parallel, uniform magnetic field, uniform gas density throughout the interaction region and uniform beam intensity across its diameter. These conditions are unlikely to be met in an apparatus of this type and for these reasons, no physical significance is attached to the secondary peaks in $T(E,\theta)$. However, the shape of the primary peak around 0° is expected to be reasonably accurate.

3.3 The Beam Tagger

Positrons were time tagged following the method developed by van House *et al* (1984) and Laricchia *et al* (1988). The beam tagger comprised a W mesh re-moderator (M2) and an annular set of (Galileo MCP10 48-208) micro-channel-plates (CEMA). Secondary electrons ejected from M2, by bombardment from the primary beam, were detected by CEMA and used to generate

timing signals. Re-emitted positrons were formed into a secondary beam by the application of a positive potential to M2.

The beam tagger is shown in figure 3.8. The primary positron beam passed through a 10mm diameter hole in the centre of CEMA1 before impinging on M2. This moderator consisted of five, superimposed, 90% transmission W meshes with an active area of around 15mm and was annealed in the same manner as the primary moderator, described in section 2.2. Immediately adjacent to M2 was a 95% transmission Cu earth grid (G1). This and M2 were held in position between Al apertures supported by nylon insulators. CEMA was mounted in a recess, machined in a ceramic holder. The inner surface of the hole through the ceramic holder was coated with graphite and held at a negative potential (-V), in order divert

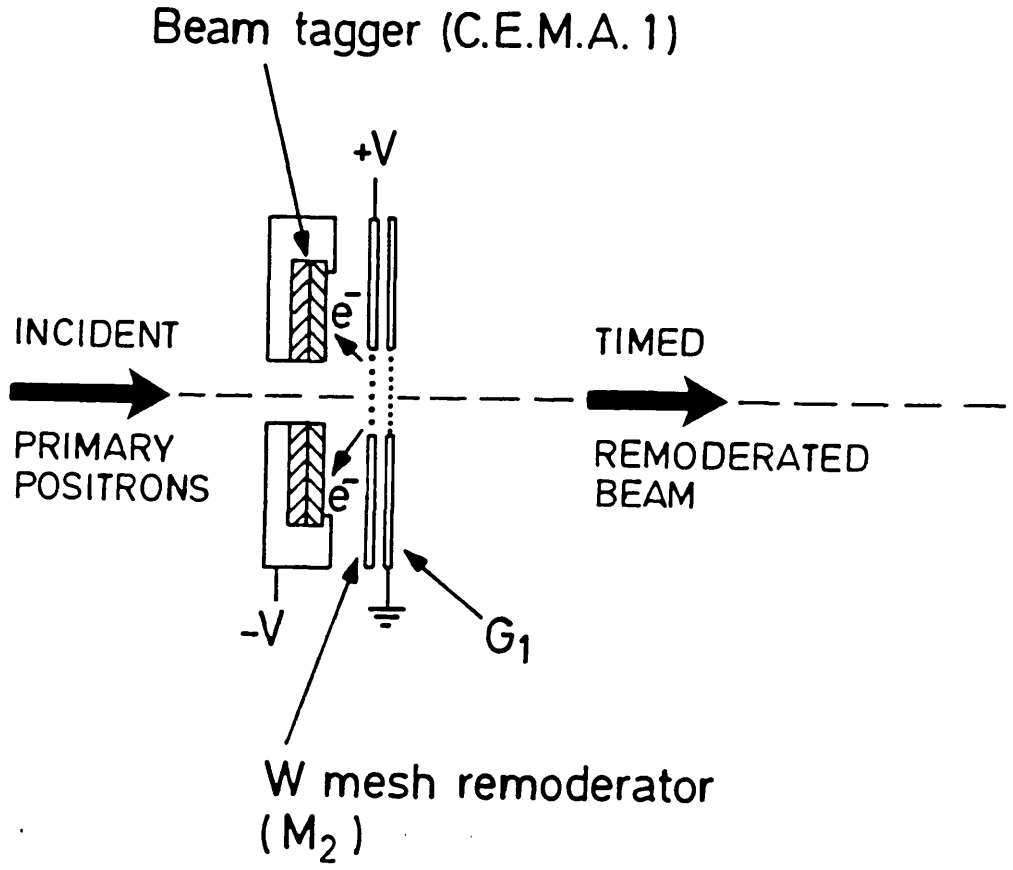

Figure 3.8. A schematic diagram of the beam tagger (not drawn to scale) showing M2 and CEMA.

electrons from M2 towards CEMA, thereby increasing the tagging efficiency. The negative potential also served to remove electrons from the primary beam, before reaching M2. The front of CEMA was held at 300V, to accelerate secondary electrons from M2 for detection. This potential also caused some of the positrons emitted from the rear of M2 to be reflected back through the meshes increasing the secondary beam intensity. The rear of CEMA was held at 3.5kV. The recess in the ceramic holder was coated with electrically conducting paint to act as a charge collector for CEMA, and held at 3.8kV. Signals were extracted from the charge collector via a decoupling capacitor. The tagger assembly was supported on a manipulator shaft, allowing the unit to be rotated or moved up and down to find the optimum position, or to be removed from the axis of the beam-line when not in use.

The performance of the beam tagger was measured using the delayed coincidence timing circuit, shown in figure 3.9. This comprised a TAC, MCA and associated pulse shaping circuitry. To make these measurements, the magnetic field strength from the scattering cell to C1 was increased to

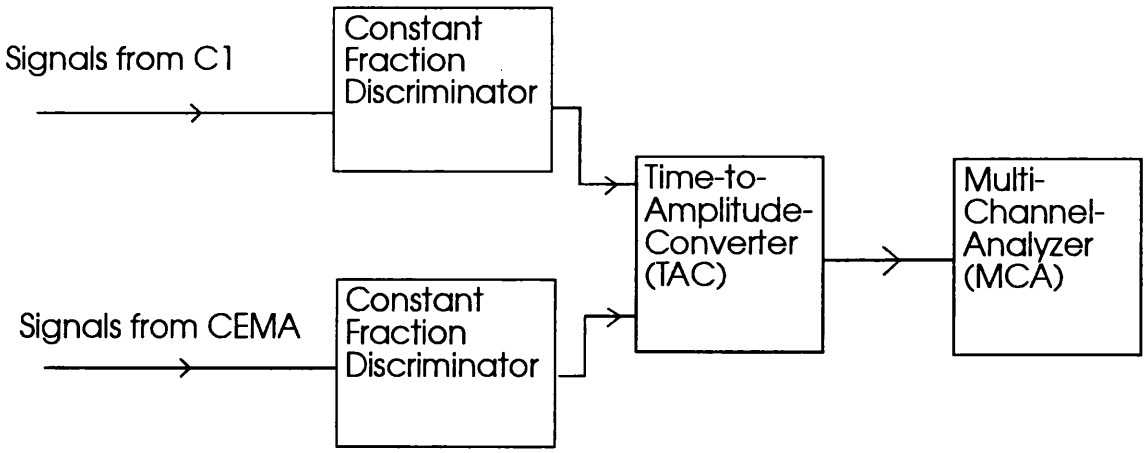

Figure 3.9. A schematic diagram of the circuit used to measure the performance of the beam tagger.

around 50G, in order to optimise the beam transport efficiency. Signals from C1 and from CEMA were converted into fast negative logic pulses by two constant-fraction discriminators, and used as the start and stop signals respectively for the TAC. Stop signals were delayed, so as to arrive at the TAC after the corresponding start pulses, thus generating an inverted TOF spectrum on the MCA. An inverted timing sequence was employed to reduce the probability of pulses from C1 arriving during the TAC dead time, due to the high count rate from CEMA ($\sim 10^4$). The spectra contained a peak, due to timed positrons, and a small background arising from randomly correlated signals. By summing the counts in the peak, the number of timed positrons was determined. This was found to be up to around 36% of the re-moderated positrons.

The use of the tagger resulted in a beam with two main components: a re-moderated secondary beam and that part of the primary beam that was transmitted through M2. The relative intensities of these two components were determined by measuring the count rate at C1 while biasing off the re-moderated beam, by applying a potential of around 6V above that applied to M2 to the analyzer grid in front of C1 (see figure 3.6). By noting the reduction in the count rate at C1 when the secondary beam was biased off, and measuring the primary beam intensity with the beam tagger removed, it was estimated that the respective intensities of the transmitted primary and secondary components were around 45% and 7%of that of the primary beam.

3.4 The Electronics

TOF spectra were obtained by using signals from C1 and CEMA to generate spectrum on a gated delayed coincidence spectrometer. Retarding field measurements were obtained by ramping a potential applied to the analyzer grid in front of C1, while measuring the count rate at C1. In both cases

signals from the ion extractor were used to gate the system so that data was only recorded when a residual ion was detected.

Figure 3.10 is a block diagram of the electronic circuit used to measure TOF spectra. During the experiment the count rate at C1 was around $60s^{-1}$ and the count rate at CEMA was of the order of 10^4s^{-1}. Pulses from C1 and CEMA were processed by two constant fraction discriminators, CFD1 and CFD2, and used as the start and stop signals respectively for the TAC. Pulses from CFD2 were delayed so that they would arrive at the TAC after the corresponding start pulse from CFD1. This was accomplished using a suitable delay cable. The TAC was operated in its strobe mode, in which the output is stored until a logic pulse is presented to the strobing input. This allowed the system to be gated by signals from the ion detector C2. The output of the TAC was fed through a normally open linear gate to the MCA. Start pulses were delayed by $12\mu s$ and then presented to one input of an OR gate. This delay was sufficient to allow an ion to be extracted from the interaction region and transported to C2. The output of the OR gate was then shaped and used to strobe the TAC. This signal was also used as a blocking pulse to inhibit the linear gate, thus preventing the output of the TAC from reaching the MCA. Hence, after $12\mu s$, if no signal had been detected from C2, the TAC would automatically be strobed while the linear gate was closed and its output would be prevented from reaching the MCA. Signals from C2 were used to trigger a third constant fraction discriminator, CFD3, the output of which was presented to the other input of the OR gate. Thus if an ion was detected, within $12\mu s$ of the ion extractor being pulsed on, the TAC would get strobed before the blocking pulse was presented to the linear gate, and the TAC output would reach the MCA.

The spectrometer was calibrated by timing a beam of positrons with a known mean kinetic energy as it travelled the accurately measured distance from M2 to C1. The true flight time was calculated and used to calibrate the

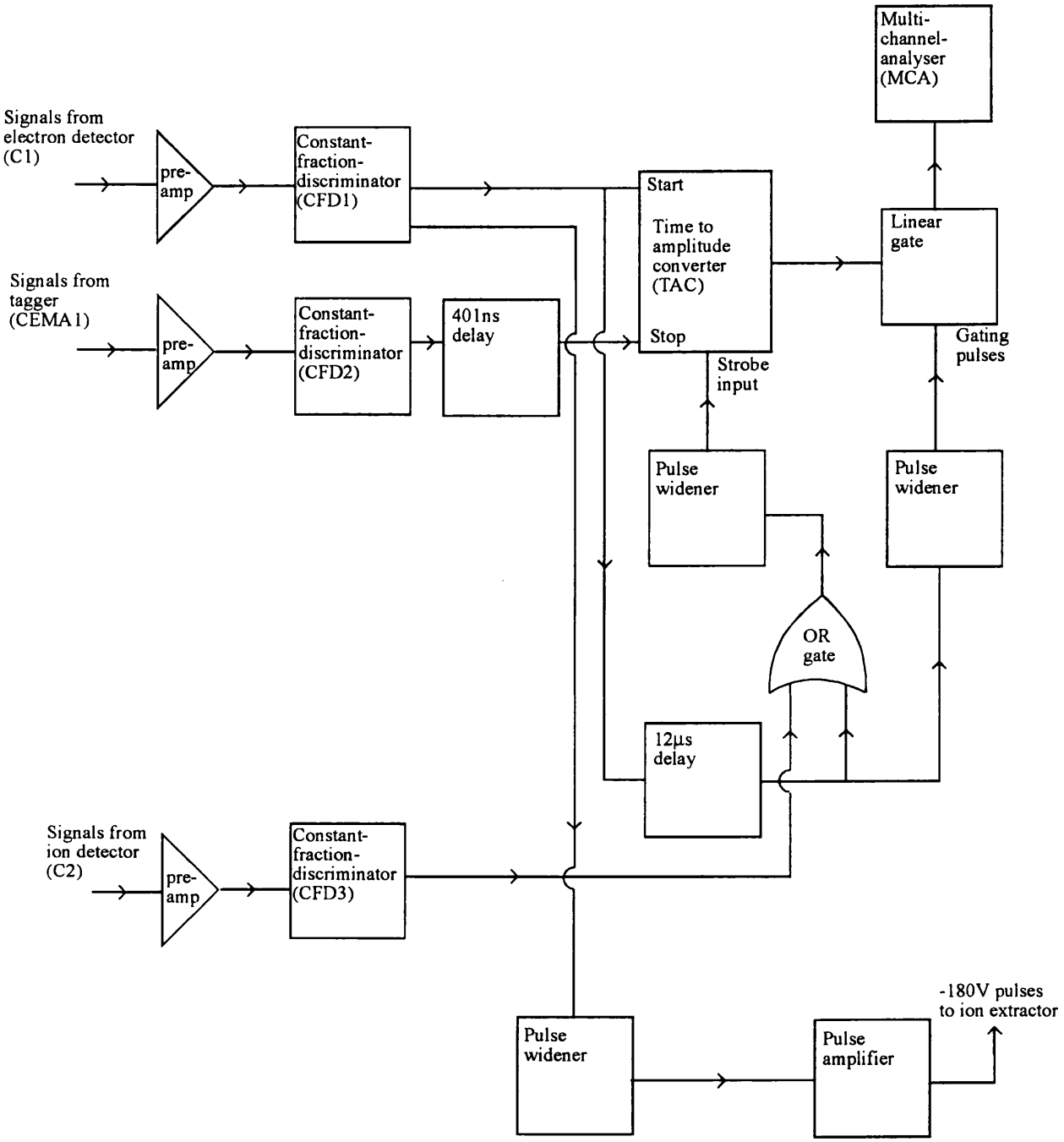

Figure 3.10. A schematic diagram of the circuit used to measure TOF spectra.

spectrometer. The spectrometer was operated with the TAC in its normal (unstrobed) mode and the blocking input to the linear gate disconnected. These measurements were made with no target gas in the scattering cell and with the ion extractor turned off. The resulting TOF spectra contained a peak, corresponding to remoderated positrons of mean energy E_+. The channel number corresponding to the peak in such spectra, $ch(E_+)$, was measured as a function of the mean beam energy E_+. The time per channel (τ) and the channel corresponding to time zero (ch_0) were then obtained from the following relationship.

$$ch(E_+) = ch_0 - \frac{d}{\tau\sqrt{2\frac{e}{m}E_+}} \qquad (3.6)$$

where d is the distance between CEMA1 and C1, and e/m is the charge to mass ratio of an electron. By plotting $ch(E_+)$ as a function of $E_+^{-1/2}$ a straight line was obtained from which τ and ch_0 were found from the gradient and vertical intercept respectively.

Retarding field measurements of the ejected electron energies were made using the circuit shown in figure 3.11. Data was collected on a 512 channel multi-channel-scaler (MCS), operated in a single sweep mode with a dwell time of 100s per channel. Pulses from C1 were used to trigger a constant fraction discriminator, CFD1, the output of which was delayed for 4μs and widened to 8μs before being presented to the input of an overlap coincidence unit. Pulses from C2 were shaped by a second constant fraction discriminator CFD2, the output of which was presented to the other input of the overlap coincidence gate. The output of this unit was fed to the data input of a MCS. Thus, if an ion was detected by C2 between 4μs and 12μs (the range of flight times for Ar ions) after an electron was detected by C1, a count was recorded on the MCS. Channel advance signals were derived from a ramp

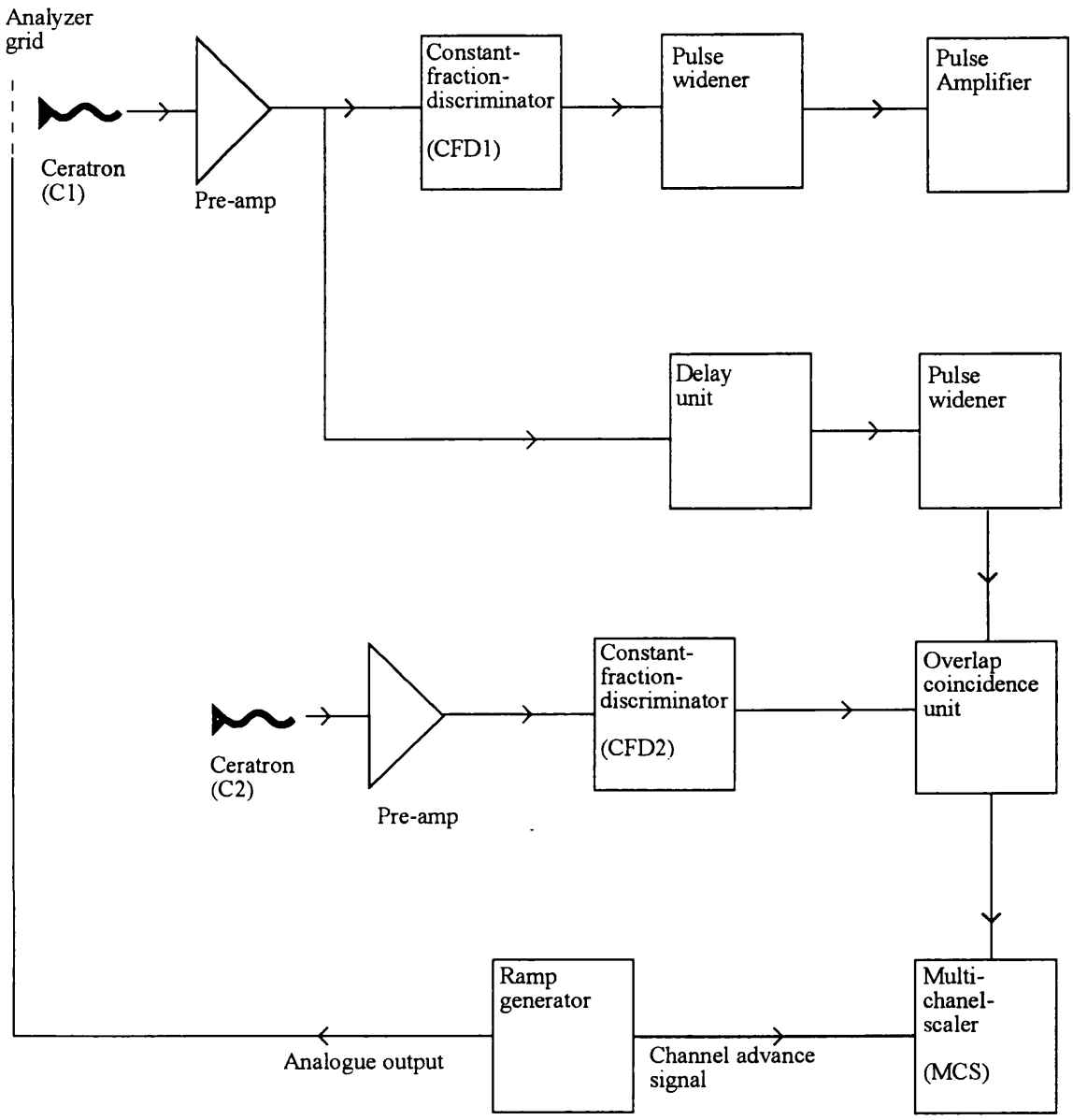

Figure 3.11. A schematic diagram of the circuit used to measure retarding potential spectra.

generator each time the output voltage increased. This voltage was amplified and applied to the analyzer grid in front of C1. In this way a retarding field spectrum was accumulated on the MCS, while data was gated by signals from the ion detector.

In both cases, in order to prevent the electric field of the ion extractor from deflecting the beam in the interaction region, the potential applied to its electrodes was pulsed on by signals from C1. The positive going output from CFD1 was widened and used to trigger the MOSFET pulse amplifier which provided 12μs long pulses of -180V for the ion extractor.

3.5 Data Restoration

Data was collected in the form of either TOF or retarding field spectra. In order subtract background contributions and derive ejected electron energy spectra, the following data restoration procedures were employed.

3.5.1 Restoration of TOF Spectra

The TOF spectra contained background contributions arising from random coincidences between signals from the three detectors. The magnitude of these contributions were assessed and where significant, corrected for. The background contributions may be divided into two categories.

The first arose from un-correlated timing signals from C1 and CEMA arriving in coincidence with a signal from C2. This was expected to contribute a flat background to a TOF spectrum, since the signals from C1 and CEMA were randomly correlated in time. The magnitude of this background was estimated by averaging counts over a number of channels in a flat part of the TOF spectra where no signal was expected. The portion of the spectra chosen for this purpose was that corresponding to ejection energies in excess of (E_+-E_I). The

average number of background counts per channel was then subtracted from each TOF spectrum.

The second form of background was caused by uncorrelated signals from C2 causing the system to time electrons not associated with the creation of an ion, such as secondary electrons ejected from grids or apertures by stray positrons. In order to determine the magnitude of this form of background, the ion signal was replaced by a pulse train from a signal generator, thus gating the system randomly, whilst timing electrons in the usual way. A spectrum taken in this way was found to contain less than 5% of the number of counts in a similar spectrum obtained when the system was gated the same number of times by signals from the ion extractor. This component of the background was considered negligible and was not subtracted.

After subtracting the background, TOF spectra were converted into electron energy spectra by summing data into bins corresponding to equal increments in electron energy. The widths of the increments were 3, 5 and 7eV for impact energies of 50, 100 and 150eV respectively. The bin widths were chosen to be as wide as possible, to reduce statistical uncertainties, and yet still be narrow enough to resolve any structure in the spectra resembling that predicted by theory. The kinetic energies (E) of the ejected electrons were calculated from the measured flight times (T) using

$$E = \left[\frac{d_-}{T\sqrt{2\frac{e}{m}} - \frac{d_+}{\sqrt{E_+}}} \right]^2 \qquad (3.7)$$

where E is in eV, d_+ is the distance from M2 to the midpoint of the scattering cell and d_- is the distance from this point to C1.

3.5.2 Restoration of Retarding Field Spectra

Retarding field spectra were converted into energy spectra by summing the data in increments corresponding to 5eV and then differentiating with respect to the retarding potential. The summation was performed to reduce the statistical scatter of the data and the bin width was chosen with the same criteria as applied to the TOF spectra, i.e. to minimise statistical scatter, without significant loss of energy resolution. The spectrum was differentiated by subtracting the data in each 5eV increment from that in the preceding one.

The magnitude of the background contribution arising from data acquired when the system was randomly gated by uncorrelated ion signals was estimated by replacing the ion signal with pulses from a pulse generator. This contribution was again found to be negligible.

3.6 Systematic Effects

The most significant sources of uncertainty affecting the measurements, their consequences and the way they were estimated, are discussed below.

Multiple scattering of incident positrons may have resulted in ionising collisions involving positrons with unknown impact energies and pitch angles. Electrons ejected by such positrons would have lower energies than those produced by unscattered positrons and would result in a distortion of the energy spectra. The probability of multiple scattering is difficult to estimate accurately, without detailed knowledge of the differential cross-sections involved. However, it is reasonable to assume that this probability is significantly smaller than that of single scattering and this may be estimated since the total scattering cross-section of Ar is well known. Values of Q_t were used to estimate beam attenuations, i.e. the fraction of the incident beam that was scattered, and all the data

presented below were obtained with small beam attenuations, thus ensuring that multiple scattering effects were small.

The scattering of ejected electrons could also result in the degradation of ejected electron energies and the scattering of electrons into, or out of, the range of angular acceptance of C1, causing a distortion of the derived energy spectra, increasing the number of counts at low energies and reducing the magnitude of any observed structure caused by ECC. The probability of an ECC electron being scattered was estimated using the electron Q_t and by assuming that, on average, an ejected electron traverses half the scattering cell, with a small pitch angle, since electrons with pitch angles greater than around 15° were unlikely to reach the detector as shown in section 3.2.1.

The repeller grid located after the scattering cell caused unscattered positrons to pass back through the interaction region. Such positrons would have sufficient kinetic energies to pass through M2 and be reflected back into the forward direction by the primary moderator. However, the increased distance (≈3m) would have resulted in flight times that were outside the range covered by the TOF spectra. This would also have no detrimental effect on the retarding field measurements, since the incident energy of the positrons would not be altered.

More significant was the effect of multiple traversals of the cell by positrons that had undergone some form of scattering and had a reduced longitudinal component of momentum allowing them to be reflected back through the scattering cell by M2. Any electrons ejected by these positrons may also have arrived at C1 with apparently delayed flight times. For example, if a 100eV positron lost a small amount of energy and re-traversed the interaction region after reflection from M2, an electron ejected with 37eV (corresponding to E_{ECC}) would appear in a TOF spectrum at a time corresponding to around 16eV. However, at 37eV the transmission probability was estimated to be almost zero for pitch angles greater than around 15° and it is unlikely that

a scattered positron would be able to pass through the scattering cell apertures and re-traverse the cell. This effect is therefore expected to be small.

The uncertainty in electron energy, measured by the TOF method, was predominantly due to the uncertainty in starting position along the length of the scattering cell ($\Delta E/E \approx \pm 10\%$), the uncertainty caused by the distribution of electron pitch angles ($\Delta E/E \approx \pm 6\%$), the timing resolution ($\Delta E/E \approx \pm 11\%$, for 50eV electrons) and the energy spread of the positron beam ($\Delta E/E \approx \pm 1.5\%$, for 100eV positrons). The net effect of these independent errors in the uncertainty in the measured electron energy is around ±16%.

The energy uncertainty in the retarding field measurements arose mainly from the incident beam energy spread and the distribution of pitch angles of the ejected electrons and was estimated to be around ±6%. The error bars on the results presented below all represent one statistical standard deviation.

3.7 Results and Discussion

The ejected electron energy spectrum shown in figure 3.12a) was derived from a retarding field spectrum measured at an impact energy of 106eV. The target gas pressure was around 0.5μmHg. From the value of the Q_t for Ar (Kauppila *et al* 1981), the probability of a positron at this energy being scattered in a single traversal of the scattering cell would be around 5%. At this impact energy E_{ECC} is around 45eV and the probability that such an electron will be scattered, when traversing half the interaction region, in a straight line, is around 5% (Golden and Bandel 1966).

The electron energy spectrum contains a large number of counts at low energies, rapidly decreasing in intensity with increasing emission energy, as expected. The distribution falls to close to zero by around 60eV. There is no evidence of any structure in this spectrum. However it does provide

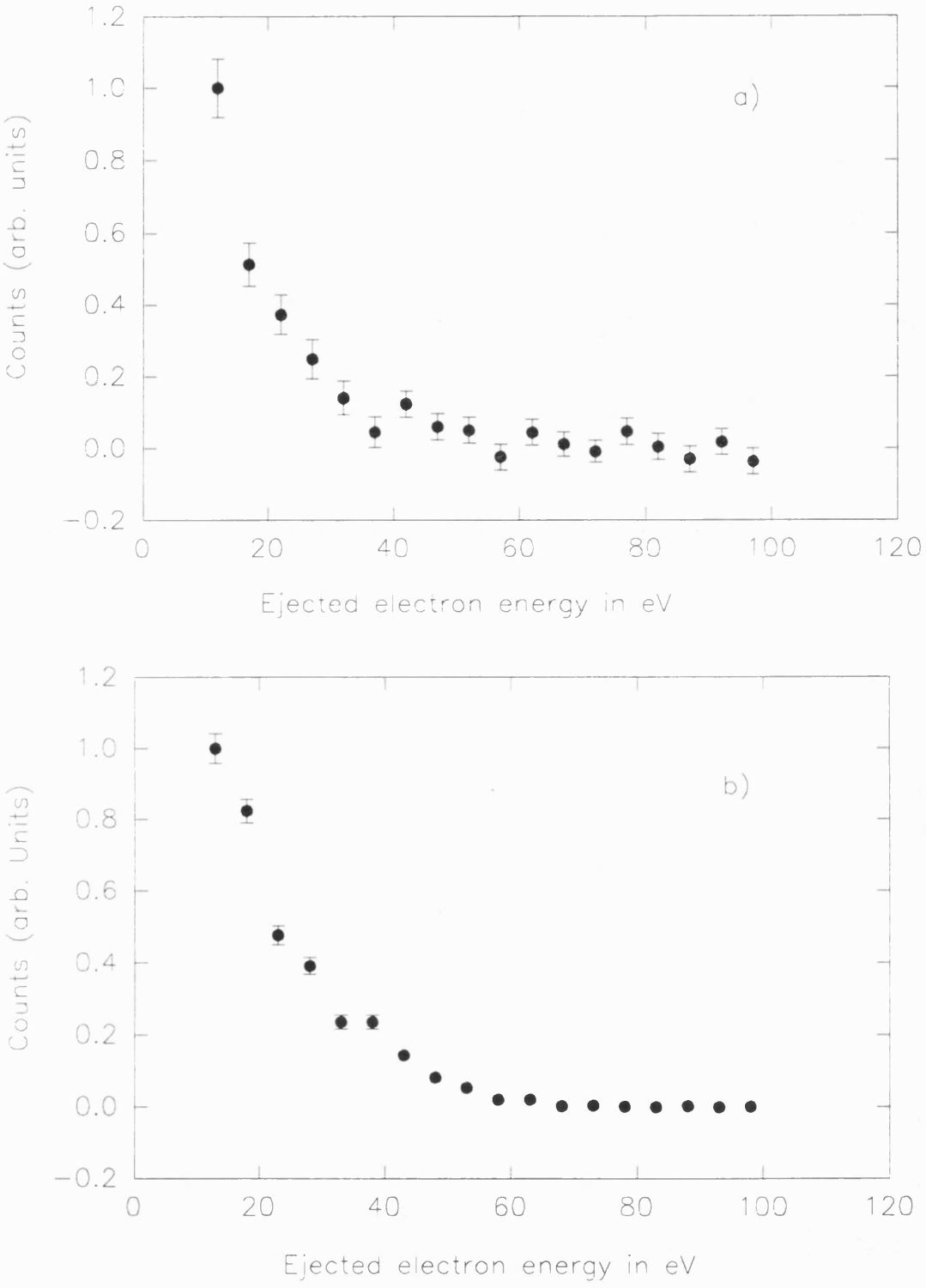

Figure 3.12. Ejected electron energy spectra obtained a) from a retarding potential spectrum at an impact energy of 106eV, and b) from a TOF spectrum at an impact energy of 100eV.

evidence of electron emission with kinetic energies in excess of E_{ECC}, since none of the systematic effects mentioned above would increase the apparent energies of the electrons, as the multiple positron scattering and electron scattering effects would result in the degradation of electron energies. The statistical uncertainties in this data would have obscured any structure resembling that predicted by Schultz and Reinhold (1990). These theoretical results have been convoluted with the estimated transmission probability function $T(E,\theta)$ and are shown in figure 3.13 for comparison. In contrast, any major structure, of the magnitude predicted by Mandal *et al* (1986) or Sil *et al* (1991), would have been resolved. The results of Sil *et al* (1991), convoluted with $T(E,\theta)$, are also shown in figure 3.13.

The remainder of the spectra presented here were obtained from TOF measurements. Here the systematic effects described above would cause the detection of electrons at delayed flight times and degraded kinetic energies. This would again lead to a distortion of the energy spectra, to increase the numbers of counts at low energies. The scattering of ECC electrons would have resulted in a reduction in the magnitude of any structure due to this process. Measurements were therefore made at pressures at which the probability of multiple scattering was small.

Figure 3.12b) shows an electron energy spectrum derived from a TOF spectrum measured with an impact energy of 100eV and at a gas pressure of 0.5μmHg. In this case E_{ECC} is around 42eV. The general shape of this spectrum is similar to that obtained from a retarding field profile, however the statistical uncertainties are smaller. There is a broad distribution of low energy electrons falling to close to zero around 60eV. A pronounced cusp of the type predicted by Mandal *et al* (1986) and Sil *et al* (1991) is not present. There is however some evidence of structure at intermediate emission energies, that is compatible with ECC. The point at 37eV lies around two standard deviations above a smooth line drawn through the other points and is therefore unlikely to

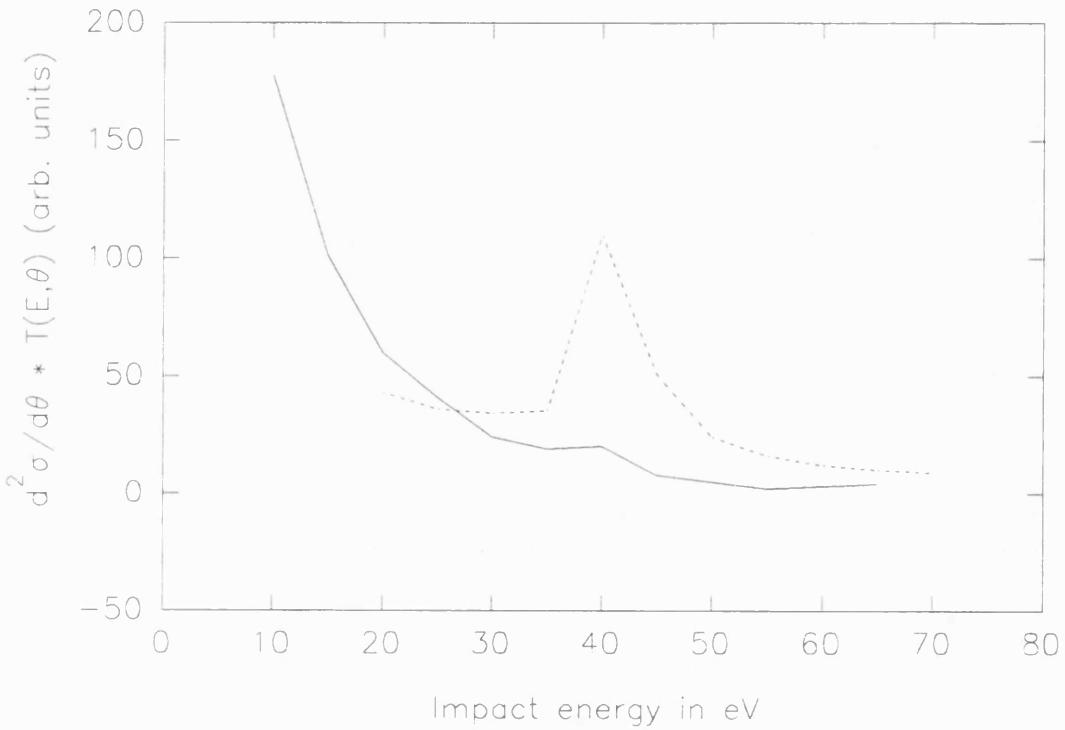

Figure 3.13. The results of Sil *et al* (1991) dashed line, and Schultz and Reinhold (1990) solid line, both convoluted with $T(E,\theta)$.

be a statistical fluctuation. Such an enhancement in the distribution resembles the structure predicted by Schultz and Reinhold (1990).

Figures 3.14 a) and b) are electron energy spectra obtained from TOF measurements at impact energies of 150eV and 50eV. The probability of a 150eV positron being scattered in a single traversal of the interaction region, is around 8% (Kauppila *et al* 1981) and approximately 6% of the ECC electrons, if they were to traverse the half the length of the scattering cell in a straight line, would be subsequently scattered (Golden and Bandel 1966). The effects of multiple scattering and electron scattering are therefore estimated to be small.

The count rate falls rapidly with increasing emission energy and is close to zero by around 90eV. One point at 60eV

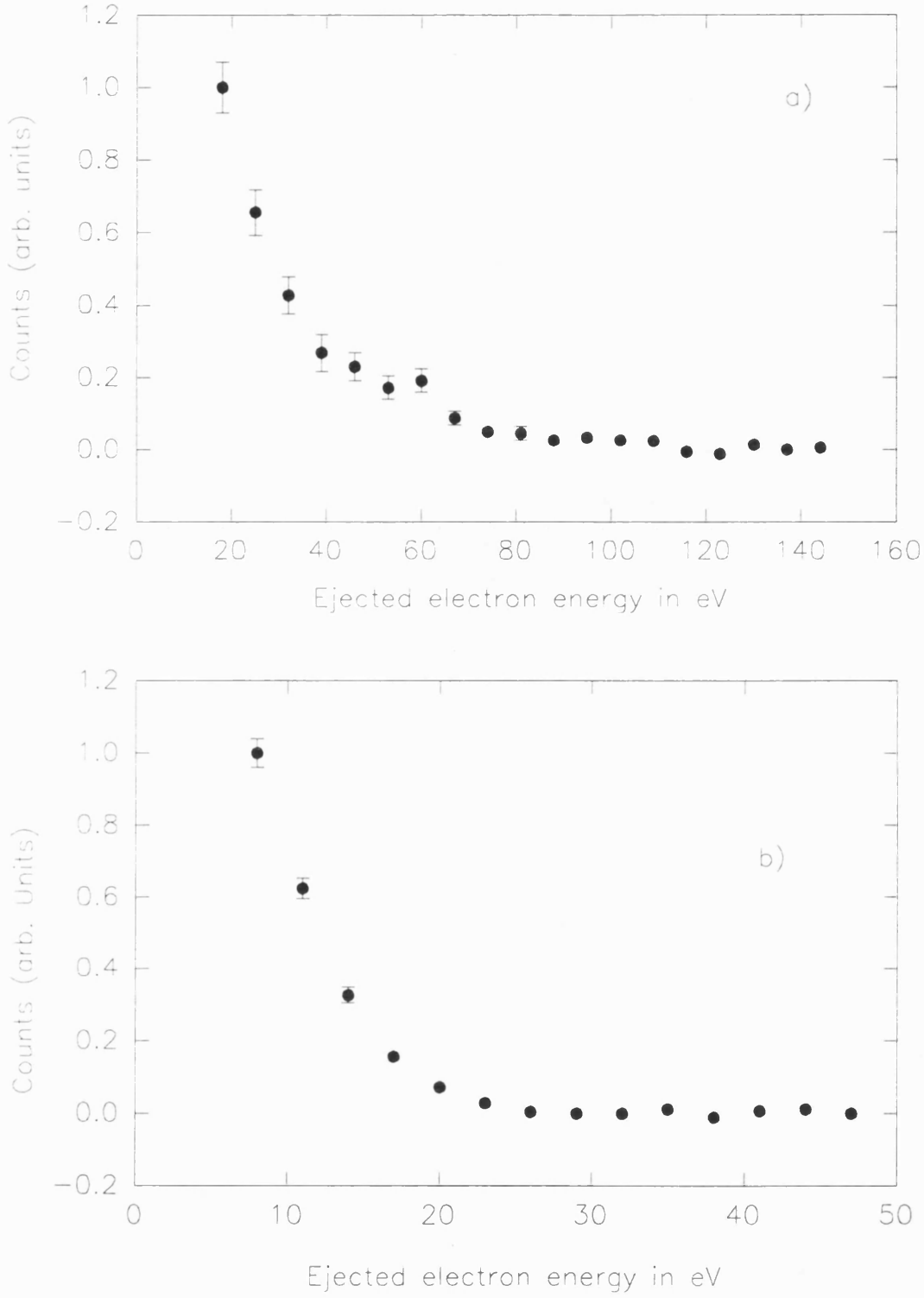

Figure 3.14. Ejected electron energy spectra obtained from TOF spectra at impact energies of a) 150 and b) 50eV.

lies around two standard deviations higher than a smooth line drawn through the other points. The ridge formed by this deviation again resembles the ECC structure predicted by Schultz and Reinhold (1990), and is close to E_{ECC} at 67eV. Again there is no evidence of a prominent cusp or peak in the vicinity of E_{ECC}.

The spectrum obtained at an impact energy of 50eV was measured at a gas pressure of 0.5μmHg. At this pressure a 50eV positron would have a 6% probability of scattering in the interaction region. At this impact energy E_{ECC} is around 17eV. Around 7% of the ECC electrons were estimated to be scattered before leaving the scattering cell (Golden and Bandel 1966). This spectrum contains no structure and decreases smoothly with increasing electron energy. The electron count rate is close to zero by around 26eV. There is no evidence of an ECC cusp.

All the spectra presented above were obtained in runs lasting typically around 24 hours. Spectra were also measured at higher gas pressures in order to increase signal rates, however no significant structure was observed, suggesting that the effects of multiple scattering and electron scattering may be significant at higher pressures. Similarly, there was no evidence of any structure in spectra obtained with an increased magnetic field strength (25G) around the interaction region. This may have been due to the reduced energy resolution or to the emission of ECC electrons being confined to small angles.

The small magnitude of the ECC structure in the measured spectra, makes it difficult to determine the energy dependence of the ECC yield. However, the contribution from ECC, albeit small, does appear to be greater at 100eV and 150eV than at 50eV. In the case of proton impact ionisation Rodbro and Andersen (1979) found that the yield of ECC electrons followed an energy dependence similar to that for capture to bound states and reached a maximum at projectile velocities around 1.4 times the orbital velocity of the captured electron. For a positron, this would occur at an

impact energy of around 30eV. However, if the low yield of ECC electrons in the forward direction is attributed to positron scattering to wide angles (Schultz and Reinhold 1990), then the yield may be influenced by the differential ionisation cross-section for the scattered positrons. This is expected to become more forwardly peaked with increasing impact energy (e.g. Schultz and Olson 1988) and may therefore cause the ECC yield in the forward direction to increase with impact energy, as observed.

3.8 Summary

The distribution of kinetic energies of electrons ejected in the forward direction from an Ar target by positron impact have been measured. These spectra have been compared with theoretical doubly differential cross-sections (Schultz and Reinhold 1990, Sil *et al* 1991, Brauner and Briggs 1986 and Mandal *et al* 1986) in order to assess the magnitude of its contribution to positron impact ionisation from ECC and compare available conflicting theories.

Electron energies were determined by a TOF technique and by a retarding electric field analyzer. In both cases the residual ion was detected and used to gate the data collection system, making it possible to discriminate between electrons ejected from the target gas and secondary electrons ejected from other parts of the apparatus.

None of the measured spectra contained any major cusp structure predicted by the theories by Mandal *et al* (1986) and Sil *et al* (1991). However, some of the spectra showed evidence of a small ridge at energies compatible with ECC, in qualitative agreement with the calculations of Schultz and Reinhold (1990). The small magnitude of these structures and the lack of a pronounced cusp suggests that ECC makes a minor contribution to ionisation by a light positively charged projectile for electron emission in the forward direction.

CHAPTER 4

TOTAL IONISATION CROSS-SECTIONS IN POSITRON-GAS COLLISIONS

4.1 Introduction

The two most significant processes by which positron impact may cause the ionisation of gaseous targets are direct ionisation and Ps formation, the latter being unique to positron scattering.

In this chapter, experimental values for the cross-sections for single ionisation by positron impact (Q_i^+) and Ps formation (Q_{Ps}) are reviewed and compared with theoretical expectations. Discrepancies are highlighted and the need for more precise measurements is discussed. In the present work, total ionisation cross-sections (Q_t^+) have been measured for a variety of atomic and molecular gases. Q_t^+, which includes contributions from all ionisation channels (including Ps formation) was determined by an ion-counting technique, using a modified version of the apparatus described in chapters 2 and 3. This work is described below.

4.1.1 Ps Formation Cross-Sections

Ps may be formed when a positron (e^+), of sufficient kinetic energy collides with an atomic or molecular target, A(M). This (capture) reaction may be expressed as

$$e^+ + A(M) \rightarrow Ps + A^+(M^+) \qquad (4.1)$$

where the Ps atom and/or the remnant ion may be left in an excited state. Since the binding energy of Ps in its ground state is 6.8eV, the threshold (E_{Ps}) for reaction (4.1), is at

(E_I-6.8eV) where E_I is the first ionisation potential of the target.

The first direct measurements of the energy dependence of Q_{Ps} were reported by Charlton *et al* (1980) for He, Ar, H_2 and CH_4, up to 12eV above E_{Ps}. The cross-sections were determined by measuring 3γ coincidences from the decay of o-Ps formed in a scattering cell. With an improved version of the apparatus, the same group measured Q_{Ps} for all the inert gases up to 150eV (Charlton *et al* 1983) and several molecular gases (Griffith 1983). However, the results were subsequently shown to have been subject to serious systematic errors (e.g. the loss of o-Ps to the walls of the scattering cell) and were up to a factor of five smaller than values of Q_{Ps} obtained in other experiments. These results will not be included in the discussion below.

Using a complementary technique, Fornari *et al* (1983) measured Q_{Ps} for He, Ar and H_2 up to around 80eV, by measuring the fraction of an incident positron beam that was lost due to Ps formation during its transmission through a scattering cell. In this experiment, the transmitted beam intensity and positron TOF spectra were measured simultaneously, with and without gas added to the cell. The fraction of the beam that underwent any kind of scattering (F) was determined by observing the attenuation of the beam in the TOF spectra. Almost all scattered positrons were constrained to reach the detector by a strong (100G) axial magnetic field, so that the fractional decrease in the beam count rate (f) was approximately equal to the fraction of the positrons that had formed Ps. After corrections for background and small angle scattering, values of Q_{Ps} were obtained from fQ_t/F, using values of Q_t available in the literature.

Measurements of Q_{Ps} were extended to higher impact energies by Diana *et al* (1986,1986a) and to the remaining inert gases by Diana *et al* (1985,1987,1989). In the region of overlap, these results agree with those of Fornari *et al* (1983) but at higher impact energies they contain unexplained structure.

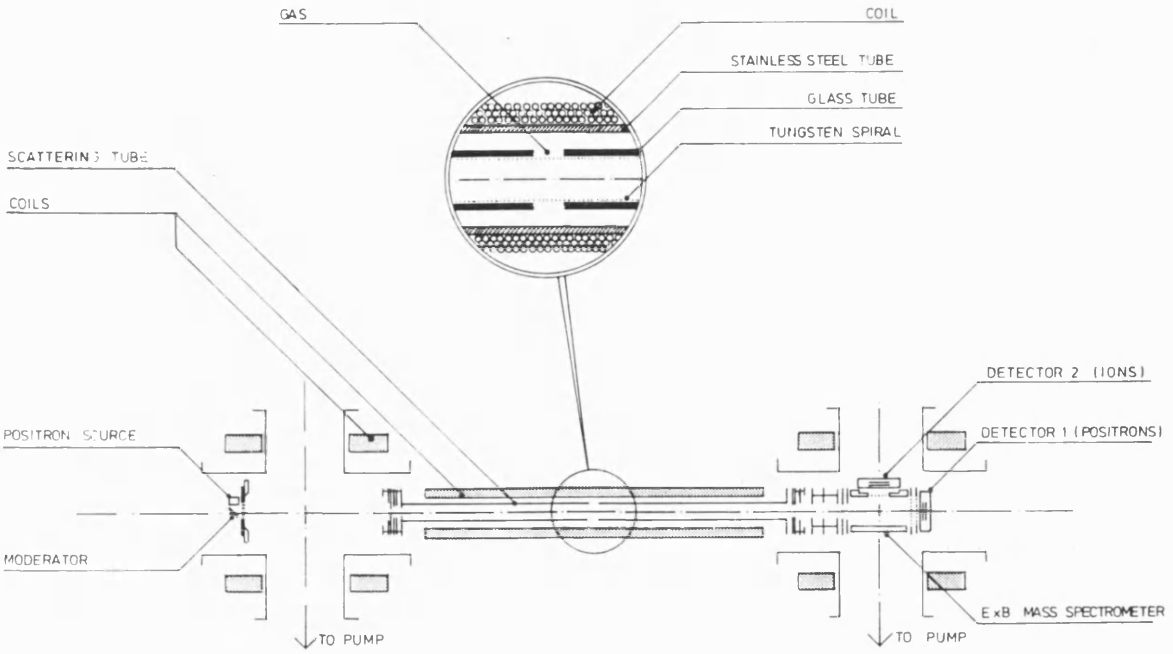

Figure 4.1. A schematic diagram of the apparatus used by Fromme *et al* (1986,1988) to measure Q_{Ps} and Q_i^+.

Fromme *et al* (1986,1988) measured Q_{Ps} for He and H_2 using the apparatus shown in figure 4.1. A longitudinal magnetic field was employed to guide the beam through a long differentially pumped scattering tube, from which ions could be extracted and detected. By measuring the total ion-yield and the number of positron-ion coincidences in ion-TOF spectra, both Q_{Ps} and Q_i^+ were measured simultaneously. The results for Q_{Ps} in He agree well with those of Fornari *et al* (1983), below 80eV, but do not contain the structure noted by Diana *et al* (1986) at higher energies.

The experimental results for He, referred to above, are shown in figure 4.2 along with the results of a polarised-orbital calculation by Khan *et al* (1985), the distorted-wave calculation of Mandal *et al* (1979) and the first-order exchange calculation by Roy *et al* (1984). Below around 30eV

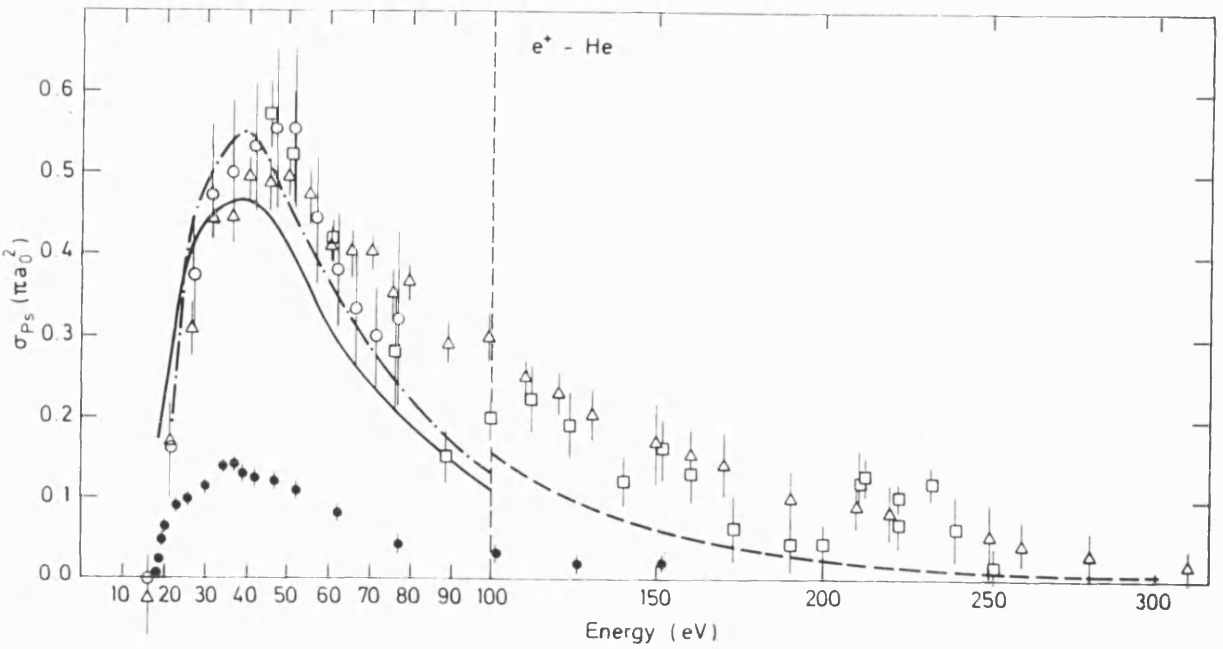

Figure 4.2. Q_{Ps} in He. Experiment: Charlton *et al* (1983),•; Fornari *et al* (1983),○; Fromme *et al* (1986),△; Diana *et al* (1986),□. Theory: Khan *et al* (1985), solid line; Mandal *et al* (1979), dash-dot line; Roy *et al* (1984) dashed line.

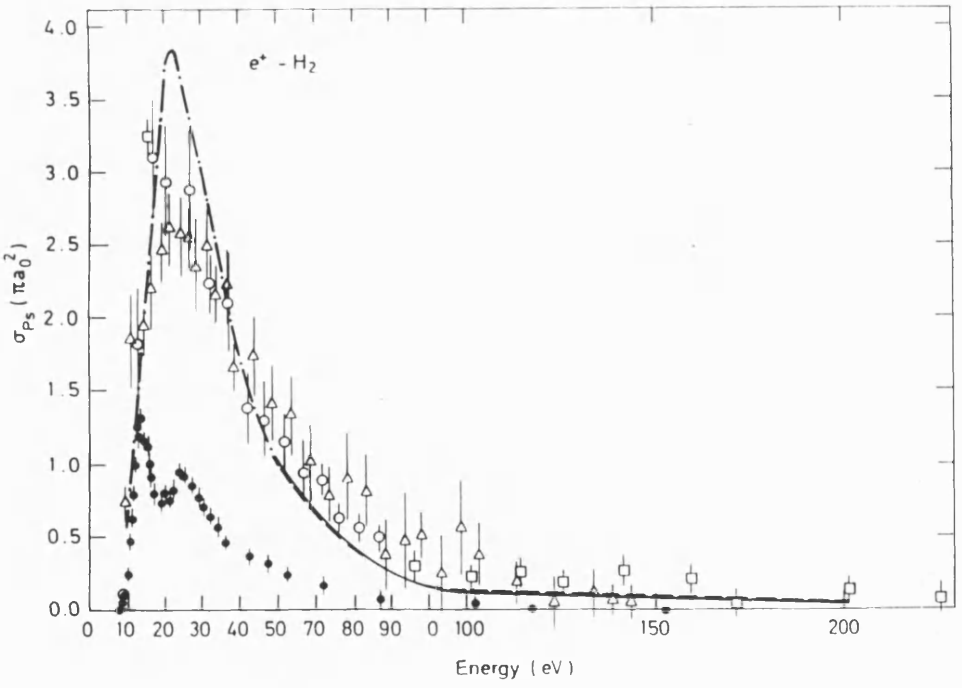

Figure 4.3. Q_{Ps} in H_2. Experiment: Charlton *et al* (1983),•; Fornari *et al* (1983),○; Diana *et al* (1986),□; Fromme *et al* (1988),△. Theory: Ray *et al* (1980), dashed line; Sural and Mukherjee (1970), solid line; Bussard *et al* (1979), dash-dot line.

the theoretical results lie above the experimental data and reach their maximum values around 10eV lower. The magnitudes of the maxima are in accord with experiment within the statistical scatter, but the theoretical results fall significantly below experiment by around 50% at 100eV. The results of the first-order exchange calculations of Roy *et al* (1984) for energies between 100eV and 300eV also lie well below the experimental results.

The results of Khan *et al* (1985) include contributions from ground state (Khan and Ghosh 1983) and first excited state Ps formation, the results of Mandal *et al* (1979) only contain contributions from Ps formed in its ground state, while the results of Roy *et al* (1984) include contributions from the first five excited states. The experimental results contain contributions from all excited states, however it is unlikely that the reason for the discrepancy between the experimental and theoretical values of Q_{Ps} can be attributed to the neglect of excited state Ps, since above around 50eV, these contributions are expected to fall off as n^{-3} where n is the principle quantum number of the Ps formed (Mandal *et al* 1980 and Khan *et al* 1984,1985).

In a CTMC calculation (not shown) Schultz and Olson (1988) found that the values of Q_{Ps} should fall with energy (E), approximately as $E^{-3.5}$ above around 100eV. These authors point out that the experimental results fall as E^{-1} to $E^{-1.5}$ whereas most of the theoretical cross-sections decay as E^{-3} to E^{-5} and suggest that the discrepancy may be due to incomplete confinement of the scattered positrons in the experiments. Results of a more recent experiment by Overton *et al* (1993) exhibit an energy dependence in better agreement with theoretical expectations.

Comparison between theory and experiment may also be made in the case of H_2, as shown in figure 4.3. Ray *et al* (1980) used a Jackson-Schiff approximation for energies above 50eV, obtaining results that are almost identical to those of a Born approximation calculation by Sural and Mukherjee (1970). Both of these are slightly lower than the

experimental values obtained by Fornari *et al* (1983), Diana *et al* (1986) and Fromme *et al* (1988) which are, as already mentioned, in reasonably good agreement with each other. Bussard *et al* (1979) estimated Q_{Ps} semi-empirically at low energies and used the results of Sural and Mukherjee (1970) at high energies, resulting in an estimate of Q_{Ps} that exceeded experiment by around 30% at the maxima in the cross-section.

Q_{Ps} in H has recently been measured by Sperber *et al* (1992) using a technique similar to that of Fromme *et al* (1986,1988). The apparatus is shown in figure 4.4. An electrostatically guided positron beam was crossed with a beam containing H, obtained from a Slevin type discharge tube (Slevin and Stirling 1981). Due to the limited angular acceptance of the positron detection system, wide angle scattering corrections were necessary. These were estimated by using the first Born approximation to calculate the fraction of ionising positrons scattered outside the angular range of acceptance of the detector (30°). Contributions from dissociative ionisation of the residual H_2 in the gas jet and Ps detection by the positron detector were found to be negligible. A mass analyzer (QMA) was used to distinguish between protons and H_2 ions. The values obtained for Q_{Ps} are shown in figure 4.5 where they are compared with theory. A large number of calculations have been performed for this simple system, but for clarity only a few representative examples are shown.

The first Born approximation calculation of Massey and Mohr (1954) predicts a cross-section with a maximum value close to that of the experiment, it does however occur at a slightly lower energy. However this approximation is not well suited to such a reaction and Sperber *et al* (1992) point out that the good agreement may be fortuitus. Other calculations which yield maximum values consistent with the experiment include the first-order exchange calculations of Mandal and Guha (1979) (not shown), the distorted wave approximation of Mandal *et al* (1979) (not shown) and the Fock-Tani calculation

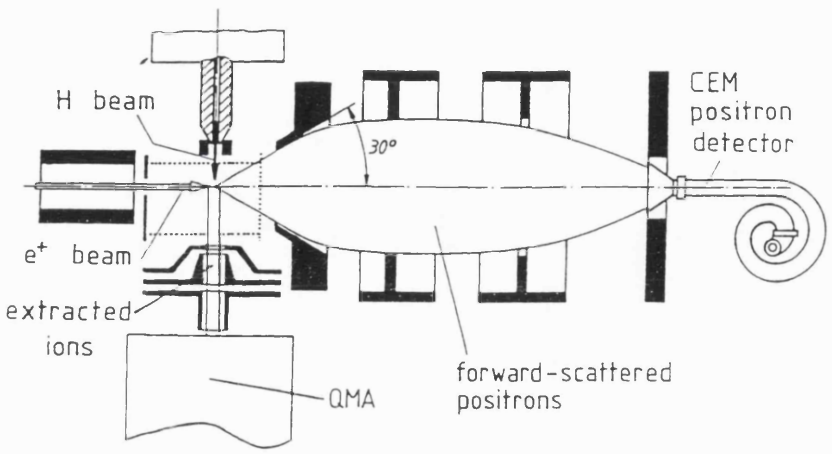

Figure 4.4. A schematic diagram of the apparatus used by Sperber *et al* (1992) to measure Q_{Ps} in H.

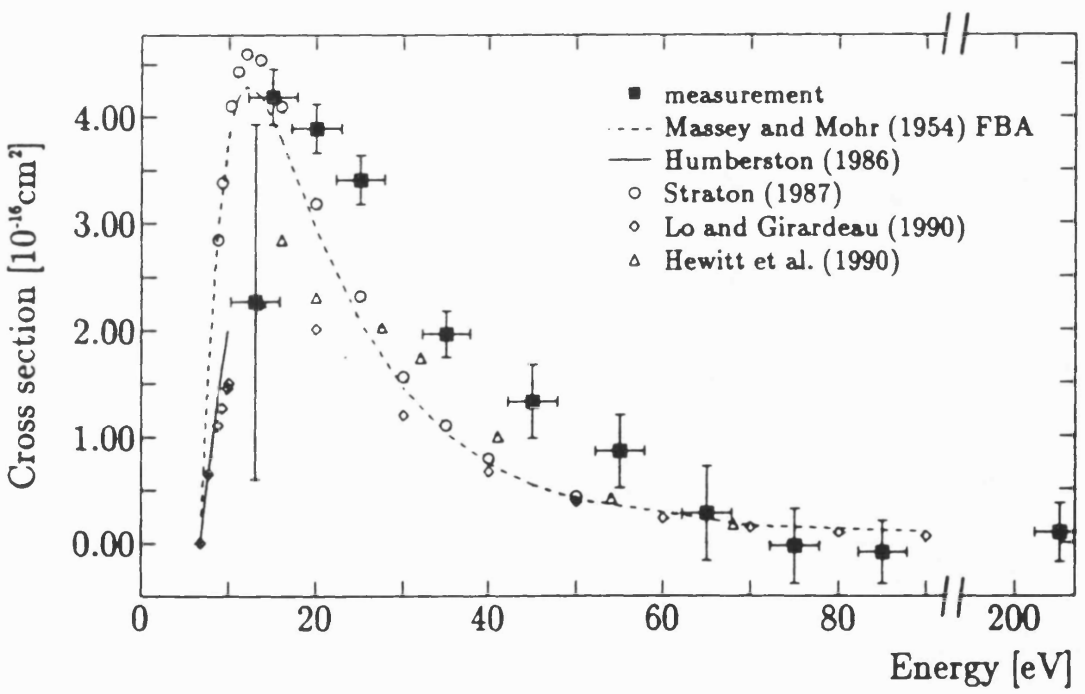

Figure 4.5. Q_{Ps} in H (Sperber *et al* 1992).

of Straton (1987), who extended an earlier calculation by Ficocelli-Varracchio and Girardeau (1983). Other theories predict cross-sections with maxima that are significantly lower than experiment. These include the Fock-Tani calculation by Lo and Girardeau (1990), a close coupling calculation by Hewitt *et al* (1990), a distorted wave Born approximation by Shakeshaft and Wadhera (1980) (not shown), an R-matrix calculation by Higgins and Burke (1991) (not shown) and the CTMC calculations by Ohsaki *et al* (1985) and Wetmore and Olson (1986) (neither of which are shown). The position of the maxima in most of these calculations are however closer to that obtained experimentally. Sperber *et al* (1992) point out that the Kohn-variational calculations of Brown and Humberston (1984) could be extrapolated above 10.2eV, the highest energy covered by the calculation, to give a cross-section consistent with the experiment.

4.1.2 Single Ionisation Cross-Sections

Single (direct) ionisation by positron impact occurs by the following reaction

$$e^+ + A(M) \rightarrow e^+ + A^+(M^+) + e^- \qquad (4.2)$$

The threshold for this process is at E_I and at higher energies the ion may be left in an excited state.

Sueoka (1982) and Mori and Sueoka (1984), using a TOF technique in conjunction with a retarding electric field, have measured Q_i^+ for He, Ne and Ar at low to intermediate energies. They obtained values of Q_i^+ that are slightly lower than the corresponding electron results, a finding that has not been corroborated by subsequent measurements, including those of Sueoka (1989). The latter are discussed below.

Fromme *et al* (1986,1988) measured Q_i^+, simultaneously with Q_{Ps} for He and H_2, using the apparatus shown in figure 4.1. The values of Q_i^+ were determined by integrating the background-subtracted TOF spectra, in order to detect

transmitted positrons in time correlation with ions. By measuring the electron single ionisation cross-section (Q_i^-) with the same apparatus, and by comparing these results with those of Montague *et al* (1984), they were able to make corrections for the energy dependence of the ion extraction efficiency. The positron results were normalised to the electron data above 750eV, where the positron and electron cross-sections were found to have the same energy dependence and were assumed to have merged. They found Q_i^+ to be significantly larger than Q_i^- at intermediate energies, as shown in figure 4.6 together with other experimental and theoretical estimates of Q_i^+. This figure does not include the later measurements of Q_i^+ made by Knudsen *et al* (1990) which are shown for He, in figure 4.8. The experimental data of Fromme *et al* (1986), Diana *et al* (1985) and Sueoka (1989) are all in good accord with each other and with the results of

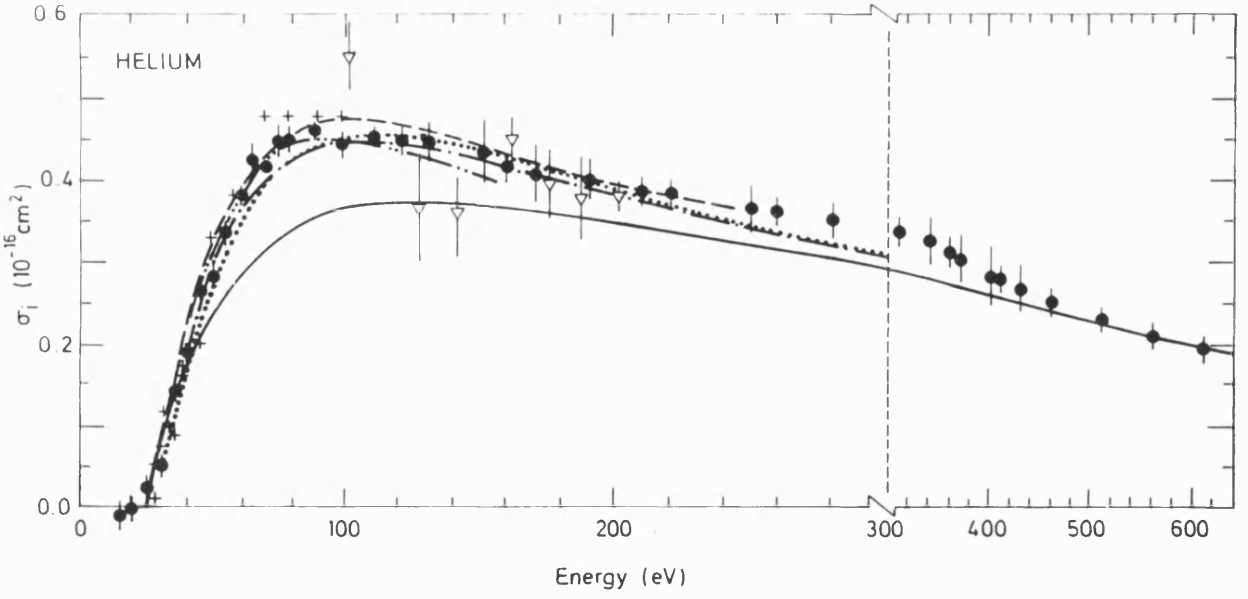

Figure 4.6. Q_i^+ for positron-He scattering. Experiment: Fromme *et al* (1986),•; Diana *et al* (1985),▽; Sueoka (1989),+. Theory: Campeanu *et al* (1987b), dashed line; Golden and McGuire (1976), dotted line; Peach and McDowell (1983), dash-dot line; Basu *et al* (1985), dash-dot-dot line. Q_i^- for He (Montague *et al* 1984), solid line.

the distorted-wave Born approximation calculations by Basu *et al* (1985) and Campeanu *et al* (1987a), as shown in figure 4.6. Good agreement is also found between the experimental results for positrons and the theoretical electron cross-section, when calculated without exchange, by Golden and McGuire (1976) and Peach and McDowell (1983). This led Fromme *et al* (1986) and Raith and Sinapius (1989) to suggest that the exchange interaction is responsible for the difference between Q_i^+ and Q_i^- at intermediate energies. A similar effect is manifest in the single ionisation cross-section for proton impact, which was found to exceed that for anti-proton impact at intermediate collision velocities both theoretically (Fainstien *et al* 1987) and experimentally (Andersen *et al* 1987). This suggests that the enhanced cross-section for the positive projectile might be due to charge effects and not the absence of the exchange interaction. From low to intermediate energies, target polarisation may enhance the ionisation cross-section for a positively charged projectile which pulls the target electrons towards itself, unlike the case of electron and anti-proton impact.

More recently, Q_i^+ has been measured by Knudsen *et al* (1990) for He, Ne, Ar and H_2, using the apparatus shown in figure 4.7. In this experiment, a positron beam was magnetically guided through a target chamber from which ions could be extracted and detected. The ion extractor was pulsed for short periods, by signals from the positron detector, thus preventing deflection of the positrons by the electric field. By measuring the time difference between the detection of transmitted positrons and remnant ions it was possible to discriminate between different ionic charge states, by virtue of their differing flight times. After background subtraction and corrections for contributions arising from Ps formation, relative values of Q_i^+ were obtained.

In figure 4.8 the results of Knudsen *et al* (1990) for He are compared with those of Fromme *et al* (1986). Also shown are values of Q_i^- measured by Krishnakumar and Srivastava (1988) and Montague *et al* 1984. In He, the results of Knudsen

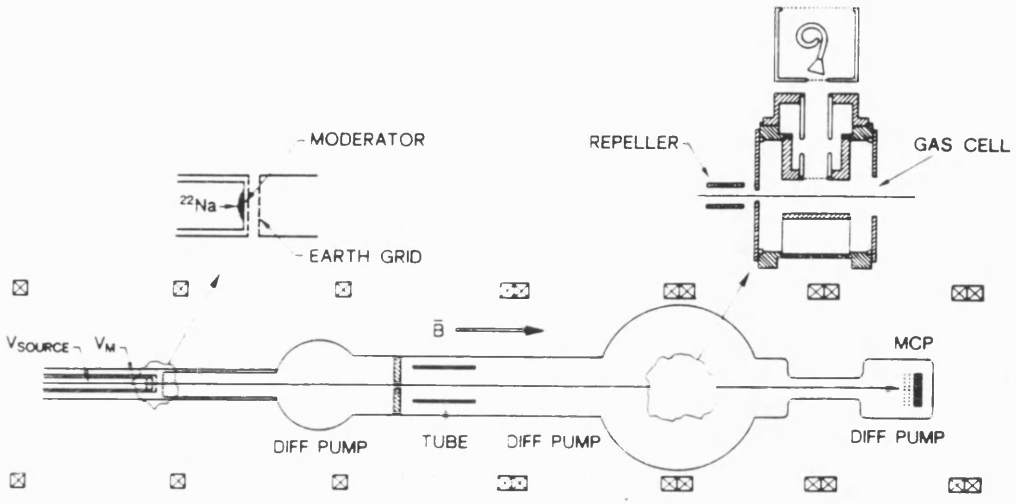

Figure 4.7. A schematic diagram of the apparatus used by Knudsen *et al* (1990).

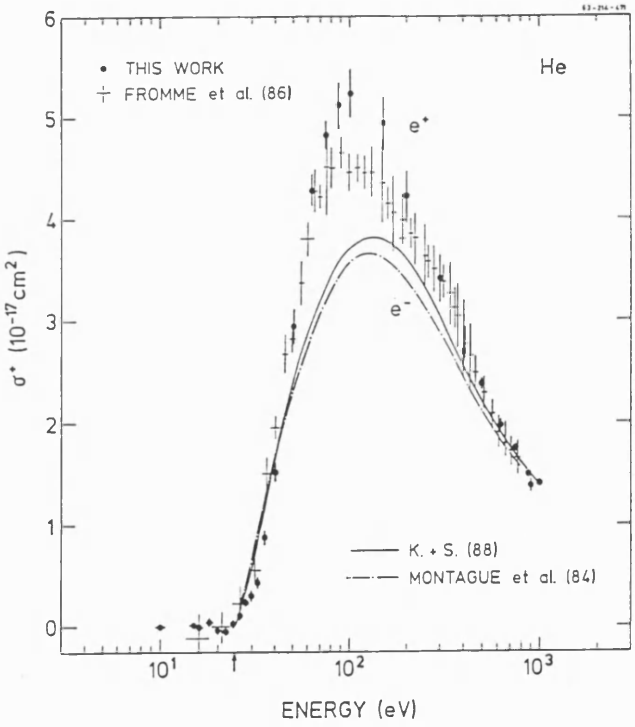

Figure 4.8. Q_1^+ for positron-He scattering (Knudsen *et al* 1990).

et al (1990) are around 15% larger than those of Fromme *et al* (1986) around the maxima, whilst for H_2 (not shown) the results of Knudsen *et al* (1990) are around 10% smaller than those of Fromme *et al* (1988). The results of Knudsen *et al* (1990) merge with those of Fromme *et al* (1986) by around 600eV and were normalised to Q_i^- (Rapp and Englander-Golden 1965) at 1keV. In figure 4.8 it is apparent that $Q_i^+ < Q_i^-$ at the lowest energies. This might be due to competition between the single ionisation and Ps formation channels and "anti-binding" effects between the atomic electrons and negatively charged projectiles (Knudsen and Reading 1992).

The values of Q_i^+ for H, shown in figure 4.9, were obtained by Spicher *et al* (1990), using an apparatus similar to that of Sperber *et al* (1992). This is shown in figure 4.4. The same crossed beam geometry was employed and positrons were again detected in delayed coincidence with ions. Measurements of Q_i^- were carried out with the same apparatus and were found to be in reasonable agreement with those of Shah *et al* (1987). The results of Shah *et al* (1987) were combined with those of Fite and Brackmann (1958) and used for normalisation of the positron data.

The resulting values of Q_i^+ are significantly higher than most theoretical predictions. Ghosh *et al* (1985) used a distorted-wave polarized-orbital approximation and obtained results around 20% lower than those obtained by Spicher *et al* (1990). The results of a similar calculation by Mukherjee *et al* (1989) lie slightly below those of Ghosh *et al* (1985), as do the CTMC results of Ohsaki *et al* (1985) and Wetmore and Olson (1986), with the results of Ohsaki *et al* (1985) around 50% lower than those of Spicher *et al* (1990) at most energies. As well as being smaller in magnitude, most of the theoretical data reach a maximum value around (20-30)eV below the experiment. In contrast, the results of a more recent distorted-wave polarised-orbital calculation by Acacia *et al* (1993) are in good agreement with Spicher *et al* (1990).

A similar experiment has recently been performed by Jones *et al* (1993). The H target was obtained from a Slevin

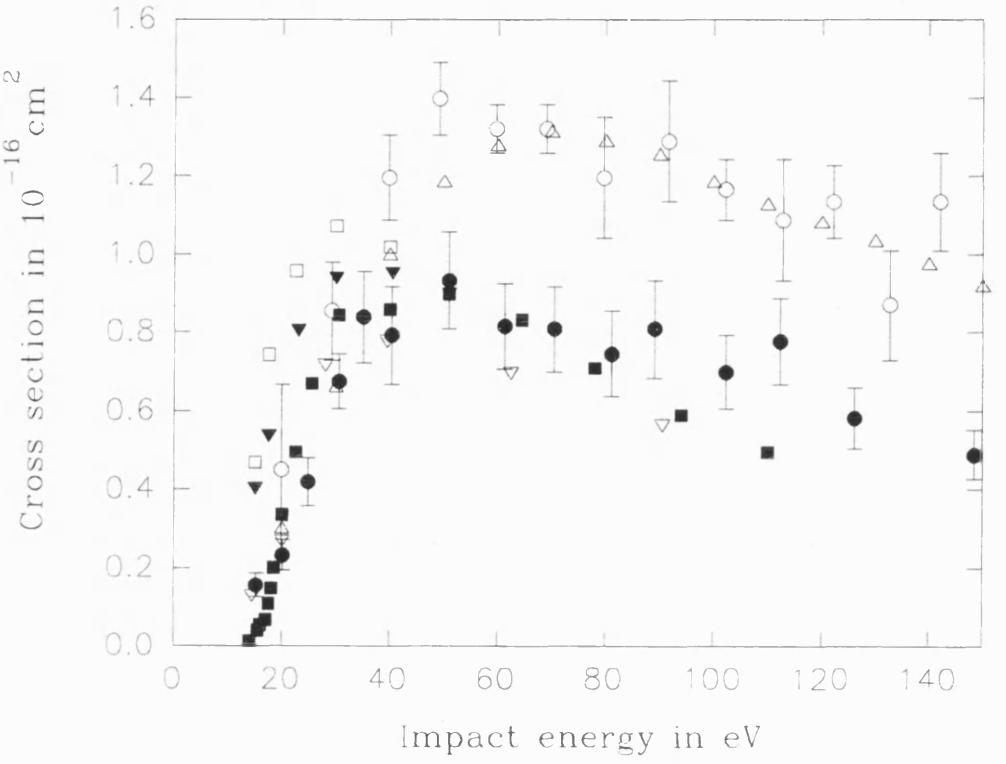

Figure 4.9. Q_i^+ for H. Experiment: Spicher *et al* (1990),o; Jones *et al* (1993),•. Theory: Ghosh *et al* (1985),□; Mukherjee *et al* (1989),▾; Ohsaki *et al* (1985),▽; Wetmore and Olson (1986),■; Acacia *et al* (1993),△.

type discharge tube, however, in contrast with the experiment of Spicher *et al* (1990), the positron beam was magnetically confined through the interaction region, thereby increasing the collection efficiency of positrons scattered to wider angles. The results were normalised to Q_i^- (Shah *et al* 1987) at 700eV. The results Jones *et al* (1993) are also shown in figure 4.9. The values obtained for Q_i^+ are significantly lower than those obtained by Spicher *et al* (1990) and are in reasonable agreement with most theoretical expectations, with the exception of the data of Acacia *et al* (1993).

4.1.3 Total Ionisation Cross-Sections and the Present Work

At least part of the difficulty in measuring Q_{Ps} and Q_i^+ (for example in the work of Fromme *et al* 1986, 1988) is caused by the problem of discriminating between reactions (4.1) and (4.2), both of which result in an ion in the final state. Another useful quantity, which is easier to measure, is the total ionisation cross-section (Q_t^+) defined as

$$Q_t^+ = Q_{Ps} + Q_i^+ + \sum Ho \qquad (4.3)$$

where ΣHo is the sum of all higher order processes contributing to ionisation (e.g. multiple ionisation) and is usually relatively small.

Even though Q_t^+ contains contributions from more than one reaction, it may still yield much important information. Neglecting annihilation, Ps formation is the first ionising channel to open. Therefore, below E_I, $Q_t^+ = Q_{Ps}$ and a knowledge of Q_t^+ can be used to investigate the near threshold behaviour of Q_{Ps}. At higher impact energies the Ps formation cross-section becomes vanishingly small and, if higher order processes are negligible, Q_t^+ becomes approximately equal to Q_i^+. Hence, Q_t^+ may be used to study the merging of Q_i^+ and Q_i^-, in accordance with the first Born approximation. As direct ionisation cross-sections become increasingly well known, it may be easier to determine Q_{Ps} by subtracting Q_i^+ from Q_t^+, instead of measuring Q_{Ps} directly. There is some evidence that Q_{Ps} might contain structure (e.g. Diana *et al* 1986, McAlinden and Walters 1992) and this might be manifest in Q_t^+. Additionally, it has been suggested that Q_{el} may contain Wigner cusps, around E_{Ps}, caused by the rapid onset of Ps formation (e.g. Campeanu *et al* 1987, Fromme *et al* 1988). The behaviour of Q_{el}, in this energy region, may be deduced by subtracting Q_t^+ from Q_t, since the latter has been accurately determined for a number of targets.

In the present work, Q_t^+ has been measured, in detail and with high precision, for a variety of atomic and molecular

targets. The experimental apparatus used to make these measurements is described in the remainder of this chapter, along with its principles of operation and the systematic checks that were carried out.

The apparatus described in chapter 2 was modified to produce a pulsed beam of slow positrons, allowing the beam and ion-extractor to be pulsed on and off in anti-phase. This prevented the ion extractor from deflecting the positrons in the interaction region. The ion-yield was measured as a function of the beam energy as described below and, where possible, existing data have been used for normalisation to obtain values for Q_t^+.

As a systematic check, the total electron impact ionisation cross-section (Q_t^-) was measured using the same technique. Here Q_t^- is defined as

$$Q_i^- = \sum_n Q_{ni}^- \qquad (4.4)$$

where Q_{ni}^- is the cross-section for ionisation to the n^{th} charge state and the summation is over all energetically accessible n values. The results of these measurements were compared with values of Q_i^- obtained from literature and used to verify that the ion extraction technique had no significant energy dependence.

4.2 Experimental Details

Figure 4.10 is a schematic diagram of the apparatus used to measure ion-yields. The apparatus of figure 3.6 was modified for this purpose by incorporating a Wien filter and two repeller tubes prior to the scattering cell. The flight tube, the repeller grid after the scattering cell and the beam tagger were removed. The Wien filter and repeller tubes were used to improve the quality of the positron beam by removing fast components and reducing its energy spread as described below.

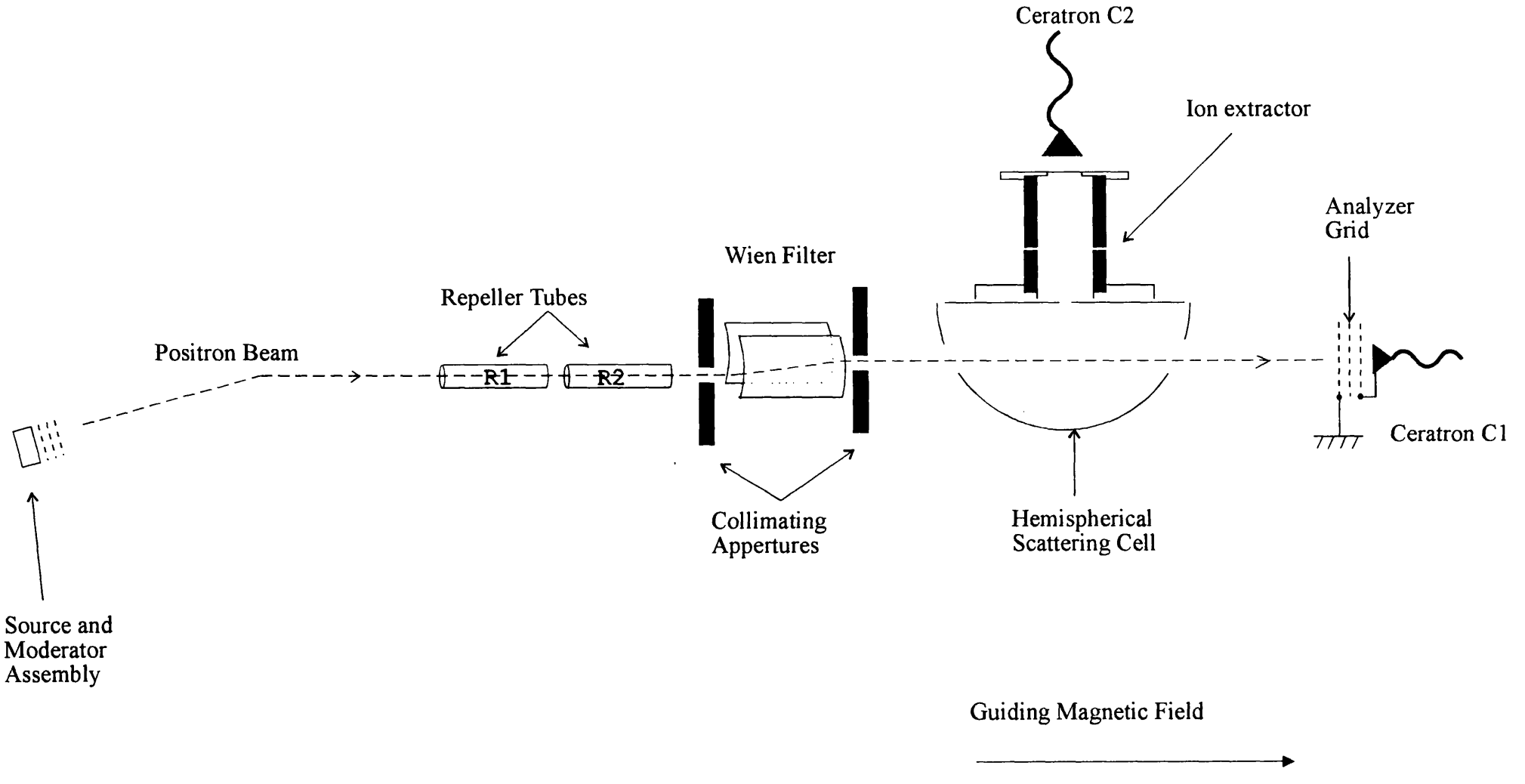

Figure 4.10. A schematic diagram of the apparatus used to measure ion-yields (not drawn to scale).

A beam of slow positrons with an intensity of around $2x10^3s^{-1}$ was obtained by the moderation of β^+ particles emitted from a 10mCi ^{58}Co radioisotope in conjunction with an annealed W mesh moderator. The source and moderator arrangement are described in chapter 2. A beam of electrons with an intensity of around 10^5s^{-1}, was obtained from the secondary electrons liberated from the moderator meshes by radiation from the source. By applying a negative potential to the moderator, electrons were accelerated to kinetic energies (E) given by

$$E = e|V_m| + \Delta E \qquad (4.5)$$

where ΔE is the kinetic energy with which an electron leaves the moderator. The energy distribution of the electron beam was measured as described in section 4.3, and ΔE was found to take values up to around 15eV, whilst in the case of a positron beam, ΔE given by equation 2.1 was found to take a maximum value of around 2.8eV. This is due to the different physical mechanism responsible for positron and electron emission from a metal surface (e.g. Schultz and Lynn 1988).

The source grid shown in figure 2.3 was removed since positrons or electrons emitted from it would have had a higher mean energy that the main beam, due to the potential difference between this grid and the moderator and its use would have broadened the beam energy distribution.

Two brass repeller tubes (R1 and R2) were inserted inside the bent solenoid, as shown in figure 4.10. When using a positron beam R1 was held at around -150V to remove secondary electrons from the beam. These electrons came from metal surfaces, such as the moderator holder and associated grids, by radiation from the positron source and, if not removed, may have caused ionisation in the interaction region. When using an electron beam R1 was grounded. A retarding potential (V_r) was applied to R2 in order to bias off a low energy portion of the beam, thereby reducing its energy spread. The effects of V_r on the energy distribution and intensities of beams of positrons and electrons are described in section 4.3.

Before entering the interaction region the beam passed through a Wien filter. This acted as a broad band velocity filter, causing the separation of the slow positrons from the background of fast particles in the beam and also allowed the beam to be modulated (chopped). A Wien filter works by creating an electric field perpendicular to the guiding magnetic field. The resulting forces acting on a charged particle, initially travelling with a velocity (v) parallel to the magnetic field, will cause the particle to be deflected a distance (d) such that

$$\underline{d} \propto \frac{1}{v} \cdot \frac{\underline{E} \times \underline{B}}{B^2} \qquad (4.6)$$

where E and B are the electric and magnetic field vectors. Since d is inversely proportional to v, this effect may be used, in conjunction with suitable collimating apertures, to produce a velocity filter. Cylindrical deflection plates have been used in this apparatus following Hutchins *et al* (1986), who demonstrated that the distortion of a beam caused by planar deflection plates (e.g. Mills 1980), may be reduced by such a geometry. The Wien filter used in the present work comprised two parallel 120mm long, part cylindrical deflection plates, separated by 10mm and having 6mm collimating apertures at each end. The average radii of the cylinders was around 20cm. When the unit was used as a velocity filter, the axes of the collimating apertures and of the beam-line before and after the filter were laterally offset by 10mm. The beam was deflected through the offset apertures by the application of suitable potentials to the plates and the beam was chopped by periodically grounding the deflection plates.

The use of the Wien filter made it difficult to transport the beam through the apparatus without severe attenuation when its mean energy was automatically ramped over a wide range (e.g 2-300eV). When making measurements over this range of impact energies, the collimating apertures were placed on the same axis and the deflection plates were

grounded. The unit did not then act as a velocity filter and in this case the beam was interrupted by applying potentials of ±180V to the deflection plates.

The pulsed beam traversed the scattering cell described in chapter 2, and was monitored at the end of the beam-line using C1. The diameter of the beam apertures in the scattering cell were increased from 8mm to 12mm to reduce the probability of intersecting the beam, since scattered particles and secondary electrons may have resulted in ionisation of the target gases, resulting in overestimates of ion-yields.

4.3 Beam Characterisation

The energy distribution and intensities of the positron and electron beams were measured as successive portions of the beams were biased off. This allowed the energy spread of the beam to be estimated and a compromise between intensity and energy resolution to be reached. Each beam was biased off by the application of a retarding potential (V_r) to R2. The beam energy distribution was measured with V_m held constant for different values of the potential difference between R2 and the moderator (V_r-V_m). V_r was set using the floating battery and potential divider shown in figure 4.11.

The beams were characterised at the end of the beam-line using a retarding electric field set up using the analyzer grid in front of C1. The circuit used for this purpose is shown in figure 4.12. The potential applied to the retarding grid was ramped while pulses from C1 were counted on the MCS. The ramp generator provided a channel advance signal for the MCS every 10s whilst simultaneously incrementing the retarding potential by 0.5V. This allowed the count rate of C1 to be measured as a function of the retarding potential.

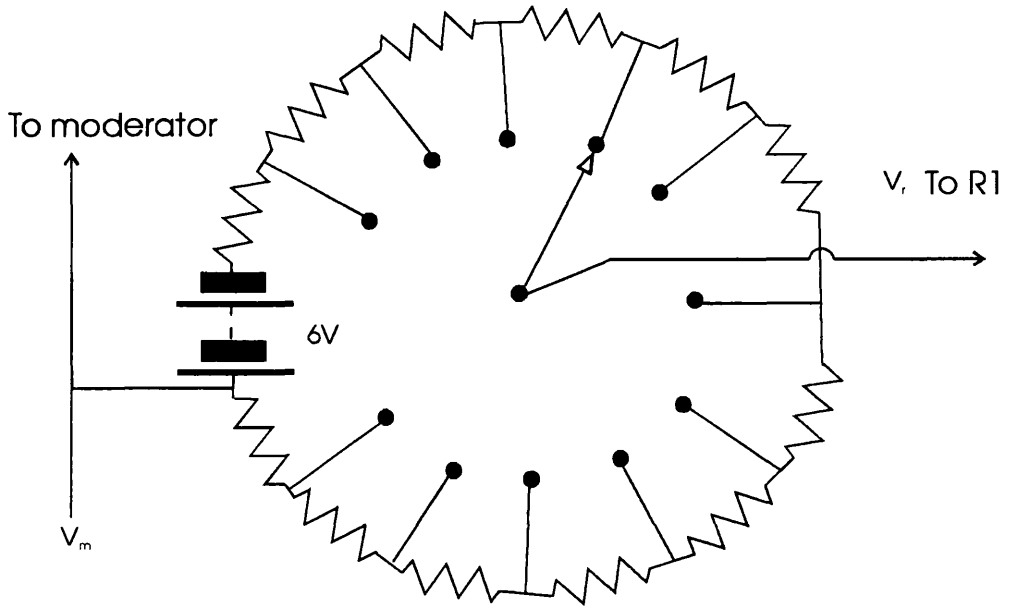

Figure 4.11. A schematic diagram of the potential divider used to derive V_r. All resistors are 1.8MΩ.

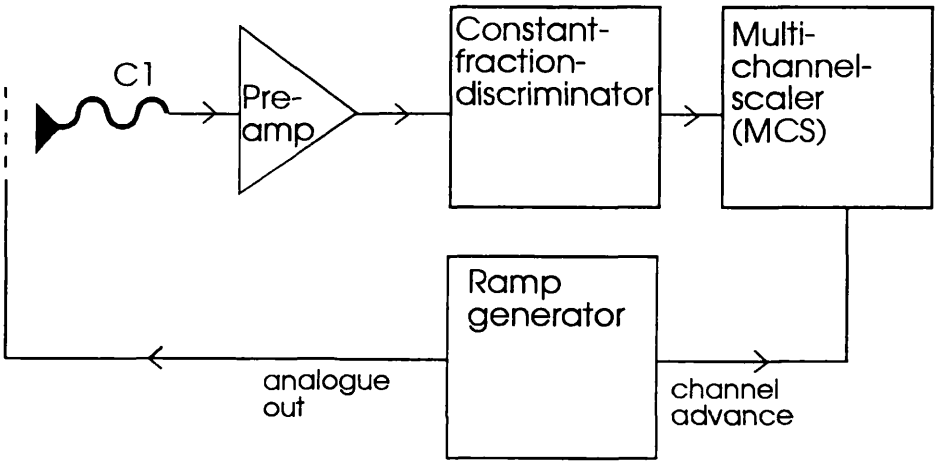

Figure 4.12. The circuit used to measure beam energy profiles.

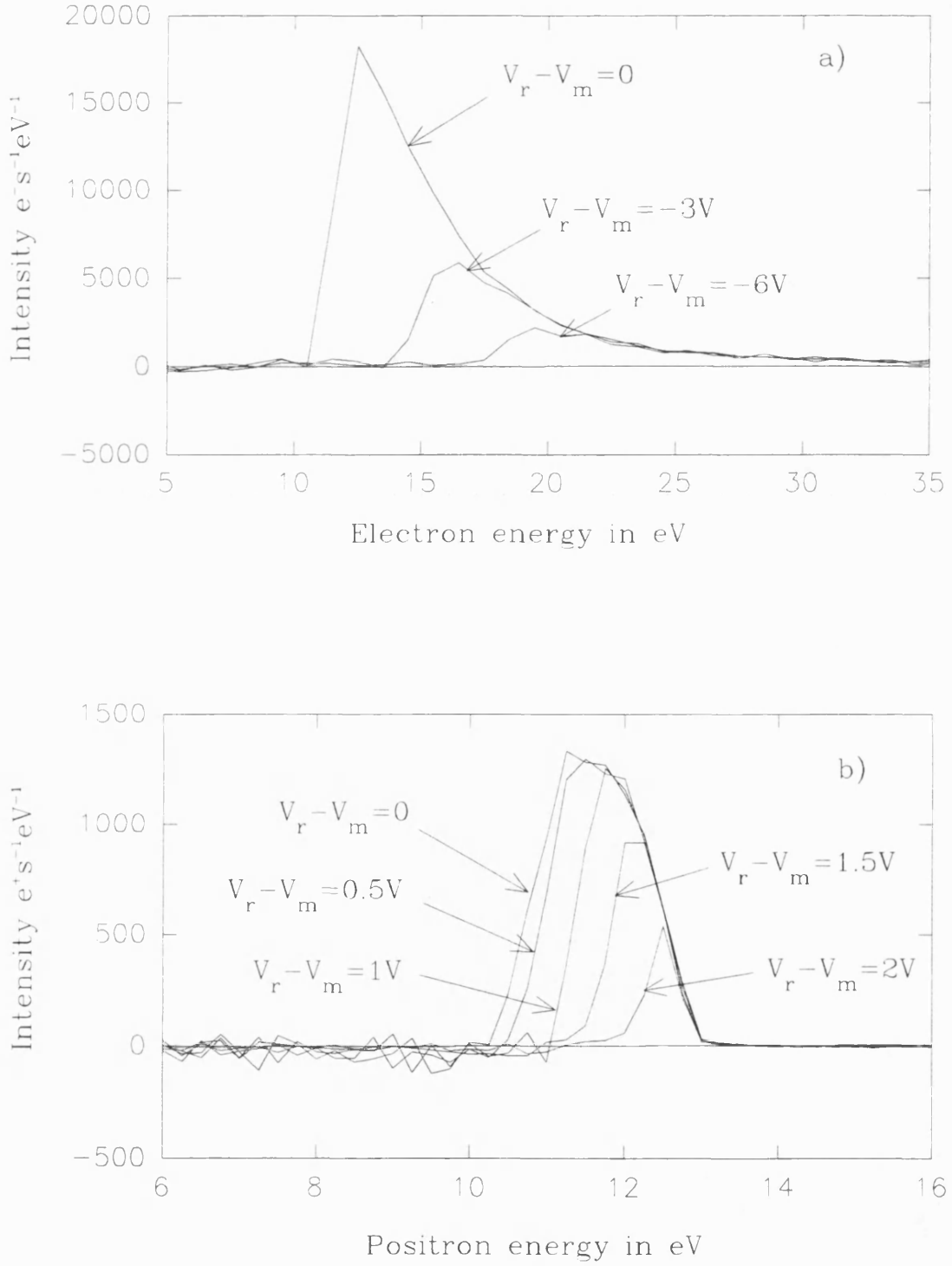

Figure 4.13. Energy distributions of beams of a) electrons and b) positrons with a moderator potential (V_m) of magnitude 10V.

In order to obtain the beam energy distributions, the retarding field profiles were differentiated with respect to the retarding potential. The results are shown in figure 4.13. This shows the energy distributions of beams of electrons and positrons obtained with $|V_m|$ = 10V for different values of V_r. These data were used to estimate the full width half maximum (FWHM) of the beam, where the FWHM is defined as the width of the distribution at half its maximum intensity.

Figure 4.13a) shows the energy distributions of a beam of electrons. The distributions are clearly asymmetric, with a high energy tail extending above 25eV. With V_r = 10V (i.e. the full beam) the distribution rises from zero at around 10eV to a maximum around 12eV and then falls to half this value by around 16eV. As a result of the high energy tail the change in shape of the distribution as V_r is increased causes the FWHM to increase.

The FWHM of the positron beam was measured for values of V_r in the range 10-12V and is shown in figure 4.13b). The energy distribution is approximately symmetric about its mean value and extends from around V_r to 12.8eV. As V_r was increased both the energy spread and FWHM of the energy distribution were reduced.

The intensities and FWHM of the beams are summarised for different values of (V_r-V_m) in table 4.1. In the case of a positron beam the reduction in intensity, as (V_r-V_m) was increased, was accompanied by a reduction in the FWHM of the energy distribution as expected. Reducing the FWHM from its intrinsic value of 1.6eV to 0.8eV, the value used in measurements described below, resulted in a reduction in intensity of around 33%. It was not feasible to reduce the FWHM of the electron beam in the same way, due to the high energy tail of the energy distribution.

Beam type	(V_r-V_m) in V	FWHM in eV	Intensity in particles s^{-1}
e^-	0	4.5	$10x10^4$
	-3.0	5.2	$41x10^3$
	-6.0	6.1	$18x10^2$
e^+	0	1.6	$21x10^2$
	0.5	1.5	$19x10^2$
	1.0	1.1	$13x10^2$
	1.5	0.8	$7x10^2$
	2.0	0.4	$2x10^2$

Table 4.1 A table showing the variation in intensity and FWHM of beams of positrons and electrons, as V_r is varied with respect to V_m.

4.4 The Electronics

Figure 4.14 shows the electronic circuit used to measure ion-yields. This allowed data to be collected on an MCS whilst ramping V_m. It also provided high voltage pulses for the ion extractor and suitable potentials to allow the Wien filter to transmit and chop the beam as its energy was ramped. The same circuit was used to measure both the ion count rates and beam intensities as a function of the mean beam energy. The two signals were of course measured in separate runs.

Data were collected on an Ortec 916 MCS card installed in a personal computer. The MCS was operated in a multiple sweep mode with a dwell time of 10s per channel. Channel advance signals were derived from a digital ramp generator, the analogue output of which was used as the reference voltage used to control a high voltage power supply which provided V_m. This was operated in its externally controlled

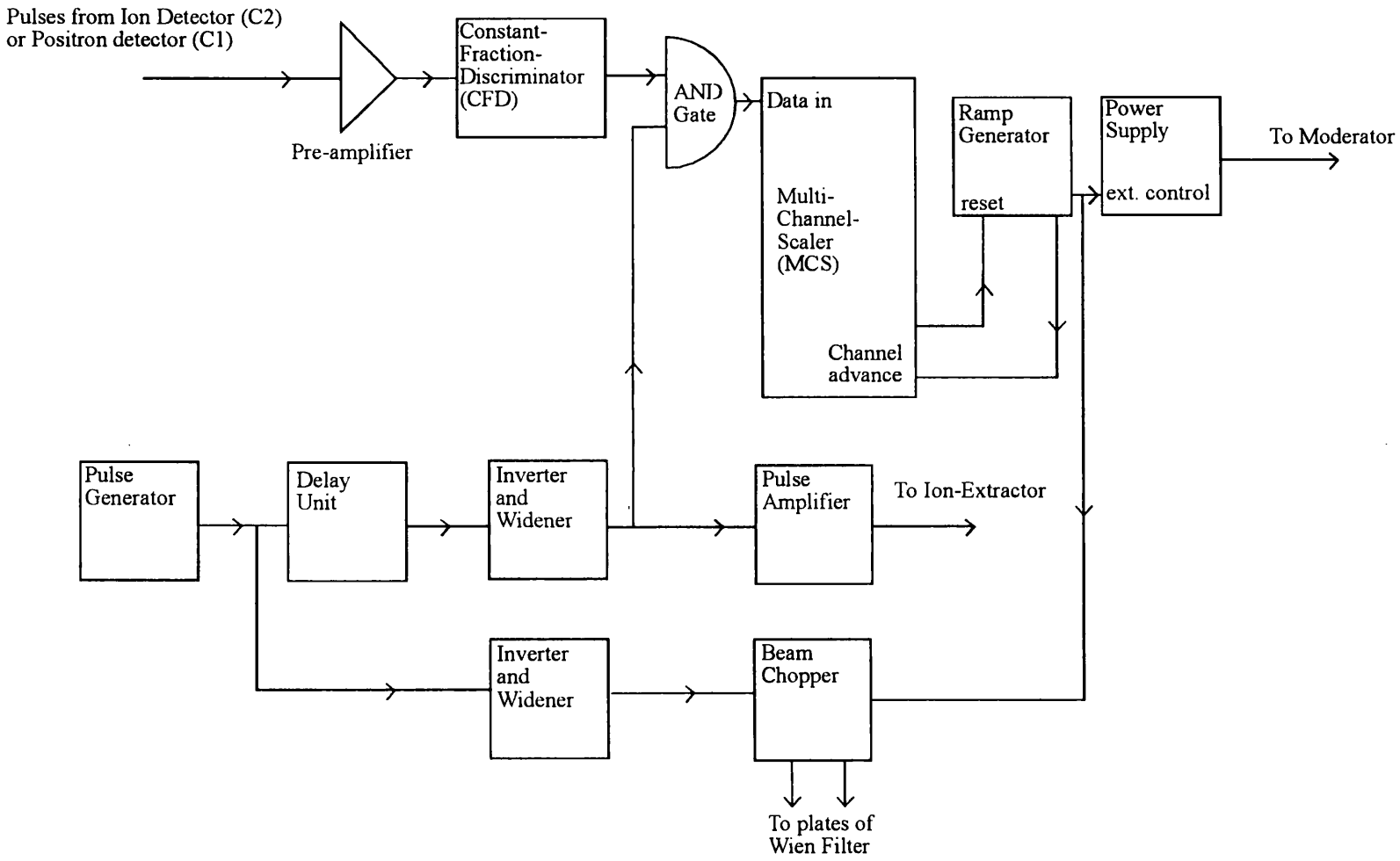

Figure 4.14. A schematic diagram of the electronic circuit used to measure ion-yields.

mode and the output gain of the ramp generator was adjusted so that V_m increased in steps of 0.5V. At the end of each pass the ramp was automatically reset to zero, thus initiating another sweep. This allowed data to be collected in long runs in multiple sweeps thus minimising the effects of instrumental drift and gas pressure fluctuations.

When the Wien filter was used as a velocity selector, it was necessary to vary the potentials applied to the deflection plates in step with V_m. This was done automatically by the device that will be referred to as the beam chopper. The beam chopper produced two variable output voltages (V_W) of equal magnitude but opposite polarity for the two deflection plates, given by

$$V_W = \pm(a.V_m+b) \qquad (4.7)$$

where a and b are constants, chosen to minimise the energy dependence of the beam intensity emerging from the filter. Since the deflection of the beam is proportional to v^{-1} (see equation 4.6), and hence to $E^{-1/2}$, this is only an approximation to the required potential. However due to the broad velocity pass-band of the Wien filter, the approximation was sufficiently good to allow the beam to be transmitted over a range of energies, for example, from (10-50)eV with a variation of intensity of typically only around 25%. The gain and the offset (a and b in equation 4.7) of the beam chopper were adjusted so as to minimise the energy dependence of the beam intensity in the following way. V_m was set to the minimum value required for a run (usually zero) and the offset was adjusted to maximise the beam intensity. V_m was then set close to the maximum value required and the gain was adjusted to maximise the beam intensity. By repeating these steps and by manipulation of the magnetic coils around the Wien filter, it was possible to arrive at values of a and b that allowed the beam to be transported through the filter over the required range of energies. As already mentioned, the beam was pulsed by periodically

grounding the plates of the Wien filter in response to a pulse train applied to the blocking input of the beam chopper. The blocking pulses were derived from a signal generator running at a frequency of 20kHz. The pulses from the signal generator were widened to 10μs and presented to the blocking input of the beam chopper, causing the positron beam to be interrupted for 10μs every 50μs. These pulses are shown in figure 4.15.

The output from the signal generator was also used to trigger the ion-extractor. This was done by delaying the pulses for 1μs, then widening them to 5μs before they triggered the high voltage pulse amplifier so that pulses with a duration of 5μs and an amplitude of -180V were applied to the ion-extractor 1μs after the beam was interrupted. This was done to allow positrons that were between the Wien filter and the scattering cell, when the beam was chopped, to pass through the scattering cell before the ion-extractor was pulsed on, thus ensuring that no positrons were in the interaction region at this time. These pulses, together with their time relationship with the pulses from the beam chopper are also shown schematically in figure 4.15.

Returning to figure 4.14, signal pulses from the ion detector, C2, were amplified by a pre-amp and used to trigger a constant fraction discriminator (CFD). The CFD threshold was set to reject noise and pulses caused by stray coupling between the ion extraction pulses and the signal line. The output from the CFD was presented to an AND gate before being stored on the MCS. The other input of the AND gate was derived from the pulses that were used to trigger the pulse amplifier for the ion extractor. This caused data to only be acquired during the periods when the ion extractor was pulsed on, thus reducing the background signal caused by detector dark counts. This was particularly useful for He since it has the smallest ionisation cross-section of the targets studied. When measuring ion-yields for the heavier targets the AND gate was disabled, since the longer flight times of the ions meant that some of them arrived at C2 after the extraction

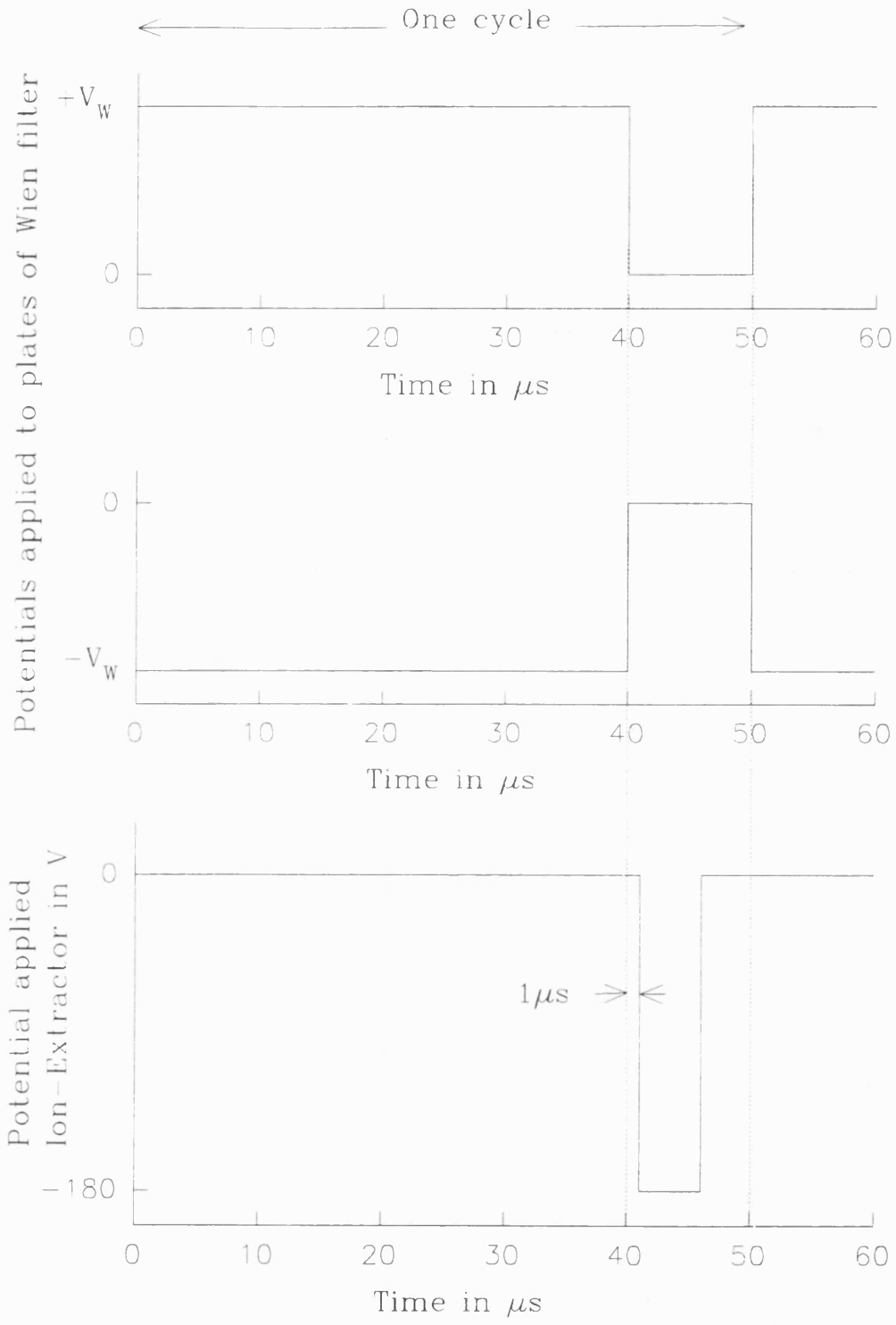

Figure 4.15. A schematic representation of the pulses applied to the ion extractor and the Wien filter.

pulse had been terminated. When measuring the beam intensity the AND gate was disabled and pulses from the CFD were presented directly to the MCS.

To test the operation of the beam chopper, the beam intensity was measured as a function of time by also using the pulse train triggering the beam chopper to start a TAC. The stop pulses were provided by C1 and the output of the TAC was monitored on a MCA. This circuit is shown in figure 4.16 whilst the variation of beam intensity with time is shown in figure 4.17. This data was obtained during preliminary measurements and the pulse length and frequency are slightly different from those used in the final data acquisition. It does, however, serve to illustrate the operation of the beam chopper.

4.5 Data Collection and Restoration

The results presented in this chapter were collected in three set of runs:

1) Electron ion-yields were measured for He, Ar and H_2 from below E_{Ps} to around 300eV, with the mean beam energy ramped in steps of 2eV. The energy dependencies of these ion-yields were compared with Q_t^-, given by equation 4.4, in order to ascertain whether the ion extraction technique was energy independent as demanded. He and Ar were studied because they are the lightest and heaviest of the atomic targets used in this work and H_2 was chosen to assess the possible effects of molecular dissociation. These measurements were made with electrons because the ionisation cross-sections are well known and the high beam intensity, compared to that obtainable with positrons, made run times considerably shorter. These measurements were made with the Wien filter used only to chop the beam.

2) Positron ion-yields were measured for He, Ar and H_2, over

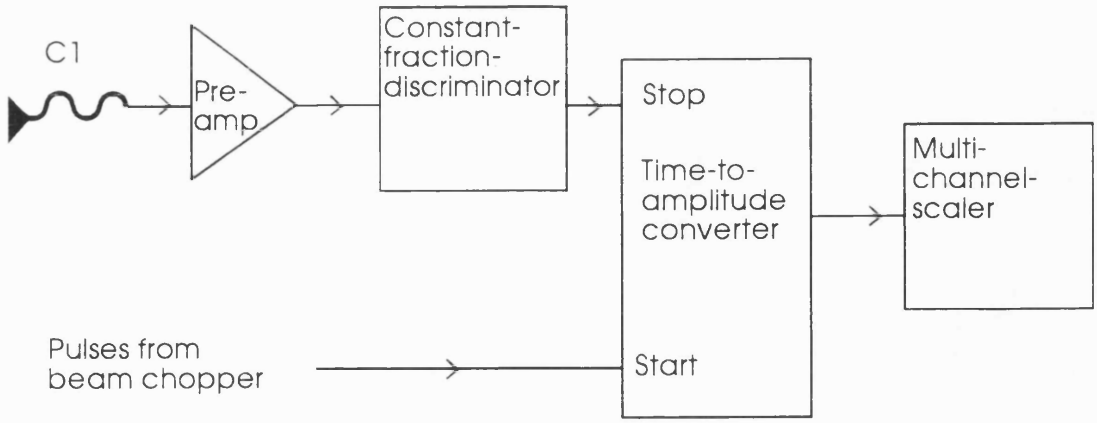

Figure 4.16. The circuit used to measure the beam intensity as a function of time.

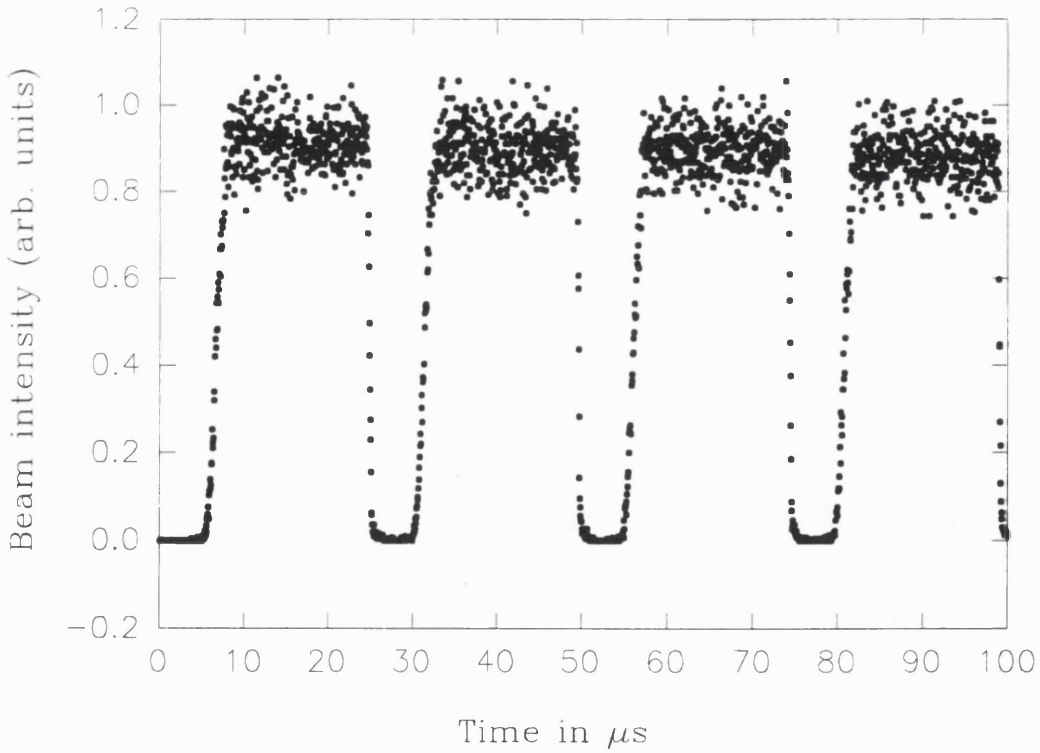

Figure 4.17. The beam intensity as a function of time.

the same range of impact energies as above, with the beam also ramped in steps of 2eV. However, the total ionisation cross-sections are not so well known for positrons and include contributions from Ps formation, making comparisons a little more difficult. These measurements were also made with the Wien filter just acting as a chopper.

3) Positron ion-yields were obtained for He, Ar and H_2 in an energy range from below E_{Ps} to some tens of eV above E_{Ps}. These measurements were made in detail with the mean beam energy ramped in steps of 0.5eV and the energy spread of the beam reduced to around 0.8eV FWHM. These results are analysed in detail in chapter 5.

Due to the differing beam characteristics, slightly different procedures were adopted in each case to subtract background contributions and to derive ion-yields from the data. These procedures are described in the next three sections.

4.5.1 Electron Ion-Yields

As pointed out in section 4.3, the electron beam was found to possess a wide energy spread with a high energy tail extending up to more than 15eV above the energy at which the maximum intensity occurred. In order to effectively improve the characteristics of the beam, ion count rate and beam intensity spectra were measured in pairs with different portions of the beam biased off. Then by taking the difference between pairs of spectra it was possible to simulate the effect of an electron beam with a narrower energy spread than that obtained directly from the moderator. In this case, ion-yields (Y_i^-) were calculated from

$$Y_i^- = \frac{N_i(-3) - N_i(-6)}{N_{e^-}(-3) - N_{e^-}(-6)} \qquad (4.8)$$

where $N_i(-3)$ and $N_i(-6)$ were the ion count rate spectra

measured with (V_r-V_m) = -3V and (V_r-V_m) = -6V respectively, and $N_{e^-}(-3)$ and $N_{e^-}(-6)$ were the corresponding beam intensity spectra. Equation (4.8) was applied to each set of four of spectra, channel by channel, to obtain the energy defence of the ion yields. By calculating ion-yields in this way, the contribution from those electrons with energies in the range $(|V_m|+3)$eV to $(|V_m|+6)$eV were obtained, thus simulating an electron beam with an energy spread of around 3eV, similar to the intrinsic energy spread of the positron beam. This also subtracted background contributions which were common to both pairs of spectra.

During preliminary measurements some spiralling of the incident electrons was evident. The ion-yields obtained using pairs of spectra obtained with (V_r-V_m) = 0 and -3V were found to exceed those obtained in the manner described above, i.e. with (V_r-V_m) = -3V and -6V. In such cases the energy dependence of the measured ion-yields was found to be distorted resulting in an enhancement at low energies. Since the electrons may be emitted from the moderator surface over 4π, with energies up to 15eV this can result in a wide range of pitch angles at low beam energies. The transverse component of velocity may be expected to remain approximately constant, hence, as the beam is accelerated to higher energies, the ratio between longitudinal and transverse components of the beam energy distribution will increase thus reducing the pitch angles of particles in the beam. This effect may then have caused the average path length of the projectiles traversing the interaction region to become energy dependent and have resulted in the observed distortion of the ion-yields. By measuring ion-yields according to equation 4.8, the spiralling particles, which would have a reduced longitudinal component of energy, were preferentially biased off, thus reducing this effect.

4.5.2 Positron Ion-Yields (2-300eV)

Due to the narrower intrinsic energy spread of the positron beam, measurements were made in pairs, with the full beam and with the beam completely biased off. The spectra obtained with the beam biased off were subtracted from the signal spectra in order to remove the background. Ion-yields (Y_i^+) for positron impact over this range of impact energies were obtained using

$$Y_i^+ = \frac{N_i(0) - N_i(6)}{N_{e^+}(0) - N_{e^+}(6)} \qquad (4.9)$$

where $N_i(0)$ and $N_{e+}(0)$ are, respectively, the ion count rate and beam intensity spectra with $(V_r - V_m) = 0$, i.e. the full beam. $N_i(6)$ and $N_{e+}(6)$ correspond to the ion and beam count rates respectively with $(V_r - V_m) = 6V$, i.e with the beam biased off. By applying equation 4.9 to corresponding spectra, channel by channel, an energy dependent ion-yield was obtained and the background was subtracted.

4.5.3 Low Energy Positron Ion-Yields

For these measurements, the axes of the beam-line were offset by 10mm and the Wien filter used as a velocity selector. As a result these spectra contained a significantly reduced background in comparison with those described in § 4.5.2. The ion-yields (Y_i) were calculated from

$$Y_i = \frac{N_i - Bkg}{N_{e^+}} \qquad (4.10)$$

where N_i and N_{e+} were the ion count rate and beam intensity spectra respectively. The background (Bkg) was determined by averaging number of counts in that part of the ion count rate spectra below the Ps formation threshold (E_{Ps}). Ion count rate

spectra were accumulated in runs lasting around $6x10^4$s and beam intensities in runs lasting around 10^3s. In all cases the beam intensities were measured with no target gas in the scattering cell.

Some ions were detected in preliminary measurements, even at beam energies below E_{Ps}. This was found to be caused by energetic secondary electrons ejected from the cone of C1 passing back through the interaction region. To eliminate this effect, the ion count rates were measured with the beam guidance coils at the end of the beam-line and the potentials applied to C1 turned off.

4.6 Results and Discussion

Since the areal target density, the ion-extraction efficiencies and the beam transport and detection efficiencies were unknown, absolute scales were assigned to ion-yields by normalising the data to values of Q_t^+ and Q_t^- derived from partial cross-sections obtained from literature. Measurements were first made over the range of impact energies from 2eV to 300eV using both electrons and positrons as projectiles. These measurements were made primarily as a systematic check of the apparatus and technique. More precise measurements were then made for the low energy part of the cross-sections using positrons.

The results presented in the next three sub-sections are arranged according to the type of projectile and impact energy range. In each case, the cross-sections used for normalisation and comparison with the present results are also shown and the degree of agreement is discussed. The error bars represent one statistical standard deviation.

4.6.1 Electron Results

The electron results for He, Ar and H_2 are shown in figure

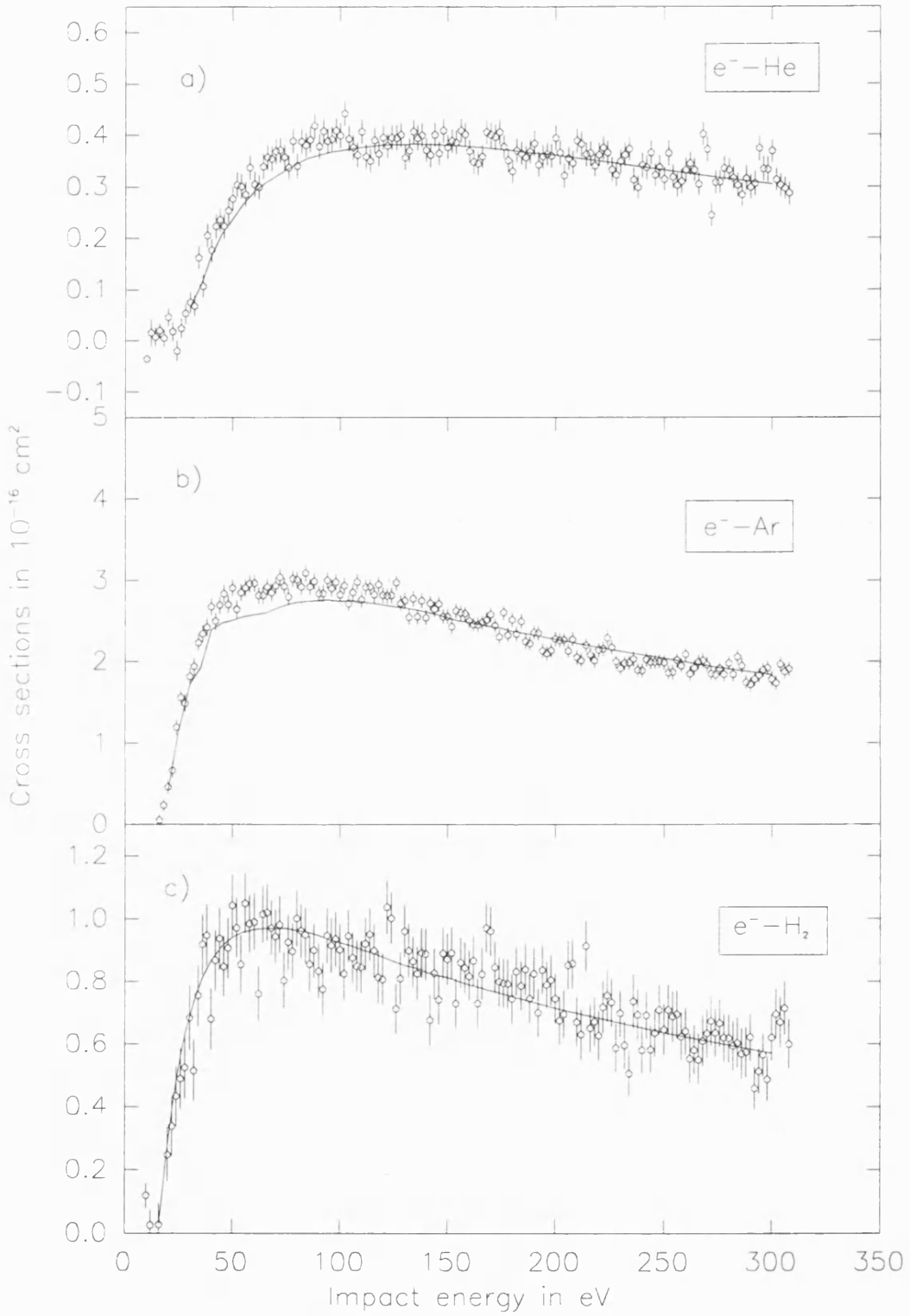

Figure 4.18. O, the present values of Q_t^- for a) He, b) Ar and c) H_2. Solid lines represent Q_t^- obtained from literature (see text).

4.18. The ion-yields were normalised to Q_t^- in all cases at around 300eV, the highest energy investigated. Normalisation was carried out at this energy, because the path length corrections due to pitch angle effects were believed to be smallest at the highest beam energies for the reasons discussed above.

Figure 4.18a) shows the present values of Q_t^- for electron impact on He. These results were obtained by normalising the ion-yield to Q_i^- measured by Krishnakumar and Srivastava (1988). These values of Q_i^- contain contributions, albeit small, from double ionisation and are therefore directly comparable with the present results. Of the gases studied, Q_t^- has the broadest maximum in He, rising from zero around threshold at 24.6eV to its maximum value around 100eV. Between 50eV and 100eV the results of Krishnakumar and Srivastava (1988) are up to around 8% lower than the present results, with the maximum discrepancy occurring around 80eV. Above 130eV the two results converge and are in agreement up to 300eV, where the data were normalised. The difference at low energies may be caused by spiralling of the beam, resulting in an overestimate of the ion-yields at low energies.

The results for Ar are shown in figure 4.18b). The values of Q_t^- were obtained by normalising ion-yields to the sum of Q_i^- and the double ionisation cross-section (Q_{2i}^-), both measured by Krishnakumar and Srivastava (1988). Higher order processes, the most significant being triple ionisation, have been neglected in the comparison. The contribution from triple ionisation is less than 0.3% that of Q_i^-, over this range of energies, according to Krishnakumar and Srivastava (1988) and are therefore negligible in the present measurements. Q_t^- rises from close to threshold at 15.7eV, to its maximum value around 80eV. The present values of Q_t^- exceed ($Q_i^-+Q_{2i}^-$) by up to approximately 10%, between 30eV and 120eV, before converging above 130eV. The small discrepancy at low energies is again attributed to spiralling effects.

The present values of Q_t^- for H_2 were obtained by

normalising the ion-yield to Q_i^- measured by Rapp and Englander-Golden (1965). Both cross-sections shown in figure 4.18c) include contributions from dissociation. Q_t^- increases rapidly above threshold at 15.4eV to its maximum value by around 30eV. It has the narrowest maxima of the gases studied. The present results are in good agreement with those of Rapp and Englander-Golden (1965), within the statistical scatter of the present data, at all energies studied.

4.6.2 Positron Results (2-300eV)

The present values of Q_t^+ for He, H_2 and Ar, over an energy range of (2-300)eV, are shown in figure 4.19. Also shown are the estimated values of Q_t^+ used for normalisation. Q_t^+ was obtained by summing appropriate partial cross-sections from literature. For consistency, the positron data was normalised around the maxima in the cross-sections, since in the case of Ar it is difficult to estimate the values of Q_t^+ above 76eV, the highest energy investigated by Fornari *et al* (1983): the results of Diana *et al* (1986a) contain unexplained structures at higher energies. For He and H_2 it was possible to obtain accurate values of Q_t^+ from Fromme *et al* (1986,1988) by summing Q_{Ps} and Q_i^+, since they measured the total ion-yield which was then partitioned into these two cross-sections.

The present values of Q_t^+ for He were obtained by normalising the ion-yield to the sum of Q_{Ps} and Q_i^+ (Fromme *et al* 1986). These are shown in figure 4.19a). The contribution to Q_t^+ from double ionisation is expected to be less than 0.4% (Charlton *et al* 1988) and is negligible within the precision of the present measurements. Within the statistical scatter of the data, the agreement between the present results and $Q_{Ps}+Q_i^+$ is excellent over the entire range of energies investigated.

The results for Ar are shown in figure 4.19b), along with the estimated values of Q_t^+ that were used for normalisation. Q_t^+ was estimated by summing Q_{Ps} measured by

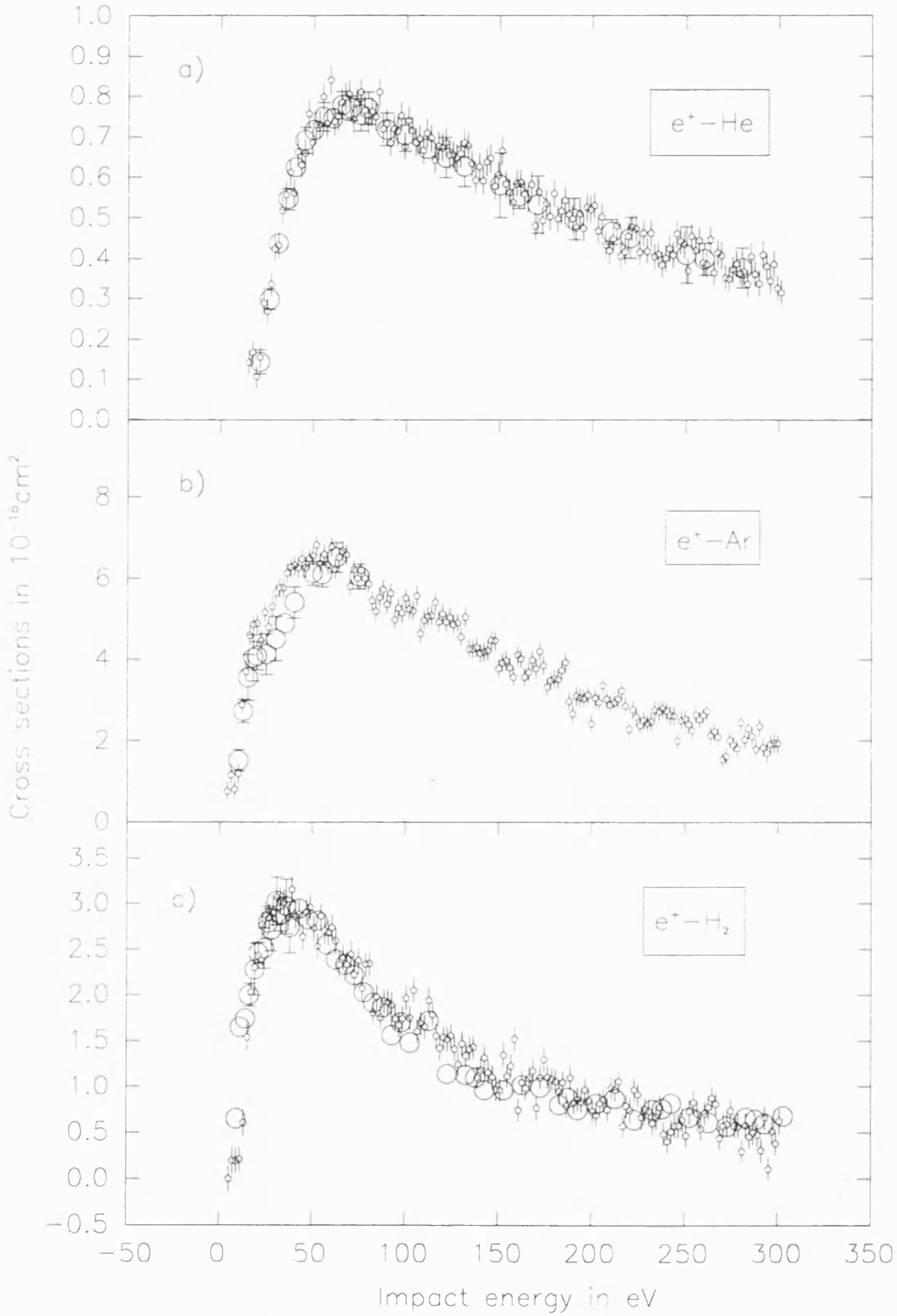

Figure 4.19. Small circles represent the present values for Q_t^+ for (2-300)eV in a) He, b) Ar and c) H_2. Large circles represent Q_t^+ obtained from literature (see text).

Fornari *et al* (1983) with Q_i^+ measured by Knudsen *et al* (1990). Where the two measurements were made at slightly different energies, the data were interpolated in order to perform the summation. The contribution to Q_t^+ from double ionisation, measured by Charlton *et al* (1989), is not expected to exceed (5.2±0.5)% the value of Q_i^+ over this range of energies, with the maximum reported value of Q_{2i}^+/Q_i^+ occurring at around 100eV.

The present values of Q_t^+ rise steeply from around threshold at 8.9eV to a maximum value at around 60eV. Q_t^+ falls below $Q_{Ps}+Q_i^+$ by up to around 20% between 20eV and 40eV. Above 60eV Q_t^+ decreases smoothly, within the statistical scatter of the data up to 300eV, the highest energy investigated. There is no evidence of any structure in Q_t^+ of the kind reported by Diana *et al* (1986a) in Q_{Ps}. The present value of Q_t^+ at 300eV is around 10% smaller than Q_i^+ measured by Knudsen *et al* (1990). The reason for the discrepancy is unknown. However, if the present results are reliable, it may be caused by inconsistencies between the absolute values of Q_{Ps} and Q_i^+, which were obtained by different groups using different techniques. This could have resulted in an inaccurate energy dependence when the two cross-sections were summed.

The H_2 results are shown in figure 4.19c). The values of Q_t^+ used to normalise the present results, were estimated by summing Q_{Ps} and Q_i^+, both measured by Fromme *et al* (1988), who found the contribution from dissociative ionisation to be negligible. Q_t^+ rises from around threshold at 8.6eV to reach a maximum value at around 40eV. Of the gases studied, Q_t^+ for H_2 reaches its maximum value at the lowest impact energy, and is most peaked around this energy. Above the maximum Q_t^+ falls rapidly and smoothly, up to 300eV, the highest energy studied. There is good agreement with the present results, except near threshold, as discussed below.

4.6.3 Low Energy Positron Results

Figures 4.20 and 4.21 show the present values of Q_t^+ from threshold to intermediate impact energies for He, H_2, Ar and Ne. As already mentioned, these measurements were made using a beam with a FWHM of around 0.8eV with its mean energy incremented in steps of 0.5eV. The values of Q_t^+ used for normalisation are also shown. These were estimated by summing partial cross-sections in the manner discussed above.

A few points deviate from a smooth energy dependence by a statistically significant amount. This behaviour was not reproduced in other runs obtained under similar conditions and hence no physical significance is attached to this behaviour.

The measured cross-sections rise from around zero, close to E_{Ps} for each gas. The small rise just below E_{Ps} is attributed to the energy spread of the positron beam. The accuracy of the beam energy determination is verified by the position of the onset of the ion-yields, which, when the energy spread of the beam is accounted for, are in good agreement with the known values of E_{Ps} for all the gases studied.

The values of Q_t^+ for He, shown in figure 4.20a), were normalised using values of Q_t^+ estimated by summing Q_{Ps} and Q_i^+ measured by Fromme *et al* (1986). At all energies investigated $Q_{Ps}+Q_i^+$ and the present values of Q_t^+ are in excellent agreement. Q_t^+ rises from close to threshold at 17.8eV, and increases smoothly, before levelling off by 60eV, the highest energy studied in this run. Of the gases studied, the increase in Q_t^+ is most gradual in He. The polarised orbital results for the sum of Ps formation in ground (Khan and Ghosh 1983) and first excited (Khan *et al* 1985) states agree with the experimental results below around 22eV, but exceed the latter by up to around 25% between 22eV and 35eV. The experimental results also include contributions from single ionisation with its threshold at 24.6eV. The distorted wave calculation values of Q_{Ps} by Mandal *et al* (1979) are slightly

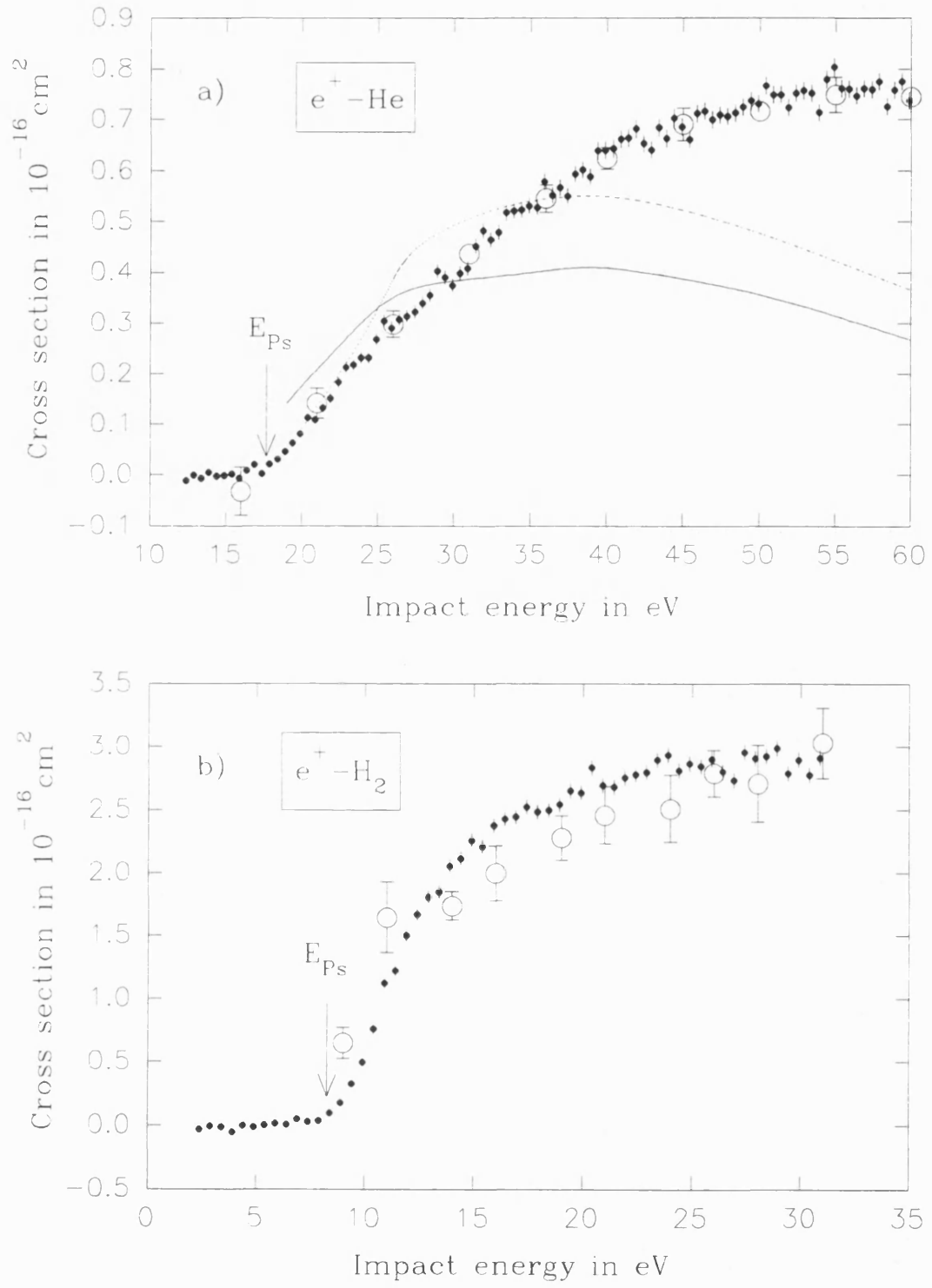

Figure 4.20. a) He: present values of Q_t^+,•; (Q_{Ps}+Q_i^+)(Fromme *et al* 1986),o; Q_{Ps} (Khan and Ghosh 1983,Khan *et al* 1985), dashed line; Q_{Ps} (Mandal *et al* 1970), solid line b) H_2: present values of Q_t^+,•; (Q_{Ps}+Q_i^+)(Fromme *et al* 1988),o.

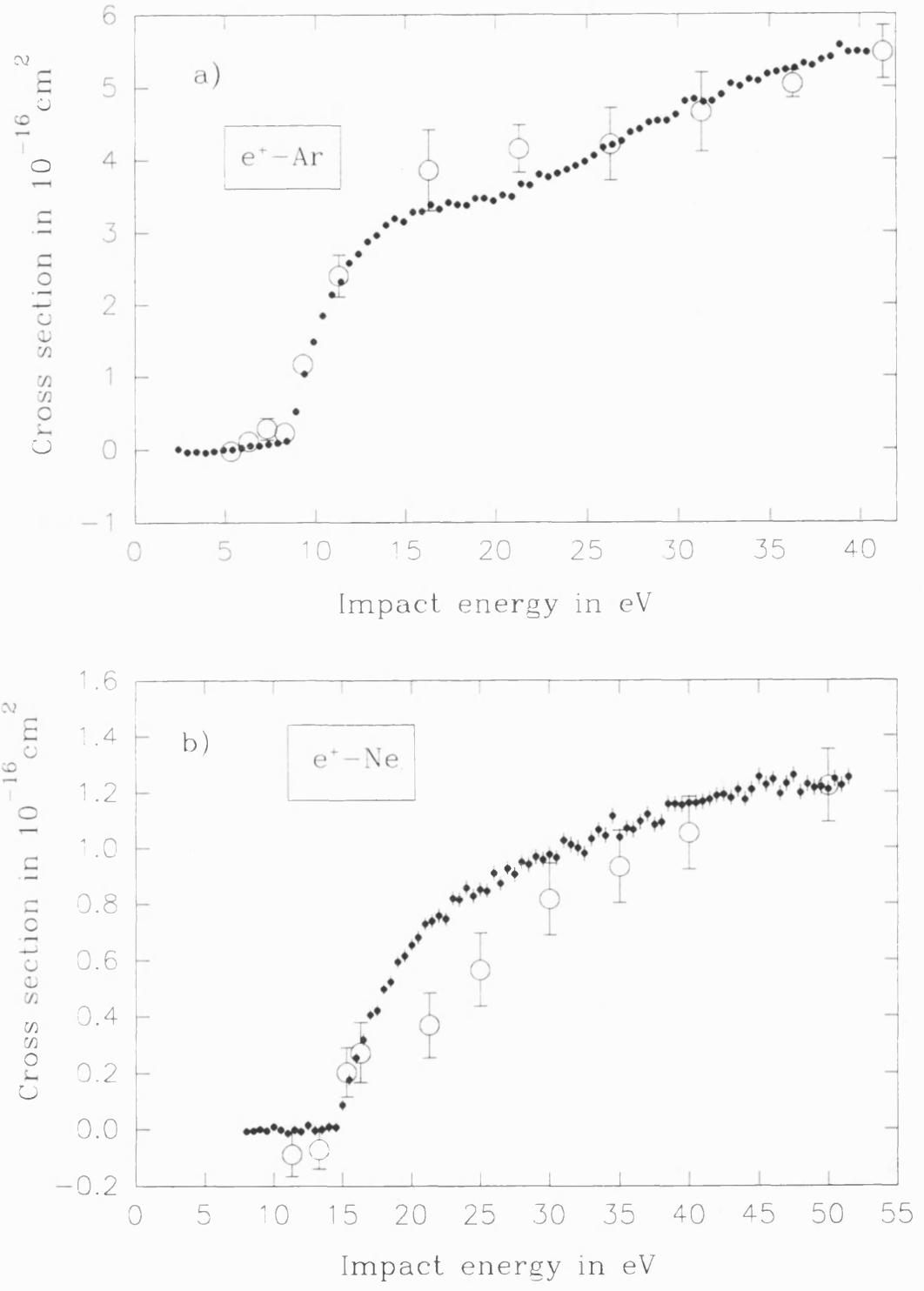

Figure 4.21. a) Ar: present values of Q_t^+,•; Q_{Ps}(Fornari *et al* 1983) + Q_i^+(Knudsen *et al* 1990),o. b) Ne: present values of Q_t^+,•; Q_{Ps}(Diana *et al* 1985a) + Q_i^+(Knudsen *et al* 1990),o.

higher than the experimental values of Q_t^+ up to around 28eV. The reason for the discrepancies are not clear, however, these calculations are not expected to be very accurate at low energies.

In the case of H_2, Q_t^+ was normalised to $Q_{Ps}+Q_i^+$ measured by Fromme *et al* (1988) and both cross-sections are shown in figure 4.20b). Q_t^+ rises steeply from close to threshold, at 8.6eV, up to around 16eV before beginning to level off. Q_t^+ appears to reach a maximum value around (25-30)eV. The present data was normalised to coincide with the corresponding measurement made over 2-300eV. However the agreement below 25eV is somewhat poorer, with the 3 points representing $Q_{Ps}+Q_i^+$ between 14eV and 18eV lying more than one standard deviation below the present values of Q_t^+ and the two points below 12eV lying significantly higher.

The present values of Q_t^+ for Ar are presented in figure 4.21a). These values of Q_t^+ were obtained by normalising the ion-yield to Q_{Ps} measured by Fornari *et al* (1983) plus Q_i^+ measured by Knudsen *et al* (1990) at around 40eV. Below 15.7eV where the contribution from direct ionisation is zero Q_t^+ is in good accord with Q_{Ps} (Fornari *et al* 1983). Q_t^+ rises very steeply close to E_{Ps} at 8.9eV before levelling off by around 16eV. Q_t^+ then begins another gradual increase at around 22eV and is still rising at 42eV, the highest energy covered by this run. The reason for the second increase in Q_t^+ beginning at around 22eV is at present unknown.

In the case of Ne, values of Q_t^+ were obtained by normalising the ion-yield to Q_{Ps} measured by Diana *et al* (1985a) plus Q_i^+ measured by Knudsen *et al* (1990) at 50eV. Normalising the data in this way gives values of Q_t^+ that are up to around 2 times greater than Q_{Ps} (Diana *et al* 1985) below E_I. Conversely, if the present data were normalised to Q_{Ps} below E_I, the value of Q_t^+ would be around half that of the quoted value of $(Q_{Ps}+Q_i^+)$ at 50eV. Therefore, the absolute values of Q_t^+ have a normalisation uncertainty of the order of ±25%. The results are shown in figure 4.21b). Q_t^+ rises from around E_{Ps} at 14.8eV and continues to do so up to 50eV, the

highest energy investigated for this gas. Q_t^+ appears to be close to its maximum value by 50eV.

4.7 Summary

A pulsed slow positron beam has been developed and used to obtain values of Q_t^+ for He, Ne, Ar, H_2. These results have been discussed, with particular attention to the degree of agreement between the present measurements and the data used for normalisation. The energy dependence of ion-yields for He, Ar and H_2, over the range of impact energies from close to threshold to around 300eV, has been compared with that obtained from summed partial cross-sections from literature and found to be in good agreement for both positron and electron impact.

The ion-yields have been measured in detail for He, Ne, Ar and H_2 from low to intermediate energies. Absolute values of Q_t^+ have been obtained by normalising ion-yields to summed partial cross-sections. The results obtained for He are in excellent agreement with the measurements of Fromme *et al* (1986) at all the energies studied. For H_2 the present values of Q_t^+ are also in good agreement with the results of Fromme *et al* (1988) above 25eV. For Ar and Ne values of Q_t^+ were obtained by normalising the ion-yields to summed partial cross-sections measured in different labs using different techniques. Here, a greater uncertainty exists in the present absolute values of Q_t^+, particularly for Ne.

CHAPTER 5

THRESHOLD EFFECTS AND CHANNEL COUPLING IN POSITRON COLLISION CROSS-SECTIONS

5.1 Introduction

Threshold effects are an example of the more general phenomena of channel coupling effects. These are due, essentially, to competition for projectile flux between different scattering channels and may be manifested as structures in the cross-sections for the competing processes. These effects have been observed and studied in a number of fields in physics.

It was first shown by Wigner (1948), in the context of nuclear reactions, that a cross-section may contain structure, in the form of cusps or rounded steps at the threshold for a new reaction. Wigner (1948) derived expressions for the energy dependence of an inelastic cross-section, close to its threshold, using R-matrix theory and showed that, for an endothermic reaction with no long range Coulomb forces, the s-wave contribution to the cross-section should have an infinite slope at threshold. From flux conservation considerations, this may result in a sharp drop in an existing cross-section, just above the reaction threshold. Below this threshold, the uncertainty principle allows virtual transitions into the inelastic channel, with increasing probability as the threshold is approached. This may result in a cusp or rounded step in the cross-section for the existing channel, centred on the inelastic threshold.

Malmberg (1956) found that $dQ_{el}/d\Omega$ for protons scattering from ^{7}Li contained cusp-like structures peaked at 1.88MeV, the threshold for neutron emission. The cusp was attributed to a threshold effect, caused by the opening of the reaction channel. The cross-section for the emission of 478keV gamma

rays was also found to have a similar structure at the same threshold by Newson *et al* (1957). They also measured the neutron emission cross-section and demonstrated that its energy dependence, close to threshold, could be fitted by the R-matrix theory of Wigner (1948).

Simple formulae for these threshold effects were derived by Baz (1958) by using the unitarity of the scattering matrix and its analytic continuation across the reaction threshold. It was pointed out by Baz (1958), that useful information such as the elastic scattering phase-shift could be obtained from experimental data by analysis of the threshold effects. The theory of threshold effects has subsequently been extended by Newton (1959) and Meyerhof (1963) and reviewed by Fonda (1961).

Evidence of similar threshold effects has also been obtained in atomic physics. For electron-alkali atom scattering, structures in $dQ_{el}/d\Omega$ have been observed in the vicinity of E_{ex} (Andrick *et al* 1972, Eyb and Hofmann 1975, Gehenn and Reichert 1972). These structures take the form of cusp-like peaks or dips, and were ascribed to the presence of the inelastic threshold. However, some doubt remains as to the origin of the structure, since Moores (1976) calculated that the threshold behaviour should only exist over a region of around $\pm 10^{-3}$eV from the threshold, and should not have been resolved in the experiments.

More recently, interest has turned to the possibility of threshold effects in positron scattering. The threshold theories mentioned above, have their simplest form if the reaction considered is the first inelastic channel to open and has no long range Coulomb forces. They are therefore suitable for the analysis of the energy dependence of Q_{Ps} and its effect on Q_{el} for positron scattering from inert gases, since a Ps atom is neutral and this is the first inelastic channel to open. The possibility of annihilation may be neglected since its cross-section has a v^{-1} dependence (equation 1.5) and is negligibly small at the energies considered here.

The first calculation of a threshold anomaly for positron scattering was obtained by Brown and Humberston (1985) who used a Kohn variational technique to calculate the d-wave contribution to Q_{el} and Q_{Ps} for positron-H scattering. These were combined with earlier results for the s- and p-wave contributions (Humberston 1982, Brown and Humberston 1984) to obtain values for Q_{el} and Q_{Ps}. The calculation was carried out over a range of impact energies from below E_{Ps} to around E_{ex} and the result is shown in figure 5.1.

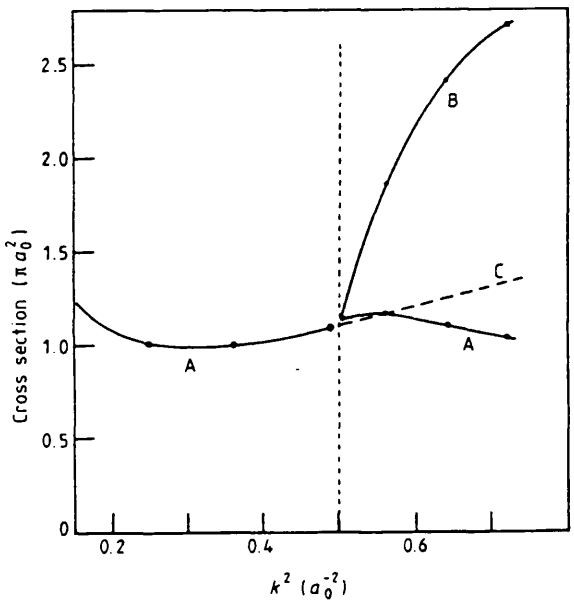

Figure 5.1. The results of Brown and Humberston (1985) showing A, Q_{el}; B, $Q_{el}+Q_{Ps}$; C, a linear extrapolation of Q_{el} from below E_{Ps}.

The elastic cross-section was found to contain a slight discontinuity across E_{Ps} which was attributed to either a "narrow cusp-like feature" in Q_{el} or to a calculational artefact, since the values of the cross-section were not calculated to the same accuracy above and below E_{Ps}. In addition, the calculated value of Q_{el} was around 20% smaller at E_{ex} than the value obtained by a linear extrapolation from

below E_{Ps}. The change in gradient in Q_{el} around E_{Ps} indicated that the reduction in Q_{el} was caused by the Ps formation channel.

The first experimental evidence of a threshold effect in Q_{el} for positron scattering, was obtained by Campeanu *et al* (1987) who made a detailed analysis of the available experimental data for He, in an attempt to partition Q_t. Campeanu *et al* (1987) subtracted Q_{Ps} and Q_i^+ measured by Fromme *et al* (1988) from Q_t obtained by Stein *et al* (1978) to deduce the "total cross-section without ionisation", namely $Q_{el}+Q_{ex}$. Below E_{ex} this is obviously equal to Q_{el}. A smooth curve passing through zero at E_{Ps} was drawn through $Q_{Ps}+Q_i^+$ and this was then subtracted from Q_t. The result is shown in figure 5.2.

The resulting estimate of Q_{el} was found to exhibit a

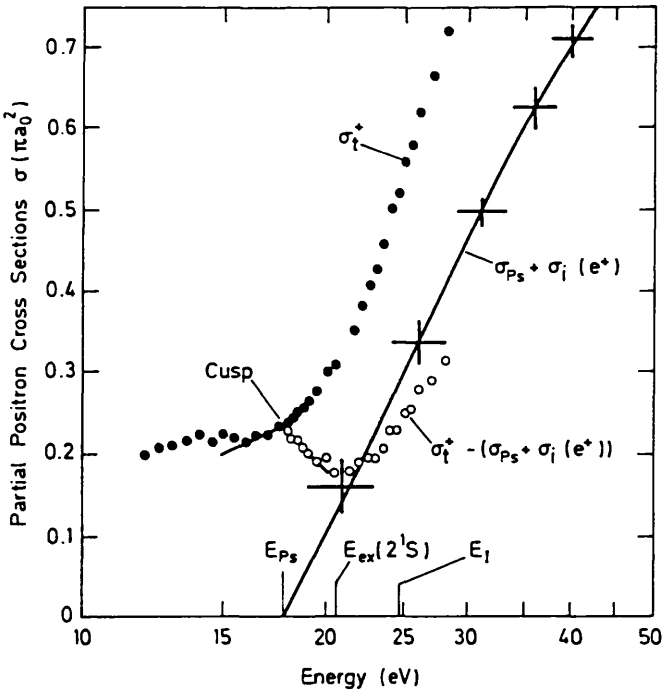

Figure 5.2. Cusp feature in Q_{el} for positron-He scattering, as obtained by Campeanu *et al* (1987).

pronounced cusp-like feature peaked at E_{Ps}, followed by a decrease of approximately 20% between E_{Ps} and E_{ex}.

A similar study was performed by Fromme *et al* (1988) after measuring Q_{Ps} and Q_i^+ for H_2, which they subtracted from Q_t measured by Hoffman *et al* (1982). Again, the analysis provided evidence of a pronounced cusp in Q_{el} at E_{Ps}, followed by a reduction of up to around 50% in the value of Q_{el} between E_{Ps} and E_{ex}.

In both the analysis by Campeanu *et al* (1987) and by Fromme *et al* (1988) a high degree of interpolation was necessary, due to the dearth of data for Q_{Ps} close to threshold. As pointed out by Campeanu *et al* (1987), the cross-sections used in the analyses were obtained by different groups under different conditions and the inferred threshold effects could have been exaggerated by differences in beam energy determination and the absolute values of the cross-sections.

These problems were circumvented by Coleman *et al* (1992) by measuring Q_t and Q_{Ps} for He using the same apparatus. The technique allowed all the measurements to be made by merely changing the potentials applied to two grids, thereby minimising systematic errors. Q_{Ps} was then subtracted from Q_t in order to determine $(Q_{el}+Q_{ex}+Q_i^+)$. This equals Q_{el}, up to E_{ex} at 20.6eV and the results are shown in figure 5.3. Due to the unknown areal target density, these measurements were normalised to the Q_t values of Stein *et al* (1978) below E_{Ps}, where Q_t and Q_{el} are equal since E_{Ps} is, in this case, the first inelastic threshold. Within the statistical uncertainties (around 10% in Q_{el}), the elastic cross-section was found to be flat up to E_{ex} suggesting that, if a threshold effect is present, it is not as pronounced as that predicted by Campeanu *et al* (1987). Above E_{ex}, $(Q_{el}+Q_{ex}+Q_i^+)$ rises as expected, with the onset of excitation and ionisation.

In this chapter, new values for Q_{el} are derived, for He, Ar and H_2 using the present values of Q_t^+ and published data for Q_t. In § 5.2 the energy dependencies of Q_{el} are examined in the vicinity of E_{Ps}, in order to search for a threshold effect

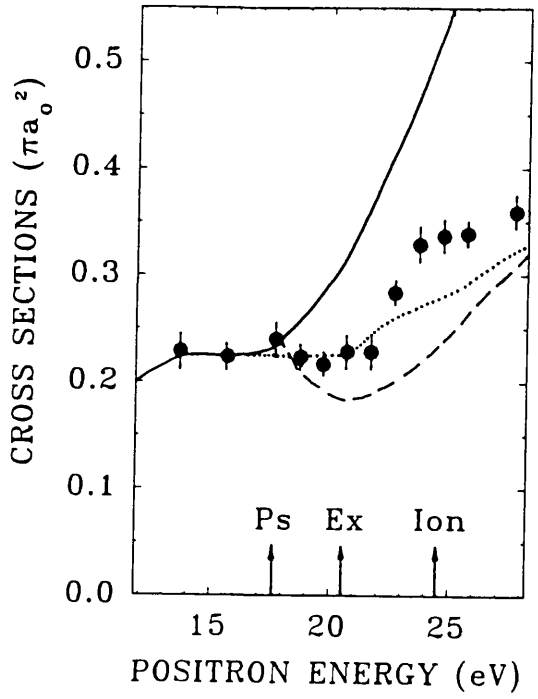

Figure 5.3. •, ($Q_{el}+Q_{ex}+Q_i^+$) from Coleman *et al* (1992); solid line, Q_t from Stein *et al* (1978); dashed line, $Q_{el}+Q_{ex}$ from Campeanu *et al* (1987).

in Q_{el}. In § 5.3 the present values of Q_t^+ for He, Ne and Ar are analyzed using threshold formulae derived from R-matrix theory. In § 5.4 the present values for Q_t^+ and the phase-shifts calculated by McEachran *et al* (1979) are used to predict the nature and magnitude of the threshold effects in Q_t for Ar. This is then compared with experiment. In § 5.5 evidence of channel coupling in Q_t^+ and Q_{ex} for O_2 is discussed.

5.2 The Energy Dependence of Q_{el}, Close to E_{Ps}

The partial cross-sections that comprise Q_t and Q_t^+, for an atomic target, are shown in table 5.1. The right hand column shows the difference between Q_t and Q_t^+, in different energy ranges from zero to above E_I. Any threshold effects, caused by the onset of Ps formation, would be expected to be

confined to a small range of impact energies around E_{Ps} and here Q_t-Q_t^+ is equal to Q_{el}.

Energy range	Q_t =	Q_t^+ =	Q_t-Q_t^+ =
$E<E_{Ps}$	Q_{el}	0	Q_{el}
$E_{Ps}<E<E_{ex}$	$Q_{el}+Q_{Ps}$	Q_{Ps}	Q_{el}
$E_{ex}<E<E_I$	$Q_{el}+Q_{Ps}+Q_{ex}$	Q_{Ps}	$Q_{el}+Q_{ex}$
$E_I<E$	$Q_{el}+Q_{Ps}+Q_{ex}+Q_i^+$	$Q_{Ps}+Q_i^+$	$Q_{el}+Q_{ex}$

Table 5.1. A table showing the partial cross-sections that contribute to Q_t, Q_t^+ and Q_t-Q_t^+, for an atomic target.

The gases that were studied are He, Ar and H_2. The cross-sections and thresholds shown in table 5.1 are for rare gases. However, in the case of H_2, Q_t also contains contributions from molecular rotation and vibrational excitation, and dissociation. These contributions are expected to be small in the range of energies of interest and are not expected to affect the present analysis. In the case of Ne a relatively large normalisation uncertainty exists in the absolute values of Q_t^+ and the Ne data was not analyzed in this way. For Ar, He and H_2, the values of Q_t^+ were subtracted from two published measurements of Q_t, in order to obtain the difference curves shown in figure 5.4, 5.5 and 5.6. Where necessary, the values of Q_t were interpolated before making the subtraction.

For all three targets $Q_{el}+Q_{ex}$ continues across E_{Ps} smoothly, within the resolution of the measurements. As already mentioned, Q_t^+ was measured with a beam energy spread of around 0.8eV FWHM and a cusp of the magnitude predicted by Campeanu *et al* (1987) should therefore be easily resolved. The uncertainties in Q_t-Q_t^+ are typically around 5%. Above E_{Ps} there is a small decrease in the values of $Q_{el}+Q_{ex}$ between E_{Ps} and E_{ex} for all three gases. None of the deduced Q_{el} contains

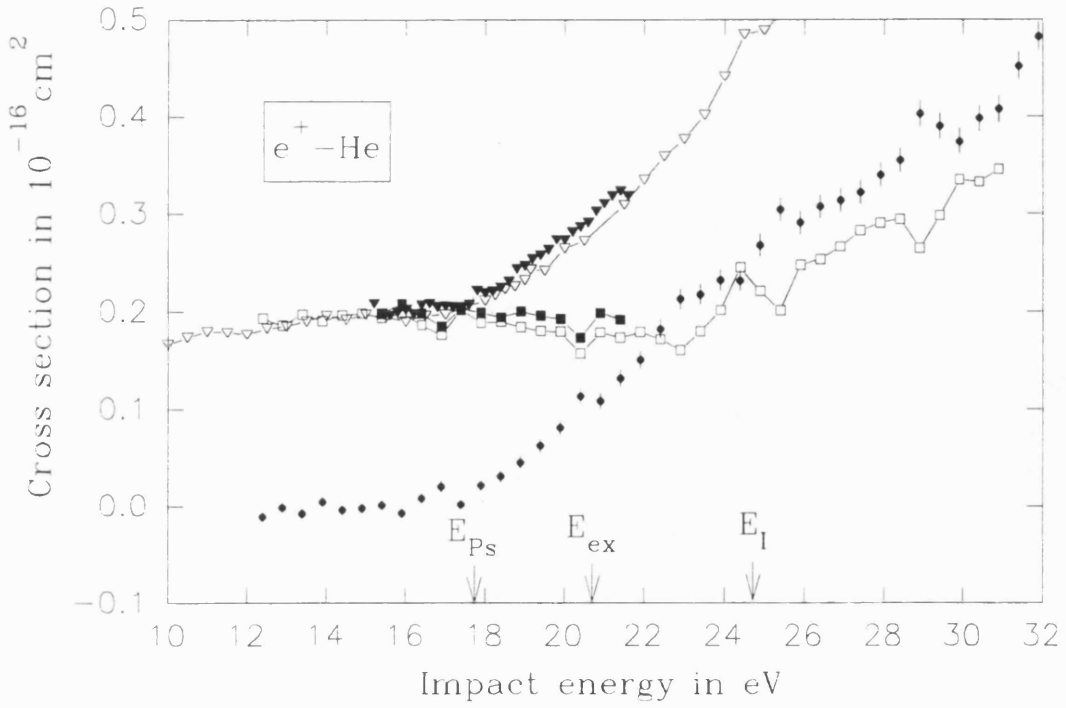

Figure 5.4. The present values of Q_t^+ for positron-He scattering, •; Q_t (Mizogawa *et al* 1985), ▾; Q_t (Stein *et al* 1978), ▿; Q_t(Mizogawa *et al* 1985)-Q_t^+, ■; Q_t(Stein *et al* 1978)-Q_t^+, □.

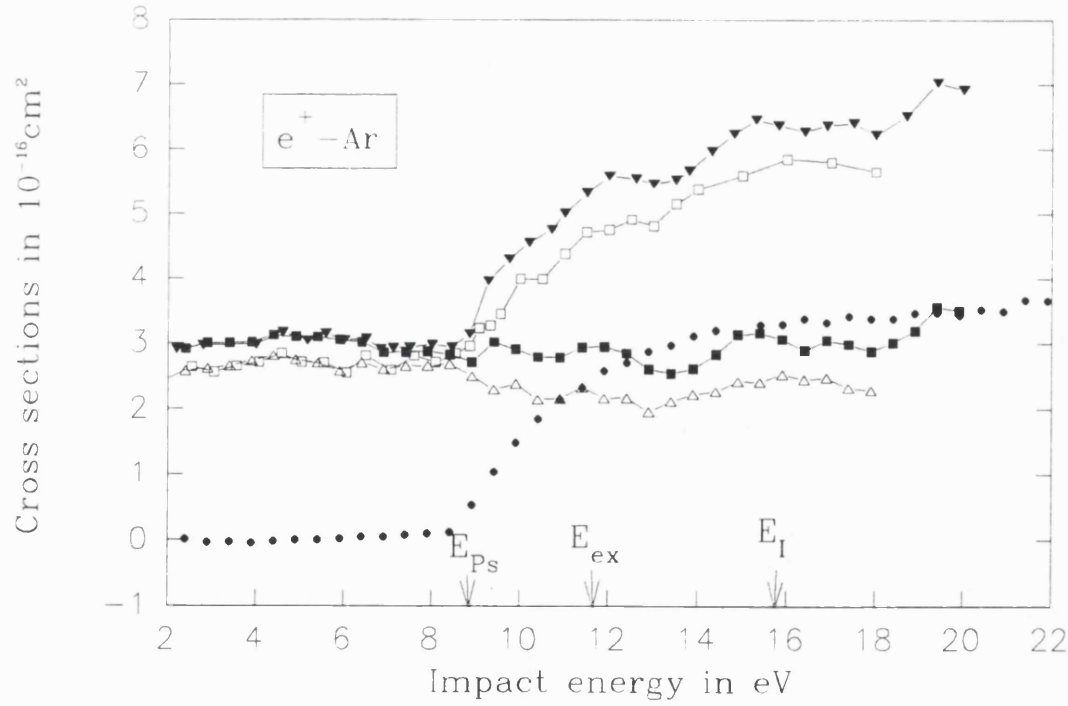

Figure 5.5. The present values of Q_t^+ for positron-Ar scattering, •; Q_t (Charlton *et al* 1984), ▾; Q_t (Kauppila *et al* 1976), □; Q_t(Charlton *et al* 1984)-Q_t^+, ■; Q_t (Kauppila *et al* 1976)-Q_t^+, ▿.

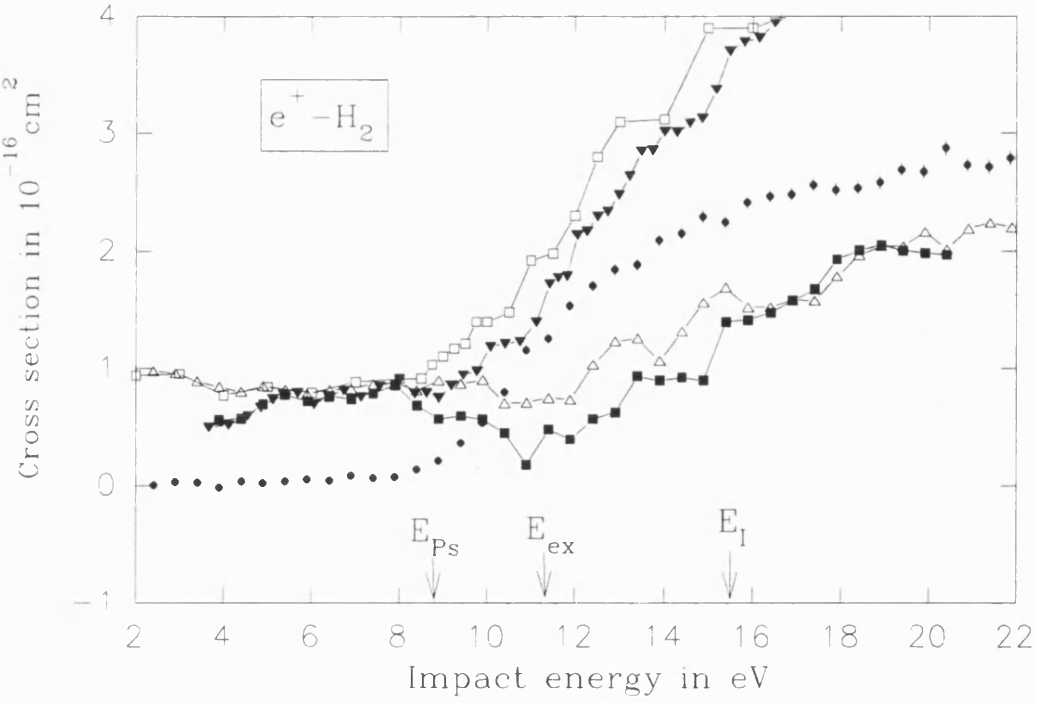

Figure 5.6. The present values of Q_t^+ for positron-H_2 scattering, •; Q_t (Hoffman *et al* 1982), □; Q_t (Charlton *et al* 1983), ▾; Q_t(Hoffman *et al* 1982)-Q_t^+, △; Q_t(Charlton *et al* 1983)-Q_t^+, ■.

a pronounced cusp-like feature peaked at E_{Ps} of the magnitude predicted by Campeanu *et al* (1987).

The behaviour of Q_t and Q_{el}, close to E_{Ps}, was then studied more closely. The values of Q_{el} in the energy range between E_{Ps} and E_{ex} are shown in figures 5.7, 5.8 and 5.9, along with the values of Q_t over a similar range of energies below E_{Ps}. E_b is an energy, the same distance below E_{Ps} as E_{ex} is above, i.e. $E_b = E_{Ps}-(E_{ex}-E_{Ps})$.

It is of interest that, in all cases, the energy dependencies of Q_t appear to have a positive slope just above E_{Ps}. In some cases there is a discontinuity between Q_t and Q_{el}, across E_{Ps}. This is due to the small non-zero values of Q_t^+, just below E_{Ps}, caused by the beam energy spread and has no physical significance. In order to obtain a quantitative estimate of the rise in Q_t below E_{Ps}, and the fall in Q_{el} above E_{Ps}, a linear least squares fit was made on the values of Q_t

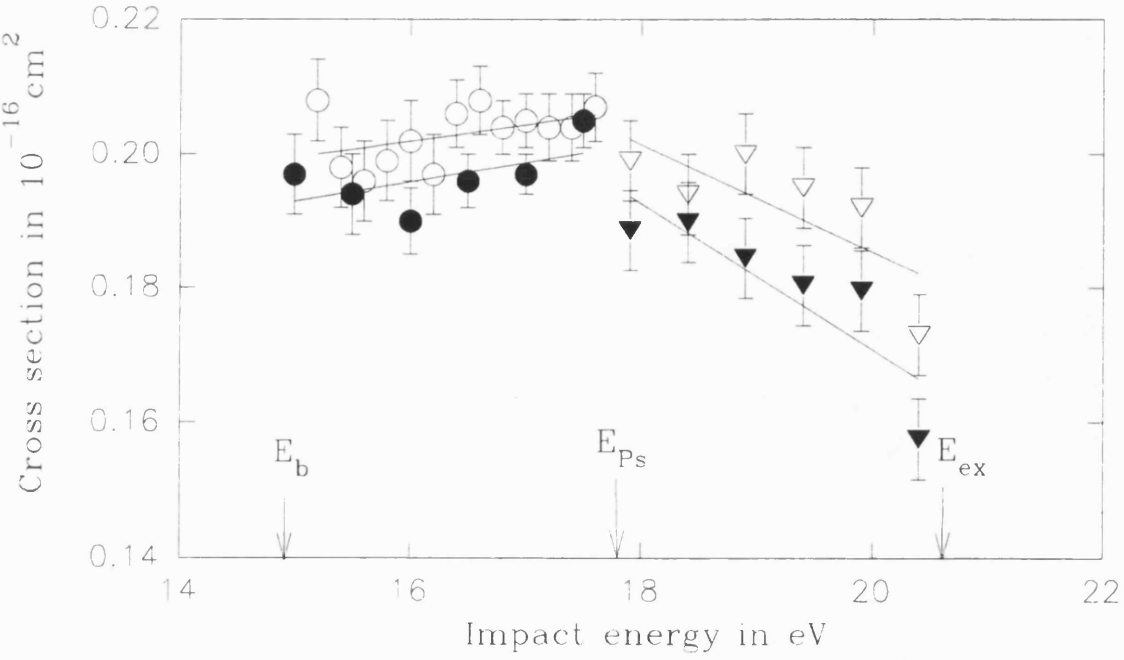

Figure 5.7. For positron-He scattering: Q_t (Mizogawa *et al* 1985), o; Q_t (Stein *et al* 1978), •; Q_t(Mizogawa *et al* 1985)-Q_t^+, ▽; Q_t (Stein *et al* 1978), ▼. The solid lines are least squares fits to the data.

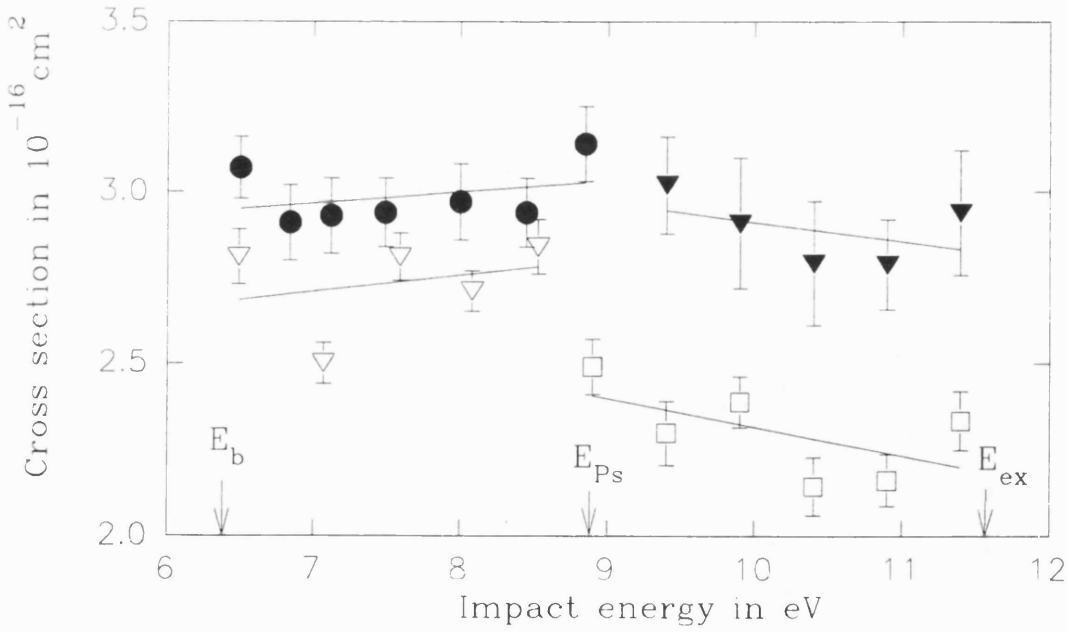

Figure 5.8. For positron-Ar scattering: Q_t (Charlton *et al* 1984), •; Q_t (Kauppila *et al* 1976), ▽; Q_t(Charlton *et al* 1984)-Q_t^+, ▼; Q_t(Kauppila et al 1976)-Q_t^+, □. The solid lines are least squares fits to the data.

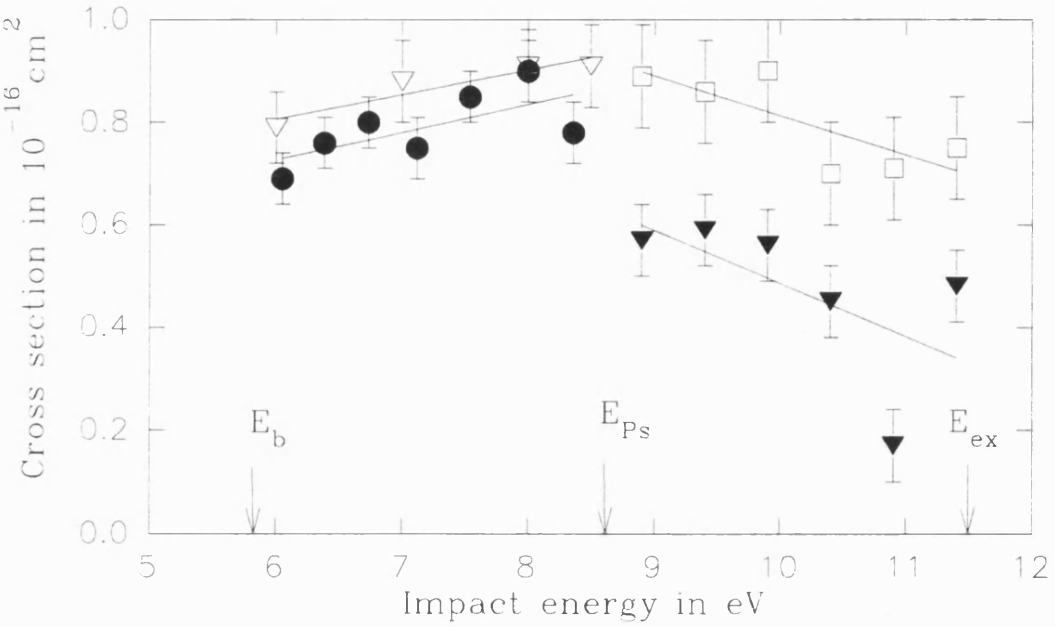

Figure 5.9. For positron-H_2 scattering: Q_t (Hoffman *et al* 1982), ▽; Q_t (Charlton *et al* 1983), •; Q_t(Hoffman *et al* 1982)-Q_t^+, □; Q_t(Charlton *et al* 1983)-Q_t^+, ▼. The solid lines are least squares fits to the data.

in the energy range E_b to E_{Ps} and on Q_{el} in the interval from E_{Ps} to E_{ex}. The fitted lines are also shown in figures 5.7, 5.8 and 5.9. The changes in Q_t (ΔQ_t) and Q_{el} (ΔQ_{el}) are defined as follows

$$\Delta Q_t = Q_t(E_{Ps}) - Q_t(E_b) \qquad (1.5.a)$$

$$\Delta Q_{el} = Q_{el}(E_{ex}) - Q_{el}(E_{Ps}) \qquad (1.5.b)$$

The values of ΔQ_t and ΔQ_{el} were obtained from the fit and are summarised in table 5.2.

Gas	Q_t used to derive ΔQ_t and ΔQ_{el}	ΔQ_t in $10^{-16}cm^2$	ΔQ_{el} in $10^{-16}cm^2$
Ar	Charlton *et al* (1984)	0.08 ± 0.11	-0.15 ± 0.15
Ar	Kauppila *et al* (1976)	0.13 ± 0.26	-0.22 ± 0.15
He	Mizogawa *et al* (1985)	0.013 ± 0.005	-0.023 ± 0.016
He	Stein *et al* (1978)	0.0087 ± 0.0043	-0.030 ± 0.010
H_2	Charlton *et al* (1983)	0.15 ± 0.075	-0.029 ± 0.18
H_2	Hoffman *et al* (1982)	0.13 ± 0.03	-0.22 ± 0.08

Table 5.2. A table showing the values of ΔQ_t and ΔQ_{el}.

In each case the fitted line has a positive slope below E_{Ps} and a negative slope above, indicating a small threshold effect due to Ps formation. Firm conclusions are inhibited by the large uncertainties in Q_t-Q_t^+ and, to a lesser extent, the energy calibration and resolution. The values of ΔQ_{el} in He are smaller than predicted by Campeanu *et al* (1987), being around 5% in the present analysis.

In addition to the analysis of Q_{el}, the values of Q_t-Q_t^+ have been used to estimate Q_{ex} of He. This was done by subtracting the average values of Q_t-Q_t^+ ($=Q_{el}$) just below E_{ex} from the values of Q_t-Q_t^+ ($=Q_{el}+Q_{ex}$) above E_{ex}. The result is shown in figure 5.10 compared with values of Q_{ex} measured by Coleman *et al* (1982) and Sueoka (1989) and the theoretical predictions by Hewitt *et al* (1992) (2S,2P) and Ficocelli-Varracchio and Parcell (1992) (2S,2P,3P). The present results for Q_{el} are those derived from values of Q_t obtained by Stein *et al* (1978).

The present values of Q_{ex} remain close to zero from threshold, at 20.6eV, up to around 23eV. The reason for the

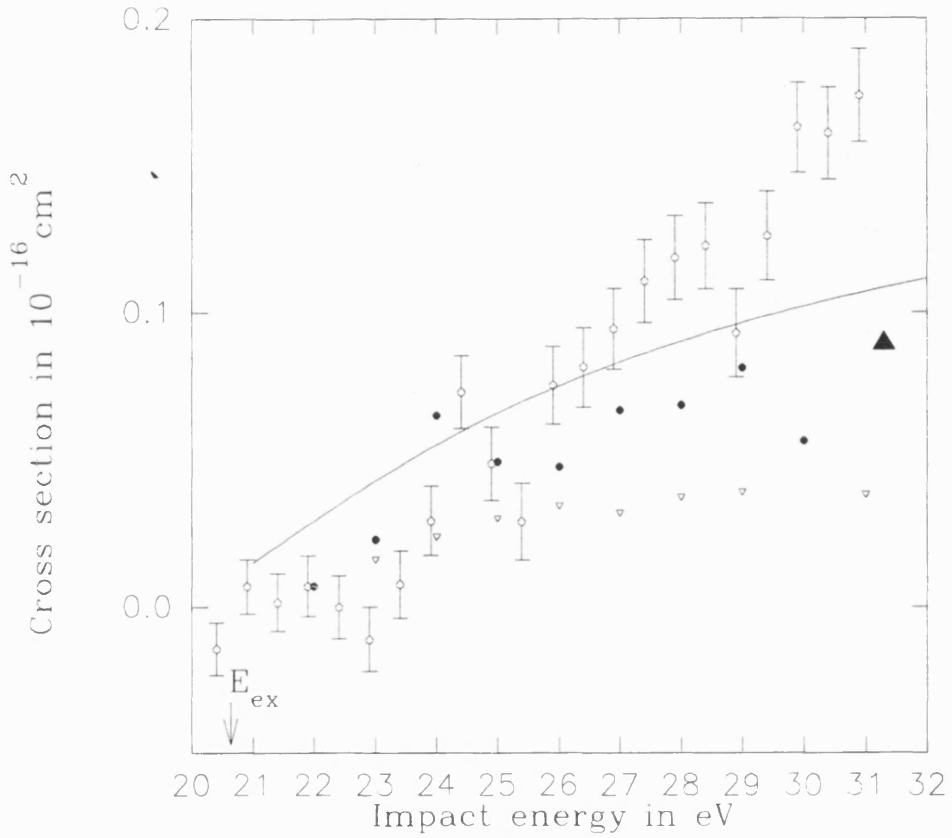

Figure 5.10. The present values of Q_{ex} for positron-He scattering, o; Q_{ex} (Sueoka 1989), •; Q_{ex} (Coleman *et al* 1982), ▽; Q_{ex} (Hewitt *et al* 1992), ▲; Q_{ex} (Ficocelli-Varraccio and Parcell 1992), solid line.

apparently zero values of Q_{ex} below 23eV is at present unknown, but may be due to uncertainties in Q_t-Q_t^+. As already mentioned, the energy calibration of the present data was confirmed by observing the position of the threshold in Q_t^+. Above 23eV Q_{ex} rises and continues to do so up to 30eV, the highest energy for which Q_{ex} was estimated. The present values of Q_{ex} are significantly greater than previous estimates. However the present results must be viewed with caution, due to the indirect manner in which they have been derived.

5.3 The Energy Dependence of Q_{Ps} Close to Threshold

The R-matrix threshold theory may be used to derive an

expression for Q_{Ps} (Moxom *et al* 1993a). For a single incoming and outgoing angular momentum, l and l′

$$Q_{Ps} = \frac{4\pi}{k^2}(2l+1) \; . \; P^{(l)}(kR) \; . \; P^{(l')}(k'R) \; . \; r^{(l,l')} \qquad (5.2)$$

where k and k′ are the wave-numbers of the positron and Ps atom respectively and R is the radius of the R-matrix sphere, outside of which the wave-functions of the incoming and outgoing particles are unaffected by the scattering centre. $P^{(l)}$ and $P^{(l')}$ are penetration factors, and the last term is a ratio of the R-matrix elements coupling the elastic and inelastic channels and is only weakly dependent on E. The first two terms are functions of k and are therefore also expected to vary slowly with E, close to E_{Ps}. Hence, close to the reaction threshold, the main energy dependence of the cross-section is determined by the second penetration factor $P^{(l')}$ and Q_{Ps} may be written

$$Q_{Ps} \approx a \; P^{(l')}(k'R) \qquad (5.3)$$

where (a) is a constant of proportionality. Since there are no long range Coulomb forces in the final channel, $P^{(l')}$ has the following form (Lane and Thomas 1958)

$$P^{(l')} = \frac{(k'R)^{2l'+1}}{1+(k'R)^{2l'}} \qquad (5.4)$$

Then, if k′R<<1, equation 5.4 becomes

$$P^{(l')} \approx (k'R)^{2l'+1} \qquad (5.5)$$

If R is of the order of an atomic radius, the inequality condition is satisfied over a range of a few eV above E_{Ps}. If E′ is the kinetic energy of the Ps atom then equation 5.3 can be written

$$Q_{Ps} \approx a \; (E')^{l'+1/2} \qquad (5.6)$$

If more than one partial wave contributes to the cross-

section this expression must be summed over all the relevant angular momenta. If the measured values of Q_{Ps} can be fitted to a curve of this form, the value of l' may be deduced. The values of l that couple to the Ps formation channel are dictated by conservation of angular momentum

$$\underline{l} = \underline{l}_{ion} + \underline{l'} \qquad (5.7)$$

and conservation of parity

$$(-1)^{l} = (-1)^{l_{ion}+l'} \qquad (5.8)$$

Here l_{ion} is the angular momentum of the ion, which for a rare gas is equal to the angular momentum of the electron captured to form Ps. This information may then be used to analyze the threshold effects in Q_{el} or Q_t as described in § 5.4.

To analyze Q_{Ps} in this way, the present results for Q_t^+ ($Q_t^+ = Q_{Ps}$ up to E_I) were least squares fitted to a curve of the form

$$Q_{Ps} = a_0 (E')^{b_0} + a_1 (E')^{b_1} \qquad (5.9)$$

which assumes that only two partial waves, e.g. $l' = 0$ and $l' = 1$, can contribute to Q_{Ps}. Initially, to test whether the data could be fitted by a single partial wave, the fit was performed with $a_1 = 0$ and using a_0 and b_0 as fitting parameters. The results are shown in figure 5.7, plotted logarithmicly, so that such a curve will yield a straight line with a gradient equal to b_0.

For Ne and Ar, the data were well fitted in this way up to several eV above threshold, indicating that close to threshold the cross-sections are dominated by single partial waves. The He data could not be fitted in this way, indicating that the cross-section contains significant contributions from more than one partial wave.

In Ar, the data could be fitted up to ~4eV above E_{Ps} with $b_0 = 0.51 \pm 0.01$. Comparison with equation (5.6) indicates therefore that predominantly $l' = 0$. For Ar, close to E_{Ps}, a positron must pick up a 3p electron to form a Ps atom and so,

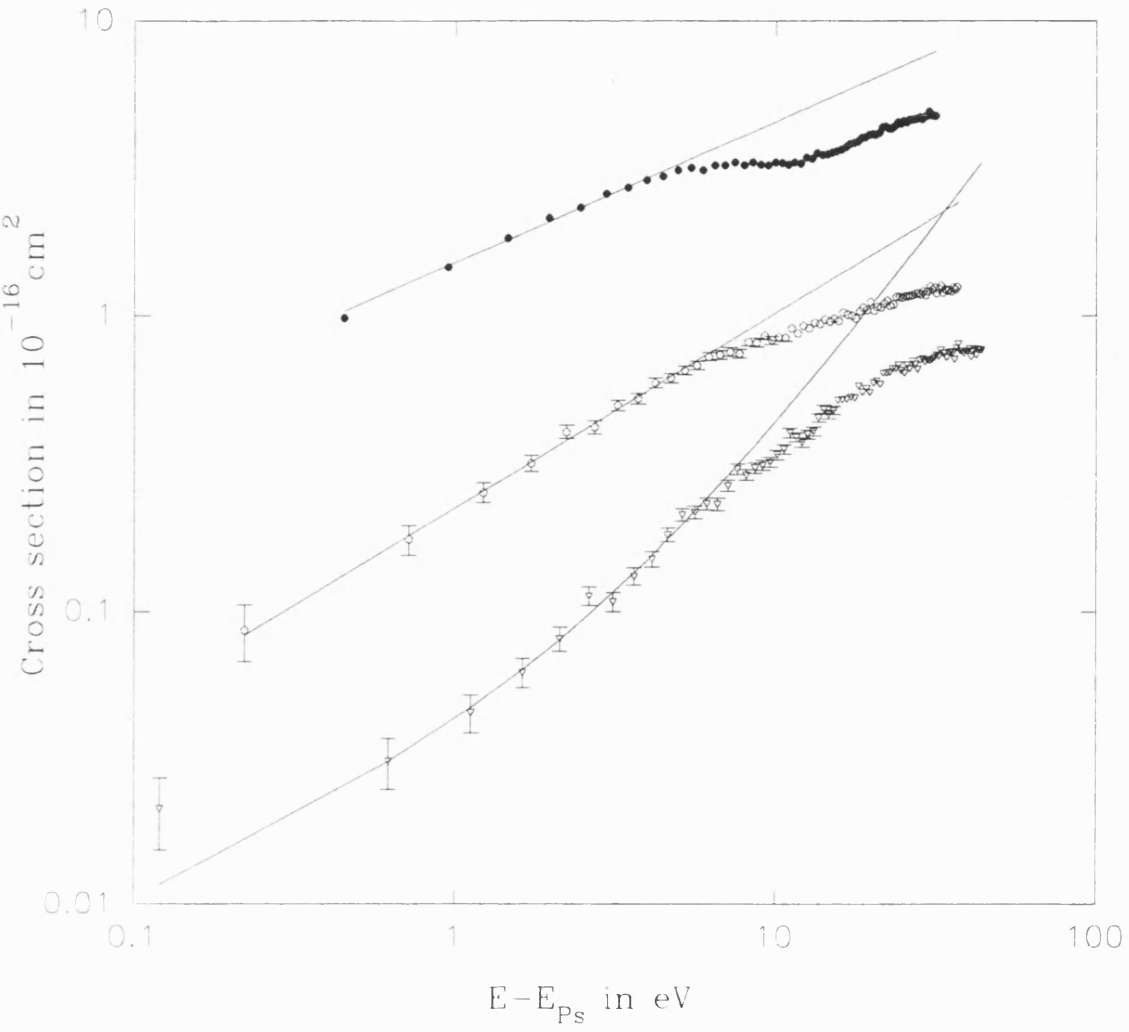

Figure 5.11. Present values of Q_i^+ for He, ▽; Ne, ○ and Ar, •. The solid lines are least squares fits to the data.

from equation (5.7) the most likely value of the incoming angular momentum that couples to the Ps channel is l = 1.

In the case of Ne the data may be fitted for up to ~6eV above E_{Ps}, by $b_0 = 0.66 \pm 0.01$. Here the situation is not quite as clear as for Ar, but suggests that the outgoing Ps is predominantly s-wave in character.

The He data was fitted by setting $b_0 = 1/2$ and $b_1 = 3/2$, i.e. assuming contributions from s- and p-waves. Then a_0 and

a_1 were used as fitting parameters. The fit was extended to around E′ = 6eV yielding a_0 = 0.031±0.003 and a_1 = 0.011±0.001 where the cross-section is in units of $10^{-16}cm^2$ and E′ is in eV. The point at 0.12eV lies above the fitted curve. This is attributed to the 0.8eV FWHM energy spread of the beam, causing the measured values of Q_t^+ this close to threshold to appear too high. Therefore this point was not included in the fit.

5.4 Threshold Effects in Positron-Ar Scattering

The cross-section in which a threshold effect occurs (Q_{el} or Q_t) may be decomposed in the following way

$$Q_{el,t}(E) = Q_0(E) + \Delta Q_{el,t}(E, E') \qquad (5.10)$$

where ΔQ_{el} (ΔQ_t) is the "threshold effect" in Q_{el} or Q_t. These effects are related by

$$\Delta Q_t = \Delta Q_{el} + Q_{Ps} \qquad (E > E_{Ps}) \qquad (5.11.a)$$

$$\Delta Q_t = \Delta Q_{el} \qquad (E < E_{Ps}) \qquad (5.11.b)$$

$$\Delta Q_t = \Delta Q_{el} = 0 \qquad (E = E_{Ps}) \qquad (5.11.c)$$

and the cross-section Q_0 is given by

$$Q_0 = \frac{4\pi}{k^2} \sum_l (2l+1) \sin^2\delta_l \qquad (5.12)$$

where δ_l is the elastic phase shift of the incident positron that couples to the Ps formation channel, calculated with the Ps formation channel hypothetically suppressed.

By definition, the threshold effects are zero at threshold and so at E_{Ps}

$$Q_0(E_{Ps}) = Q_t(E_{Ps}) = Q_{el}(E_{Ps}) \qquad (5.13)$$

By considering the unitarity of the scattering matrix, and its analytic continuation across the threshold, the following formulae may be derived (Meyerhof 1963).

$$\Delta Q_{el} = Q_{Ps} \begin{cases} -1+\cos 2\delta_l & (E>E_{Ps}) \qquad (5.14.a) \\ (-1)^{l'+1} \sin 2\delta_l & (E<E_{Ps}) \qquad (5.14.b) \end{cases}$$

$$\Delta Q_t = Q_{Ps} \begin{cases} \cos 2\delta_l & (E>E_{Ps}) \qquad (5.14.c) \\ (-1)^{l'+1} \sin 2\delta_l & (E<E_{Ps}) \qquad (5.14.d) \end{cases}$$

As before, if more than one partial wave contributes to Q_{Ps}, the expressions must be summed over all the relevant angular momenta.

In order to evaluate the threshold effects in Q_{el} or Q_t, it is first necessary to know l', Q_{Ps} and δ_l. By analysing the energy dependencies of Q_{Ps}, as described in the previous section, the appropriate values of l' to be used in the analysis may be determined. Then, using theoretical phase shifts (e.g. McEachran *et al* 1979), the present values of Q_{Ps} may be used to calculate the magnitude and shape of the threshold effect in Q_{el} and Q_t. These may then be compared with experiment. This was done for Ar, since, according to the analysis of § 5.3, only one outgoing angular momenta contributes significantly to Q_{Ps} close to E_{Ps}. This is the s-wave indicating that $l = 1$. Thus the p-wave elastic phase shifts of McEachran *et al* (1979) must be used to calculate the threshold effects and Q_0. Close to threshold, these phase shifts are small and positive. Therefore, according to

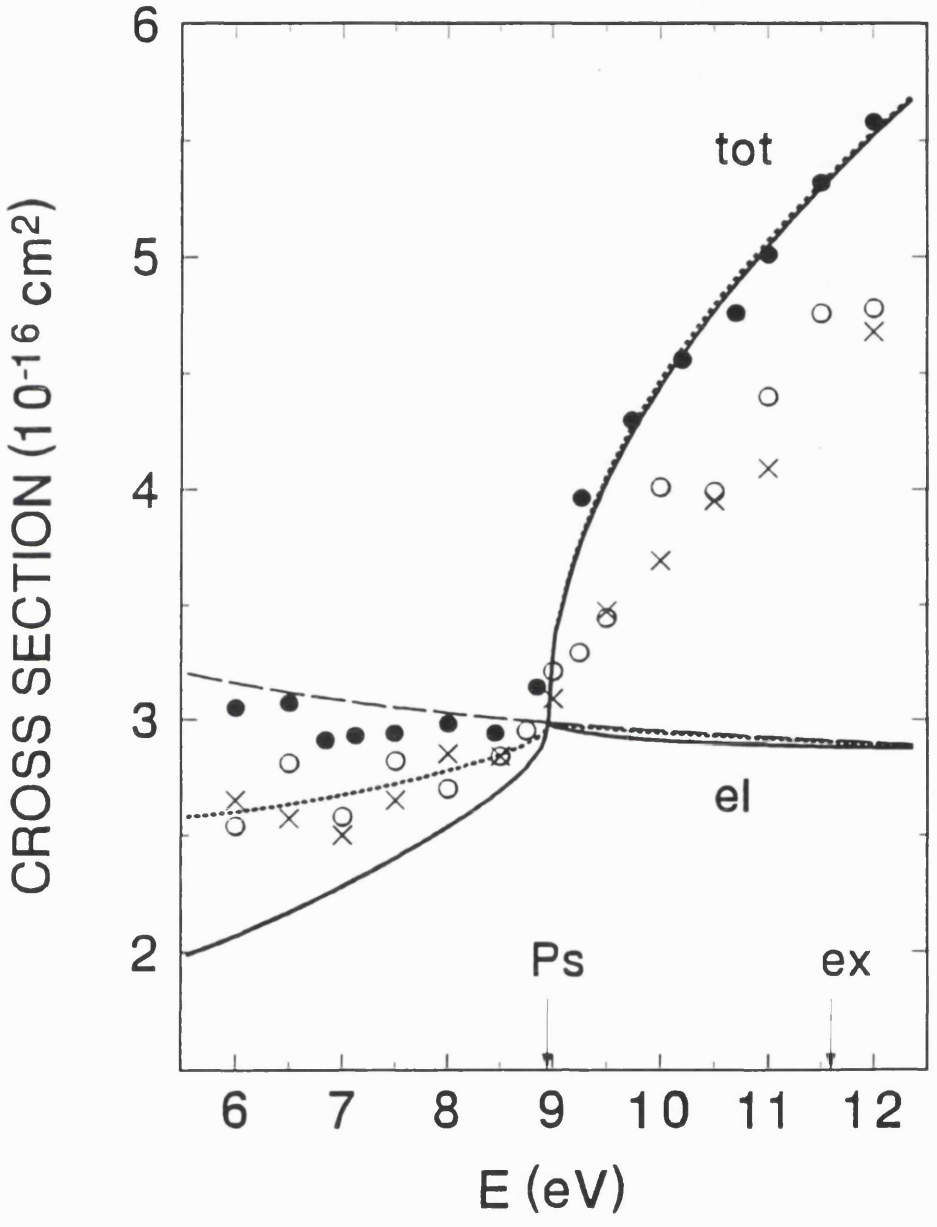

Figure 5.12. Q_t values from Kauppila *et al* (1976) ○, Coleman *et al* (1980) • and Charlton *et al* (1984) ×. Dashed curve is Q_0, solid curves are Q_{el} and Q_t derived using δ_1 from McEachran *et al* (1979) and dotted curves are Q_{el} and Q_t derived using $\delta_1 \div 2$.

equation (5.14.b), the threshold effects in Q_{el} are small and negative both above and below E_{Ps} and are expected to lead to a small cusp in Q_{el}. In order to smooth out statistical fluctuations, the values of Q_{Ps} used in this analysis are those obtained by fitting the data to a curve, as described in § 5.3.

In order to proceed with the analysis, the values of Q_0 obtained from the p-wave elastic phase shifts of McEachran *et al* (1979) must be fitted, so that equation 5.13 is satisfied. One way to do this is to multiply the theoretical values of Q_0 by a constant (f). Figure 5.12 shows the Q_t values of Charlton *et al* (1984), Kauppila *et al* (1976) and Coleman *et al* (1980). This figure also shows Q_0 from McEachran *et al* (1979) fitted to Q_t with f = 1.1 and the predicted behaviour of Q_{el} and Q_t from equations (5.14.a-d) and 5.10. Above E_{Ps}, the derived Q_t is in good agreement with the data of Charlton *et al* (1984), however, the values of Q_t measured by Kauppila *et al* (1976) and Coleman *et al* (1980) are slightly smaller. Below E_{Ps} all three measurements lie above the derived Q_t. This indicates that the phase shifts of McEachran *et al* (1979) may be too large. If they are arbitrarily halved, the agreement for $E < E_{Ps}$ is generally improved, as shown. Above E_{Ps} the threshold effect is small and relatively insensitive to changes in the value of δ_1, since it follows the cosine dependence given by equations (5.14.a) and (5.14.c). Hence, above E_{Ps}, doubling the phase shift makes very little difference to ΔQ_t, with the prediction remaining in good agreement with the results of Charlton *et al* (1984).

A similar analysis in the case of He is complicated by the fact that more than one partial wave seems to contribute significantly to Q_{Ps}.

5.5 Near Threshold Effects in Positron O_2 Scattering

Evidence of another form of channel coupling effect has been observed in the case of O_2. Here a broad dip in Q_t^+ has been

found, corresponding to a broad maximum in the cross-section for excitation to the Schuman-Runge continuum (Q_{SR}), as measured by Katayama *et al* (1987).

At the time these measurements were made the gain of the ion detector (C2) had greatly deteriorated due to ageing. This resulted in output pulses that were small in comparison with the noise on the ion signal line due to stray coupling with the high voltage pulses from the ion extractor. It was therefore not possible to pulse the ion-extractor and instead, a d.c. potential of a few volts was applied in conjunction with a d.c. beam. The effect of this potential on the ion-yield was investigated and no effect on the energy dependence of the ion-yield or on the beam intensity was observed when measurements were made with V_{ex} less than 2V. The ion count rates and beam intensities were measured in the same way as before, with V_m ramped in steps of 0.5V. These measurements were made with a beam with a FWHM of around 1.1eV.

Figure 5.13 shows an ion-yield obtained for O_2. This data was obtained by averaging 4 runs lasting around ($8-24 \times 10^4$)s. The values of Q_t^+ used for normalisation were estimated by averaging Q_t measured by Charlton *et al* (1983) below E_{Ps} (between 2 and 4eV) and subtracting this value from Q_t above E_{Ps}. The ion-yield was then normalised to these values between 5 and 7eV to obtain an estimate of Q_t^+.

Q_t^+ rises very steeply from close to E_{Ps} at 5.3eV and continues to rise up to around 8eV. This is followed by a decrease in Q_t^+ of around 12% at around 12eV, above which Q_t^+ begins a more gradual rise over the remainder of the energies investigated. This energy dependence is significantly different from that observed in all the other gases studied (He, Ne, Ar and H_2). In these gases Q_t^+ was found to increase smoothly with impact energy. Also shown in figure 5.13 is Q_{SR} measured by Katayama *et al* (1987). This cross-section has a broad maximum around 12eV which corresponds to the dip in Q_t^+. It is interesting to note that the decrease in Q_{SR} begins close to E_I at 12.1eV, around which Q_t^+ begins to rise again.

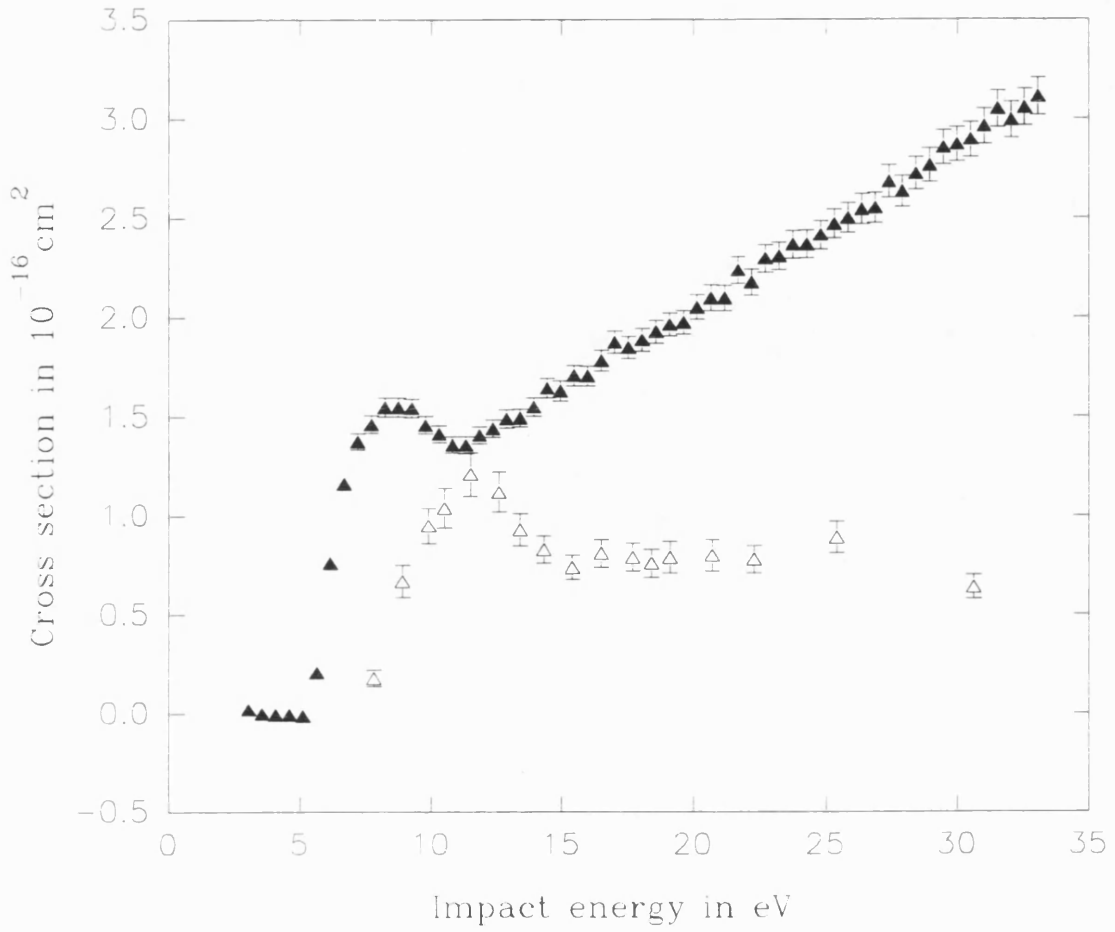

Figure 5.13. Present values of Q_t^+ for positron-O_2 scattering ▲ and Q_{SR} from Katayama *et al* (1987) △.

This correlation indicates that there is coupling between the channels, similar to that between Q_{Ps} and Q_{el} for He, Ar and H_2. However in the case of O_2 the effect seems to be more pronounced and the cross-section containing the effect (Q_t^+) has been observed directly.

5.6 Summary

The energy dependencies of Q_{el} for positron scattering in He, Ar and H_2 have been derived from the present values of Q_t^+. There is no evidence of a Wigner cusp at E_{Ps} of the magnitude

expected by Campeanu *et al* (1987), however a small change in the slope of Q_{el} is apparent in the vicinity of E_{Ps}, suggesting that there is a small threshold effect caused by coupling between the Ps formation and elastic scattering channels.

The energy dependencies of Q_{Ps} have been analyzed for He, Ne Ar and H_2 and the dominant partial waves that contribute to Q_{Ps} have been deduced. In the case of Ar, the Ps appears to be almost entirely s-wave in character. This information has been used to predict the threshold effects in Q_t, using the elastic scattering phase shifts calculated by McEachran *et al* (1979). The expected behaviour has been compared with experiment and this indicates that the true phases shifts are smaller than estimated by McEachran *et al* (1979). The small phase shifts are in qualitative accord with the hypothesis that, for positron scattering, the interaction potential is weak due to a partial cancelation of the static and polarisation interactions.

Q_t^+ has been measured for O_2. Structure has been observed in Q_t^+ for this target, which is not present in the other gases studied and this is ascribed to coupling between the Ps formation and excitation to the Schuman Runge continuum channels as suggested by Laricchia and Moxom (1993).

CHAPTER 6

CONCLUSIONS

The work presented in this thesis concerns experimental investigations of positron impact ionisation phenomena. The phenomenon of electron capture to the continuum (ECC) was studied and the total ionisation cross-sections measured for a variety of atomic and molecular targets. In the latter case, the energy dependence of the Ps formation cross-section, close to its threshold, and channel coupling phenomena received particular attention.

ECC arises if a high degree of correlation exists between a scattered positively charged projectile and an ejected electron. It has been shown that, in collisions involving protons and positive ions as projectiles, ECC may give rise to cusp-like peaks in the ejected electron energy spectra (e.g. Crooks and Rudd 1970, Rodbro and Andersen 1979). It has also been suggested that ECC may result in structures in the double and triple differential cross-sections in the case of positron-atom(molecule) scattering. However, theoretical results (Schultz and Reinhold 1990, Mandal *et al* 1986, Sil *et al* 1991, Brauner and Briggs 1986) disagree as to the magnitude and shape of such structures.

In the present work, the significance of ECC in positron-Ar scattering has been assessed by measuring the ejected electron energy spectra. This was done using two different methods involving TOF and retarding potential measurements. A novel ion extractor was developed and employed to allow the detection of ions formed in a long scattering cell. In both cases the remnant ion was detected and used to gate the data acquisition system, in order to discriminate between electrons originating from the target

gas and background electrons originating from metal surfaces in the apparatus.

No major cusp-like structures of the type predicted by Mandal *et al* (1986) and Sil *et al* (1991) were found, however some spectra showed evidence of minor structures at energies compatible with ECC. The shape of this structure resembles the small ridge predicted by Schultz and Reinhold (1990) in the case of positron-H scattering. Its magnitude suggests that, in the case of a light positively charged projectile, ECC makes a minor contribution to ionisation at small forward emission angles. The absence of any major structures in these spectra have now been confirmed by Kover *et al* (1993) using an electrostatically transported positron beam which enabled an angular resolution of ±6° and an energy resolution of 4% to be achieved.

The total ionisation cross-section (Q_t^+), including contributions from Ps formation, was measured for a range of atomic and molecular gases. Values of Q_t^+ were derived from ion-yields obtained by a particle counting technique. These were measured for He, Ar and H_2, over the range of impact energies from below threshold to around 300eV, using a technique involving pulsed electron or positron beams with a narrow energy spread. The beam and ion extractor were pulsed on and off in anti-phase, in order to avoid deflection of the beam during the collision. The energy dependence of the ion-yields obtained by electron impact have been compared with total ionisation cross-sections obtained by summing partial cross-sections available in the literature, in order to verify that the ion extraction technique had no significant energy dependence. Ion-yields have been obtained for positron impact over a similar energy range and, furthermore, the near threshold behaviour for He, Ne, Ar and H_2 has been examined in greater detail.

Absolute cross-sections were deduced from the ion-yields by normalisation to existing data. These values of Q_t^+ were used to derive new estimates of Q_{el}, close to E_{Ps} for He, H_2 and Ar. No evidence was found of a Wigner-like cusp around E_{Ps} of

the magnitude suggested by Campeanu *et al* (1987). A small threshold effect, however, appears to be present in Q_{el}. This is believed to be consistent with the weak interaction between a positron and an atom, resulting from the partial cancellation between the static and polarisation potentials.

Below E_I the energy dependencies of Q_t^+ for He, Ne and Ar were analyzed using formulae derived using R-matrix theory (Wigner 1948) and the dominant partial waves in the Ps formation channel close to threshold deduced. Additionally, the magnitude of the threshold effects in Q_{el} and Q_t for Ar were computed using the present results for Q_t^+ together with the purely elastic scattering cross-sections calculated by McEachran *et al* (1978). Comparison with available measurements of Q_t suggests that the phase shifts of McEachran *et al* (1979) might be too large.

In the near threshold behaviour of Q_t^+ for O_2, structure was found in the form of a minimum in Q_t^+ which coincides with a maximum in the cross section for excitation to the Schuman-Runge continuum. This is attributed to coupling between the two inelastic channels.

It is planned to make more precise measurements of Q_t^+ and to extended this work to a wider range of targets. By extending measurements to higher energies, where Q_t^+ is expected to equal Q_t^-, it is hoped that absolute values of Q_t^+ may be obtained at low energies without having to normalise to existing positron data.

In order to deduce the behaviour of Q_{el} across E_{Ps}, measurements of total cross-sections, using the same apparatus as that employed to measure Q_t^+ would be highly valuable. It is also expected that the investigation of threshold effects may soon be extended to differential measurements, where a higher degree of sensitivity is expected.

With the availability of positron beams of ever increasing intensity and quality, experiments will be performed with significantly higher precision and resolution. Interesting results in this field are anticipated.

References

Acacia P, Campeanu R I, Horbatsch M McEachran R P and Stauffer A D (1993) submitted to *J. Phys. B*

Adachi S, Chiba M, Hirose T, Nagayama S, Nakamitsu Y, Sato T and Yamada T (1990) *Phys. Rev. Leyy* **65** 2634

Adkins G S (1983) *Ann. Phys.* (N.Y) **146** 18

Amusia M Ya, Cherepkov N A, Chernysheva L V and Shapiro S G (1976) *J. Phys. B* **9** L531

Andersen L H, Hvelplund P, Knudsen H, Moller S P Sorensen A H, Elsener K, Rensfelt K G and Uggerhoj E (1987) *Phys. Rev. A* **36** 3612

Anderson C D (1932) *Phys. Rev.* **41** 405

Andrick D, Eyb M and Hoffman H (1972) *J. Phys. B* **5** L15

Basu M, Mazumdar P S and Ghosh A S (1985) *J. Phys. B* **18** 369

Bartschat K, McEachran R P and Stauffer A D (1988) *J. Phys. B* **21** 2789

Baz A I (1958) *Soviet Phys. JETP* **6** 709

Billoire A, Lacaze R, Morel A and Navelet H (1978) *Phys. Lett.* **78B** 140

Blackett P M S and Occchialini G P S (1933) *Proc. Roy. Soc A* **B** 699

Brandes G R, Canter K F, Horsky T N, Lippel P H and Mills A P (1988) Rev. *Sci. Inst.* **59** 228

Brauner M and Briggs J S (1986) *J. Phys. B* **19** L325

Brown B L (1986) in "Positron Studies of Solids, Surfaces and Atoms" ed. A P Mills, W S Crane and K F Canter (World Scientific, Singapore)

Brown C J and Humberstom J W (1984) *J. Phys. B* **17** L423

Brown C J and Humberstom J W (1985) *J. Phys. B* **18** L401

Brunings J (1934) *Physica* **1** 996

Bussard R W, Ramaty R and Drachman R J (1979) *Astrophys. J.* **228** 928

Campeanu R I, Fromme D, Kruse G, McEachran R P, Parcell L A, Raith W, Sinapius G and Stauffer A D (1987) *J. Phys. B*

20 3557

Campeanu R I, McEachran R P and Stauffer A D (1987b) J. Phys. B 20 1635

Canter K F, Coleman P G, Griffith T C and Heyland G R (1972) *J. Phys. B* **5** L167

Caswell W E and Lepage G P (1976) *Phys. Rev. A* **20** 36

Chang Tian-Bao, Tang Hsiaowei, and Li Yaoqing (1985) "Positron Annihilation" (eds. Jain P C, Singru R M and Gopinathan K P world scientific) p.212

Charlton M (1985) *Rep. Prog. Phys.* **48** 737

Charlton M, Andersen L H, Brun-Nielsen L, Deutch B I, Hvelplund P, Jacobsen F M, Knudsen H, Larrichia G, Poulsen M R and Pedersen J O (1988) *J. Phys. B* **21** L545

Charlton M, Brun-Neilsen L, Deutch B I, Hvelplund P, Jacobsen F M, Knudsen H, Larrichia G and Poulsen M (1989) *J. Phys. B* **22** 2779

Charlton M, Clark G, Griffith T C and Heyland G R (1983) *J. Phys. B* **16** L465

Charlton M, Griffith T C, Heyland G R Lines K S and Wright G L (1980) *J. Phys. B* **13** L757

Charlton M, Griffith T C, Heyland G R and Wright G L (1983) *J. Phys. B* **16** 323

Charlton M, Laricchia G, Griffith T C, Wright G L and Heyland G R (1984) *J. Phys. B* **17** 4945

Charlton M and Larrichia G (1990) *J. Phys. B* **23** 1045

Charlton M, Laricchia G, Zafar N and Jacobsen F M (1987) in "Atomic Physics with Positrons" ed. Humberston J W and Armour E A G (Plenum) p.15

Cherry W (1958) PhD thesis, Princeton University

Coleman P G (1986) in "Proceedings of the 3rd International Workshop on positron (electron)-Gas Scattering" (World Scientific) ed. Kauppila W E, Stein T S and Wadhera J M p.25

Coleman P G, Griffith T C, Heyland G R and Killeen T L (1975) *J. Phys. B* **8** 1734

Coleman P and Hutton J T (1980) *Phys. Rev. Lett.* **45** 2017

Coleman P, Hutton J T, Crook D R and Chandler C A (1982) *Can.*

J. Phys. **60** 584

Coleman P, Johnston K A, Cox A M G, Goodyear A and Charlton M (1992) *J. Phys. B* **25** L585

Coleman P and McNutt J D (1979) *Phys. Rev. Lett.* **42** 1130

Coleman P, McNutt J D, Diana L M and Burgiaga (1979) *Phys. Rev. A* **20** 145

Coleman P, McNutt J D, Diana L M and Hutton J T (1980) *Phys. Rev. A* **22** 2290

Coleman P, McNutt J D, Hutton J T, Diana L M and Fry J L (1980) *Rev. Sci. Inst.* **51** 935

Costello D G, Groce D E, Herring D F and McGowan J W (1972) *Phys. Rev. B* **5** 1433

Costello D G, Groce D E, Herring D F and McGowan J W (1972a) *Can J. Phys.* **50** 23

Crooks G B and Rudd M E (1970) *Phys. Rev. Lett.* **25** 1599

Dale J M, Hulett L D and Pendyala S (1980) *Surf. Int. Anal* **2** 199

Deutsch M (1951) *Phys. Rev.* **82** 455

de Heer F J McDowell M R C and Wagenaar R W (1977) *J. Phys. B* **10** 1945

Dewangan D P and Walters H R J (1977) *J. Phys. B* **10** 637

Diana L M, Brooks D L, Coleman P G Chaplin R L and Howell (1989) in "Positron Annihilation" ed. Dorikens-Vanpraet L, Dorikens M and Segers D (Singapore: World Scientific) p.311

Diana L M, Coleman P G, Brooks D L and Chaplin R L (1987) in "Atomic Physics with Positrons" ed. Humberston J W and Armour E A G (New-York: Plenum) p.55

Diana L M, Coleman P G, Brooks D L, Pendleton P K and Norman D L (1986) P*hys. Rev. A* **34** 2731

Diana L M, Coleman P G, Brooks D L, Pendleton P K, Norman D M, Seay B E and Sharma S C (1986a) in "Positron(Electron)-Gas Scattering" ed. Kaupplia W E, Stein T S and Wadhera J M (Singapore: world Scientific) p.296

Diana L M, Fornari L S,Sharma S C, Pendleton P K and Coleman P G (1985) in "Positron(Electron)-Gas Scattering" ed.

Kaupplia W E, Stein T S and Wadhera J M (Singapore: world Scientific) p342

Diana L M, Sharma S C, Fornari L S, Coleman P G, Pendleton P K, Brooks D L and Seay B E (1985a) in "Positron Annihilation" ed. Singru R M and Jain P C (Singapore: World Scientific) p.428

Dirac P.A.M. (1930a) *Proc. Roy. Soc.* **A** 126 360

Dirac P.A.M. (1930b) *Proc. Camb. Phil. Soc.* **26** 361

Dou L, Kauppila W E, Kwan C K and Stein T S (1992) *Phys. Rev. Lett.* **68** 2913

Drachman R J (1966) *Phys. Rev.* **144** 25

Dubois R D and Rudd M E (1975) *J. Phys. B* **8** 1474

Eyb M and Hoffman H (1975) *J. Phys. B* **8** 1095

Fainstein P D, Ponce V H and Rivarola R D (1987) *Phys. Rev. A* **36** 3639

Ficocelli-Varracchio E and Girardeau M D (1983) *J. Phys. B* **16** 1097

Ficocelli-Varracchio E and Parcell L A (1992) *J. Phys. B* **25** 3037

Fite W L and Brachmann R T (1958) *Phys. Rev.* **112** 1142

Floeder K, Honer P, Raith W, Schwab A, Sinapius G and Spicher G (1988) *Phys. Rev. Lett.* **60** 2363

Fonda L (1961) *Nuovo Cimento Suppl.* **20** 116

Fornari L S, Diana L M and Coleman P G (1983) *Phys. Rev. Lett.* **51** 2276

Frieze W E, Gidley D W and Lynn K G (1985) *Phys. Rev. B* **31** 5628

Fromme D, Kruse G, Raith W and Sinapius G (1986) *Phys. Rev. Lett* **5** 3031

Fromme D, Kruse G, Raith W and Sinapius G (1988) *J. Phys. B.* **21** L261

Fulton T and Martin P C (1954) *Phys. Rev.* **95** 811

Gehenn W and Reichert E (1972) *Z. Phys.* **254** 28

Ghosh A S, Mazumdar P S and Basu M (1985) *Can. J. Phys.* **63** 621

Gidley D W, Rich A, Sweetman E and West D (1982) *Phys. Rev. Lett* **49** 525

Golden D E and Bandel H W (1966) *Phys. Rev.* **149** 58
Golden J E and McGuire J H (1976) *Phys. Rev. A* **13** 1012
Griffith T C (1983) in "Positron Scattering in Gases" ed. Humberston J W and McDowell (New York:Plenum) p.53
Groce D E, Costello D G, McGowan J W and Herring W F (1969) in "Book of Abstracts 6th ICPEAC" 757
Guang-yan P, Hvelplund P, Knudsen H, Yamazaki Y, Brauner M and Briggs J S (1992) *Phys. Rev. A* **47** 1531
Haghgooie M, Mader J J and Berko S (1978) *Phys. Lett. A* **69** 293
Harris I and Brown L (1957) *Phys. Rev.* **105** 1656
Harrison K G and Lucas M W (1970) *Phys. Lett.* **33A** 142
Hewitt N R, Noble C J and Brandsden B H (1990) *J. Phys. B* **23** 4185
Hewitt N R, Noble C J and Brandsden B H (1992) *J. Phys. B* **25** 557
Heyland G R, Charlton M,Griffith T C and Wright G L (1982) *Can. J. Phys.* **60** 503
Higgins K and Burke P G (1991) *J. Phys. B* **24** L343
Hoffman K R, Dababneh M S, Hsieh Y F, Kauppila W E, Pol V, Smart J H and Stein T S (1982) *Phys. Rev. A* **25** 1393
Humberston J W (1979) "Advances in Atomic and Molecular Physics" eds. Bates D R and Bederson B (Academic Press, New York) **15** 101
Humberston J W (1982) *Can. J. Phys.* **60** 591
Humberston J W (1986) *Adv. At. Mol. Phys.* **22** 1
Humberston J W and Campeanu R I (1980) *J. Phys B* **13** 4907
Hutchins S M, Coleman P G, Stone R J and West R N (1986) *J.Phys E* **19** 282
Hyder G M A, Dababneh M S, Hsieh Y-F, Kauppila W E, Kwan C K, Mahdavi-Hezavah M and Stein T S (1986) *Phys. Rev. Lett.* **57** 2252
Jacobsen F M, Charlton M, Chevallier J, Deutch B I, Laricchia G and Poulsen M (1990) *J. App. Phys.* **67** 575
Jaduszliwer B and Paul D A L (1973) *Can. J. Phys.* **51** 1565
Jaduszliwer B and Paul D A L (1974) *Can. J. Phys.* **52** 1047
Jochian C J and Potvliege R M (1987) *Phys. Rev. A* **35** 4873

Jones G O, Charlton M, Slevin J, Laricchia G, Kover A, Poulsen M R and Nic Chormaic S (1993) *J. Phys. B* **26** L483

Katayama Y, Sueoka O and Mori S (1987) *J. Phys. B* **20** 1645

Kauppila W E, Stein T S and Jesion (1976) *Phys. Rev. Lett.* **36** 580

Kauppila W E, Stein T S, Smart J H, Dababneh M S, Ho Y K, Downing J P and Pol V (1981) *Phys. Rev. A* **24** 725

Khan P and Ghosh A S (1983) *Phys. Rev. A* **28** 2181

Khan P, Mazumdar P S and Ghosh A S (1984) *J. Phys. B* **17** 4785

Khan P, Mazumdar P S and Ghosh A S (1985) *Phys. Rev. A* **31** 1405

Knudsen H, Andersen L H and Jensen K E (1986) *J. Phys. B* **19** 3341

Knudsen H, Brun-Neilsen L, Charlton M and Poulsen M R (1990) *J. Phys. B* **23** 3955

Knudsen H and Reading J F (1992) *Phys. Rep.* **212** 107

Kover A, Laricchia G and Charlton M (1993) *J. Phys. B* **26** L575

Krishnakumar E and Srivastava S (1988) *J. Phys. B* **21** 1055

Kubica P and Stewart A T (1975) *Phys. Rev. Lett.* **34** 852

Kwan C K, Kauppila W E, Lukaszew R A, Parikh S P, Stein T S, Wan Y J and Dababneh M S (1991) *Phys. Rev. A* **44** 1620

Lane A M and Thomas R G (1958) *Rev. Mod. Phys.* **30** 257

Lang N D and Kohn W (1971) *Phys. Rev. B* **3** 1215

Laricchia G, Davies S A, Charlton M, Beling C and Griffith T C (1988) *J. Phys. E* **21** 886

Laricchia G Moxom J and Charlton M (1993) *Phys. Rev. Lett.* **70** 3229

Lo C and Girardeau M D (1990) *Phys. Rev. A* **41** 158

Lynn K G, Gramsh E, Usmar S G and Sferlazzo P (1989) *Appl. Phys. Lett.* **55** 87

Lynn K G (1988) unpublished, from Schultz and Lynn (1988)

Macek J (1970) *Phys. Rev. A* **1** 235

MacKenzie I K, Khoo T L, McDonald A B and McKee B T A (1967) *Phys. Rev. Lett.* **19** 946

Madanski L and Rasetii (1950) *Phys. Rev.* **79** 397

Madey J M J (1969) *Phys. Rev. Lett.* **22** 784

Malmberg P R (1956) *Phys. Rev.* **101** 114

Mandal P and Guha S (1979) *J. Phys. B* **12** 1603

Mandal P, Guha S and Sil N C (1979) *J. Phys. B* **12** 2913
Mandal P, Guha S and Sil N C (1980) *Phys. Rev. A* **22** 2623
Mandal P, Roy K and Sil N C (1986) *Phys. Rev. A* **33** 756
Manuel A A (1981) in POS81 581
Massey H S W and Burhop E H S (1938) *Proc. Roy. Soc A* **167** 53

Massey H S W and Mohr C B O (1954) *Proc. Roy. Soc. London A* **67** 695
Massoumi G R, Schultz P J, Lennard W N and Ociepa J (1980) *Nucl. Inst. Methods* **30** 592
McAlinden M T and Walters H R J (1992) *Hyp. Int* **73** 65
McCoyd G (1965) Ph.D thesis St. Johns University New York.
McEachran R P, Horbatsch M and Stauffer A D (1991) *J. Phys. B* **24** 1107
McEachran R P, Morgan D L, Ryman A G and Stauffer A D (1977) *J. Phys. B* **10** 663
McEachran R P, Ryman A G and Stauffer A D (1978) *J. Phys. B* **11** 551
McEachran R P, Ryman A G and Stauffer A D (1979) *J. Phys. B* **12** 1031
McEachran P R and Stauffer A D (1986) *Positron (Electron)-Gas Scattering* ed. W E Kauppila, T S Stein and J M Wadehra (Singapore: World Scientific) p.122
Merrison J P, Charlton M, Deutch B I and Jorgensen L (1992) *J. Phys. Condens. Matter* **4** L207
Meyerhof W E (1963) *Phys. Rev.* **129** 692
Mikhailov A I and Porsev S G (1992) *J. Phys. B* **25** 1097
Mills A P (1980) *Appl. Phys.* **23** 189
Mills A P (1981) *Phys. Rev. Lett.* **46** 717
Mills and Gullikson E M (1986) *Appl. Phys. Lett.* **49** 1121
Mills A P, Platzman P M and Brown B L (1978) *Phys. Rev. Lett.* **41** 1076
Mizogawa T, Nakayama Y, Kawaratani T and Tosaki M (1985) *Phys. Rev. A* **31** 593
Mohorovicic S (1934) Astron Nachr 235 94
Montague R G, Harrison M F A and Smith A C H (1984) *J. Phys. B* **17** 3295

Montgomery R E and LaBahn R W (1970) *Can. J. Phys.* **48** 1288
Moores D (1976) *J. Phys. B* **9** 1329
Mori S and Sueoka O (1984) *At. Col. Res. Jap.* **12** 8
Moxom J, Laricchia G and Charlton M (1993) *J. Phys. B* **26** L367
Moxom J, Laricchia G, Charlton M, Kover A and Meyerhof W E (1993a) in preparation
Mukherjee K K, Singh N R and Muzumdar P S (1989) *J. Phys. B* **22** 99
Murray C A and Mills A P (1980) *Solid State Comm.* **34** 789
Nahar S J and Wadhera J M (1987) *Phys. Rev. A* **35** 2051
Newson H W, Williamson R M, Lones K W, Gibbons J H and Marshak H (1957) *Phys. Rev.* **108** 1294
Newton R G (1959) *Phys. Rev.* **123** 2312
Nico J S, Gidley D W, Skalsey M and Zitzewitz P W (1991) in "Book of Abstracts, 9th ICPA" 132
Nieminen R M and Hodges C H (1976) *Solid State Commun.* **18** 1115
Nieminen R M and Oliva J (1980) *Phys. Rev. B* **22** 2226
Ohsaki A, Watanabe T, Nakanishi K and Iguchi K (1985) *Phys. Rev. A* **32** 2640
Oldham W J (1965) *Phys. Rev.* **140** A1477
Oldham W J (1967) *Phys. Rev.* **161** 1
O'Malley T F, Spruch L and Rosenberg L (1961) *J. Math. Phys* **2** 491
Ore A and Powell J L (1949) Phys. Rev. 75 1696
Overton N, Mills R J and Coleman P G (1993) submitted to *J. Phys. B*
Parcell L A, McEachran R P and Stauffer A D (1983) *J. Phys. B* **16** 4249
Parcell L A, McEachran R P and Stauffer A D (1987) *J. Phys. B* **20** 2307
Parikh S P, Kauppila W E, Kwan C K, Lukaszew R A, Przybyla D, Stein T S and Zhou S (1993) *Phys. Rev. A* **47** 1535
Peach G and McDowell (1983) unpublished
Pendyala S, Bartell D, Girouard F E and McGowan J W (1976) *Can. J. Phys* **54** 1527
Perkins A and Carbotte J P (1970) *Phys. Rev. B* **1** 101

Phelps J O and Lin C C (1981) *Phys. Rev. A* **24** 1299
Raith W and Sinapius G (1989) *Comment. At. Phys.* **22** 199
Ramsauer C (1921) *Ann. Phys.* (Liepzig) **66** 546
Ramsauer C (1923) *Ann. Phys.* (Liepzig) **72** 345
Ramsauer C and Kollath R (1929) *Ann. Phys.* (Liepzig) **3** 536
Rapp D and Englander-Golden P (1965) *J. Chem. Phys.* **43** 1464
Ray A, Ray P P and Shah B C (1980) *J. Phys. B* **13** 1464
Rodbro M and Andersen F D (1979) *J. Phys. B* **12** 2883
Roy P K, Guha S, Sihha C and Sil N C (1984) *Ind. J. Pure Appl. Phys* **22** 398
Ruark A E (1945) *Phys. Rev.* **68** 278
Rudd M E, Sautter C A and Bailey C L (1966) *Phys. Rev.* **151** 20
Salin A (1969) *J. Phys. B* **2** 631
Schrader D M (1979) *Phys. Rev. A* **20** 918
Schultz P and Lynn K G (1988) *Rev. Mod. Phys.* **60** 701
Schultz D R and Olson R E (1988) *Phys. Rev. A* **38** 1866
Schultz D R and Reinhold C O (1990) *J. Phys. B* **23** L9
Schwentner N, Himpsel F J, Saile V Skibowski M Steinmann W and Koch E E (1975) *Phys. Rev. Lett.* **34** 528
Shah M B, Elliot D S and Gilbody H B (1987) *J. Phys. B* **20** 3501
Shakeshaft R and Wadhera J M (1980) *Phys. Rev. A* **22** 968
Shearer J W and Deutch M (1949) *Phys. Rev* **76** 462
Sil N C, Roy K and Mandal P (1991) Proc 17th Int. Conf. on Physics of Electronic and Atomic Collisions (Brisbane) (Bristol: Adam Hilger) Abstracts p354
Sinapius G, Raith W and Wilson W G (1980) *J. Phys. B* **13** 4079
Slevin J and Stirling W (1981) *Rev. Sci. Inst.* **52** 1780
Smith S J, Kauppila W E, Kwan C K and Stein T S (1989) Proc. 15th Int. Conf. on Physics of Electron Atom Collisions (Amsterdam: North-Holland) p 403
Sperber W, Becker D, Lynn K G, Raith W, Schwab A, Sinapius G, Spicher G and Weber M (1992) *Phys. Rev. Lett.* **68** 3690
Spicher G, Olsson B, Raith W, Sinapius G and Sperber W (1990) *Phys. Rev. Lett.* **46** 1019
Srivastava S K, Tanaka H, Chutjian A and Trajmar S (1981) *Phys. Rev. A* **23** 2156

Stein T S, Gomez R D, Hseih Y-F, Kauppila W E, Kwan C K and Wan Y J (1985) *Phys. Rev. Lett.* **55** 488

Stein T S and Kauppila W E (1986) *Advances in Atomic and Molecular Physics* ed. D Bates and Bederson (Academic press New-York) 18 p53

Stein T S, Kauppila W E, Kwan C K and Zhou S (1993) in book of abstracts, 18th int. conf. on the Physics of electronic and Atomic Collisions **2** 416

Stein T S, Kauppila W E, Pol V, Smart J H and Jeison G (1978) *Phys. Rev. A* **17** 1600

Stein T S, Kauppila W E and Roellig L O (1974) *Rev. Sci. Inst* **45** 951

Straton J C (1987) *Phys. Rev. A* **35** 3725

Sueoka O (1982) *J. Phys. Soc. Jap.* **51** 3757

Sueoka O (1982a) *J. Appl. Phys.* **21** 102

Sueoka O (1989) private communication in Charlton and Larrichia (1980)

Sural D P and Mukherjee S C (1970) *Physica* **40** 249

Tong B Y (1972) *Phys. Rev. B* **5** 1436

Townsend J S and Bailey V A (1922) P*hilos. Mag.* **43** 593

Van House J, Rich A and Zistewitz P W (1984) *Origins of life* **14** 413

Vehanen A, Lynn K G, Schultz P J and Eldrup M (1983) *App. Phys. A* **32** 163

Vehanen A and Makinen J (1985) *App. Phys. A* **36** 97

Wadehra J M, Stein T S and Kauppila W E (1981) *J. Phys. B* **14** L783

Walters H R J (1976) *J. Phys. B* **9** 227

Walters H R J (1988) *J. Phys. B* **21** 1893

Ward S J, Horbatsth M, McEachran R P and Stauffer A D (1989) *J. Phys. B* **22** 1845

Wetmore A E and Olsen R E (1986) *Phys. Rev. A* **34** 2822

Weyl H (1931) *Gruppentheorie und Quantenmechanik* 2nd ed. p234

Wheeler J A (1946) *Ann. N.Y. Acad. Sci* **48** 219

Wigner E P (1948) *Phys. Rev.* **73** 1002

Wilson W G (1978) *J. Phys. B* **11** L629

Winick J R and Reihardt W P (1978) *Phys. Rev. A* **18** 925

Yamazaki Y, Kuroki K I, Andersen L H, Horsdal-Pedersen E, Knudsen H, Moller S P, Uggerhoj E and Elsener K (1990) *J. Phys. Soc. Japan* **59** 2642

Yang C N (1950) *Phys. Rev.* **77** 242

Zafar N, Chevallier J, Jacobsen F M, Charlton M and Lariccia G (1988) *Appl. Phys. A* **47** 409

Zafar N, Chevallier J and Charlton M (1989) *J. Phys. D* **22** 868

Zhou S, Kauppila W E and Stein T S (1993) *Abstracts of Contributed Papers* 18th International Conference on the Physics of Electronic and Atomic Collisions **2** p411

J. Phys. B: At. Mol. Opt. Phys. 26 (1993) L367–L372. Printed in the UK

LETTER TO THE EDITOR

Total ionization cross sections of He, H_2 and Ar by positron impact

J Moxom, G Laricchia and M Charlton

Department of Physics and Astronomy, University College London, London WC1E 6BT, UK

Received 13 December 1992, in final form 8 February 1993

Abstract. Total positron impact ionization cross sections, including contributions from positronium formation, have been measured for He, H_2 and Ar from below the positronium formation threshold, E_{Ps}, up to 60 eV, 31 eV and 41 eV respectively. These cross sections have been subtracted from corresponding total cross section measurements and a small decrease in the elastic cross section between E_{Ps} and the threshold for excitation has been deduced for all three targets.

Brown and Humberston (1985) calculated the elastic scattering cross section (Q_{el}) and the positronium (Ps) formation cross section (Q_{Ps}) for positron (e^+) scattering from atomic hydrogen over a range of impact energies up to the excitation threshold (E_{ex}) at 10.2 eV. A slight discontinuity was found in the calculated value of Q_{el} across E_{Ps}. It was thought that this may have been due to a 'narrow cusp-like feature' in Q_{el} in the vicinity of E_{Ps}, or a calculational artefact, since Q_{el} above E_{Ps} was not evaluated with the same accuracy as below that energy. Additionally, above E_{Ps} the calculated values of Q_{el} were smaller than the values obtained by a linear extrapolation from below E_{Ps}, with the difference being nearly 20% at 10.2 eV.

A comparison of experimental data on e^+–helium scattering carried out by Campeanu *et al* (1987) indicated that a cusp may be present in Q_{el}, at E_{Ps}, followed by a decrease of approximately 20% between E_{Ps} and E_{ex}. The behaviour of Q_{el} was deduced by adding together Q_{Ps} and the single ionization cross section (Q_i^+) of Fromme *et al* (1986), fitting a curve to these points and then subtracting this from the total cross section (Q_t) of Stein *et al* (1978). Fromme *et al* (1988) have also measured Q_i^+ and Q_{Ps} for e^+–H_2 scattering and have subtracted these from Q_t of Hoffman *et al* (1982). A similar behaviour in Q_{el} was deduced as in the case of e^+–He scattering, with a reduction in Q_{el} of up to approximately 60% between E_{Ps} and E_{ex}. In both cases, however, the scarcity of available data for Q_{Ps} at low energies introduced a significant uncertainty in the deduced behaviour of Q_{el} near E_{Ps}.

A recent experiment by Coleman *et al* (1992), in which both Q_t and Q_{Ps} were measured using the same apparatus, has produced no evidence of a cusp in Q_{el} at E_{Ps} for e^+–helium scattering, of the magnitude found by Campeanu *et al* (1987). This result is depicted in the inset of figure 1. Q_{el} was also found to be, within the uncertainty of the measurements, flat up to E_{ex}. For He E_{Ps} is at 17.8 eV and E_{ex} is at 21.2 eV.

0953-4075/93/130367+06$07.50

In order to shed more light on the behaviour of Q_{el} in the vicinity of E_{Ps}, a more detailed knowledge of Q_{Ps} at low impact energies is needed. In the work described here, the total ionization cross section Q_t^+ has been measured, in detail, for He, H_2 and Ar for a range of impact energies from below E_{Ps} to 60 eV, 31 eV and 41 eV respectively. The measured values of Q_t^+ have been used to deduce Q_{el} above E_{Ps}, by subtraction from available Q_t data. Throughout this work Q_t^+ is defined,

$$Q_t^+ = Q_{Ps} + Q_i^+ + \sum Q_{ho}^+$$

where Q_{Ps} includes contributions from excited states and $\Sigma\, Q_{ho}^+$ is the sum of all higher order processes. This final term is zero for He and Ar over the range of energies for which data are presented here whilst, following Knudsen *et al* (1990), the dissociative contribution for H_2 is expected to be small.

A magnetically guided positron beam of variable kinetic energy, with an intensity of around $900\,s^{-1}$, was passed through a differentially pumped gas scattering cell, incorporating the ion extractor used by Moxom *et al* (1992). The energy spread of the beam was reduced to around 0.8 eV FWHM by biasing off the low energy portion of the beam. A Wien filter was employed, prior to the scattering cell, in order to remove fast particles emitted by the radioisotope from which the positrons were obtained. To prevent the positrons from being accelerated by the ion extractor, a random ion extraction technique was used. The beam was pulsed off (i.e. chopped) and, shortly after chopping the beam, the ion extraction field was pulsed on. This cycle was repeated at a frequency of 20 kHz and ensured that no positrons were in the scattering cell while the electric field was present. This technique benefited from the fact that the ion lifetime in the scattering cell was long in comparison with the period of the pulse cycle. Data were collected on a multichannel scaler (MCS), in multiple sweeps with a dwell time of 10 s per channel. Spectra were obtained by ramping the potential applied to the moderator in steps of 0.5 V, so that the data in each channel of the MCS corresponded to the count rate with a different mean beam energy. Ion count rates and beam intensities were measured in separate runs and the ion count rate was divided by the beam intensity channel by channel to obtain an ion yield. The beam intensity was measured with no target gas in the scattering cell using a Ceratron detector. This unit was switched off when the ion count rates were measured in order to prevent electrons ejected from its cone from passing through the scattering cell.

A detailed description of the apparatus and the systematic checks which were carried out will be given in a future publication (Moxom *et al* 1993). Amongst these checks, ion yields were measured over the range of impact energies between 2 eV and 300 eV in steps of 2 eV, using the full beam with an energy spread of 1.6 eV FWHM. The energy dependence of the ion yields was in good agreement with existing data, indicating that the ion extraction efficiency had no significant energy dependence over a wide range of impact energies. Ion yields were compared with published cross sections in order to obtain absolute values for Q_t^+. In the cases of He and H_2, ion yields were normalized to the sum of Q_{Ps} and Q_i^+, both of which have been measured by Fromme *et al* (1986, 1988). Ion yields were normalized at energies at which $Q_{Ps} + Q_i^+$ reached its maximum value, by fitting the present data to $Q_{Ps} + Q_i^+$ by eye. This procedure was found to give good agreement, within the statistical scatter of the data, over the whole range of impact energies for He and for all energies above 30 eV for H_2. In the case of Ar, the ion yields were normalized to measurements of Q_{Ps} by Fornari *et al* (1983) below 15.7 eV, where the contribution from direct ionization was zero. The Ar data were normalized in this way because of the uncertainty in Q_t^+ at higher energies. This

uncertainty arises from multiple ionization contributions and poor knowledge of Q_{Ps} above 76 eV, the highest energy investigated by Fornari *et al* (1983).

More detailed measurements were then made for the three targets over a narrower range of impact energies and it is these measurements which are reported here. The cross sections, Q_t^+, for the three gases are shown in figures 1, 2 and 3. The error bars represent one standard deviation. These data were in fact based upon ion yields obtained in a single run for each target and are typical of those found under different conditions (e.g. gas pressure and pulse frequency). The energy scale was fixed by measuring the beam energy with a retarding electric field set-up using a grid in front of the Ceratron. Verification of the beam energy determination was obtained from the position of the onset of the ion yields for the three targets.

The cross sections rise in each case, as expected, from an energy close to E_{Ps}. The small increase apparent just below this threshold (see for example Ar in figure 3) is attributed to the energy spread of the e^+ beam. The data presented in figures 1–3 show Q_t^+ varying smoothly with energy. A few points, however, appear to deviate from this behaviour by a statistically significant amount. No physical significance is attached to these points, since this behaviour probably arose from noise on the ion signal line and was not reproduced in runs taken under similar conditions. As mentioned above, the data were obtained from a single run consisting of multiple sweeps of the e^+ energy.

Figure 1 shows that the onset of Q_t^+ at E_{Ps} is most gradual in He, in comparison with Ar and H_2. The present data are in excellent agreement with $Q_{Ps}+Q_i^+$ of Fromme *et al* (1986) at all energies for He. The agreement in the case of H_2 is poorer below

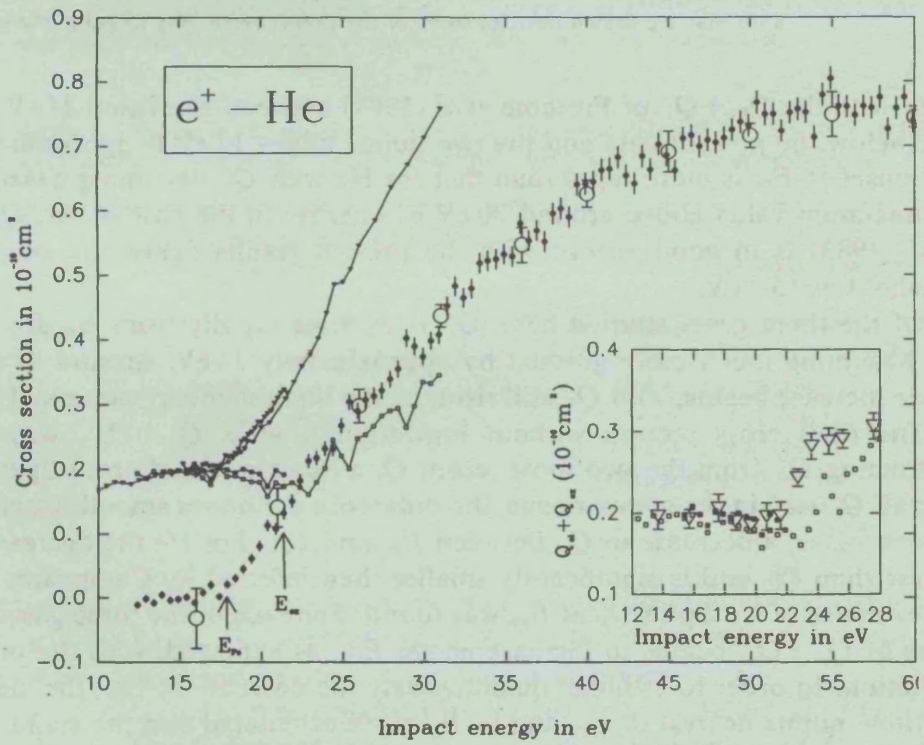

Figure 1. Present values of Q_t^+ (♦), $Q_{Ps}+Q_i^+$ of Fromme *et al* (1988) (◇), Q_t of Mizogawa *et al* (1985) (▼), Q_t of Stein *et al* (1978) (▽), the difference between Q_t of Mizogawa *et al* (1985) and Q_t^+ (■), the difference between Q_t of Stein *et al* (1978) and Q_t^+ (□), $Q_{el}+Q_{ex}$ of Coleman *et al* (1992) (▽) (inset). The lines that are drawn through some of the points serve only to guide the eye.

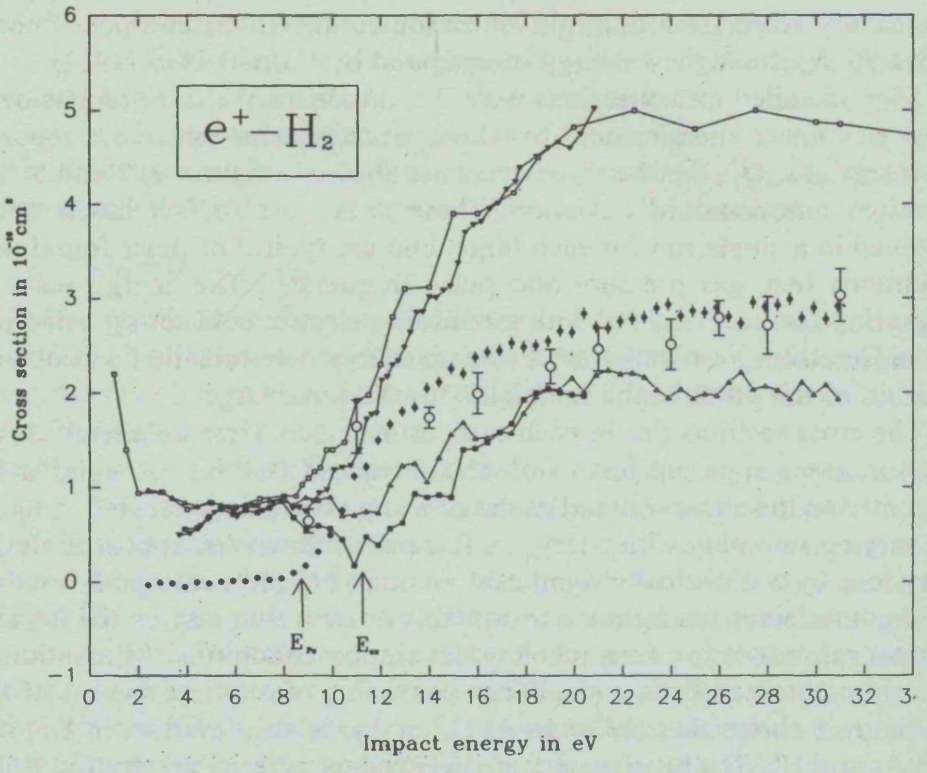

Figure 2. Present values of Q_t^+ (♦), $Q_{Ps}+Q_i^+$ of Fromme *et al* (1988) (◌), Q_t of Hoffman *et al* (1982) (□), Q_t of Charlton *et al* (1983) (▼), the difference between Q_t of Hoffman *et al* and Q_t^+ (△), the difference between Q_t of Charlton *et al* (1983) and Q_t^+ (■). The lines that are drawn through some of the points serve only to guide the eye.

30 eV with the $Q_{Ps}+Q_i^+$ of Fromme *et al* (1988) between 14 eV and 24 eV lying around 15% below the present data and the two points below 12 eV lying significantly higher. The onset at E_{Ps} is more rapid than that for He with Q_t^+ becoming nearly constant at its maximum value above around 20 eV e^+ energy. In the case of Ar, Q_{Ps} of Fornari *et al* (1983) is in good accord with the present results below the single ionization threshold at 15.7 eV.

Of the three gases studied here, Q_t^+ rises most rapidly from E_{Ps} for Ar, with the rise becoming much more gradual by approximately 14 eV. Around 22 eV a second, gentle increase begins, with Q_t^+ still rising at the highest energy presented here (41 eV).

The total cross section without ionization, that is $Q_{el}+Q_{ex}$, was deduced by subtracting Q_t^+ from the two most recent Q_t measurements. For all three targets and with all Q_t used in the comparisons, the difference continues smoothly across E_{Ps} with, in most cases, a decrease in Q_{el} between E_{Ps} and E_{ex}. For He the decrease appears to be less than 8% and is significantly smaller than inferred by Campeanu *et al* (1987). No evidence of a cusp in Q_{el} at E_{Ps} was found. For each of the three gases the inferred value of $Q_{el}+Q_{ex}$ begins to increase above E_{ex}, as expected, with the onset of target excitation. In order to estimate quantitatively the decrease in Q_{el}, the mean values of the three points nearest to E_{Ps} and to E_{ex} were calculated and the standard deviation used to estimate the uncertainty. The change in Q_{el} between E_{Ps} and E_{ex} is expressed, as a percentage, in table 1, along with the source of Q_t used to deduce Q_{el}.

The inset of figure 1 compares, for e^+–He collisions, the present derived values of $(Q_{ex}+Q_{el})$ with those measured by Coleman *et al* (1992). Between E_{Ps} and E_{ex} both experiments find Q_{el} nearly unchanged from its value just below E_{Ps}. Above E_{ex} the

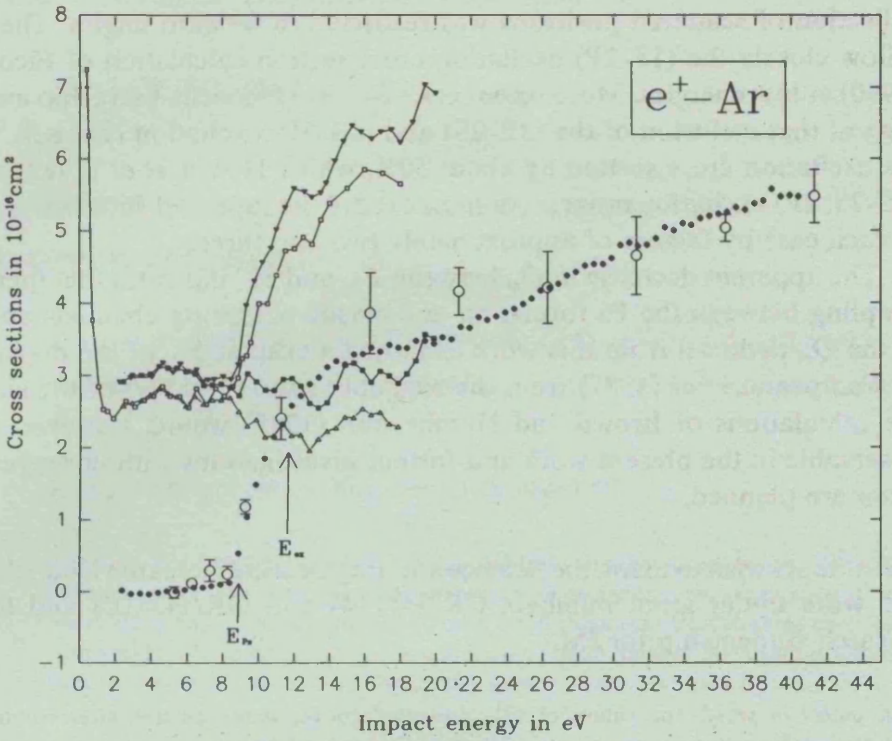

Figure 3. Present values of Q_t^+ (♦) (some of the error bars are encompassed by the points), Q_{Ps} of Fornari *et al* (1983) + Q_i^+ of Knudsen *et al* (1990) (◇), Q_t of Charlton *et al* (1984) (▼), Q_t of Kauppila *et al* (1976) (□), the difference between Q_t of Charlton *et al* (1984) and Q_t^+ (■), the difference between Q_t of Kauppila *et al* (1976) and Q_t^+ (△). The lines that are drawn through some of the points serve only to guide the eye.

Table 1. Change in the deduced values of Q_{el} between E_{Ps} and E_{ex}, for each target gas, expressed as a percentage, together with the source of Q_t used to deduce Q_{el}.

Target	% change in deduced value of Q_{el} between E_{Ps} and E_{ex}	Source of Q_t used to deduce Q_{el}
He	−5.5% ± 5.0%	Mizogawa *et al* (1985)
He	−8.3% ± 2.6%	Stein *et al* (1978)
H_2	−14.9% ± 4.4%	Hoffman *et al* (1982)
H_2	−50% ± 24%	Charlton *et al* (1983)
Ar	+2.1% ± 4.2%	Charlton *et al* (1984)
Ar	−10.5% ± 6.4%	Kauppila *et al* (1976)

two measurements do not agree, with the results of Coleman *et al* (1992) rising from around 21–22 eV, whilst for the present ($Q_{el} + Q_{ex}$) data the increase is not apparent until around 24 eV. The origin of this discrepancy is at present unknown.

An estimate of Q_{ex} in He was obtained by linearly extrapolating $Q_{el} + Q_{ex}$ from below E_{ex} to 30 eV. The difference between the extrapolated value of Q_{el} and the measured value of $Q_{el} + Q_{ex}$ was between 1.7×10^{-17} cm^2 and 2.1×10^{-17} cm^2 at 30 eV. This range of values is about three times higher than the corresponding measurement of Sueoka (1982), who employed a time-of-flight method to obtain energy-loss spectra. These measurements are believed to represent a lower estimate of Q_{ex} since the

collection of scattered positrons was restricted to forward angles. They do, however, follow closely the (1S–2P) excitation cross section calculation of Ficocelli-Varrachio (1990) at low energies. More recent calculations (Ficocelli-Varrachio and Parcell 1992) suggest that inclusion of the (1S–2S) and (1S–3P) excitation channels would increase the excitation cross section by about 50%, whilst Hewitt *et al* (1992) have found the (1S–2S, 2P) excitation cross sections to exceed the results of Ficocelli-Varrachio (1992) in each case by factors of approximately two and three.

The apparent decrease in Q_{el} between E_{Ps} and E_{ex} indicates that there may be some coupling between the Ps formation and elastic scattering channels above E_{Ps}. None of the Q_{el} deduced from this work exhibited a cusp at E_{Ps} of the magnitude obtained by Campeanu *et al* (1987) from the available data. A feature of the size indicated by the calculations of Brown and Humberston (1985) would, however, not have been observable in the present work and further investigations with improved energy resolution are planned.

The authors wish to thank the Science and Engineering Research Council for supporting this work under grant numbers GR/H41744 and GR/H25188 and for providing a research studentship for JM.

Note added in proof. The values of Q_t^+, presented above, were obtained after ssubtracting a constant background from the ion count rates. The true background however, appears to contain a small energy dependent contribution, resulting in non-zero values of Q_t^+ below E_{Ps} in the case of Ar, and the small differences between the deduced values of Q_{el} and Q_t below E_{Ps}. The authors wish to thank Professor W E Meyerhof for drawing our attention to this point.

References

Brown C J and Humberston J W 1985 *J. Phys. B: At. Mol. Phys.* **18** L401
Campeanu R I, Fromme D, Kruse G, McEachran R P, Parcell L A, Raith W, Sinapius G and Stauffer A D 1987 *J. Phys. B: At. Mol. Phys.* **20** 3557
Charlton M, Griffith T C, Heyland G R and Wright G L 1983 *J. Phys. B: At. Mol. Phys.* **16** 323
Charlton M, Laricchia G, Griffith T C, Wright G L and Heyland G R 1984 *J. Phys. B: At. Mol. Phys.* **17** 4945
Coleman P G, Johnston K A, Cox A M G, Goodyear A and Charlton M 1992 *J. Phys. B: At. Mol. Opt. Phys.* **25** L585
Ficocelli-Varrachio E 1990 *J. Phys. B: At. Mol. Opt. Phys.* **23** L779
Ficocelli-Varrachio E and Parcell L A 1992 *J. Phys. B: At. Mol. Opt. Phys.* **25** 3037
Fornari L S, Diana L M and Coleman P G 1983 *Phys. Rev. Lett.* **51** 2276
Fromme D, Kruse G, Raith W and Sinapius G 1986 *Phys. Rev. Lett.* **57** 3031
—— 1988 *J. Phys. B: At. Mol. Opt. Phys.* **21** L261
Hewitt R N, Noble C J and Bransden B H 1992 *J. Phys. B: At. Mol. Opt. Phys.* **25** 557
Hoffman K R, Dababneh M S, Hsieh Y F, Kauppila W E, Pol V, Smart J H and Stein T S 1982 *Phys. Rev.* A **25** 1393
Kauppila W E, Stein T S and Jesion G 1976 *Phys. Rev. Lett.* **36** 580
Knudsen H, Brun-Nielsen L, Charlton M and Poulsen M R 1990 *J. Phys. B: At. Mol. Opt. Phys.* **23** 3955
Mizogawa T, Nakayama Y, Kawaratini T and Tosaki M 1985 *Phys. Rev.* A **31** 2171
Moxom J, Laricchia G and Charlton M 1993 in preparation
Moxom J, Laricchia G, Charlton M, Jones G O and Kover A 1992 *J. Phys. B: At. Mol. Opt. Phys.* **25** L613
Stein T S, Kauppila W E, Pol V, Smart J H and Jesion G 1978 *Phys. Rev.* A **17** 1600
Sueoka O 1982 *J. Phys. Soc. Japan* **51** 3757

Physics letters A 174 (1993) 255–257
North-Holland

PHYSICS LETTERS A

Ionization of CO_2 by positron impact

G. Laricchia and J. Moxom
Department of Physics and Astronomy, University College London, Gower Street, London WC1E 6BT, UK

Received 22 October 1992; revised manuscript received 18 January 1993; accepted for publication 20 January 1993
Communicated by B. Fricke

The total ion yield by positron impact on CO_2 has been measured, for the first time, in the range 3–20 eV incident energy. An enhancement of this yield is observed at around 11 eV consistently with formation of positronium simultaneous to target excitation. An estimate of the total ionization cross section is obtained.

The total cross section of CO_2 for positron (e^+) impact is typical of many atomic and molecular targets in that it shows a substantial increase close to the threshold for positronium (Ps) formation, E_{Ps}. In CO_2, however, an additional notable increase exists *before* the threshold for ionization, E_i, at approximately 4–5 eV above E_{Ps} [1,2]. This observation prompted the suggestion [3] that it might be associated with the formation of Ps in the first excited state. As a consequence of this hypothesis, CO_2 was expected to be a good target for the observation that had eluded researchers for nearly thirty years, namely the formation of $n=2$ Ps by scattering e^+ in gaseous media. In the event, this process was first observed with simpler atomic and molecular targets [4], whilst CO_2 gave rise to unexpected results [5]. Summarizing, the technique employed a delayed coincidence circuit between a low energy photon detector (sensitivity $600 \geqslant \lambda \geqslant 200$ nm) and an annihilation photon counter. Detection of Lyman-α (243 nm) photons from the de-excitation of Ps (2P) in coincidence with one of the annihilation photons from the resulting Ps ($1\,^3S_1$) produced an exponential with the characteristic decay constant of ground-state triplet Ps. Supplementary verification of Ps (2P) detection was obtained by inserting a glass shutter in front of the phototube to reduce its sensitivity to ($600 \geqslant \lambda \geqslant 285$ nm), thus blocking out the Lyman-α photons.

In CO_2, however, signal levels consistent with a cross section of the order of 10^{-16} cm^2 were observed on both sides of the analyzer time-zero, implying that at least some of the signal originated from coincidences between an annihilation photon *followed*, in time, by the low energy photon. Furthermore the signal persisted upon insertion of the shutter. Subsequent studies and more extensive analysis of the data identified the origin of the signal as Ps formation simultaneous to the excitation of the remnant ion [6]. From the attenuation by the shutter, a photon energy of 3.5 eV was deduced and it was suggested that it originated from the ($^2\Pi_u$–$^2\Pi_g$) transition of CO_2^+.

In the present work, the total ion yield of CO_2 has been measured, for the first time, in the range 3–20 eV positron impact energy. By "total ion yield" we mean the yield of ions associated with *and* without Ps formation. This was done in order to test the deductions of Laricchia et al. [6] and verify their estimation of the cross section associated with the process.

A magnetically guided beam of quasi-monoenergetic positrons ($\Delta E \approx 1.1$ eV FWHM) was passed through the hemispherical gas cell described in ref. [7]. The base of the cell consisted of a set of concentric electrodes producing a radial field to extract ions from all parts of the cell. Unlike Moxom et al. [7] who used a pulsed extraction field, dc potentials were applied to the electrodes, the most negative being applied on the innermost. The perturbation on the collision produced by the static extraction potential was investigated by varying the magnitude of

the dc potential in the range 0.7–2.5 V. Within the statistical uncertainties of the data and at the present level of energy resolution, no effect due to the static field was discerned below 2 V extraction voltage.

The (vacuum) positron beam rate and the (gas) ion count rate versus beam energy were collected on a multi-channel-scaler. This was controlled by an external ramp providing the advance pulse in synchronism to increases in the voltage of the moderator (0.5 V steps, in this case) and of the set of $E \times B$ plates which separated the e^+ beam from the flux of fast particles originating from the β^+ source. The data, shown in fig. 1, represents the total ion yield, namely the ion count rate divided by the e^+ rate, obtained from a 90 mm long cell filled with CO_2 to a pressure of 0.4 μm of Hg. The spectrum was collected over a ~60 ks period consisting of ~150 cycles. A constant background, originating primarily from the ion detector dark counts, was determined by averaging the counts in the first five channels and subtracting it from the raw ion count rate. The correctness of this procedure was checked by collecting a spectrum with the e^+ beam repelled just prior to the $E \times B$. The signal, *at all energies*, was found to increase linearly with target pressure in the range 0.4–1 μm of Hg.

As can be seen in fig. 1, the variation of the total ion yield with energy displays features similar to those found in the total cross section [1,2]. The sharp ion yield onset is notable at around 7 eV, the Ps formation threshold. After rising for a couple of eV, the yield appears to have a plateau for a further few eV before starting to rise again approximately 3–4 eV *below* the single ionization threshold. This behaviour was reproduced in all runs taken under different conditions of gas pressure and ion extraction voltage, adding further statistical significance to the plateau and subsequent rise in the ion yield. This enhancement is therefore associated with Ps formation. Additionally its onset at 10–11 eV is in close agreement with the signal threshold previously observed [6] and it supports, by energy conservation considerations, the deduction of 3.5 eV as the energy of the photon involved. The postulated photon source, a CO_2 ion, has now been directly observed.

It is interesting that the excitation of the product ion apparently results in an increased Ps formation probability. A recent calculation of low energy s-wave

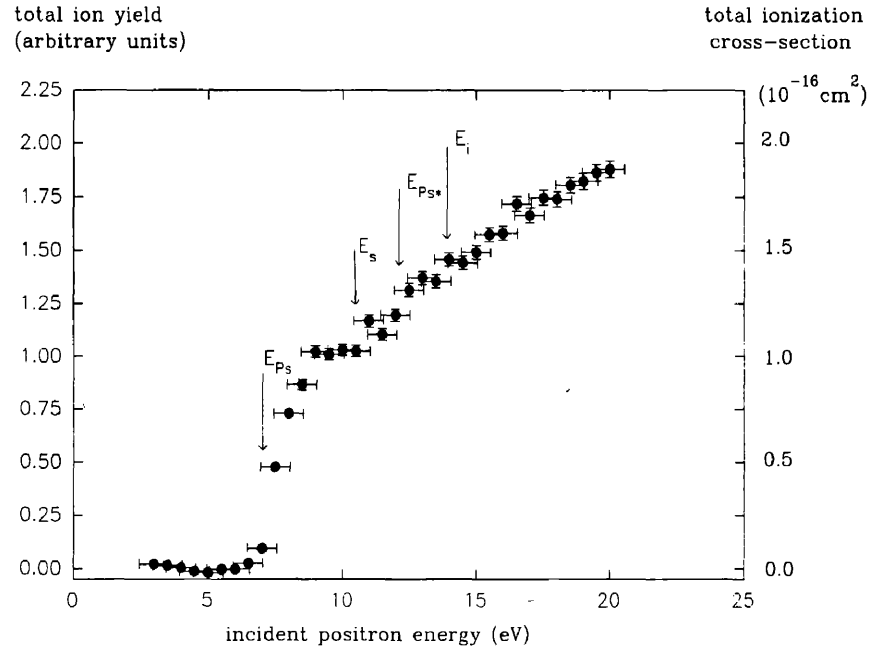

Fig. 1. The variation with impact energy of the total ion yield (l.h.s) and total ionization cross section (r.h.s) in positron–CO_2 scattering. The vertical bars denote statistical errors whilst the horizontal bars serve to illustrate the energy width of the beam. The thresholds for Ps formation in the ground (E_{Ps}) and first excited state (E_{Ps^*}), Ps formation simultaneous to ionic excitation (E_s) and single ionization (E_i) are shown.

positron–Li scattering employing the Kohn variational method has predicted a significant increase in the Ps formation cross section just below the threshold for target excitation [8]. This might be analogous to the present case since we note that the C-state of CO_2 lies at 10.56 eV above the ground-state, i.e. only 60 meV above the threshold for Ps formation simultaneous to ion excitation (see table 1). It seems as if Ps formation proceeds via a quasi-excitation of the molecule, followed by capture of the excited electron by a near-stationary positron, the remnant ion absorbing the difference in binding energies. We intend to test this conjecture by increasing our energy resolution and extending these studies to other targets.

An estimate of the absolute total ionization cross section was obtained as follows. The total cross section [1] between 5 and 7 eV was extrapolated linearly and subtracted from the values above the Ps formation threshold. The ion yields were then normalized to these values in the range 8–10 eV. The absolute scale thus obtained is shown on the r.h.s. vertical axis of fig. 1. It provides, to our knowledge, the first measure of the total ionization cross section of CO_2 by e^+ impact thus contributing to the data library which now comprises Ps formation and ionization cross sections by positron impact on inert atoms, molecular and, most notably, atomic hydrogen [9].

Table 1
Energy thresholds for various processes in e^+–CO_2 scattering.

Process	Threshold (eV)
(X-A) target excitation	5.70
ground state Ps formation	6.98
(X-B) target excitation	8.99
Ps formation with ionic excitation	10.50
(X-C) target excitation	10.56
excited state Ps formation	12.08
ionization	13.78

It is a pleasure to acknowledge illuminating discussions with Drs. John Humberston and Jonathan Tennyson. The Science and Engineering Research Council is also gratefully acknowledged for supporting this work under grant number (GR/H/25188) and for providing a research studentship to JM.

References

[1] K.R. Hoffman, M.S. Dababneh, Y.-F. Hsieh, W.E. Kauppila, V. Pol, J.H. Smart and T.S. Stein, Phys. Rev. A 25 (1982) 1393.
[2] M. Charlton, T.C. Griffith, G.R. Heyland and G.L. Wright, J. Phys. B 16 (1983) 323.
[3] K.Ch. Kwan, Y.-F. Hsieh, W.E. Kauppila, S.J. Smith, T.S. Stein, M.N. Uddin and M.S. Dababneh, Phys. Rev. Lett. 52 (1984) 1417.
[4] G. Laricchia, M. Charlton, G. Clark and T.C. Griffith, Phys. Lett. A 109 (1985) 97.
[5] M. Charlton and G. Laricchia, in: Proc. 3rd Positron (electron)-gas scattering conference, eds. W.E. Kauppila, T.S. Stein and J.M. Wadehra (World Scientific, Singapore, 1986) pp. 73–84.
[6] G. Laricchia, M. Charlton and T.C. Griffith, J. Phys. B 21 (1988) L227.
[7] J. Moxom, G. Laricchia, M. Charlton, G. Jones and A. Kover, Hyp. Int. 73 (1992) 217.
[8] M.S.T. Watts and J.W. Humberston, J. Phys. B (1992), in press.
[9] M. Charlton and G. Laricchia, J. Phys. B 23 (1990) 1045; W. Raith, Hyp. Int. 43 (1992) 3; H. Knudsen and J.F. Reading, Phys. Rep. 212 (1992) 107.

Near Threshold Effects in Positron-O_2 Scattering

G. Laricchia, J. Moxom, and M. Charlton
Department of Physics and Astronomy, University College London, Gower Street, London WC1E 6BT, United Kingdom
(Received 11 January 1993)

Structure has been observed in the total ionization cross section of O_2 above 8 eV positron impact energy. A comparison with available data on the excitation to the Schumann-Runge continuum indicates that coupling effects between the positronium formation, excitation, and direct ionization channels may be responsible.

PACS numbers: 34.80.Gs, 36.10.Dr

In atomic and nuclear physics, anomalous behavior in the form of discontinuous energy derivatives of partial cross sections, at the threshold for a new scattering channel, have been interpreted in terms of flux conservation using essentially classical arguments, and quantum mechanically according to virtual transitions allowed by the uncertainty principle [1]. Such interplay between various (elastic and inelastic) scattering channels constitutes one of the current topics of major interest in positron-atom (molecule) collisions [2].

A reduction in the probability for elastic scattering just above the positronium (Ps) formation threshold has been predicted in e^+-H collisions [3]. Some experimental evidence of such a coupled-channel effect has been derived from cross sections for e^+ impact on He [4,5], Ar [5], and H_2 [5,6]. More convincingly, structure has recently been observed at intermediate energies in the differential elastic scattering cross section when plotted at a fixed angle versus the energy of positrons incident on an Ar target [7]. This structure is manifested by a decrease of a factor of 2 at 60° occurring near the energy at which the ionization cross section reaches a maximum and has been interpreted as a coupled-channel shape resonance between the elastic scattering and the Ps formation and/or single-ionization channels. Recent calculations have found further evidence of such resonances in e^+-H [8] and e^+-inert atom [9] collisions.

In this work, channel-coupling effects in e^+ scattering have been observed *directly*, for the first time, in an integral partial cross section *close to the threshold* for a new inelastic channel. This observation has resulted from the measurement of the total ion yield from e^+ impacting on molecular oxygen. This yield is directly proportional to the total ionization cross section, σ_i^I, which comprises all allowed scattering channels resulting in at least one ion in the final state and therefore may be represented by

$$\sigma_i^I = \sigma_{Ps} + \sigma_i^+ + \sum \sigma_{HO},$$

where σ_{Ps} is the cross section for Ps formation in all allowed quantum states, σ_i^+ is the single-ionization cross section, and $\sum \sigma_{HO}$ is the sum over higher-order processes [10]. Contributions from this latter term are expected to be negligible, however, in the energy range investigated here.

A magnetically guided beam of quasimonoenergetic positrons ($\Delta E \approx 1.0$ eV FWHM) was passed through a hemispherical gas cell [11]. Its base consisted of a set of concentric electrodes producing a dc radial field used to extract ions from all parts of the cell. The perturbation on the collision produced by the static extraction potential was investigated by varying the magnitude of the dc potential in the range 0.7–2.0 V, corresponding to maximum potentials at the beam position approximately an order of magnitude lower. Within the statistical uncertainties of the data and at the present level of energy resolution, no effect due to the static field was discerned across the whole voltage range.

The (vacuum) positron beam rate and the (gas) ion count rate versus beam energy were collected on a multichannel scalar. This was driven by an external voltage ramp generator which provided the advance pulse in synchronism to increases in the voltage of the β^+ moderator (0.5 V above ground) and of the set of E×B plates employed to separate the e^+ beam from the flux of fast particles originating from the β^+ source. The total ion yield, namely, the ion count rate divided by the e^+ rate, obtained from the 90 mm long cell filled with O_2 gas at a given pressure was then calculated. The signal, at all energies, was found to increase linearly with target pressure in the range 0.07–0.13 Pa. Spectra were typically collected over 1–3 day periods consisting of several hundred ramp cycles. A constant background, originating primarily from the ion detector dark counts, was determined by averaging the counts below 4 eV (i.e., in the first four channels) and subtracting it from the raw ion count rate. The validity of this procedure was checked by comparison with a spectrum collected with the e^+ beam repelled prior to the gas cell.

An estimate of the absolute total ionization cross section was obtained as follows. An average of the total cross section [12] was determined between 2–4 eV and subtracted from the values above the Ps formation threshold. The average values of four ion-yield measurements were then normalized to these differences in the range 5–7 eV. In these measurements, the maximum ion extraction potential at the beam position was ≤ 0.15 V. The results thus obtained are shown in Fig. 1 where the total ionization cross section is seen to rise, as expected,

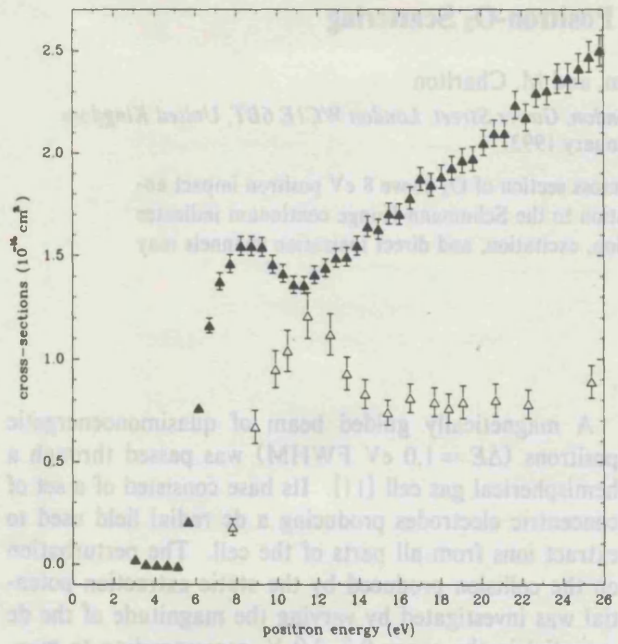

FIG. 1. Positron scattering from O_2: ▲, total ionization cross section (present results); △, cross section for excitation to the Schumann-Runge continuum [14].

near the threshold for Ps formation at 5.27 eV, before decreasing above approximately 9 eV impact energy. After reaching a minimum at around 11 eV, it is seen to rise over the remaining range of energies investigated. This energy dependence is markedly different from that observed for He, Ar, and H_2 [5,6,13] where both σ_i^+ and σ_{Ps} are found to vary smoothly with projectile energy, peaking, respectively, at approximately 3–4 times and twice the first ionization potential of the target. While the uncertainty in the energy dependence of the ion yields is approximately $\pm 3\%$, the absolute scale assigned to the total ionization cross section is considerably less certain, its uncertainty (up to $\pm 50\%$) arising primarily from the unknown energy dependences, above the Ps formation threshold, of the preexisting cross sections, namely, those for elastic scattering and excitation to the $A^3\Sigma_u^+$ state.

Also shown in Fig. 1 are the measurements of Katayama, Sueoka, and Mori [14] for the cross section σ_{ex} for excitation, by positron impact, to the Schumann-Runge continuum, a broad photoabsorption band in the ultraviolet region. It is interesting to note that the location of the dip in σ_i^+ appears to correspond with the maximum in σ_{ex}. This correspondence is evidence of coupling between the two channels. Indeed the increase of σ_i^+ is arrested in the vicinity of the threshold for the excitation $X^3\Sigma_g^- \rightarrow B^3\Sigma_u^-$ at 6.2 eV while the decrease in σ_{ex} appears close to the threshold for single ionization at 12.07 eV around which energy σ_i begins to rise again. This behavior is qualitatively similar to that expected in the elastic cross section in the vicinity of the Ps formation threshold [3]. The difficulty of extracting an accurate energy dependence of a preexisting cross section across the threshold for a new scattering channel, as in the case of elastic scattering (over all space) and Ps formation [4,15], does not arise in the present study where the relevant channel is observed directly.

In conclusion, structure has been observed in the total ionization cross section in e^+-O_2 scattering which reflects coupling effects with the cross section for excitation to the Schumann-Runge continuum [14]. The energy dependence of the latter is found to complement qualitatively the present measurements. Further investigations employing a higher energy resolution system and other targets are planned.

It is a pleasure to thank A. Kover, W. E. Meyerhof, and J. F. McCann for illuminating discussions. Also the Science and Engineering Research Council is gratefully acknowledged for supporting this work under Grant No. GRH25188 and providing a research studentship for J.M.

[1] For example, R. G. Newton, *Scattering Theory of Waves and Particles* (Springer, New York, 1982), 2nd ed.
[2] For example, L. Parcell (editor), Hyperfine Interact. **73**, 1–232 (1992).
[3] C. J. Brown and J. W. Humberston, J. Phys. B **18**, L401 (1985).
[4] R. I. Campeanu *et al.*, J. Phys. B **18**, 3557 (1987).
[5] J. Moxom, G. Laricchia, and M. Charlton, J. Phys. B (to be published).
[6] D. Fromme *et al.*, J. Phys. B **21**, L261 (1988).
[7] L. Dou *et al.*, Phys. Rev. Lett. **68**, 2913 (1992).
[8] K. Higgins and P. G. Burke, J. Phys. B **24**, L343 (1991).
[9] M. T. McAlinden and H. R. J. Walters (Ref. [2]).
[10] For example, for electron impact dissociative ionization, see D. Rapp *et al.*, J. Chem. Phys. **42**, 4081 (1965); for Ps formation accompanied by excitation, see G. Laricchia and J. Moxom, Phys. Lett. A (to be published).
[11] J. Moxom *et al.*, J. Phys. B **25**, L613 (1992).
[12] M. Charlton *et al.*, J. Phys. B **16**, 323 (1983); M. S. Dababneh *et al.*, Phys. Rev. A **38**, 1207 (1988).
[13] D. Fromme *et al.*, Phys. Rev. Lett. **57**, 3031 (1986).
[14] Y. Katayama, O. Sueoka, and S. Mori, J. Phys. B **20**, 1645 (1987).
[15] P. G. Coleman *et al.*, J. Phys. B **25**, L585 (1992).